Stellingen

behorende bij het proefschrift:

'Seismic reservoir characterisation employing factual and simulated wells'

- 1. Het combineren van diverse ondergrondse gegevens en kennis vereist dat deze vergelijkbaar gemaakt worden middels een consistente beschrijving aan de hand van een geologisch model (dit proefschrift, hoofdstuk 2).
- 2. Het integratie framework, zoals gedefinieerd in dit proefschrift, is een generieke beschrijving van de ondergrond die het mogelijk maakt lithostratigrafie, sequentie-stratigrafie, genetische eenheden en fysische eigenschappen te verbinden en in een computer te manipuleren (dit proefschrift, sectie 2.4.3).
- 3. Het visualiseren en interpreteren van seismische horizon patronen, bijvoorbeeld door middel van de segmentatie techniek heeft de potentie om uit te groeien tot een standaard techniek bij 3D-seismische intepretatie studies (dit proefschrift, hoofdstuk 6).
- 4. Bij veel op objecten gebaseerde geologische modellering systemen, wordt de geologische realiteit ondergeschikt gemaakt aan het rekenkundige model.
- 5. Het gebruik van fractalen voor het modelleren van geologische schaalniveaus is onjuist wanneer men op verschillende schalen de vorm van de geologische entiteiten betracht (b.v. Fig. 2.3 van dit proefschrift).
- 6. De aandacht besteed aan de ontwikkeling van een olieveld is vaak omgekeerd evenredig met zijn omvang.
- 7. De toekomst van geofysische inversie ligt in de geologie en niet in de fysica.
- 8. De projectmatige benadering van onderzoek in Europa mist een economische en strategische invalshoek. Voor innovaties buiten direct project verband is geen plaats in de huidige cultuur.

- 9. De complexiteit van geologische processen, de fragmentarische kennis van de ondergrond en de onzekerheden betreffende voorspellingen in de geologische tijd zou tot een éénduidig verbod moeten leiden ten aanzien van oplossingen voor het ondergronds opbergen van nucleair afval waarbij terugwinning uitgesloten wordt.
- 10.Het zou interessant zijn te onderzoeken hoeveel professionele hulpverleners hulp behoeven.

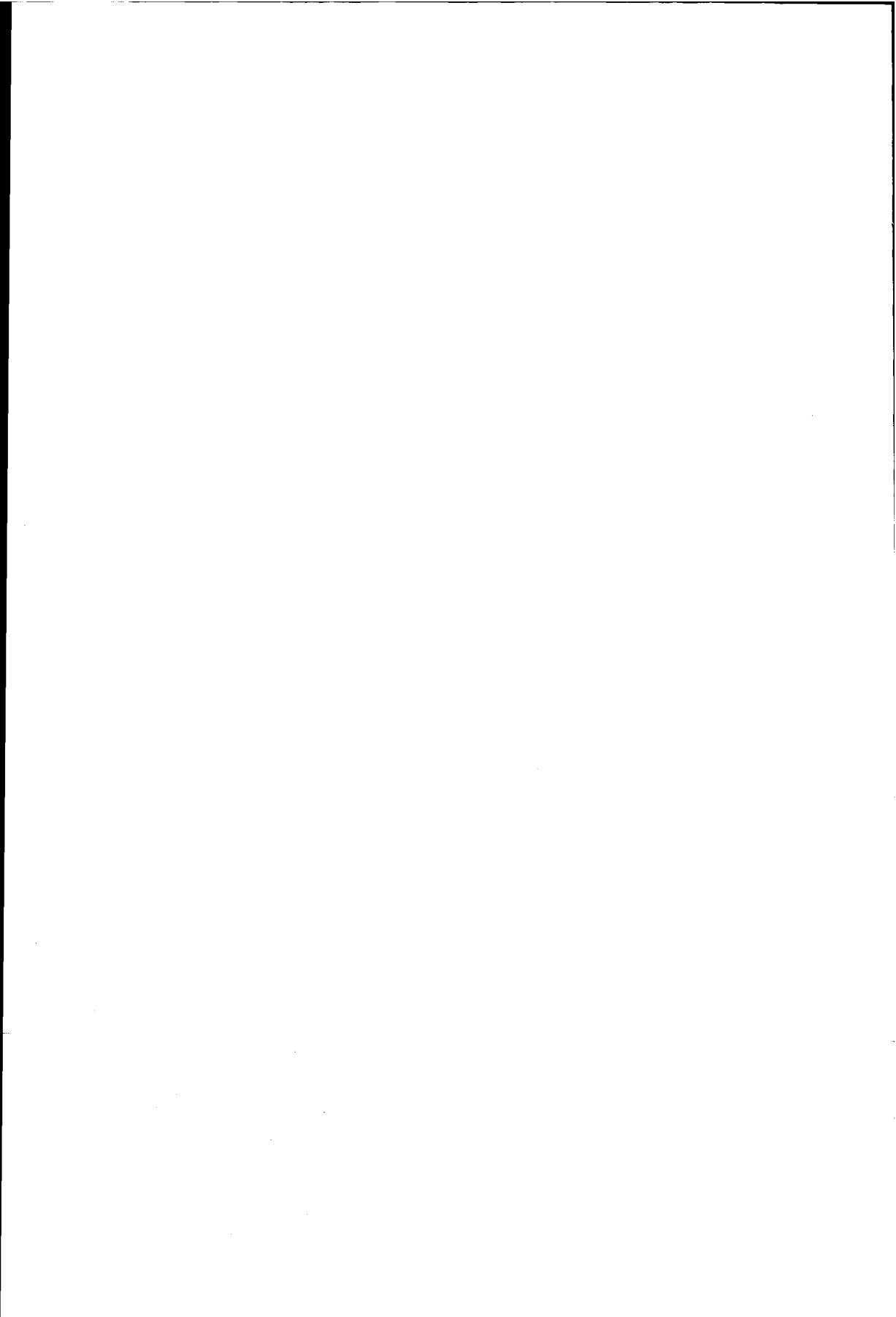
Enschede, 20 september 1995

Paul de Groot

633900 3182934 TR diss 2696.

TR diss 2616

Seismic reservoir characterisation employing factual and simulated wells



Seismic reservoir characterisation employing factual and simulated wells

PROEFSCHRIFT

ter verkrijging van de graad van doctor aan de Technische Universiteit Delft, op gezag van de Rector Magnificus Prof. ir. K.F. Wakker, in het openbaar te verdedigen ten overstaan van een commissie, door het College van Dekanen aangewezen, op woensdag 20 september 1995 te 10:30 uur

door

Paul Franciscus Maria DE GROOT

Mijnbouwkundig ingenieur geboren te Enschede



Dit proefschrift is goedgekeurd door de promotoren

Prof. ir. K.J. Weber en Prof. dr. ir. J.T. Fokkema

Samenstelling promotiecommissie:

Rector Magnificus, voorzitter

Prof. ir. K.J. Weber, TU Delft, promotor

Prof. dr. ir. J.T. Fokkema, TU Delft, promotor

Prof. ir. C.P.J.W. van Kruijsdijk, TU Delft

Prof. dr. ir. A.J. Berkhout, TU Delft

Dr. ir. A.J.W. Duijndam, TU Delft

Dr. C. Schweitzer, BEB Erdöl und Erdgas GMBH, Hannover

Dr. A.E. Campbell, TNO-GG, Delft

Published and distributed by:

Delft University Press

Stevinweg 1

2628 CN Delft

The Netherlands. Telephone +31 15 783254. Fax +31 15 781661

CIP-DATA KONINKLIJKE BIBLIOTHEEK, DEN HAAG

Groot, Paul Franciscus Maria de

Seismic reservoir characterisation employing factual and simulated wells / Paul Franciscus Maria de Groot. - Delft : Delft University Press. III.

Thesis Delft University of Technology. - With ref. - With summary in Dutch.

ISBN 90-407-1163-1

NUGI 836

Subject headings: reservoir characterisation / seismic inversion / neural network

Copyright © 1995 by P.F.M. de Groot

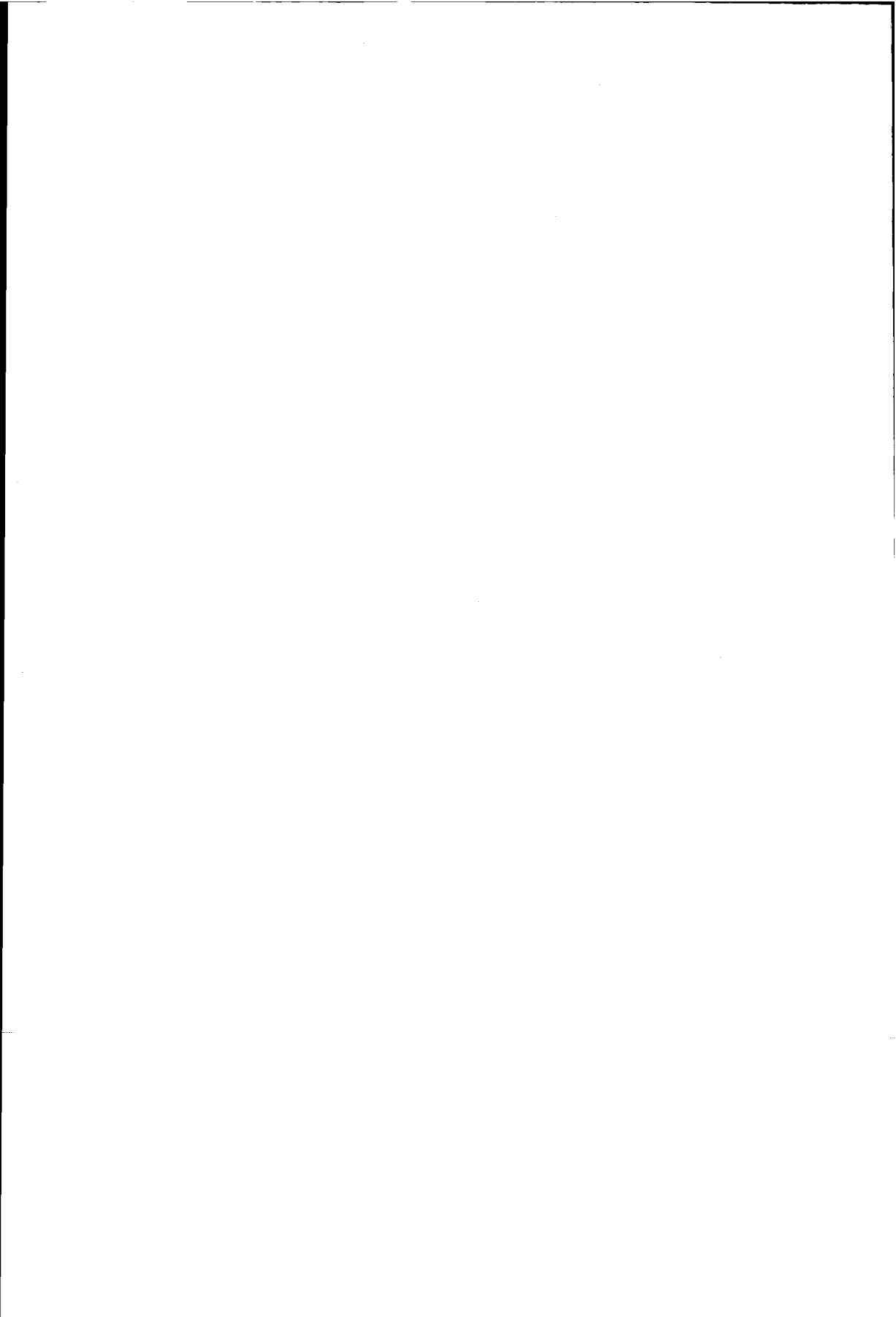
All rights reserved.

No part of the material protected by this copyright notice may be reproduced or utilised in any form or by any means, electronic or mechanical, including photocopying, recording or by any information storage and retrieval system, without permission from the publisher: Delft University Press, Stevinweg 1, 2628 CN Delft, The Netherlands.

Printed in The Netherlands.

Cover design: Jos Rietstap

Voor Mieke



PREFACE

In the beginning of 1991, I was transferred from Shell Petroleum Development Company of Nigeria to Shell International Petroleum Maatschappij in The Netherlands. In my new position as interpretation support geophysicist I came across artificial neural networks and realised that here was a tool with potential for seismic reservoir characterisation studies. By the middle of 1991 I decided that the best way to develop my ideas was to start my own company: Quest Geophysical Services B.V.

With the support of TNO Institute of Applied Geoscience in Delft, the Netherlands, whom I joined in 1992, I was able to achieve the first part of my quest by the end of 1992, i.e. the formation of the PROBE consortium. The objective of PROBE was to develop and test, in proprietary case studies, a seismic reservoir characterisation system based on neural networks and stochastic modelling techniques. PROBE attracted sponsorship from Saudi Arabian Oil Company, BEB Erdöl und Erdgas GMBH, IBM Nederland N.V., High Tech Automation B.V., SINTEF, TNO, the European Union and the Norwegian Research Council.

The greater part of the research which finally led to this thesis has been carried out within the PROBE project. I wish to thank the participating companies for making this possible and also for the interest and stimulating discussions during the sponsor meetings. Special thanks go to Saudi Arabian Oil Company and BEB for the permission to use their data in this thesis.

PROBE was jointly carried out by TNO and the Norwegian R&D organisation SINTEF. I wish to thank my Norwegian colleagues: Ragnar Havaaldsen Jr, Mats Carlin, Bjørn Lillekendlie and Gunnar Berre, for their

dedication and enthusiasm, which resulted in the neural network module of the GeoProbe system. Special thanks to my counterpart in the project: Tom Kavli. Thanks Tom, for many interesting discussions and for your willingness to implement the segmentation approach, even though the money was gone. It not only saved the project, it also saved my thesis!

Many thanks also to all TNO colleagues who participated in the PROBE project. I specifically like to mention the contributions of Harry Wedemeijer, Wim Immers, Bert Bril, Ewan Campbell and Frans Floris. Harry implemented the seismic processing module and became indispensable when data had to be loaded. Wim helped me greatly with many of the drawings that appear in this thesis. Bert Bril is one of the very rare persons who combines domain expertise with extra-ordinary software engineering skills. Bert has designed the GeoProbe software system and a.o. invented the coding system for the integration framework. Ewan played a crucial role in the case studies which are described in Chapter 6 of this thesis. Moreover, he edited my Dutch-English into Scottish-English and was never tired of searching for yet another reference that I could not omit. Frans Floris has solved the problem of drawing correlated multi-variate stochastic variables one-by-one, which is included as Appendix I of this thesis. This solution is inspired by earlier work of Peter Defize from TNO-TPD.

I also wish to thank Eddie Szulc and Koen Schilders of High Tech Automation for their work early on in the project and Rosana Cisneros, an independent consultant, for testing the software and applying it to another proprietary case study.

Special thanks are due to my promoters Prof. Weber and Prof. Fokkema for reviewing my work. I especially appreciated the sessions with Prof. Fokkema and Ir. Peet and thank them for their constructive criticism regarding my writing.

Finally, sincere thanks to my family. Marieke, Michelle, Nadine and Bart I'm sorry I could not give you the attention you deserved. Mieke, all credits and thanks go to you. I could not have done this without you.

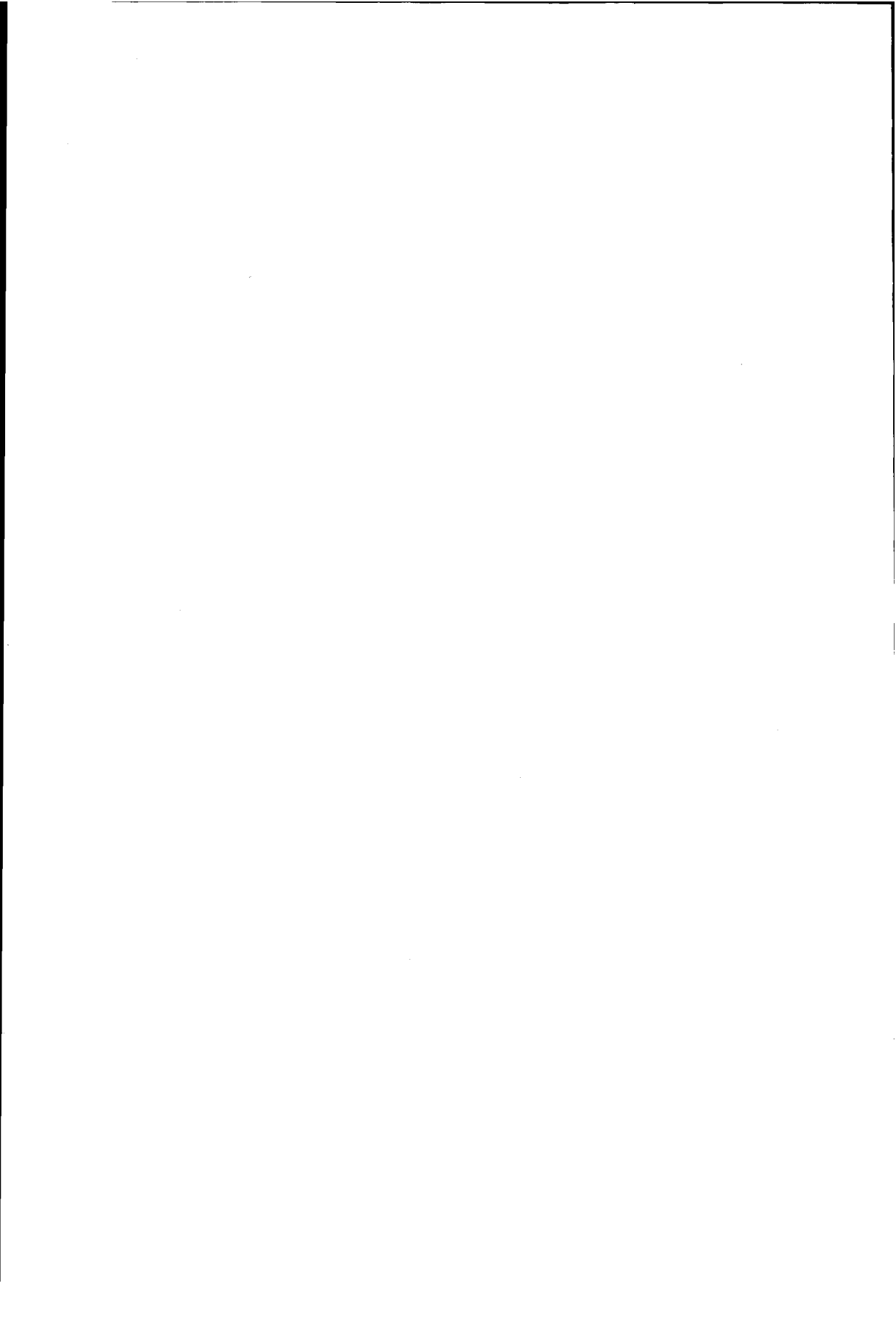
Paul de Groot Delft, July 1995

TABLE OF CONTENTS

Preface	i
Table of Contents	iii
Introduction	
1.1 Statement of the problem	
1.2 Total space inversion	
1.3 Outline of this thesis	4
Seismic Reservoir Characterisation	7
2.1 Introduction	
2.2 Assumptions	8
2.3 Overview existing techniques	10
2.3.1 General	10
2.3.2 Attribute analysis	
2.3.3 Acoustic impedance inversion	
2.3.4 Stochastic simulations	
2.4 Towards a new technique	
2.4.1 General	13
2.4.2 The scale problem	
2.4.3 The integration framework	21
2.4.4 Total space inversion	24
Introducing the various Techniques	27
3.1 Introduction	27
3.2 Artificial Neural Networks	28
3.2.1 General	
3.2.2 Multi-layer perceptrons (MLP)	29
3.2.3 Radial Basis Function Neural Networks (RBF)	
3.2.4 Unsupervised Vector Quantiser (UVQ)	35

3.3 Monte Carlo Statistics	39
Simulating wells	43
4.1 Introduction	43
4.2 Simulation algorithm	43
4.3 Simulation example	48
Experiments with simulated data	53
5.2 Initial model	33 51
5.3 Experiments	
5.3.1 Network design	
5.3.2 Geological model complexity	57
5.3.3 Seismic bandwidth variations	39
5.3.4 Additional information	64
5.4 Discussion of the results	64
5.5 Conclusions	69
Case studies	
6.1 Introduction	
6.2 Rotliegend case study	72
6.2.1 Available data	72
6.2.2 Geology	73
6.2.2.1 Tectonic Overview	
6.2.2.2 Stratigraphy	
6.2.2.3 Depositional Facies and Reservoir Geole	
6.2.3 Integration framework	
6.2.4 Well data preparation	
6.2.5 Direct inversion	
6.2.6 Segmentation	
6.3 Middle Eastern case study	
6.3.1 Available data	
6.3.2 Geology	
6.3.2.1 Tectonic Overview	
6.3.2.2 Stratigraphy	
6.3.2.3 Depositional facies and reservoir geolog	
6.3.3 Integration framework	
6.3.4 Segmentation	
6.4 Conclusions	117
Practical aspects	.119
7.1 Introduction	119
7.2 True amplitude seismic processing	
7.3 Seismic trace balancing	121
7.3 Reference horizon	122
7.4 Applicability	

Suggestions for future work	127
8.1 Introduction	
8.2 Geostatistical implementation	128
8.3 Pre-stack implementation	129
8.4 Fluid replacement simulations	130
8.4 Well log preprocessor	133
8.5 Supervised segmentation	134
8.6 Step-wise inversion	135
8.7 General use of the integration framework	135
Conclusions	137
9.1 General	
9.2 Conclusions	138
References	141
Monte Carlo statistics	149
Simulation specifications	157
Performance statistics simulated data experiments.	165
Summary	177
Samenvatting	179
Curriculum Vitae	183



INTRODUCTION

1.1 Statement of the problem

The seismic reflection method measures the response of the subsurface, in space and time, due to a generated source wavefield (Fig. 1.1). On land, dynamite and seismic vibrator sources are commonly used to generate the source wavefield. In general for the marine case airgun sources are used. The response is measured by a distribution of geophones (land) or hydrophones (marine). The seismic experiments are repeated multiple times, at different locations, in order to obtain a proper sampling of the subsurface. If the seismic measurements are acquired along a line, a two-dimensional profile is acquired (2D-seismic). If the measurements are acquired such that the seismic coverage is equal, to and perpendicular to, the recording direction, a three-dimensional dataset is acquired (3D-seismic). In the seismic processing phase, the measurements are transformed to sections in space and time (sometimes space and depth) of the subsurface. These sections need then to be interpreted in order to obtain structural images of the subsurface.

Apart from information on the structural framework of the subsurface, the seismic measurements, also carry information about rock and fluid properties in the subsurface. This type of information is valuable, from an economic perspective, for characterising zones of interest, such as hydrocarbon reservoirs. This process of inferring information about the subsurface properties from the seismic measurements is called *seismic reservoir characterisation*. It plays an important part in total field development and reservoir management.

1. Introduction 2

Seismic reservoir characterisation must be approached from a geological perspective. The reason for this is that seismic reservoir characterisation results must ultimately be combined with results obtained from other data inversions and interpretations aimed at delineating and describing the reservoir model. The only way to obtain commensurable results is to use a common subsurface model for all relevant data descriptions. This common subsurface model must be based on a geological description.

The goal of this thesis is to describe a seismic reservoir characterisation method, based on a geological approach, that is aimed at extracting the greatest possible stratigraphic and lithological detail from post-stack migrated seismic data.

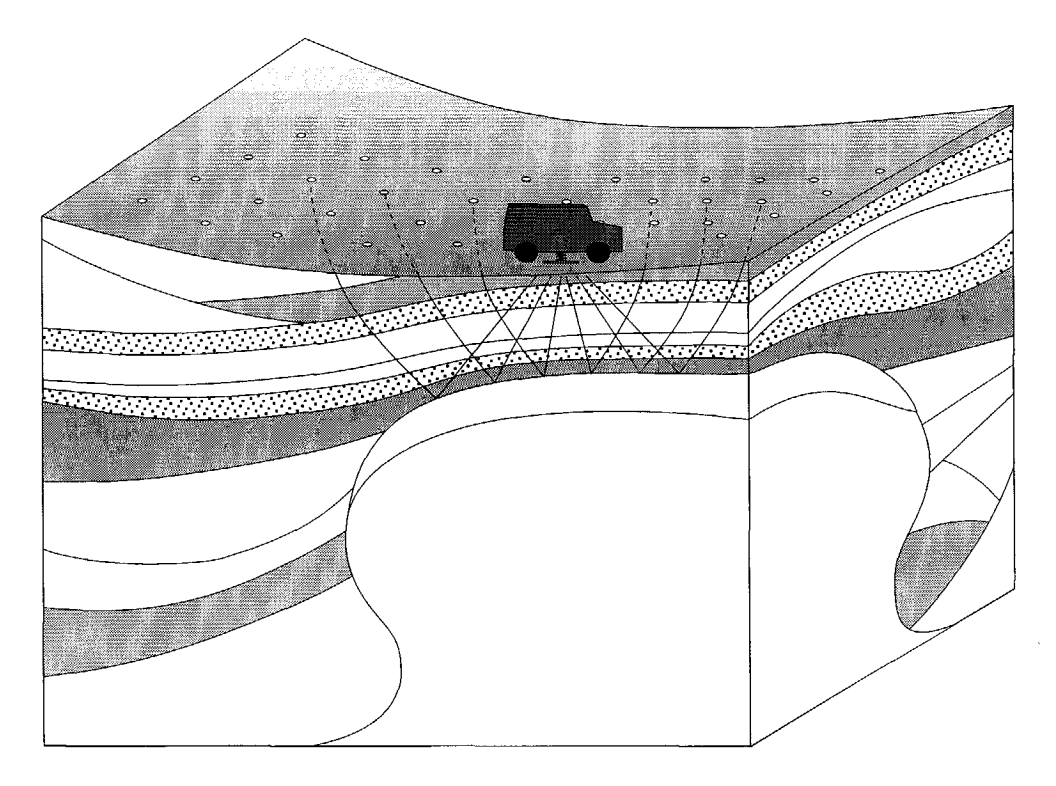


Fig. 1.1 The principle of the seismic method. Seismic waves are generated by a seismic source. They propagate through the subsurface, get reflected by layer boundaries and propagate back to the surface where they are recorded by the geo-/hydrophones.

1.2 Total space inversion

Seismic reservoir characterisation techniques have a requirement to integrate data and knowledge from other sources and disciplines. Integration of such data and information is not trivial because of the varying datatypes, scales and accuracies involved. Another major problem is that well data is often limited and geological knowledge and reasoning can best be entered into the problem via stochastic methods. Hence, there is a requirement to combine stochastic and deterministic data.

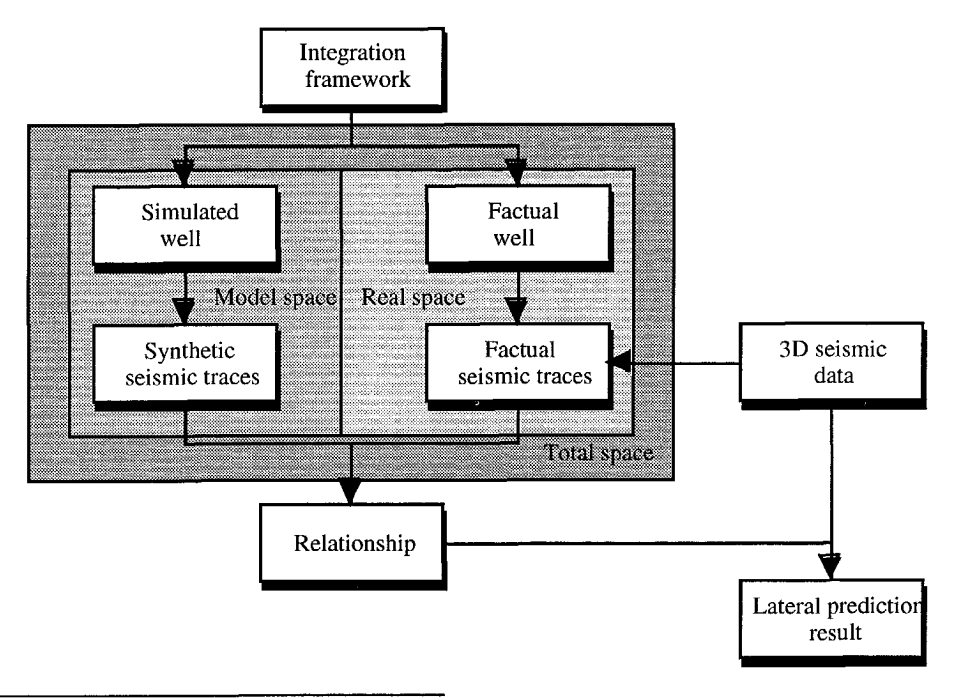


Fig. 1.2 Total space inversion concept.

Relevant data, from a seismic reservoir characterisation perspective, are described, in this thesis, in terms of a common subsurface model: the *integration framework*. Factual wells, i.e. one-dimensional (1D) stratigraphic profiles with attached physical properties, and simulated wells, described in terms of the integration framework, are commensurable. The factual well data is combined with the surface seismic traces at the well locations. This part of the problem space is defined as *real space*. Simulated wells and corresponding synthetic seismograms are part of the problem space that is defined as *model space*. The combination of real space and model space is defined as *total space*. Datasets consisting of wells with corresponding seismic responses can then be compiled from factual and/or

1. Introduction

4

simulated data. The objective is to arrive at a dataset that is representative of the target zone in a particular study area. The seismic reservoir characterisation technique uses the representative dataset to establish relations between seismic response and underlying salient well properties. The technique is referred to as *total space inversion*.

1.3 Outline of this thesis

This thesis after outlying existing seismic reservoir characterisation techniques, describes how neural network technology and Monte Carlo statistics, can be applied to total space inversion. The method is then applied to two case studies and the results evaluated.

The thesis is divided in 9 chapters as follows:

Chapter 1 is an introduction to the problem and an outline of the thesis.

Chapter 2 is an introduction to seismic reservoir characterisation. The basic assumptions made in this thesis are presented here and an overview of existing techniques given. The problems related to the integration of different data types, scales and accuracies are then discussed. An introduction to the integration framework and the total space inversion technique follows.

Chapter 3 introduces the techniques used in this thesis for seismic reservoir characterisation, namely, artificial neural networks and Monte Carlo statistics. The network paradigms described here are:

- Multi-Layer-Perceptrons (MLP)
- Radial Basis Functions (RBF) and the
- Unsupervised Vector Quantiser (UVQ).

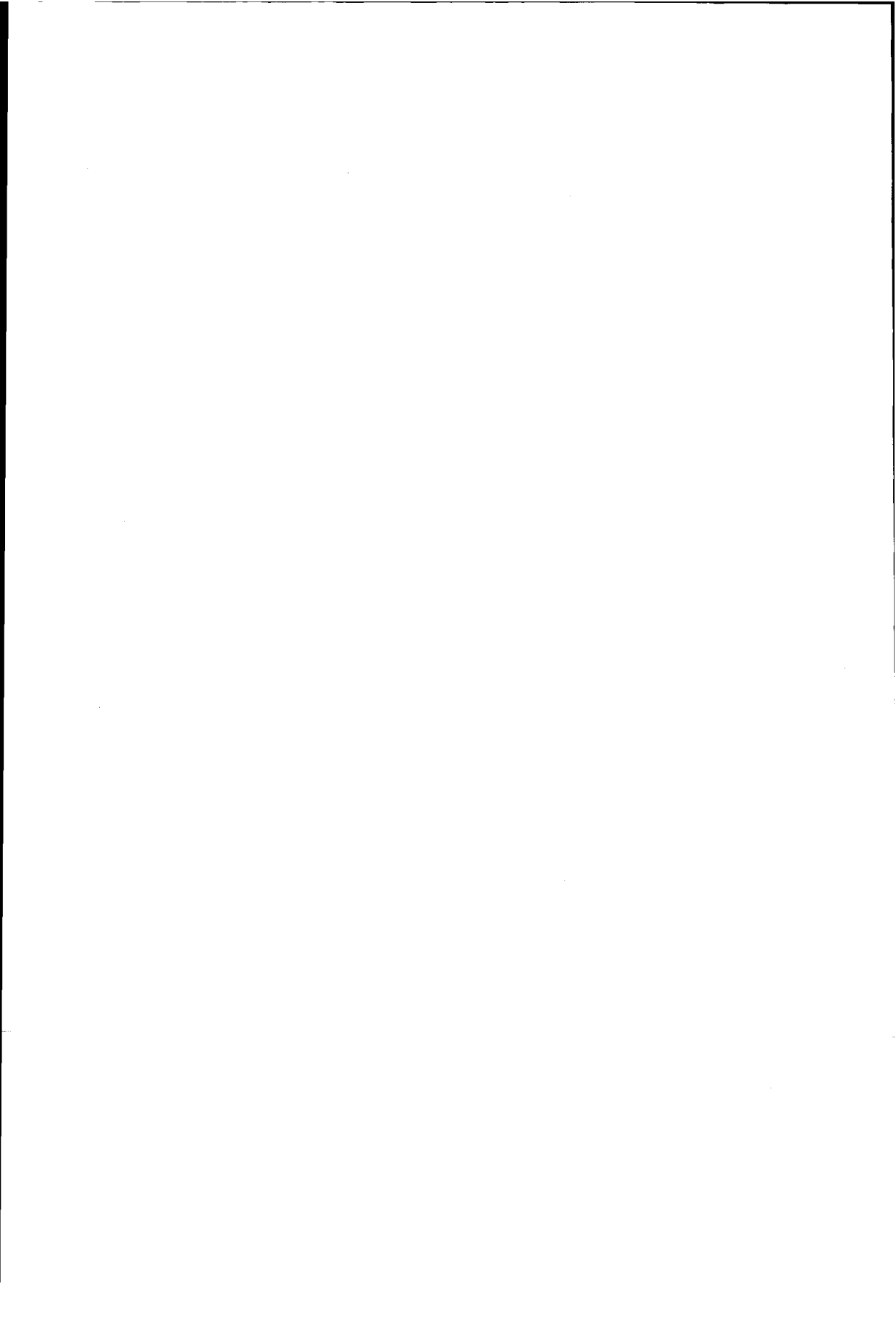
The simulation algorithm used to generate wells is then introduced. This simulation algorithm is discussed in more detail in Chapter 4. In Chapter 5 experiments with simulated data, aimed at determining the feasibility of direct inversion, are discussed.

In Chapter 6, the application of the total space inversion method to two separate case studies is described. The first study deals with an aeolian gas-

filled reservoir. The second study examines an oil-filled fluviatile reservoir model.

In Chapter 7, practical aspects, dealing with the application of the total space inversion method are discussed. Chapter 8 puts forward suggestions for future applications of the technique while the conclusions are presented in Chapter 9.

Appendix I contains the mathematics behind the Monte Carlo simulation algorithm. In Appendix II, the simulation specifications used to simulate wells in Chapters 4 and 6 are given. Finally, in Appendix III, the neural network performance statistics for the experiments described in Chapter 5, are presented.



SEISMIC RESERVOIR CHARACTERISATION

2.1 Introduction

Post-stack seismic reservoir characterisation (or lateral prediction) studies have been carried out since the first "bright spots" were recognised some 25 years ago (Brown, 1991). In the early days seismic attributes were measured along an interpreted seismic horizon. These attributes were then calibrated at well locations to physical rock properties, such as porosity. The attribute measurements away from the well bore yielded prediction results for the calibrated rock property. In the eighties acoustic impedance inversion was introduced as an alternative seismic reservoir characterisation technique (e.g. Savit and Changseng Wu, 1982, Neidel et.al., 1986). The aim of acoustic impedance inversion is to increase the seismic band-width in order to increase the amount of detail that can be extracted from the data. In general, acoustic impedance inversion is followed by additional inversion steps, in which the seismic impedance traces are transformed into physical rock properties. In the nineties stochastic simulations were introduced (e.g. Haas and Dubrule, 1994). With this technique, objects, or properties, are generated and distributed in space. The simulated data can be constrained by the recorded seismic data. A number of stochastic models are generated for each seismic location. These stochastic models can then be analysed to obtain information on physical rock properties.

The ultimate aim of seismic reservoir characterisation is to delineate and describe, in the greatest possible detail, reservoir properties from recorded seismic data. The final output is a prediction of subsurface properties. These properties can be physical properties, such as porosity or fluid content, or they can be geological properties, such as lithology and bed thicknesses.

Invariably, seismic reservoir characterisation techniques have a requirement to combine data and information from other sources in order to be able to relate seismic response with the properties of interest. A major problem is that, in general, information is available from a variety of sources, over a wide range of scales and with greatly varying accuracies. Integration of all relevant information cannot be achieved using existing techniques. Consequently, it seems impossible to arrive at a reservoir model that is consistent with all information available, unless the diverse data types are made commensurable.

In this thesis seismic reservoir characterisation is approached from a geological perspective. It is argued that integration can be achieved only if one consistent subsurface model is used throughout to describe all relevant data and information. The model used here incorporates an acoustic-stratigraphic integration framework. The scale problem is solved by grouping framework entities at three scale levels.

1D-stratigraphic profiles with physical properties, i.e. factual wells, are described in terms of framework entities. Physical properties are attached to the smallest scale entities. For example, sonic and density log measurements are blocked at this scale and parameterised at top and bottom. Factual wells described in this way are combined with the recorded seismic trace at the well location. The combined seismic and well data is then used to generate a dataset, representative of the target zone, that is used in the seismic reservoir characterisation process. Wells with corresponding physical properties can also be simulated. The simulated acoustic properties can then be used to synthesise seismic traces. Because the simulated dataset is described using the same integration framework, factual and simulated data can be combined to create a representative dataset when well data is scarce.

In Section 2.2 the basic assumptions made in this thesis are outlined. This is followed by a section in which the most popular existing seismic reservoir characterisation techniques are presented. In the next section it is described how geological and engineering data and information can be integrated with seismic data via an integration framework. Finally, the "total space inversion" concept is introduced.

2.2 Assumptions

This thesis deals with post-stack seismic reservoir characterisation. The seismic datasets used are three-dimensional post-stack datasets comprising P-waves, or compressional waves, only. It is assumed that seismic

processing has correctly imaged and focused the seismic signals and has removed unwanted energy, such as multiples. It is assumed that "True Amplitude" seismic processing has preserved the amplitude information of the seismic reflection events, see Section 7.2. Variations in the post-stack response are assumed to be directly related to lateral geological variations.

If sonic and density logs are used, it is assumed that these logs have been edited for noise bursts, cycle skips, fluid replacement etc.

When seismic data is synthesised, the convolutional model is assumed. A discrete seismic trace $s_n = s(n\Delta t)$ n = 1,...,N, where Δt is the temporal sample rate is computed as:

$$s_n = \sum_{i=1}^{L} w_i m_{n-i}, \qquad n = 1, ..., N,$$
 (2.1)

where:

 $w_i = w(i\Delta t)$ is the discrete version of the seismic wavelet with i = 1, ..., L, $m_i = m(i\Delta t)$ is the discrete impulse earth response filter with i = 1, ..., N.

The convolutional model for the generation of a seismic trace is based on the following assumptions:

- The subsurface can be described as a one-dimensional space. In other words it consists of stacked horizontal homogeneous layers without lateral variations.
- The seismic wavelet does not change as it travels through the subsurface.
- The seismic trace is reasonably represented by compressional plane waves that arrive at layer boundaries at normal incidence. In other words, shear waves are not taken into account.

When seismic wavelets are used in this thesis, it is assumed that a single wavelet can be used to synthesise seismic traces. It is further assumed that this wavelet can be obtained, either, via seismic processing (e.g. Verschuur, 1991), or, via a statistical wavelet estimation procedure in which a match between synthetic seismic trace and field seismic trace is enforced. Both procedures of wavelet determination have been applied in this thesis.

2.3 Overview existing techniques

2.3.1 General

Conventional lateral prediction comprises a group of techniques in which seismic reflection amplitudes are analysed and transformed via true-amplitude processing and integration into acoustic impedance values. The acoustic impedance values are subsequently interpreted in terms of reservoir properties. Most conventional lateral prediction techniques can be applied to both 2D- and 3D-seismic data. The term 'conventional' is used here to indicate that these techniques are applied to post-stack seismic data involving only P-waves (compressional waves).

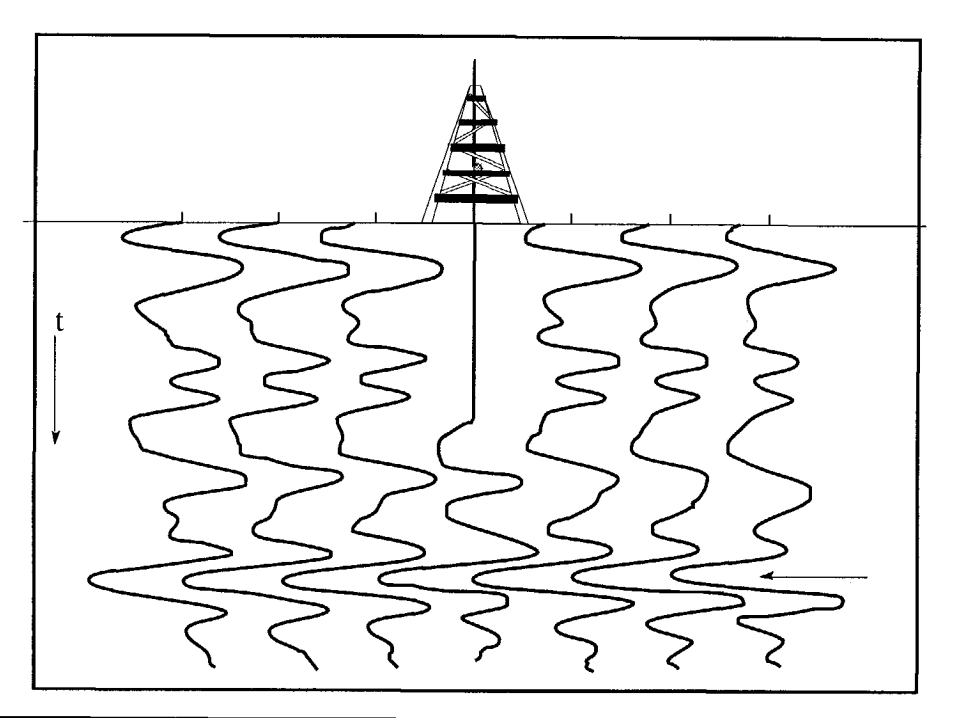


Fig. 2.1 Well-to-seismic calibration. The synthetic seismic trace is spliced into the surface seismic section at the well location (Courtesy K. J.Weber., Delft University of Technology).

The basic concept in conventional lateral prediction is calibration of the seismic response to well log measurements. Variations in the response, away from the well, are then assumed to reflect changes in rock properties. Seismic data can be calibrated at well locations with the aid of acoustic impedance and reflectivity logs. Acoustic impedance is defined as the

product of seismic wave propagation velocity and medium density. Therefore, an acoustic impedance log may be derived from sonic and density logs. From the acoustic impedance log a reflectivity log can be derived. The reflectivity logs are converted from depth to time and resampled to the seismic sampling rate. After convolution with the seismic wavelet, the resulting synthetic seismic trace can be compared with the recorded field seismic traces. The seismic events can now be identified and tied to the well data. It is noted, that after wavelet processing the synthetic seismograms and the field seismic traces should have the same amplitude and phase characteristics. A separate trace balancing step might be required should the amplitudes differ due to different processing histories. An example of a well-to-seismic calibration is shown in Fig. 2.1.

Seismic reservoir characterisation techniques can be, arbritarily, divided into three groups of techniques. The first group uses attributes, derived from the seismic response, to predict reservoir properties. The second group aims to increase the vertical seismic resolution by transforming the seismic time response into broad-band acoustic impedance profiles. This is known as acoustic impedance inversion. The third group is that of stochastic simulations where objects or properties are generated and distributed in space.

2.3.2 Attribute analysis

Seismic attributes are features extracted from a seismic signal at or near an interpreted seismic event. They have been studied for over 25 years. Initially attributes were extracted in special cases only, e.g. to map direct hydrocarbon indicators. Nowadays different attributes are routinely measured and displayed as part of a 3D-seismic interpretation (Brown, 1991). A variety of features can be extracted from a seismic signal. Examples are: minimum amplitude, maximum amplitude, loop area, zero-crossing positions, peak-to-peak amplitudes etc. Other types of seismic attributes can be obtained after signal transformations such as Fourier or Hilbert transformations. Examples of these attributes are: dominant frequency, instantaneous amplitude, instantaneous phase, instantaneous frequency etc.

The extraction of seismic attributes on modern seismic workstation is a routine task. Analysis of the results, aimed at establishing a relation between measured attributes and meaningful reservoir properties, is, however, not trivial and can be time-consuming. Many techniques have been tried by different workers. Examples are classical statistical methods,

such as regression analysis, discriminant analysis, cluster analysis etc. Sometimes the same attributes are measured on simulated data in a controlled experiment. For example, Neff (1992) uses synthetic seismic data to measure seismic amplitudes and isochrons (time-delay between two events). He then uses three-variable cross-plot analyses to determine the net-pay zone of a reservoir formation. The derived cross-plot information is then applied to the amplitudes and isochrons measured along an interpreted horizon of the factual data. This method has some similarity with the total space inversion method introduced in Section 2.4.3.

2.3.3 Acoustic impedance inversion

Acoustic impedance inversion aims at increasing the seismic band-width in order to increase the amount of detail that can be extracted from the data. The method is known by a number of different names, such as broadband constrained inversion, stratigraphic inversion, or geology-based inversion. Usually the resulting acoustic impedance profiles are considered to be an intermediate result. The acoustic impedance traces are related to lithologies and/or reservoir properties only in subsequent steps. An example of this is the method by Martinez et. al. (1992) which will be described here.

The method is a step-wise inversion scheme applied to a 2D-seismic survey. The method comprises three consecutive steps. In the first step the seismic section is transformed into an acoustic impedance section. An initial acoustic impedance model is first built, using the available well data and seismic structural and stratigraphic interpretations; the geological a priori constraints. This model is then parameterised in terms of event reflectivity and delay time. A synthetic seismic trace is generated from the model and compared with the field seismic trace. This yields a residual error which is used to update the model parameters. Constraints provided by the model and data variances are used to control the stability and resolution of the inversion process. In the case of Martinez et. al. (1992) the solution is based on a Bayesian approach to inversion (Duijndam, 1988). For the set of all possible impedance cross-sections an a priori (Gaussian) probability function is defined. This a priori probability function is described by the expectation, being the initial acoustic impedance model and the corresponding covariance operator. The optimal model is found by maximising the a posteriori probability function given the observation, i.e. the measured seismic data (the maximum-likelihood criterion). Several iterations may be required to converge to a final model due to the non-linear relationship between the parameters.

In the second inversion step well logs are inverted to estimate lithological parameters. In this particular case, sonic, density and gamma ray logs are inverted into sand and shale volume fractions and porosities.

The third and last inversion step in this scheme combines the broadband acoustic impedance model with the sand and shale volume fractions and porosities at the well locations. This last inversion step yields a final model for each of the lithologic parameters.

2.3.4 Stochastic simulations

Stochastic simulations have been used for some years for reservoir modelling (Dubrule 1989). Two main categories of stochastic reservoir modelling can be distinguished (Haldorsen and Damsleth, 1990):

- Object-based simulations; geological bodies are generated and distributed in space (e.g. Chessa, 1995).
- Pixel-based techniques; distributions of properties are obtained as a set of gridded values (e.g. Haas and Dubrule, 1994).

Only recently is seismic data being used as a constraint in the construction of stochastic simulations. For example Haas and Dubrule (1994) describe a method in which seismic impedance traces are simulated along vertical traces conditioned by well data information using a Gaussian sequential geostatistical algorithm. A simulated impedance trace is converted into a synthetic seismic trace and compared with the factual seismic trace. If the comparison is not considered satisfactory, another impedance trace is simulated. When the impedance trace is accepted, another location is selected by random draw and the procedure is repeated. Operating in this way for each location a number of impedance traces are generated. These impedance traces are subsequently analysed and used to derive petrophysical variables (porosity, permeability etc.) or lithologic parameters (sand, shale, bed-thickness etc.).

2.4 Towards a new technique

2.4.1 General

Sherrif (1992) defines reservoir geophysics as 'the use of geophysical methods to assist in delineating, describing, or monitoring a hydrocarbon reservoir'. In this definition geophysics can play an important role in every

step of the field's life cycle from appraisal and early development through to production and enhanced recovery (EOR) schemes. In fact, for economic reasons early and accurate characterisation of the reservoir warrants geophysical techniques to be employed early in the cycle for many cases. High resolution geophysical measurements such as 3D-seismic, VSP's and cross-hole tomography, closely integrated detailed geological and engineering data, are becoming increasingly important in the description and characterisation of the reservoir.

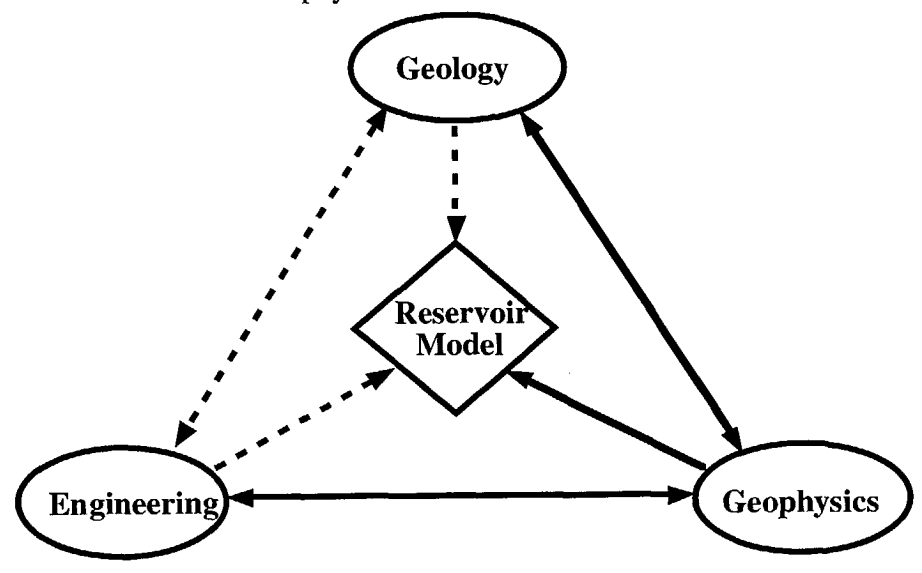
The economic optimisation process, called reservoir management, is the driving force behind the application of these reservoir characterisation techniques. Robertson (1989) defines reservoir management as 'maximising the economic value of a reservoir by optimising recovery of hydrocarbons while minimising capital investments and operating expenses'. Reservoir geophysics plays an important role in the definition of the reservoir model, a key parameter in reservoir management. The interaction between the three basic disciplines; geology, geophysics and engineering (pertrophysical as well as reservoir) is schematically shown in Fig. 2.2.

Three-dimensional seismic surveying is the geophysical tool that has had the greatest impact in reservoir management. Numerous case studies have been reported in geophysical literature on the applications of 3D-seismic data to reservoir management (e.g. Sherrif, 1992). Such applications include improvements in the definition of the geometric framework, predictions of rock and fluid properties and flow surveillance in EOR schemes.

Seismic reservoir characterisation is the objective of this thesis. As described in the previous section various techniques have been, and are being, employed to extract reservoir properties from seismic data. These techniques have a common requirement to integrate data from other sources. There are three reasons for this requirement:

- The seismic signals must be calibrated and transformed to meaningful reservoir properties.
- Additional non-seismic information is required to constrain the inherent non-unique seismic inversion solution.
- The seismic reservoir characterisation result delineates and describes only part of a reservoir model. This result must be consistent with results obtained from other sources such as production history matching results and high resolution sequence stratigraphic interpretations.

depositional environment, lithology, paleontology, correlation panels, iso-pach maps, depth sections, continuity of pay zones etc.



logs, core analyses, net-togross payzones, fluid samples, well tests, reservoir models, reservoir simulations, economics etc. 2D and 3D seismic, VSP's, cross-hole seismology, horizon maps, fault maps, continuity of zones, aquifer size etc.

Fig. 2.2 The role of reservoir geophysics (solid lines) in the definition of the reservoir model and the relationship between the three basic disciplines (solid + dashed lines); geology, geophysics and engineering (petrophysical as well as reservoir). Modified after Richardson and Sneider (1992).

Here, it is argued that the only way to obtain seismic reservoir characterisations that are consistent with other data inversion and interpretation results, is to use a common subsurface model for all data descriptions. It is further argued that this subsurface model must be based on geologic parameters (lithology, sequence stratigraphy, bed-thickness etc.) rather than physical parameters (density, wave-propagation velocity etc.). The argument is based on the fact that geological events have a one-to-many relation with physical parameters. In other words many physical

parameters can be attached to a single geological event such as a sandstone layer. In the following section, the different data types, scales and accuracies involved in seismic reservoir characterisation are discussed.

2.4.2 The scale problem

Information about a reservoir is, in general, obtained from different data sources with greatly varying relative scales and accuracies. The scale of the information ranges from the 100-1000 km, basin scale to the 10-100 μm , grain and pore scale. The complete description of a reservoir from an engineering perspective requires integration of all these data types and knowledge (Fig. 2.3).

At the basin scale, important parameters are the basin size, the subsidence rate and regional tectonic events. At the reservoir level the stress fields related to these parameters may have influenced the stratigraphy and the position and direction of faults and fractures. Techniques operating at this scale are 2D-seismic and gravity measurements. These techniques are, however, in general, primarily acquired for exploration purposes. Gravity data is usually acquired to determine the basin depth. Regional 2D-seismic lines are acquired to delineate (seismic-)stratigraphic units and tectonic events.

At the formation scale we are interested in describing the geometric framework and the overall reservoir stratigraphy (i.e. sand, shale, sandy shale etc.). The most important technique operating at this scale is the 3D-seismic method. The scales involved are in the 1-10 km's range laterally and in the 100-1000 m range vertically. Horizons, faults and unconformities are mapped at this scale. Seismic interpretation techniques include structural as well as seismo-stratigraphic mapping.

At the layer scale the internal architecture of the reservoir is described in terms of sediment bodies, such as channels, barrier bars, point bars etc. At this scale we wish to describe the dimensions, shapes, orientations and spatial disposition of these bodies. The size of the sediment bodies is in the 100-1000 m range laterally and in the 5-50 m range vertically. Subsurface information is obtained from the interpretation of well-log shapes and (under favourable conditions) from surface seismic data. Seismic lateral prediction techniques operate at this scale.

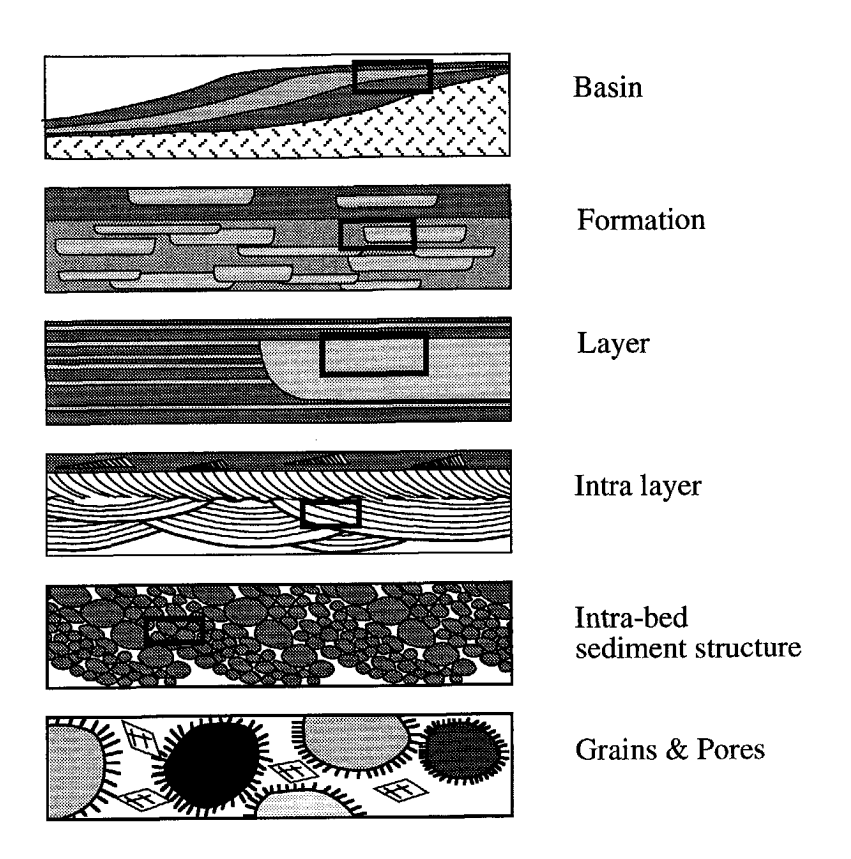


Fig. 2.3 Relevant geological scales for reservoir modelling. Ranges are typical ranges that can vary considerably for different geological settings. Modified after Weber (1986).

The intra-layer scale is in the meters range. It is the scale at which the internal heterogeneity of sediment bodies and their effect on fluid flow are described. It is typically the scale at which net-to-gross ratios in a reservoir are determined. The information is obtained primarily from well logs, such as the gamma-ray, neutron, resistivity, sonic and density logging tools. High resolution geophysical techniques, such as offset VSP's, cross-well seismology operate at this scale.

	Dimension X Y Z	Regional 2D- seismic	3D-seismic	Offset VSP's
Dimension X Y Z Resolution X Y Z Basin	- 100-1000 km by 100-1000 km by	10-100 km by 10-100 km by 1-5 km 1-10 km by 1-10 km by 1-10 km by 10-50 m	5-20 km by 5-20 km by 1-5 km 10-50 m by 10-50 m by 10-50 m	200-1000 m by 0 m by 1-2 km 10-25 m by 0 m by 10-25 m
	1-10 km	tectonics, stress fields, subsidence rates, seismo- stratigraphic events	-	
Pormation.	1-10 km by 1-10 km by 100-1000 m	geometric framework, faults, stratigraphic units, volumes, dimensions, shapes etc.	geometric framework, faults, stratigraphic units, volumes, dimensions, shapes etc.	fault position, seismic- well-tics, lateral continuity stratigraphic units, dips, prediction ahead of the bit etc.
Layer	100-1000 m by 100-1000 m by 5-50 m	fluid contacts, boundaries, lithology etc.	volumes, dimensions, shapes, orientations, small scale faults, fluid contacts, lithology etc.	lateral continuity, small scale faults, fluid contacts, boundaries etc.
Intra layer	1-10 m by 1-10 m by 1-10 m	-		
Intra-bed sediment	1-10 cm by 1-10 cm by 1-10 cm	<u> </u>	<u>-</u>	<u>-</u>
Grains & Pores	10-100 μm by 10-100 μm by 10-100 μm		14	

Dimensions at which the integration framework in this thesis operates.

Cross-well tomography /	Logs	Cores / Side Wall	Thin sections / SEM ¹	
seismology 100-250 m by 0 m by 100-250 m 1 m by 0 m by 1 m m by	0 m by 0 m by 2-3 km 0 m by 0 m by 1-30 cm depositional environment	5-20 cm by 5-20 cm by 10-100 m 0-1 cm by 0-1 cm by 0-1 cm	0-1 cm by 0-1 cm by 0-1 mm 10-100 μm by 10-100 μm by	Dimension X Y Z Resolution X Y Z Basin
	fault positions, formation tops, dips, etc.	<u>.</u>	<u> </u>	Formation
lateral continuity, small scale faults, fluid contacts,	depositional environment	_		Layer
boundaries, lateral continuity etc.	hydrocarbon saturations, net-to-gross payzones, fluid contacts, porosities, fracture identification, permeabilities etc.	depositional environment, characterisation of sedimentary bodies, fractures, porosities, permeabilities, saturations etc.	-	Intra laver
-	lithology, vertical heterogeneity, porosity, permeability etc.	lithology, vertical heterogeneity, porosity, permeability etc.		Intra-bed sediment structure
-	grain density, clay volume and typing, sandstone classification, porosity etc.	grain density, mineralogy, cementation, porosity, permeability etc.	grain and pore-size distribution, pore-wall roughness, packing arrangement, porosity type, mineralogy, cementation, diagenesis etc.	Grains & Pores

¹ Scanning Electron Microscope

Table 2.1 Tools and techniques in relation to the geological objects to be described. Ranges are typical ranges that can vary considerably for different geological settings.

The next scale of interest is that of the, intra-bed sedimentary structure. Subsurface information at this scale is available from cores and logs. The resolution is in the order of 10⁻² m for core descriptions and the highest resolution logs such as the televiewer. Information obtained at this scale typically describes reservoir properties such as saturations, permeabilities, porosities, lithologies, depositional environments and heterogeneities i.e. cross bedding, laminations and fractures. Logs and cores provide us with 1D-continuous profiles along the well track.

The smallest scale relevant to the geological reservoir model, is the scale at which grains and pores are studied. The subsurface information comes from cores, side wall samples and cuttings. Thin sections are studied using optical microscopes, or, Scanning Electron Microscopes (SEM). Pore and grain size distributions, mineralogy, cementation, diagenisis and other microscopic factors are determined. The scale of objects under a SEM are in the order of 10^{-5} m.

Well testing and sampling is another important source of information in the characterisation of a reservoir. Information on formation pressures, pressure gradients, fluid contacts, permeability estimates and water-cut estimates can be obtained from devices such as the Repeat Formation Tester (RFT). In addition physical fluid samples can be retrieved from the reservoir yielding information on the chemical composition and physical properties of the fluids.

In this review of scales and accuracies in reservoir characterisation dynamic aspects have, so far, been excluded. Dynamic aspects deal with changing reservoir properties over time intervals. Examples are pressure histories, coning effects and sweep efficiencies in Enhanced Oil Recovery (EOR) schemes. Seismic reservoir characterisation techniques have been employed to study dynamic effects (e.g. Greaves and Fulp, 1987). The method requires the 3D-seismic acquisition to be repeated at regular time intervals. This is called time-lapse 3D-seismic and may be used to monitor reservoirs under production.

Table 2.1 summarises the geological objects and the techniques used to characterise these. The dimensions and resolutions given in this table are typical values that may vary considerably.

2.4.3 The integration framework

In the previous section, the problem associated with integrating data from different sources with widely varying relative accuracies has been reviewed. This section will show how these data, relevant to seismic reservoir characterisation, can be combined (or integrated). First, the integration requirements are discussed followed by a description of the solution presented in this thesis: the integration framework.

To define the requirements for data integration from a seismic reservoir characterisation perspective it is useful to first realise what the seismic tool is actually measuring. În this thesis we are only considering post-stack seismic data, comprising P-waves, or compressional waves (Section 2.2). These data contain information about acoustic properties of the sub-surface. Acoustic properties comprise the bulk density of the medium and seismic wave-propagation velocity. Seismic reflections occur when the acoustic properties of the medium changes. The earth's reflectivity is related to geological changes, such as changes in lithology, fluid content, or stratigraphy. The measured seismic signal is the composite response of the earth's reflectivity to the seismic wavelet. The vertical resolution of the seismic tool ultimately determines the detail of information that can be extracted from the seismic signals. On vertical seismic sections the reflections occur in patterns corresponding roughly to geological structure and stratigraphy. The study of these patterns has triggered the discipline of seismic-stratigraphy which in turn has fuelled the development of the geological concept of sequence-stratigraphy (e.g. Vail et al., 1977, Wagoner et.al., 1990).

Successful data integration from a reservoir characterisation perspective has the following requirements:

- It must be possible to include information on lithology, fluid content and sequence-stratigraphy.
- It must be possible to enter acoustic properties.
- It must be possible to enter other properties.

The last requirement has been included because it is feasible that the seismic response may be related to other properties. This is possible even when the underlying rock physics are not known. Such examples include production rates, or permeabilities which might be related to the shale content, or fracturing and hence, the seismic response of a reservoir unit.

These requirements have led to the definition of a generic integration framework (Table 2.2).

In this generic framework the geology of the target zone is defined in terms of acoustic-stratigraphic entities. The entities are grouped at three hierarchical scale levels; units, sub-units and lithologies, respectively. The smallest scale level (the lithology level) typically corresponds to beds in the 1-10 m range with a similar lithological composition, e.g. sand, shale, silt etc. The intermediate scale level (the sub-unit level) typically corresponds to a stratigraphic para-sequence or depositional facies consisting of one or more, lithologies. The largest scale level (the units level) typically corresponds to a lower order stratigraphic sequence and consists of one, or more, sub-units. It is stressed that the scale levels are user-defined and should not be confused with, or constrained to, strict geological stratigraphic classifications. They are chosen such that the geological setting is represented in an optimal way. This is area and target dependent. It is very possible to define an integration framework based on a combination for litho-stratigraphy, sequence-stratigraphy and genetic units. The key issue to be addressed during definition of the integration framework, is how important geological entities must be specified. These entities can then used to describe factual and simulated wells. Individual codes for each entity ensure that all elements of the model can be uniquely identified.

unit	sub-unit	lithology	rocktype	code
A	I	a	reservoir	A.I.a
		b	seal	A.I.b
	II	a	reservoir	B.II.a
		С	waste	B.II.c
В	-	a	reservoir	B.I.a
	I	b	waste	B.I.b
		c	reservoir	B.I.c
С	III	d	reservoir	B.III.d

 Table 2.2
 Part of an integration framework, showing the hierarchy of scale levels.

The typical scale range that is covered by the integration framework is indicated in Table 2.1. A rocktype is assigned to each lithology in the framework, to accommodate the requirement for entering fluid contents. Three rocktypes are defined: seals, reservoirs and waste rocks. Seals are used to attach hydrocarbon columns. Reservoir rocks are defined as lithologies that can have a moveable fluid-fill. Waste rocks are considered non-economic but non-sealing. The requirement of integrating other

properties is fullfilled by allowing user-defined parameters to be attached to any framework entity. For example it is possible to attach a production rate either to the entire framework, or, to any defined entity in the framework, either unit, sub-unit or individual lithology.

Wells (factual and simulated) can now be described in terms of the integration framework. The following rules for this description apply:

- Units always occur in the sequence that they have been entered into the integration framework. They are, either, present, or, absent. They cannot repeat.
- Sub-units may occur in any order and multiple times within the unit they belong to. They may be missing. Sub-units occurring more than once get an occurrence number attached to the code, such that they can be identified uniquely. Sub-units can be ordered if necessary.
- Lithologies can occur in any order and multiple times within the sub-unit they belong to. They may be missing. Lithologies occurring more than once get an occurrence number attached to the code, such that they can be identified uniquely. Again, lithologies can be ordered or random as required.

Litho- Stratigraphy	Well description				Blocked	l logs	
	unit	sub-unit	lithology	rock type	code	★	•
	A	A I	a	reservoir	A.I.a		
			b	seal	A.I.b		
T I		II	a	reservoir	B.II.a.gas B.II.a	1	<u></u>
	B I	В	с	waste	B.II.c		- E
			a	reservoir	B.I.a	.	
		d	waste	B.I.b			
		е	waste	B.I.e(2)	₹	₹	
	С	III	a	reservoir	C.III.d	M	AW.
	ı	•				sonic	density

Fig. 2.4 Description of well information in terms of the integration framework. Acoustic information is parameterised at the top and bottom of the smallest scale framework entities (lithologies, or reservoir layers with similar fluid content).

When the stratigraphy of the well has been described, the acoustic properties can be entered. These are attached to the smallest scale entities: the lithology level, or, in case of reservoir layers, acoustic blocks with similar fluid contents. The acoustic properties: sonic logs (i.e. acoustic slowness) and density logs, are parameterised at top and bottom of each block (Fig. 2.4). The boundaries of the acoustic blocks must coincide with those of the most basic framework entities. User-defined physical properties, such as production rates, permeabilities etc., are also entered (or simulated).

When a number of factual wells have been described in this way, the physical properties can be analysed. Each property can be analysed at each scale level of the integration framework. For example it is possible to study the thickness variations associated with unit A, or sub-unit II of unit B, or all lithologies 'a' within sub-unit II of unit B. It is even possible to examine variations in physical properties associated with, say the fifth occurrence of lithology 'a' within the second occurrence of sub-unit II of unit B, should the need arise.

2.4.4 Total space inversion

In the previous section it has been shown that a generic integration framework can be created to describe the data required for seismic reservoir characterisation. Factual and simulated wells, described in terms of this framework, are commensurable. Consequently, it is thus feasible to combine both factual and simulated data. This is the basic precept behind the seismic reservoir characterisation technique described in this thesis.

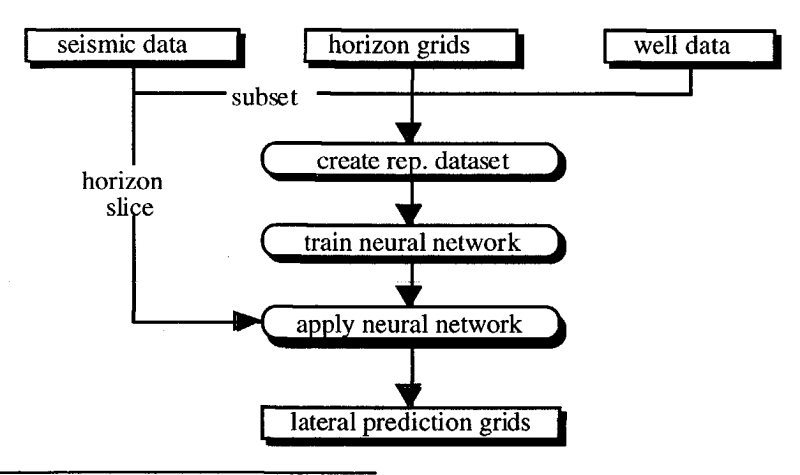


Fig. 2.5 Direct inversion flow diagram

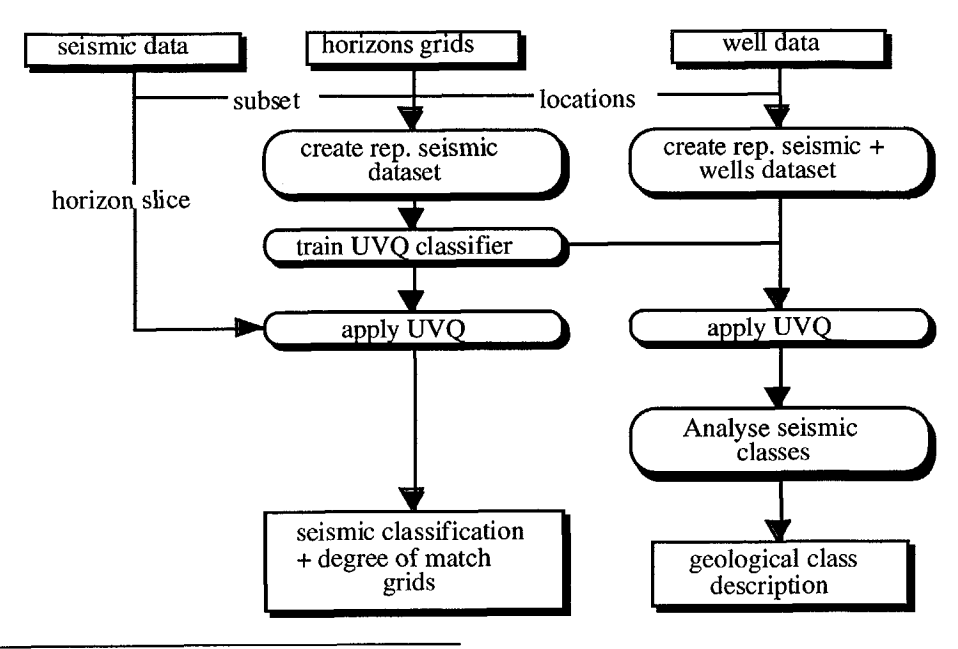


Fig. 2.6 Segmentation flow diagram

Datasets comprising well information and corresponding seismic responses are compiled from factual and/or simulated data (Fig. 1.2). The factual well data is combined with the surface seismic traces at the well locations. The seismic data for simulated wells come from synthetic seismograms. The objective is to arrive at a dataset that is representative of the target zone in the study area. This dataset can then be used in the reservoir characterisation process.

A software product utilising the total space inversion concept has been developed. This product, called GeoProbe has been used extensively in this thesis. In the GeoProbe system there are two options available for analysing the relationship between seismic response and salient well properties: direct inversion and segmentation (Fig. 2.5 and 2.6, respectively).

In direct inversion, artificial neural networks, i.e. Multi-Layer Perceptrons (MLP's) or Radial Basis Functions (RBF's) networks, are trained to recognise specific well properties from the seismic response. Optionally, the data are transformed prior to analysis, e.g. seismic attributes are calculated, or a reservoir property is calculated from acoustic properties. Application of the trained network to a seismic horizon slice, yields one lateral prediction output grid per network output node.

In segmentation the seismic response is clustered (or segmented). First, a subset of a seismic horizon slice is selected. As with direct inversion it is possible to combine the selected seismic responses with simulated responses. In general, however, this is not done. The selected seismic responses are presented to an Unsupervised Vector Quantiser (UVQ) network, which will train itself to cluster the data into a number of classes. Application of the trained UVQ to the entire horizon slice yields two output grids: a seismic classification grid and a degree of match grid. The latter grid shows how close the response is to the centroid of the winning class for each seismic trace. The seismic classification output grid can be used for subjective geological interpretation. To quantify the meaning of the different seismic classes, the UVQ can also be applied to a seismic dataset with known well information (factual and/or simulated). The clusters can then be analysed to yield a statistical description of the clusters in terms of the framework entities.

In the following section, the basic techniques (artificial neural networks and Monte Carlo statistics) as used in this thesis will be introduced.

INTRODUCING THE VARIOUS TECHNIQUES

3.1 Introduction

In the previous chapter it was shown that many techniques exist to extract reservoir properties from seismic data. These geophysical inversion methods have a common requirement to integrate data and knowledge from other sources and disciplines. It has been argued that the only way to obtain a seismic reservoir characterisation result, consistent with other data inversion and interpretation results, is to use a common subsurface model for all data descriptions. The requirements for such a subsurface model have now been defined. This has resulted in the definition of a generic, acoustic-stratigraphic integration framework. This allowed factual and simulated wells to be described in terms of this integration framework, which makes them commensurable. From this aspect came the total space inversion method. In this method factual and simulated wells with corresponding factual and synthetic seismic responses may be combined into a dataset, representative of the target interval. This dataset is used in the seismic reservoir characterisation process.

Many inversion algorithms can, in principle, be used for the total space inversion method, to establish relations between seismic response and salient reservoir properties. For instance classical statistical techniques such as regression analysis, discriminant analysis and cluster analysis may be employed. In this thesis, however, artificial neural networks have been chosen for the inversion step. The main reasons for this choice are the expected higher performance and user-friendliness of neural networks.

An algorithm is used for the simulation of wells, which combines geological reasoning with stochastic input. The algorithm makes use of an innovative Monte Carlo statistics procedure in which correlated multivariate stochastic variables are drawn one-by-one.

In this chapter, an introduction to artificial neural networks and Monte Carlo statistics is given.

3.2 Artificial Neural Networks

3.2.1 General

Artificial neural networks, or connectionist models as they are sometimes referred to, have been inspired by what is known as the 'brain metaphor'. This means that these models try to copy the capabilities of the human brain into computer hardware or software. The human brain has a number of properties that are desirable for artificial systems (e.g. Schmidt, 1994):

- It is robust and fault tolerant. Even if nerve cells in the brain die (which is known to happen every day), the performance of the brain does not deteriorate immediately.
- It is flexible. This means that the human brain can adjust itself to new situations and can learn by experience.
- It can deal with information that is inconsistent, or contaminated with noise.
- It can handle unforeseen situations by applying knowledge from other domains and extrapolating this to new circumstances.
- It can deal with large amounts of input data and quickly extract the relevant properties from that data.
- It is highly parallel, hence it has a high performance.

Neural network research started in the forties. McCulloch and Pitts (1943) described the logical function of a biological neuron. They described that the transmission of neural signals is an all-or-nothing situation. A neuron fires only, if the cell has been stimulated above a certain threshold. The output signal will, in general, have a constant strength. In their paper, McCulloch and Pitts, described that networks consisting of many neurons might be used to develop the universal Turing machine (a kind of computer described

by Turing (1937) that could, in principle, solve all mathematical problems). Research in neural networks was suddenly stopped following a publication by Minsky and Papert (1969). In this paper, it was shown that a relatively simple problem (the so-called XOR-problem) could not be solved by the linear algorithms used at the time. The major breakthrough which relaunched the interest in this technique has been the discovery in the eighties of a non-linear optimisation algorithm overcoming the previous limitations (Rumelhart et. al. 1986).

Neural networks have emerged in the last decade as a promising computing technique which enable computer systems to exhibit some of the desirable brain properties. Various types of networks have been applied successfully in a variety of scientific and technological fields. Examples are applications in industrial process modelling and control, ecological and biological modelling, sociological and economical sciences, as well as medicine (Kavli, 1992). Within the exploration and production world, neural network technology is now being applied to geologic log analysis (Doveton, 1994) and seismic attribute analysis (Schultz, 1994).

In this thesis neural networks are used for pattern recognition. Three approaches can be recognised in neural network pattern recognition (Lippmann, 1989): supervised training, unsupervised training and combined supervised-unsupervised training. Supervised training approaches require the existence of representative datasets. Unsupervised techniques find structure in the data themselves, thereby extracting the relevant properties. In this thesis Multi-Layer Perceptrons and Radial Basis Function networks are used in the supervised training approach. A vector quantiser is used for the unsupervised approach. In this thesis, the vector quantiser network is called UnSupervised Vector Quantiser. The networks used in this thesis are introduced in the following sections.

3.2.2 Multi-layer perceptrons (MLP)

The most general and most widely used neural network model is the 'multi-layer perceptron (MLP)'. The basic building block of this model is the perceptron (Fig. 3.1), a mathematical analogue of the biological neuron, first described by Rosenblatt (1962).

The mathematical expression of the biological neuron can be written as an activation function A applied to a weighting function W, defined as:

$$W(\mathbf{y}) = \sum_{i=0}^{L} w_i y_i, \qquad (3.1)$$

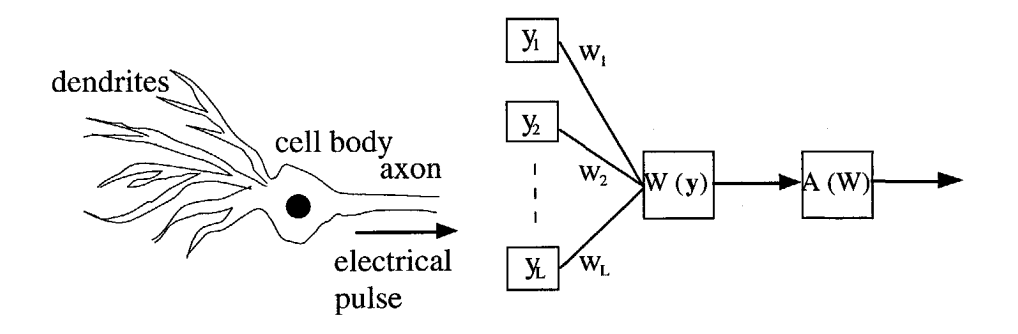


Fig. 3.1 A biological neuron and a Perceptron

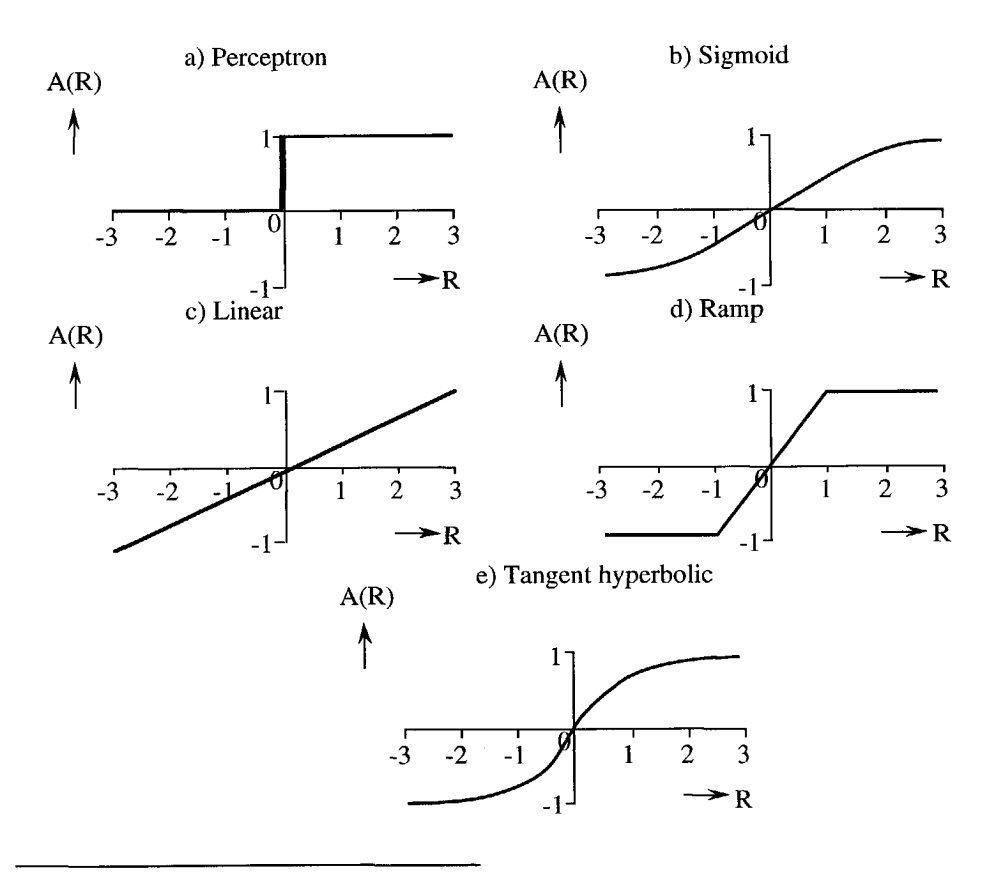


Fig. 3.2 Different activation functions for MLP networks. The Linear, Ramp, Sigmoid and Tangent hyperbolic functions have been used in this thesis (Chapter 5).

where:

y is the neural network input vector written as y_i with i = 1,...,L and weighting vector w_i with i = 1,...,L.

The activation function of the classical perceptron (Fig. 3.2a) can now be written in the following form:

$$A(W) = \begin{cases} 1 & W > 1 \\ 0 & W \le 0 \end{cases}$$
 (3.2)

In MLP's the binary activation function is often replaced by a continuous function. The most widely used activation function is the sigmoid function (Fig. 3.2b). This function has the following form:

$$A(W) = \frac{2}{1 + \exp(-W)} - 1. \tag{3.3}$$

Other activation functions used in this thesis are the linear, ramp and tangent hyperbolic functions. The linear function (Fig. 3.2c) is defined as:

$$A(W) = W. (3.4)$$

The ramp function (Fig. 3.2d) is given by:

$$A(W) = \begin{cases} -1 & W < -1 \\ W & -1 \le W \le 1. \\ 1 & W > 1 \end{cases}$$
 (3.5)

The tangent hyperbolic function (Fig. 3.2e) is written as:

$$A(W) = \frac{\exp(W) - \exp(-W)}{\exp(W) + \exp(-W)}.$$
 (3.6)

Two other activation functions are used in this thesis: the prime-sigmoid and prime-tangent hyperbolic. These functions have the same mathematical expressions as equations (3.3) and (3.6), respectively. The training

algorithm treats the two types of functions differently. For the sigmoid and tangent hyperbolic functions, the derivative is used to update the weighting vector (Rich and Knight, 1991). For the prime-sigmoid and prime-tangent hyperbolic functions an offset is added to the absolute value of the derivative. This is done exclusively to avoid saturation problems during learning, where saturation means that continued learning does not lead to improved network performance. This modified procedure is used to update the weighting vector.

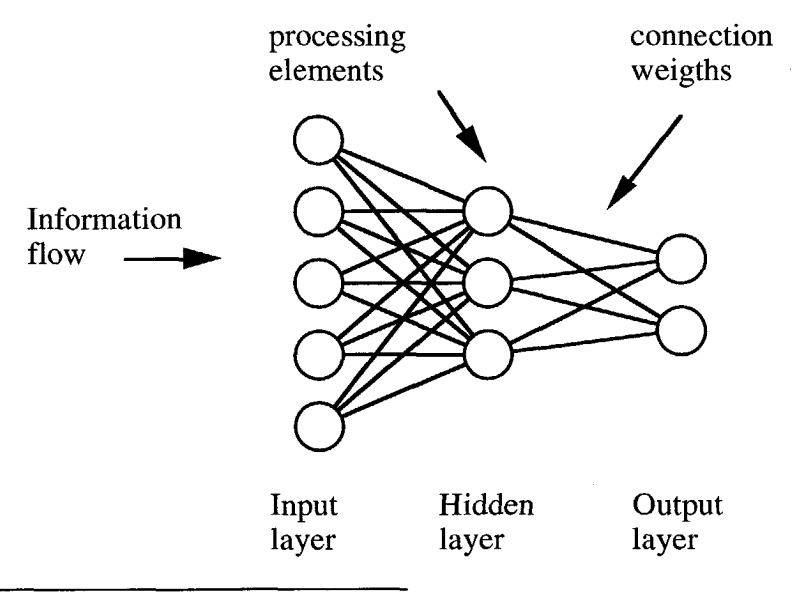


Fig. 3.3 Schematic representation of a feed-forward layered neural network, such as a Multi-Layer Perceptron and a Radial Basis Function network.

In a MLP the perceptrons are organised in layers (Fig. 3.3). In its simplest form, there are three layers; an input layer, a hidden layer and an output layer. There are no connections between neurons belonging to the same layer. The data flow between the layers is feed-forward. MLP's are trained on a representative dataset. This is a form of supervised learning. Known examples, consisting of input patterns and corresponding output patterns, are repeatedly offered to the network during the training phase. The 'back-propagation', learning, algorithm that is widely used to train this type of network attempts to minimise the error between the predicted network result and the known output by adjusting the weights of the connections. The algorithm was derived independently by a number of researchers. The modern form of back-propagation is often credited to Werbos (1974),

LeCun (1985), Parker (1985) and Rumelhart et. al. (1986). A fast variation of backpropagation is given by Fahlman (1988).

MLP's have two properties of interest: abstraction and generalisation. Abstraction is the ability to extract the relevant features from the input pattern and discard the irrelevant ones. Generalisation allows the network, once trained, to recognise input pattern which were not part of the training set.

3.2.3 Radial Basis Function Neural Networks (RBF)

Radial basis functions have been used for data modelling (curve fitting) by many researchers, e.g. Powell (1987) and Poggio and Girossi (1989). Recently these functions have been put in a neural network paradigm in what is called Radial Basis Function (RBF) Neural Networks (Broomhead and Lowe (1988), Moody and Darken (1988), Lee and Kil (1988), Platt (1991)). Schultz et.al. (1994) applied RBF networks in a seismic reservoir characterisation study.

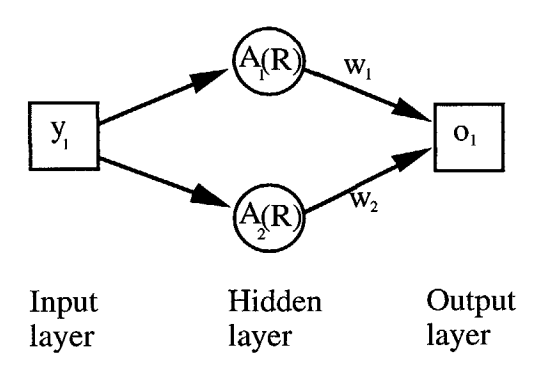


Fig. 3.4 Schematic representation of a Radial Basis Function network for the case of a single input variable, two basis functions and one output variable.

RBF networks have the same feed-forward layered architecture as MLP networks (Fig. 3.1), but the weighting function W and the activation function A are different. With RBF networks, there are only weights between output layer and hidden layer (Fig. 3.4). Each node in the hidden layer has a unique function, called the basis function. For the simple network of Fig. 3.4 with a single input, single output and two basis functions, the output is given by the sum of the two basis functions, each multiplied with its own weighting factor. In principle, any type of function

can be used to act as basis function. For example, spline functions are used (Kavli, 1992), but the identification RBF network, applies only if radial basis functions are used.

Radial basis functions give local support to data points. The output of the hidden nodes, peaks when the input is near the centroid of the node, and then falls of symmetrically as the Euclidean distance between input and the centroid of a node increases (Fig. 3.5). The consequence of this behaviour is that RBF networks are good for data interpolation, but not good for data extrapolation.

Several different radial basis functions are in use, with the Gaussian function (Fig. 3.5a), being the most widely used. If the radial basis centre R is defined as:

$$R = \sqrt{\sum_{i=1}^{L} \frac{\left(y_i - \mu_i\right)^2}{\sigma_i^2}},$$
(3.7)

where:

 μ_i represents the centre location of each basis and σ_i indicates a scaling of the width of each basis, then the Gaussian activation function is given by:

$$A(R) = \exp\left(-\frac{R^2}{2}\right). \tag{3.8}$$

Multiplication of the activation function A(R) with a weighting factor w then yields the output o (Fig. 3.4).

Another widely used RBF function is the so-called Inverse Multi-Quadratic Equation (IMQE, Fig. 3.4b), defined as:

$$A(R) = \frac{1}{\sqrt{R + k^2}},\tag{3.9}$$

where:

k is an empirically determined smoothing factor. In this thesis a value of 0.5 has been used for k.

Note, that the widths in RBF functions are specified independently from each input dimension, making the functions elliptic rather than spherical. Note as well, that unlike the activation functions for MLP's no bias is included in the RBF functions.

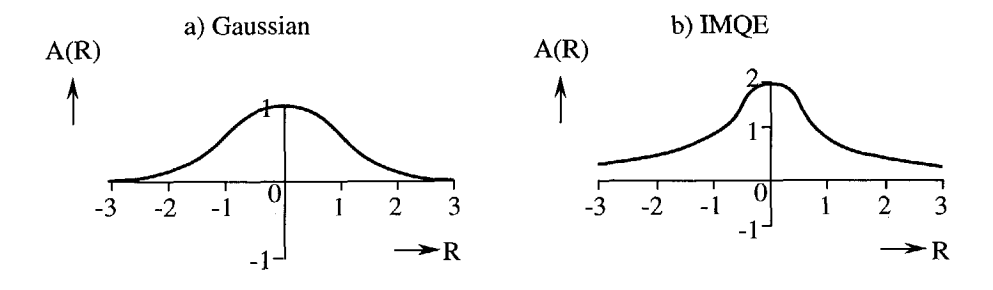


Fig. 3.5 Activation functions used in this thesis for RBF networks. The Gaussian function has a μ of 0 and a σ of 1. The IMOE function has a μ of 0, a σ of 1 and a k of 0.5.

Centre locations are typically determined by randomly selecting training examples from a large set of training data. The smoothing parameters and the number of nodes are typically adjusted empirically during training. RBF neural networks and MLP's have been compared by many workers. Kavli (1992) reported consistently better performance of RBF networks in five independent experiments. Another important aspect when comparing RBF networks and MLP's is the training speed. RBF networks can be trained within a fraction of the time that is required for training MLP's. RBF networks, however, generally require more nodes to obtain similar performances.

The training algorithm used in this thesis for RBF's is the so-called HSOL algorithm (Lee and Kill, 1989, Carlin, 1992). HSOL uses standard back propagation for updating the function parameters, but this learning algorithm also dynamically allocates new nodes in the hidden layer during training.

3.2.4 Unsupervised Vector Quantiser (UVQ)

In the preceding sections Multi-Layer Perceptrons and Radial Basis Functions networks were introduced. Both types belong to the category of supervised learning approaches. Datasets with known input and target vectors are used to train and test these networks. In this section a type of network is introduced that belongs to the category of unsupervised, or

competitive learning: the Unsupervised Vector Quantiser (UVQ). The general aim of competitive learning is to find structure in the data themselves and thereby extracting the relevant properties or features. In the case of the UVQ the aim is to segment (cluster, classify) the data. Similar input vectors must be classified in the same category. The classes are found by the network itself from the correlations of the input data. Therefore, these networks are sometimes referred to as self-organising networks.

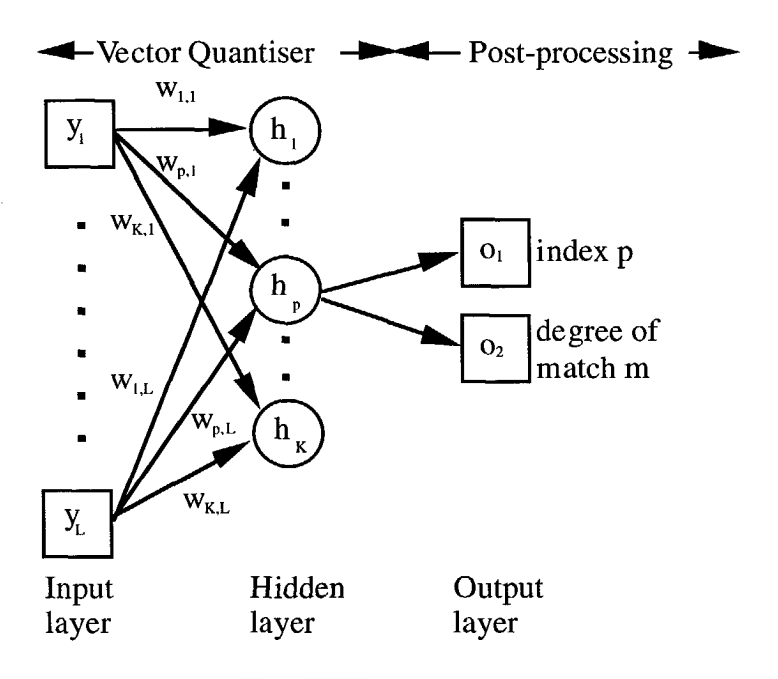


Fig. 3.6 Schematic representation of the Unsupervised Vector Quantiser, as implemented in this thesis. The network consists of a vector quantiser part and a post-processing part. Two outputs are generated: the index of the winning hidden node (i.e. the class) and a degree of match, which indicates how close the input vector is located near the centre of the class.

The UVQ in this thesis is a modified version of a Learning Vector Quantiser (LVQ). Vector quantisation is an important application of competitive learning for data encoding and compression (Hertz et. al., 1991, and Haykin 1994). In vector quantisation an input vector is replaced by the index of the winning output unit. Vector quantisation requires a set of classes, or codebook to exist. Normally, a set of prototype vectors is used.

The class is found by calculating the Euclidean distance to the prototype vectors. The nearest prototype vector is the winner. LVQ's are a supervised version of vector quantisation. In this case the prototype vectors are updated closer to the input, following a successful classification and further away from it when the classification is unsuccessful.

The unsupervised vector quantiser (UVQ) is quite similar to the LVQ. The prototype vectors are in the unsupervised case initialised as random vectors. The vector closest to the input vector is updated in the direction of the input vector.

The UVQ, implemented in this thesis, consists of a two-layer vector quantiser followed by a post-processing output-layer (Fig. 3.6). In the vector quantiser part of the network, a single layer of hidden nodes h_i with i = 1, ..., K, where K indicates the number of classes, is fully connected with a set of input nodes y_j with j = 1, ..., L via excitatory connections $w_{i,j}$. For each hidden node the net output is computed as:

$$h_i(\mathbf{y}) = \sum_{j=1}^{L} w_{i,j} y_j \quad i = 1, ..., K.$$
 (3.10)

In the learning phase the net outputs of all hidden nodes (classes) are compared in the post-processing layer. The hidden node with the smallest net output is designated the winner. The weighting vector $\boldsymbol{w}_{p,j}$ associated with the winning node p is then updated according to:

$$w_{i,j}' = \begin{cases} w_{i,j} & i = 1, ..., p-1, p+1, k \quad j = 1, ..., L \\ w_{p,j} + \eta (y_j - w_{p,j}) & j = 1, ..., L, \end{cases}$$

(3.11)

where:

 η is a empirically determined learning rate parameter and $w_{i,j}$ is the updated weighting matrix. This update rule is known as the standard

competitive learning rule. Updating is continued until no noticeable changes in the prototype vectors are observed.

In the application phase, the output layer consists of two nodes: one giving the index number of the winning node, and one giving a degree of match between the input vector and the prototype vector of this node. The degree of match m is computed as:

$$m = \left(1 - \frac{d}{r\sqrt{L}}\right),\tag{3.12}$$

where:

d is the Euclidean distance given by:

$$d = \sqrt{\sum_{j=1}^{L} (y_j - w_{p,j})^2},$$
 (3.13)

and r is the variation range for the training data.

In this thesis, the input variables are rescaled so that they all fall in the range from -0.8 to 0.8 (therefore, r=1.6). The degree of match m can thus vary from 0 (minimum match) to 1 (perfect match).

The implication of rescaling is that all input variables will contribute equally to the classification result. In our application seismic signals are classified by feeding the UVQ network amplitudes at discrete sample positions. The samples are selected relative to a reference horizon (Section 7.3). The rescaling procedure equalises the dynamic range at each sample position. It must be realised that some situations may exist where this approach does not yield an optimum result. For example, if, for the signals to be classified, a maximum amplitude and a zero-crossing always occur at the same sample positions, than the amplitude variations around the zero-crossing are relatively amplified.

This concludes the discussion on neural networks and their use in seismic inversion. In the following section, Monte Carlo statistics and there use in forward modelling are introduced.

3.3 Monte Carlo Statistics

Monte Carlo statistics is a procedure which involves sampling based on probabilities to approximate the solution of mathematical or physical problems. Monte Carlo statistics are used for a variety of different problems and have a long history of application (e.g. Tarantola, 1987). In geoscientific applications, the method is used e.g. for reserves estimations, prospect evaluations and modelling litho-stratigraphic sequences (e.g. Sinvhal and Sinvhal, 1992). In this thesis, Monte Carlo statistics are used to simulate wells, i.e. 1D-stratigraphic profiles with attached physical properties. The simulated sonic and density log responses of these wells are used to compute acoustic impedance and reflectivity logs, which in turn are converted to synthetic seismic traces by wavelet convolution and resampling processes. The simulated wells can be combined with factual wells in order to arrive at a representative dataset for the target level of the study area (Section 1.2).

Variables are simulated in a computer using a (pseudo-) random number generator. When random variables are correlated, however, it is not simple to simulate random draws using a (pseudo-) random number generator. The conventional way to solve this problem is to transform the dependent system to a system where stochastic variables can be drawn independently. Back transformation than yields the correlated stochastic vectors. In case of normally distributed random variables, it is possible to draw the variables consecutively from the marginal distributions. Each time a variable is drawn, its marginal distribution must first be updated for the already drawn variable to with it is correlated.

There are two main advantages in drawing stochastic variables instead of stochastic vectors:

- the random draw can be controlled by geological reasoning
- the drawn value can be evaluated against hard constraints.

The statistical description of the simulation algorithm is given in Appendix I. A theorem is presented for the drawing of a variable which is correlated to an already drawn other variable, e.g. drawing a sonic value for a particular lithology with a given density value. This theorem requires a full correlation matrix, which is, in general, not supplied by the user. Therefore, a second theorem gives the way to fill missing elements of the correlation matrix. An example is given to illustrate how the correlation matrix is filled and a set of values for correlated variables drawn.

In the simulation algorithm wells are constructed from integration framework entities. The selection of framework entities is a stochastic process, controlled by the user with a set of geology-related rules. These rules, determine for example that a particular sub-unit must be filled with lithologies in a random, or sequential order. The wells are constructed one-by-one. Each well is constructed from top to bottom following the scheme of the framework. For each of the selected framework entities, thicknesses and properties (acoustic, user-defined) are simulated, one-by-one, by random draws. The simulated properties are attached to the selected framework entities in the same way as factual wells have been described in the system.

A hypothetical simulation based on the framework of Table 3.1 will be used as an example to illustrate the simulation procedure.

unit	sub-unit	lithology	rocktype	code
top	marine	shale-a	seal	top.mar.shl
	deltaic	sand-a	reservoir	bas.del.snd
		shale-b	waste	bas.del.shl
base		sand-b	reservoir	bas.flu.snd
	fluvial	silt-a	waste	bas.flu.slt
		shale-c	waste	bas.flu.shl

 Table 3.1
 Hypothetical integration framework.

The following input has been specified to control the simulation:

- Probability density functions describing the thickness variations of the individual framework entities (top, marine, shale-a, base, deltaic, sanda, shale-b, fluvial, sand-b, silt-a and shale-a).
- A probability density function describing the thickness variation of the gross gas-column. The gas-column is attached to a sealing shale-a.
- Probability density functions describing the variations in acoustic properties (sonic and density at top and bottom) of the acoustic blocks (shale-a, water-filled sand-a, gas-filled sand-a, shale-b, water-filled sand-b, gas-filled sand-b, silt-a and shale-c).
- An xor rule with a 60/40 ratio, attached to the base unit. This implies that a simulated well can have, either, a deltaic sub-unit, or, a fluvial

sub-unit. Sixty percent of all simulated wells will have a deltaic sub-unit and forty percent a fluvial sub-unit.

- Iterate random rules attached to the deltaic and fluvial sub-unit. This implies that first a thickness will be simulated for the sub-unit. Then a lithology for that sub-unit is selected at random and a thickness for the selected lithology is simulated. This process is repeated until the sub-unit is completely filled.
- A generation constraint of 20 percent attached to the shale-b lithology. This implies that the shale-b lithology has a reduced chance of being selected as compared to the sand-a lithology during the filling up process described above. The result is that sand-rich deltaic sub-unit are simulated.
- Correlation coefficients for pairs of sonic and density variables.
- A hard constraint set to the maximum gross gas-column.

Given these input constraints and rules wells can be simulated thus:

- Unit defined as Top is selected and a thickness is simulated.
- The marine sub-unit is selected; the thickness is set to the thickness of unit Top.
- Shale-a is selected; the thickness is set to the thickness of the marine sub-unit.
- The acoustic properties for shale-a are drawn at random.
- A gross gas-column is drawn at random. The value is evaluated against the hard constraint and is drawn again if necessary.
- Unit defined as Base is selected and a thickness is simulated.
- Either, the deltaic sub-unit, or, the fluvial sub-unit, is selected. Let us assume the deltaic sub-unit is selected (it has a higher chance of being selected). The thickness of the deltaic sub-unit is set to the thickness of unit Base.
- Either, sand-a, or, shale-b, is selected. A thickness is simulated by random draw for the selected lithology.

- The acoustic properties for the selected lithology are simulated by random draw. If the lithology is sand-a, it is evaluated whether the sand falls within the gross gas-column. If so, the acoustic properties are drawn from the gas-filled acoustic probability density functions. If sand-a falls partly within the gross gas-column, acoustic properties are simulated for both the gas-filled and the water-filled part.
- The last two steps are repeated until the cumulative thickness of the simulated lithologies exceeds the thickness of the deltaic sub-unit. The thickness of the last lithology simulated is clipped accordingly.

The procedure is repeated for as many wells as the user desires. The algorithm is capable of simulating user-defined properties. Each time a framework entity is selected, it is evaluated whether, or not, a user-defined property has been defined in the integration framework. If so, it is simulated by random draw.

This concludes the discussion on the statistical framework used in this thesis. In the next chapter, the simulation algorithm and the different geology-related rules that have been implemented in the GeoProbe system are described.

SIMULATING WELLS

4.1 Introduction

In the previous chapter the techniques used in the total space inversion method have been introduced. It was stated that, in principle, many types of inversion algorithms can be used to establish relations between seismic response and salient reservoir properties. In this thesis artificial neural networks have been chosen for the inversion step, because of the expected good performance and user-friendliness. Three types of neural networks have been introduced: Multi-Layer-Perceptrons, Radial Basis Functions and Unsupervised Vector Quantisers.

For the simulation of wells, i.e. 1D-stratigraphic profiles with attached physical properties, an algorithm, based on Monte Carlo statistics, has been introduced. The algorithm simulates correlated stochastic variables one-by-one. Therefore, at any time, it can be evaluated whether a variable must be simulated, and which constraints should be satisfied. The mathematics is explained in Appendix I. In this chapter the simulation algorithm will be described in more detail. The capabilities of the algorithm are demonstrated by describing an existing oil field with a fluvio-deltaic, labyrinth-type reservoir.

4.2 Simulation algorithm

The aim of the simulation is to generate a set of 1D-stratigraphic profiles with attached physical properties. These simulated wells with their corresponding synthetic seismograms can be combined with factual wells which in turn have been combined with factual seismic traces (Section 1.2).

Operating in this way a representative dataset is generated which can be analysed for relations between seismic response and underlying well properties.

Input to the simulation algorithm is a combination of stochastic information and geological knowledge. It is considered important that simulated models are realistic representations of the subsurface. This implies that the simulation must be controlled by geological reasoning and that unrealistic stochastic realisations can be redrawn. The algorithm has some similarities with Markov chain models (see e.g. Sinhval and Sinhval, 1992). In Markov chains, stratigraphic sequences are simulated using probabilities that a series of lithologies follow each other in a predictable pattern. In our simulation algorithm the predictable patterns are captured in terms of geology-related rules and constraints attached to the entities of the defined integration framework (Section 2.4.3). The rules will be explained hereafter.

Two types of constraints are used by the algorithm: simulation constraints and hard constraints. Simulation constraints are a special kind of geology-related rules. They determine the probability of a framework entity to be used in the construction of a well. Hard constraints are constraints set on the upper and lower boundary of probability density functions (pdfs). Stochastic realisations are evaluated against these boundaries. If the hard constraints are not satisfied, the value can either, be drawn again, or, the boundary value is accepted.

To deal with the uncertainty, stochastic input is supplied in the form of pdfs and correlation coefficients. Pdfs and correlation coefficients are in practice determined from factual well data. For this purpose the GeoProbe system offers a well data analysis module. The information derived from factual data may be modified in the simulation to reflect geological probabilities of area's not penetrated by the drill-bit.

The simulation algorithm requires the following input to be specified:

- Pdfs for each of the physical properties: thickness of geological entity, sonic and density at the top of each lithology.
- Hard constraints on the upper and lower boundary of the pdfs.
- Correlation coefficients between pairs of stochastic variables.
- Geology-related rules. The following rules have been implemented in the GeoProbe system: xor, sum, iterate, relative. The last three rules have two versions: one in which the smaller scale entities are selected in

a random order and one in which they are selected in the order in which they have been defined in the framework.

These rules are best explained with an example. We will describe the simulation of the deltaic sub-unit of the hypothetical framework of Table 3.1. For convenience, this table is repeated here (Table 4.1).

Attaching the xor rule to the deltaic sub-unit means that sand-a and shale-b are mutually exclusive. The thickness of the deltaic sub-unit is simulated from the defined pdf, the thickness of the selected lithology is made equal to the simulated deltaic sub-unit thickness. The xor rule supports an optional parameter to indicate the probability for a smaller scale entity to be selected. For example xor 40/60 denotes that sand-a has a 40% chance to be selected against a 60% chance for shale-b.

Attaching the sum rule to the deltaic sub-unit means that the subunit is constructed from one sand-a and one shale-b lithology. The thickness of the deltaic sub-unit is the sum of the simulated thicknesses of sand-a and shale-b.

Attaching the iterate rule to the deltaic sub-unit means that the sub-unit is constructed from as many sand-a and shale-b lithologies as are required to fill the simulated sub-unit thickness. First a thickness for the sub-unit is simulated from the defined pdf. Subsequently, lithologies sand-a and shale-b are selected and thicknesses for these are simulated from their respective pdfs. This process is continued until the sum of the lithology thicknesses exceeds the simulated sub-unit thickness. The thickness of the last selected lithology is adjusted accordingly.

Attaching the relative rule to the deltaic sub-unit means that the sub-unit contains one sand-a and one shale-b lithology while the thickness-ratio is maintained in the final realisation. The thicknesses of the simulated lithologies are adjusted (stretched or squeezed) to fit the simulated thickness of the deltaic sub-unit. In other words, the relative thickness (or thickness-ratio) is kept constant.

• Simulation constraints. The following rules have been implemented in the GeoProbe system: presence, generation, occurrence.

These constraints are used in combination with the geology-related rules explained above. To illustrate these constraints we will again describe the simulation of the deltaic sub-unit of the hypothetical framework (Table 4.1).

The presence constraint operates on the full simulation dataset. It denotes that the entity can be present in a percentage of the simulated wells only. A 60% presence attached to the deltaic sub-unit means that only 60% of the simulated wells comprise the deltaic sub-unit.

The generation constraint indicates the probability of an entity to be selected. An 80% generation attached to sand-a and a 20% generation attached to shale-b, in combination with the iterate rule attached to the deltaic sub-unit indicates that the sub-unit will be sand-prone.

The occurrence constraint operates on a well-by-well basis. It denotes the number of occurrences of the entity per well. An occurrence of 2 attached to sand-a, in combination with the iterate rule attached to the deltaic sub-unit indicates that only 2 sand-a lithologies can be selected to fill the sub-unit.

Additional input can optionally be specified in the form of:

- Pdfs for sonic and density at the bottom of each lithology in order to simulate linear trends as a function of depth over an interval.
- Pdfs for gross hydrocarbon column lengths.
- Pdfs for hydrocarbon filled sonic and density variables at the top of each reservoir lithology.
- Pdfs for hydrocarbon filled sonic and density variables at the bottom of each reservoir lithology.
- Pdfs for user-defined variables.

Combination of rules, constraints and correlations are used to control the simulation. Various stratigraphic settings can be simulated in this way. Examples of what can be done with these input specifications are presented hereafter.

unit	sub-unit	lithology	rocktype	code
top	marine	shale-a	seal	top.mar.shl
	deltaic	sand-a	reservoir	bas.del.snd
		shale-b	waste	bas.del.shl
base		sand-b	reservoir	bas.flu.snd
	fluvial	silt-a	waste	bas.flu.slt
	_	shale-c	waste	bas.flu.shl

 Table 4.1
 Hypothetical integration framework.

Correlations are used for variables which are dependent. For example, sonic and density variables are often correlated negatively. Also bed-thicknesses may be correlated to reflect a thickening sequence. User-defined physical properties, such as production rates or permeabilities may be correlated with acoustic properties, such as the density of a reservoir sand.

Simulation constraints determine whether a framework entity can be selected. The presence constraint dictates how many wells, out of the total number of simulations, will feature a specified entity. It can be used for example to control erosional effects. The generation constraint determines the frequency of framework entities per well. The constraint is evaluated before a framework entity is selected and is used in combination with the geological iteration rule. Generation is used to control the composition of an entity that is being filled up. The occurrence constraint dictates how often an entity can occur per simulated well. Occurrence is typically used for entities that defy normal stratigraphic behaviour. It could be used e.g. to simulate a volcanoclastic layer cutting through a sedimentary sequence.

Hard constraints are evaluated after a variable is drawn from its marginal distributions. If the simulated value does not satisfy the hard constraints, it is either drawn again, or the boundary cut-off value is accepted. Hard constraints are used to eliminate non-realistic values. For example, when simulating gross hydrocarbon columns, a hard constraint can be set to the maximum column length in order to avoid simulating unrealistically large columns.

Geology-related rules are attached to units and to sub-units. The rules dictate how thicknesses of larger scale entities are determined and how these are filled with smaller scale entities. The xor rule can be used in situations where large lateral changes in a geological entity occur. For example to simulate a shaling-out sand package. The sum rule is typically used in area's with laterally extensive units, such as in carbonate platform environments. Iteration is used e.g. to simulate cyclicity as observed in deltaic settings. If

the iteration rule is applied in combination with the generation constraint, it is possible to control the composition of the entity. The relative rule is used, for example, to simulate pinch outs.

In general, the input information for the simulation algorithm will be derived from factual well data. The available factual wells will be analysed to obtain information on thickness, presence, occurrence, acoustic properties etc. For this purpose, a well data analysis module has been implemented in the GeoProbe system. Additional information on sediment architecture and transition probabilities can always be obtained from literature (e.g. Mijnssen et.al., 1993).

This concludes the discussion on the simulation algorithm. In the next section a simulation example is described.

4.3 Simulation example

The simulation algorithm is applied to simulate wells in the oil field that will be described as the labyrinth case study in Chapter 6. The reservoir is an Upper Carboniferous to Lower Permian fluvial / fan assemblage sitting unconformably on Silurian marine shales. The reservoir formation is in turn conformably covered by Upper Permian carbonates. The field can be considered a labyrinth of interconnecting and isolated reservoir bodies. Oil production rate is primarily a function of reservoir development. Considerable volumes of oil can be produced from relatively thin (3-8 m) sandstone intervals. The reservoir formation deposits are predominantly floodplain and playa lake deposits with reduced sand / shale ratios. Between the wells, there are no laterally correlatable horizons within the reservoir formation, but the top reservoir can be mapped on seismic data. Fig. 4.1 is a hypothetical cross-section through the crest of the structure. The geological setting is described in detail in Chapter 6.

An integration framework was established for the field, based on the major structural elements and sedimentology (Section 6.3.3, Table 6.6). Integration sub-unit subdivisions and lithology typing were derived from analysis of well data and formation analysis logs of the real field. Based on the factual well data and the geological setting it was decided to feed the simulation algorithm with the following information:

• The random iterate rule for Carbonate D unit, Reservoir unit and each of the sub-units.

- The sum sequential rule for Carbonate C, Seal and Bottom units.
- Pdfs for thicknesses of all framework entities, for gross oil column thickness, for sonic and density of each lithology, for sonic and density of oil-filled reservoir lithologies.
- Correlations for sonic and density, for sonic of oil-filled and sonic of brine-filled reservoir lithologies to reflect that porefill is independent of rock properties, for the sonic of the Type 3 sand with the sonic of all other reservoir lithologies to reflect reservoir compaction and diagenesis.
- A hard constraint for the minimum and maximum oil column length and minimum and maximum thickness of the Reservoir unit. Values were redrawn until these constraints were met.
- Generation constraints for the reservoir lithologies to control the sand/silt ratios of the various sub-unit entities.

The complete simulation specification are given in Appendix II.

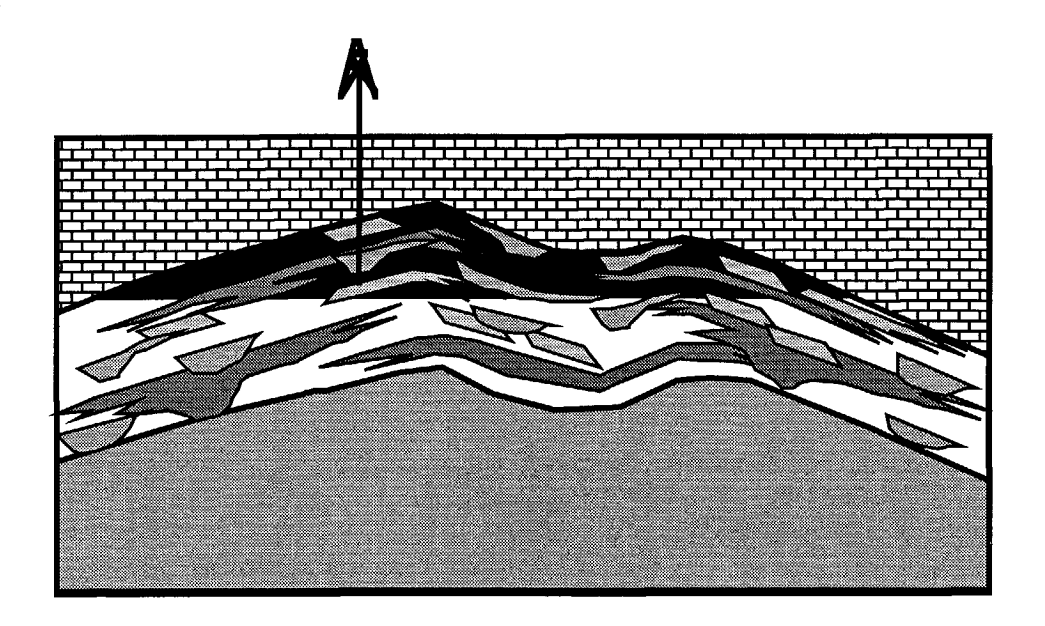
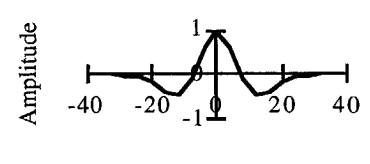


Fig. 4.1 Hypothetical cross-section through the oil field.





Time (ms)

Fig. 4.2 30 Hz Ricker wavelet used to generate synthetic seismograms.

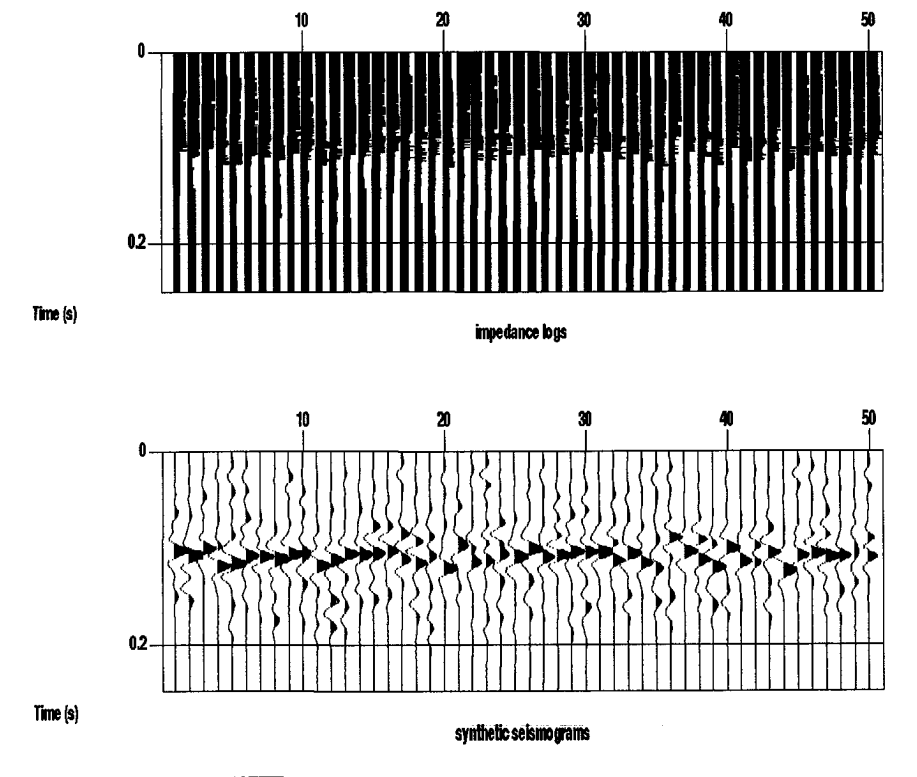


Fig. 4.3 Acoustic impedance logs for the simulated wells with corresponding synthetic seismograms. The top reservoir coincides with the large impedance break on the logs at around 100 ms.

The simulation algorithm was used to simulate 50 wells. The acoustic properties of these wells were used to create reflectivity logs. These were converted into synthetic seismograms by depth-time conversion, anti-alias filtering to 2 ms and convolution with a 30 Hz Ricker wavelet (fig. 4.2). The acoustic logs with corresponding synthetic seismograms are shown in Fig. 4.3. It must be realised that for each of the simulated wells, the complete stratigraphic sequence, described in terms of the integration framework, is also available.

In this chapter the well simulation algorithm, used in this thesis, has been described in detail. In the following chapter the algorithm is used to simulate wells in different geological settings. The simulated wells with corresponding synthetic seismograms are then used to test the performance of different neural network paradigms and architectures.

EXPERIMENTS WITH SIMULATED DATA

5.1 Introduction

The previous chapter described the algorithm used to simulate realistic 1D-stratigraphic profiles with attached physical properties. The simulated acoustic properties of these wells can be used to generate synthetic seismograms. Datasets generated in this way can be used in feasibility studies aimed at establishing relations between seismic response and underlying well properties. Based on simulated data only, it can be determined how far the seismic data can be pushed in the inversion process. It is important to know which inversion technique gives the best performance. As stated in Section 3.1, many techniques can, in principle, be used in the inversion phase. In the GeoProbe system, artificial neural networks have been chosen to carry out the inversion. The paradigm (MLP or RBF), the architecture (number of layers, number of nodes) and the type of activation functions (sigmoid, ramp, tangent hyperbolic etc.) are important factors influencing the network performance.

In this chapter a number of experiments with simulated data are described. In the first set of experiments, the network design, i.e. number nodes in the input and hidden layer and the type of activation function, is varied. After each variation, the network performance on the test data set is measured. In the second set of experiments, the network is fixed, but the geological model is made more complex by introducing new variables that affect the seismic response. In the third set of experiments the seismic bandwidth is varied. In the final experiment it is demonstrated how network performance can be increased by feeding the network additional (non-seismic) information.

In the following section (5.2), the initial model is described. The experiments are presented in Section 5.3. This is followed by a discussion of the results in Section 5.4. Conclusions are given in Section 5.5.

5.2 Initial model

The starting model is a gas field, consisting of a sealing shale with constant acoustic properties overlying a carbonate reservoir (Fig. 5.1). The acoustic properties of this reservoir vary due to changing porosities and fluid content. The framework of this model is given in Table 5.1.

The simulation specifications for this model are given in Table 5.2. The simulation algorithm was used to generate 200 wells. The acoustic properties of the simulated wells were used to create reflectivity logs. These were converted into synthetic seismograms by depth-time conversion, antialias filtering to 4 ms and convolution with a 30 Hz Ricker wavelet (Fig. 4.2). Sample impedance logs and corresponding synthetic seismic traces are shown in Fig. 5.2.

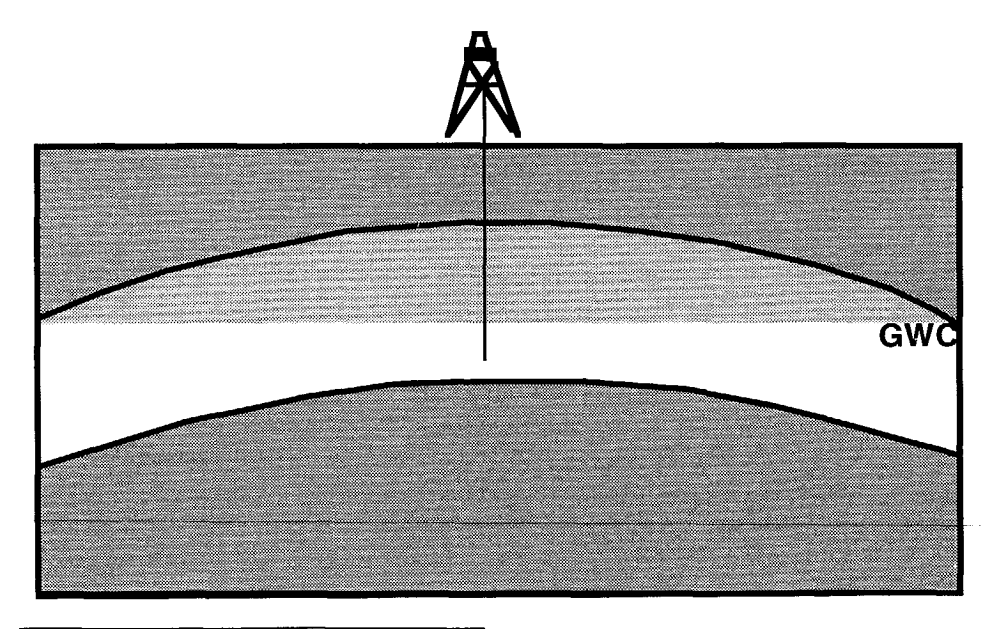


Fig. 5.1 Cross-section through the simulated field

Unit	Sub-unit	Lithology	Type	Code
Тор	Marine	Shale	Seal	top.mar.shl
Bottom	Marine	Carbonate	Reservoir	bot.mar.car

Table 5.1 The integration framework for the initial model

Code	Thickness (m)	Sonic (us/m) *	Density (kg/m^3) *
top.mar.shl	c 91.4	c 377	c 2500
bot.mar	c 91.4		
bot.mar.car		n 278.9 11.5	n 2280 50
bot.mar.car.gas **		n 295.3 16.4	n 2100 100
Gas column ***	n 15.2 15.2		

^{*} Sonic and density distributions are correlated negatively (cor. coefficient=-1); the sonic distribution of the gas filled carbonate is correlated positively (cor. coefficient=1) with the sonic distribution of the brine filled carbonate.

Table 5.2 Initial model simulation specifications. Probability density functions are specified as normal distributions with a mean and a standard deviation (n value1 value2) or as constants (c value).

5.3 Experiments

In all experiments training and test data sets consist of 100 patterns each. Sampling rate of the seismic data is 4 ms. A 30 Hz Ricker wavelet was used to generate the synthetic seismic traces in experiments 1 until 6 and 8. In experiment 7 different Ricker wavelets (20,30,40,50 Hz frequency) were used. The reference time for selecting the seismic data was the time corresponding to the top of the reservoir. Selected seismic samples were interpolated relative to this reference time.

In all experiments, networks are trained to estimate the net thickness of the gas column and the average density of the gas-filled reservoir rock from the seismic response. The average density is calculated as:

^{**} The acoustic properties of the carbonate reservoir depend on the fluid content

^{***} Maximum thickness = 45.6, minimum = 0. Values are repicked until these constraints are met.

$$\rho = \frac{\sum_{i=1}^{n} \rho_i \lambda_i}{\sum_{i=1}^{n} \lambda_i},$$
(5.1)

where:

 ρ is the density, λ the layer thickness, i the layer index and n the number of layers.

The network specifications are presented per set of experiments in a table. The performances of the test dataset are summarised in Table 5.12 for all experiments. Complete performance statistics and graphics are given in Appendix III. The results are discussed in Section 5.4.

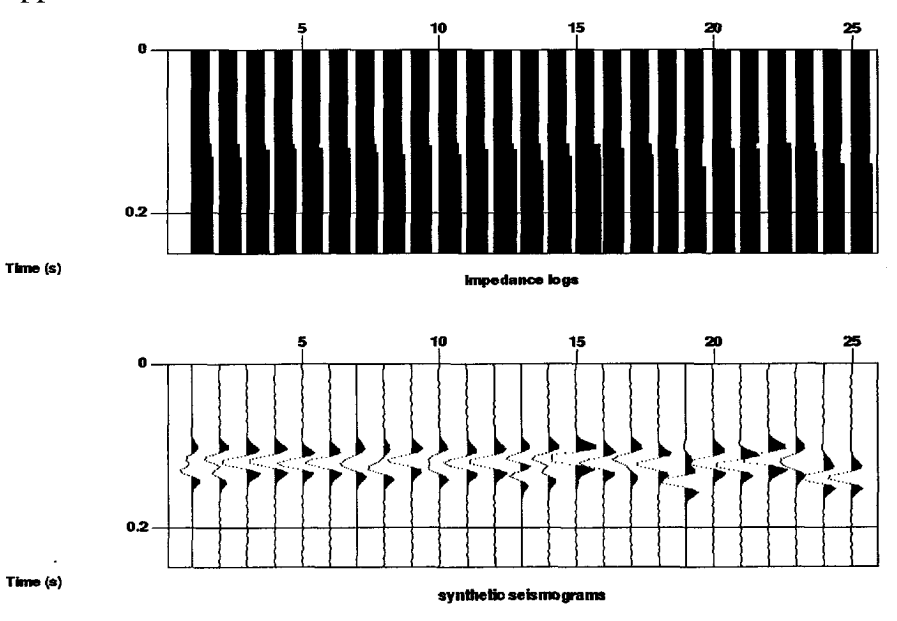


Fig. 5.2 Example of impedance logs and corresponding synthetic seismic traces of the initial model.

5.3.1 Network design

In this experiment 1 the network design is varied. The size of the input layer is progressively reduced from 25 in experiment A to 13, 7 and 1, in experiments B, C and D, respectively.

Experiment 1		
Network paradigm	Multi-Layer-Perceptron	
Number of nodes: input-hidden- output	B) 13-3-2 C) 7-3-2 D) 1-3-2	
Seismic time gate relative to the reference time-pick (ms)	A) -25 - 75 B) -25 - 25 C) -12 - 12 D) 0 - 0	
Output	average density, net gas column thickness	
Activation function input layer	none	
Activation function hidden layer	sigmoid	
Activation function output layer	linear	
Training algorithm	backpropagation	

 Table. 5.3
 Experiment 1 network specifications. The size of the input layer is varied

In experiment 2 the size of the hidden layer is varied. In experiment A, the size of the hidden layer is first increased to 9. Then in experiment B, the size is reduced to 1 node. In experiment C, the network size is increased again with the introduction of a second hidden layer. The results of these experiments can be compared with the results of experiment 1A where three nodes were used in the hidden layer.

In experiment 3 Radial Basis Function networks are tested. In experiment A, a Gaussian activation function is used in the hidden layer and in experiment C the IMQE activation function is used (see Section 3.2.2). Training is stopped after 50.000 patterns. This is identical to other experiments, described in this chapter. Training is continued for another 150.000 patterns, because the RBF networks are still learning. The results of these prolonged training sessions for experiments A and C are reported in experiments B and E, respectively. In the RBF experiments, the HSOL training algorithm of Lee and Kill (1989) and Carlin (1992) is used.

Experiment 2	
Network paradigm	Multi-Layer-Perceptron
Number of nodes: input-hidden- output	B) 25-1-2 C) 25-9-3-2
Seismic time gate relative to the reference time-pick (ms)	
Output	average density, net gas column thickness
Activation function input layer	none
Activation function hidden layer	sigmoid
Activation function output layer	linear
Training algorithm	backpropagation

Table. 5.4 Experiment 2 network specifications. The size of the hidden layer is varied

Experiment 3			
Network paradigm	Radial Basis Functions		
Number of nodes: input-hidden-	25-3-2 (end of training 25-3-2)		
output			
Seismic time gate relative to the	-25 - 75		
reference time-pick (ms)			
Output	average density, net gas column thickness		
Activation function input layer	none		
Activation function hidden layer	A) Gaussian		
j	B) Gaussian		
` ·	C) IMQE		
	D) IMQE		
Activation function output layer	linear		
Training algorithm	HSOL		
	A) 50.0000 patterns trained		
	B) 200.000 patterns trained		
	C) 50.0000 patterns trained		
	D) 200.000 patterns trained		

Table. 5.5 Experiment 3 network specifications. Radial Basis Functions; activation functions are varied along with the number of patterns trained.

In experiment 4, the final design experiment, different activation functions of the hidden layer are tested for MLP networks. In experiment A, a tangent hyperbolic function is used, followed by a prime tangent hyperbolic, a prime sigmoid, a ramp and a linear function, in experiments B, C, D and E, respectively (see Section 3.2.1). The results can be compared with the results of experiment 2A, where a sigmoid activation function is used in the hidden layer in a similar network configuration.

Experiment 4	
Network paradigm	Multi-Layer-Perceptron
Number of nodes: input-hidden- output	
Seismic time gate relative to the reference time-pick (ms)	
Output	average density, net gas column thickness
Activation function input layer	none
Activation function hidden layer	A) tangent hyperbolic B) prime tangent hyperbolic C) prime sigmoid D) ramp E) linear
Activation function output layer	linear
Training algorithm	backpropagation

Table. 5.6 Experiment 4 network specifications. MLP network with varying activation functions in the hidden layer.

5.3.2 Geological model complexity

In the following experiments the geological model complexity is increased by introducing new variables that affect the seismic response. The network specifications are kept constant in these experiments (Table 5.7).

In the first geological complexity experiment (Experiment 5), shale intercalations are introduced into the carbonate reservoir. The framework is given in Table 5.8 and the simulation specification in Table 5.9. Examples of impedance logs with corresponding seismic responses are shown in Fig. 5.3.

Experiments 5, 6 and 7	
Network paradigm	Multi-Layer-Perceptron
# of nodes: input-hidden-output	25-9-2
Input time gate	-25 to 75 ms
Output	average density, net gas column thickness
Activation function input layer	none
Activation function hidden layer	tangent hyperbolic
Activation function output layer	linear
Training algorithm	backpropagation

Table 5.7 Network specification experiments 5, 6 and 7.

Unit	Sub-unit	Lithology	Type	Code
Тор	Marine	Shale	Seal	top.mar.shl
Bottom	Marine	Carbonate	Reservoir	bot.mar.car
		Shale	Waste	bot.mar.shl

Table 5.8 The integration framework for the carbonate-shale model

Code	Thickness (m)	Sonic (us/m) *	Density (kg/m^3) *
top.mar.shl	c 91.4	c 377.3	c 2500
bot.mar	c 91.4		
bot.mar.car	n 9.14 3.05	n 278.9 11.5	n 2280 50
bot.mar.car.gas ***		n 295.3 16.4	n 2100 100
bot.mar.shl	n 1.5 1.5	n 360.9 6.6	n 2550 50
Gas column ***	n 15.2 15.2		

- Sonic and density distributions are correlated negatively (cor. coefficient=-1); the sonic distribution of the gas filled carbonate is correlated positively (cor. coefficient=1) with the sonic distribution of the brine filled carbonate.
- ** The acoustic properties of the carbonate reservoir depend on the fluid content
- *** Maximum thickness = 45.6, minimum = 0. Values are repicked until these constraints are met.

Table 5.9 Carbonate-shale simulation specification. Probability density functions are specified as normal distributions with a mean and a standard deviation (n value1 value2) or as constants (c value).

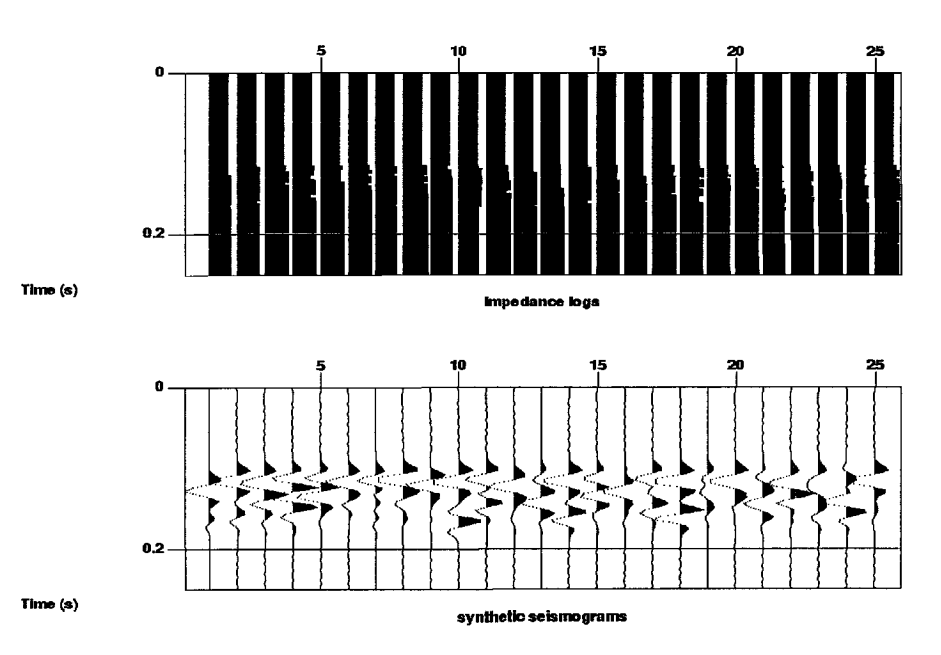


Fig. 5.3 Examples of acoustic impedance logs and corresponding synthetic seismic traces of the carbonate-shale model.

Code	Thickness (m)	Sonic (us/m) *	Density (kg/m^3) *
top.mar.shl	c 91.4	n 377.3 16.4	n 2500 500
bot.mar	c 91.4		
bot.mar.car	n 9.14 3.05	n 278.9 11.5	n 2280 50
bot.mar.car.gas ***		n 295.3 16.4	n 2100 100
bot.mar.shl	n 1.5 1.5	n 360.9 6.6	n 2550 50
Gas column ***	n 15.2 15.2		

- Sonic and density distributions are correlated negatively (cor. coefficient=-1); the sonic distribution of the gas filled carbonate is correlated positively (cor. coefficient=1) with the sonic distribution of the brine filled carbonate.
- ** The acoustic properties of the carbonate reservoir depend on the fluid content
- *** Maximum thickness = 45.6, minimum = 0. Values are repicked until these constraints are met.

Table 5.10 Overburden model simulation specifications Probability density functions are specified as normal distributions with a mean and a standard deviation (n value1 value2) or as constants (c value).

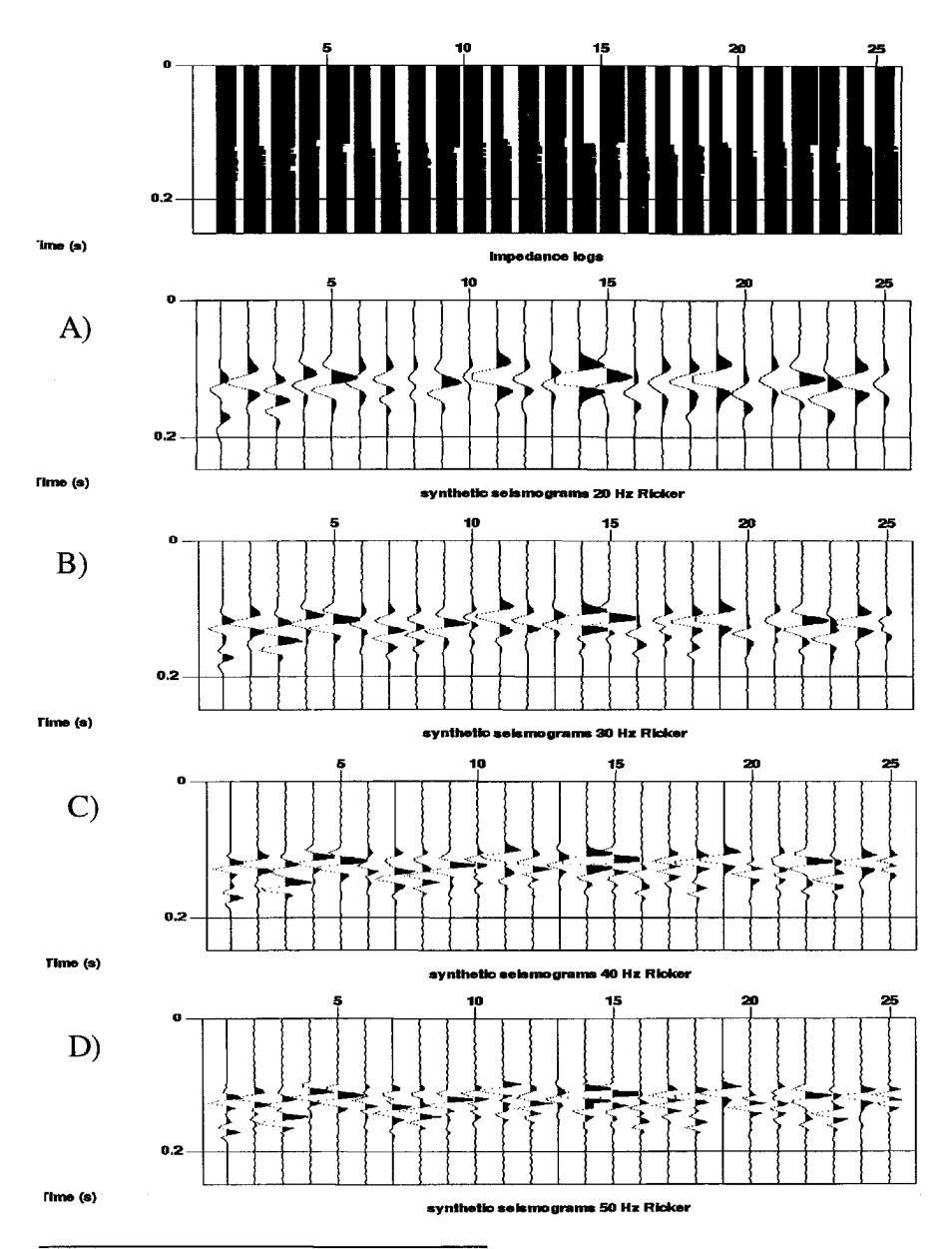


Fig. 5.4 Impedance logs of the overburden model with corresponding synthetic seismograms (A=20, B=30, C=40 and D=50 Hz Ricker wavelets).

In experiment 6 carbonate-shale model complexity is increased by varying the acoustic impedance properties of the overburden. The simulation specification are given in Table 5.10 and examples of acoustic impedance logs with corresponding seismic responses are shown in Fig. 5.4B. When interpreting these results, it must be realised that the standard deviation of the acoustic properties of the overburden is much larger than that of the target zone layers.

5.3.3 Seismic bandwidth variations

In the following experiment (Experiment 7), the synthetic seismic traces of the overburden model are convolved with different wavelets to investigate the influence of the seismic bandwidth on the inversion results. The wavelets are 20, 30, 40 and 50 Hz zero-phase Ricker wavelets (Fig. 5.5). The impedance logs and various synthetic seismic traces are presented in Fig. 5.4. The network specification are given in Table 5.7.

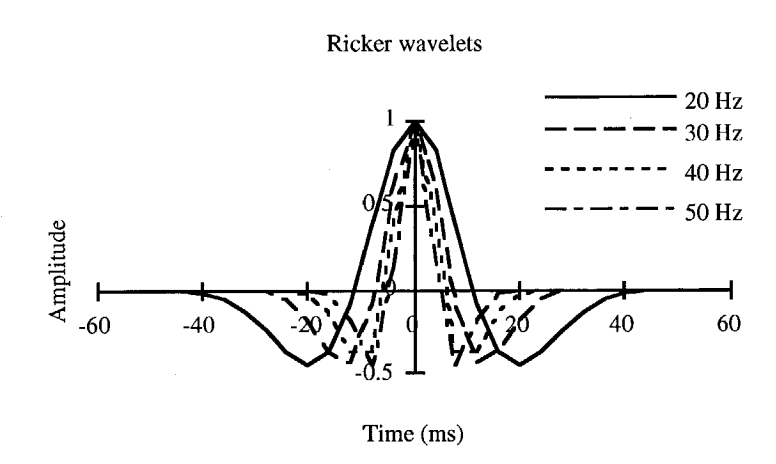


Fig. 5.5 Ricker type wavelets used to generate synthetic seismograms

Experiment 8	
Network paradigm	Multi-Layer-Perceptron
# of nodes: input-hidden-output	26-9-2 (25 seismic samples + gross gas-column)
Input time gate	-25 to 75 ms
Output	average density, net gas column thickness
Activation function input layer	none
Activation function hidden layer	tangent hyperbolic
Activation function output layer	linear
Training algorithm	backpropagation

Table 5.11 Network specifications of experiment 8.

5.3.4 Additional information

In the following experiment a carbonate-shale model with a constant overburden acoustic impedance is used (Table 5.9). The network input consists of 26 input nodes which are fed by 25 seismic samples and a gross gas-column thickness. There are no constraints to the design of networks in the GeoProbe system. It is possible to design (and train) networks that are fed by a combination of seismic and well data. Application of such networks to the factual horizon slice, is possible as well. The only condition is, that the well information is supplied in the form of a XYZ grids. Therefore, any property that can be mapped, can, in principle, be used to constrain the inversion process. In the case of experiment 8, a gross gas-column grid should be supplied together with the seismic horizon slice.

The network specification of experiment 8 is presented in Table 5.11.

This concludes the description of the experiments with simulated data. The results have been summarised in Table 5.12 and will be discussed hereafter. Additional performance statistics are presented in Apendix III.

5.4 Discussion of the results

Experiment 1 shows that gas column thickness prediction depends on the size of the input layer. The normalised RMS error increases from 0.33 through 0.44 and 0.54 to 0.97, when the number of input nodes is reduced from 25 to 13, 7 and 1, respectively. This behaviour can be explained as follows: when the number of nodes is reduced, the network is offered a

smaller time-gate around the reference time. Large gas columns will have a seismic effect outside this gate. The network must therefore extrapolate, rather than interpolate the data. Consequently the prediction results deteriorate.

Experiment	Norm. RMS Density	Norm. RMS Gas column
1A	0.28	0.33
1B	0.29	0.44
1C	0.32	0.54
1D	0.51	0.97
2A	0.24	0.32
2B	0.93	0.48
2C	0.31	0.39
3A	0.46	0.37
3B	0.33	0.30
3C	0.45	0.31
3D	0.29	0.19
4A	0.18	0.25
4B	0.18	0.27
4C	0.22	0.36
4D	0.13	0.44
4E	0.13	0.43
5	0.29	0.58
6	0.83	0.60
7A	0.87	0.61
7B	0.83	0.60
7C	0.85	0.66
7D	0.83	0.60
8	0.28	0.21

Table 5.12 Normalised RMS errors on the test datasets for the average density of the gas-filled carbonate rock and the net gas-column thickness.

The density prediction depends much less on the size of the input layer. This is because the density variations (= impedance variations, since density and sonic were correlated with a -1 correlation coefficient in the simulation) affect the seismic amplitudes and not the waveform. Because of tuning effects, seismic amplitudes are not linearly related to density, however. For this reason, a one-node network cannot predict the density as well as the

larger-size networks, normalised RMS errors are 0.28, 0.29, 0.32 and 0.51 for 25, 13, 7 and 1 input nodes.

In experiment 2 the size of the hidden layer was varied. These results can be compared with the results of experiment 1A. It is clear that with one node in the hidden layer, experiment 2B, two variables cannot be predicted simultaneously. The training performance graph (App. III) shows that training initially gives a reasonable result for the density prediction. When training is continued, the gas column prediction improves at the expense of the density prediction performance. The best results are obtained with 9 nodes in the hidden layer, with normalised RMS errors of 0.24 for density and 0.32 for gas column prediction. Adding another hidden layer, experiment 2C, deteriorates the prediction results to 0.31 and 0.39 for density and the gas column, respectively.

Radial Basis Functions networks were tested in experiment 3. These networks are normally applied to lower dimensional problems (up to 5 dimensions), where a strong correlation exists between the input variables. In these experiments a strong correlation between the input variables does exist, but the dimension of the problem is much larger than in standard RBF applications. Still RBF networks give good results, especially for the prediction of the gas column thickness where a normalised RMS error of 0.19 is reached after prolonged training using the IMQE activation function. In comparison with MLP networks, RBF networks take longer to converge. The IMQE activation function performs better than the Gaussian function in these experiments.

In experiment 4 different activation functions in the hidden layer were tested. These experiments can be compared with experiment 2A, where the sigmoid function was used. Comparing experiments 2A and 4A shows that the tangent hyperbolic activation function performs better than the sigmoid function. Normalised RMS errors for density and gas column are 0.18 and 0.25 for tangent hyperbolic and 0.24 and 0.32 for sigmoid functions, respectively. Also the prime tangent hyperbolic function scores better (0.18 and 0.27) than the sigmoid and prime sigmoid (0.22 and 0.36). The ramp and linear functions score very well when predicting the density (both 0.13), but perform less well when predicting the more difficult gas column thickness (0.44 and 0.43, respectively). The good performance on the density can be explained by the fact that seismic amplitudes outside the tuning range are related linearly to the density.

In experiments 5 and 6, the geological model was made more complex. These results are compared with the results of experiment 4A.

Shale intercalations introduced in experiment 5 have a considerable effect on the gas column prediction. The normalised RMS error decreases from 0.25 in experiment 4A to 0.58 in experiment 5. This result can be explained by the fact that non-unique solutions exist in the carbonate-shale model space. The introduction of shale layers into the reservoir, will have a large effect on the net column thickness and the seismic response. These effects, however, are not necessarily related, and, depending on the random selections made in the Monte Carlo simulations, completely different seismic signals might be related to similar net gas columns. The seismic amplitudes are less affected by the introduction of shale intercalations. Moreover, the average density is corrected for thickness of individual layers (Equation 5.1). Therefore, the decrease in performance of the density prediction is not so significant (from 0.18 in experiment 4A to 0.29 in experiment 5).

In experiment 6 the geological model complexity was increased by introducing a variation in the acoustic impedance properties of the overburden. Such variations affect the seismic amplitudes and hence the prediction performance of the reservoir density. Performance decreases from 0.29 in experiment 5 to 0.83 in experiment 6. Please note, however, that the standard deviation of the acoustic properties of the overburden is almost a factor of 10 higher than the standard deviations of the acoustic properties of the carbonate rock (Table 5.6). Changes in seismic amplitude are, therefore, primarily caused by changes in the overburden, which are completely independent of the property of interest. The performance of the gas column prediction is hardly affected by the variations in the overburden; a slight decrease in normalised RMS errors was observed: from 0.58 to 0.60.

In experiment 7 the seismic bandwidth was varied. The results show that the frequency content of the seismic data does not affect the performance of the density prediction. The normalised RMS errors are 0.87, 0.83, 0.85 and 0.83 for 20 Hz, 30 Hz, 40 Hz and 50 Hz Ricker wavelets, respectively. Since the density prediction depends primarily on the seismic amplitudes, this result is in line with the expectations. The performance of the gas column prediction was expected to be affected by the frequency content. The vertical resolution increases with increasing bandwidth, hence an increase in gas column prediction performance was anticipated with increasing frequency. The results do not show this increase. Instead the gas column prediction performance is independent of the frequency content. The normalised RMS errors are 0.61, 0.60, 0.66 and 0.60 for 20 Hz, 30 Hz, 40 Hz and 50 Hz Ricker wavelets, respectively. A possible explanation for this behaviour is that the property of interest, i.e. the gas column thickness, was calculated at the well data scale, while the inversion works on the seismic scale. In the up-scaling from well data to seismic data, the impedance logs

were resampled to the seismic sampling rate. This non-linear transformation determines whether, or not, the seismic response is related to a well property.

In experiment 8 the gross gas-column was supplied to the network in addition to 25 seismic samples. These results are compared with the results of experiment 5 where the network was trained on seismic samples only. As expected the average density is predicted equally well by both networks (normalised RMS errors are 0.29 and 0.28 for experiment 5 and 8, respectively. Also, as can be expected, the prediction of the net gas-column thickness is far better for experiment 8 then for experiment 5 (normalised RMS errors are 0.21 and 0.58, respectively.

5.5 Conclusions

From the aforementioned experiments, the following conclusions are drawn:

- In order to avoid extrapolation of results, the seismic time-gate to be analysed must cover the response of the largest thickness, for thickness-related inversions.
- The size of the hidden layer should not be chosen too small.
- A one node hidden layer can predict one variable only.
- One hidden layer is sufficient.
- Performance of RBF networks is comparable to MLP networks. RBF networks performed slightly better on the thickness inversion and slightly worse on the density inversion.
- Convergence of RBF networks is slower than that of MLP networks.
- The tangent hyperbolic activation function gives the best overall prediction performance for MLP network. For RBF networks the IMQE activation function gave a better performance than the Gaussian function.
- Prediction performance of the linear and ramp activation functions is good for the density because this is a linear problem outside the tuning range.
- Network performance deteriorates when new variables are introduced which affect the seismic response and the target variable independently.

In other words; performance deteriorates when non-unique solutions are introduced in the training set.

- Variations in the impedance of the overburden affect the seismic amplitudes and therefore the prediction performance of impedancerelated properties of the target level.
- The introduction of new layers affect the seismic waveform and therefore the prediction performance of thickness-related properties of the target level.
- Performance of the predictions of density and gas-column thickness are independent of the seismic band-width.
- Performance of the prediction can be increased by supplying additional (non-seismic) information to the network.



CASE STUDIES

6.1 Introduction

It has been shown that simulated data and factual data are commensurable if they are described in terms of the same subsurface model. The subsurface model used to describe the data has been defined as the integration framework. Artificial neural networks are used in the seismic inversion phase while 1D-stratigraphic profiles with attached physical properties are simulated using Monte Carlo statistics. So far, the performance of different network paradigms and architectures have only been investigated on simulated data.

In this chapter the total space inversion method is applied to real data, in two separate case studies.

The first study is a Rotliegend unit comprising gas-filled aeolian sandstones located in onshore Germany. The study area is covered by 3D-seismic data and is a subset of a study which included information from 19 wells.

The second case study involves a fluvial-clastic oil reservoir from the Middle East. The reservoir unit consists of sands and silts in a labyrinth type architecture. The area is covered by 3D-seismic data and the reservoir has been extensively penetrated by numerous wells, 61 of which were used in this study.

In both studies, the objective was to extract the greatest possible detail from the seismic response in order to delineate the sediment architecture and define an accurate depositional history of the reservoir unit. For each study, the available data will first be described, along with a summary of the geological setting. This is followed by the application of the techniques and a discussion of the results.

6.2 Rotliegend case study

6.2.1 Available data

The Rotliegend case study area is covered by a 1991-1992 vintage 3D-seismic dataset. The data have been acquired using a combination of dynamite and vibroseis sources. The field layout consisted of 8 parallel receiver lines, each with 60 geophone groups. Source and receiver intervals were 50 m, yielding a 25 by 25 bin size with a nominal fold of 15. Acquisition sampling rate of 2 ms was resampled to 4 ms in processing. The vibroseis data have been matched to the dynamite data in two steps, prestack and post-stack. A post-stack zero-phasing filter was applied at the end of the processing sequence which included 2 passes of residual statics, DMO and post-stack 3D-migration.

Several seismic horizons were mapped by the client. The top Wustrow horizon, corresponding to the top of the main reservoir unit, is the reference horizon used in this study (Fig. 6.11).

In the greater Rotliegend area some 40 wells have penetrated the target interval. From these, 28 wells lie inside the study area, 19 of which were selected and loaded into the GeoProbe system. The area shown in this thesis is a subset containing 11 wells (Fig. 6.1). A full suite of logs was available in digital format for the 19 wells. These included: sonic, density, neutron, calliper, gamma-ray, resistivity, corrected elan-litho logs, time-depth curves, and blocked acoustic impedance curves for Rotliegend and basal Zechstein. In addition cross-plots of acoustic impedance vs. porosity and permeability, and a set of stratigraphic profiles were also available on paper copies.

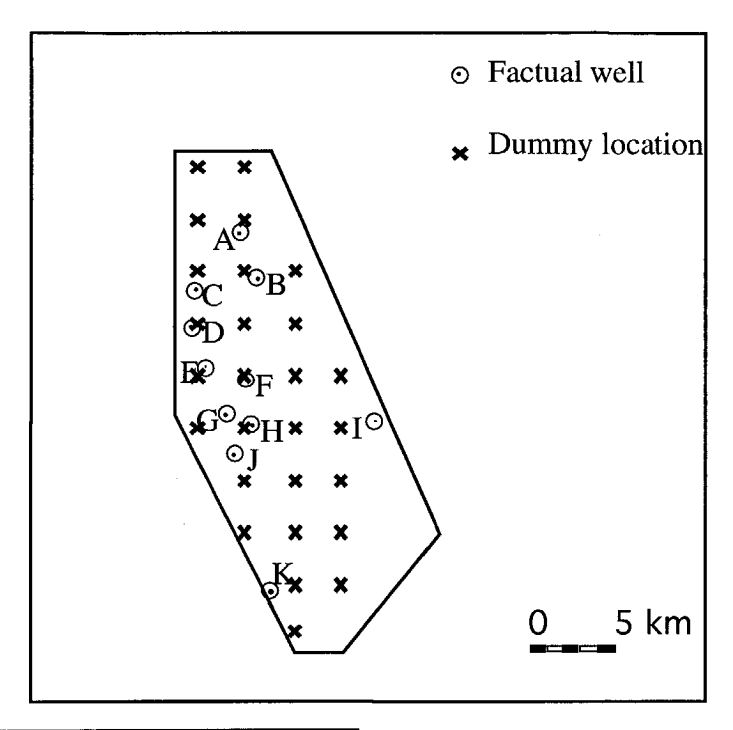


Fig. 6.1 Well locations

6.2.2 Geology

6.2.2.1 Tectonic Overview

The structural history of the Rotliegend gas play area is typical of the structural development of Northern Germany. An overview of this can be found in Ziegler (1990).

An extensional tectonic regime dominated prior to deposition of the Zechstein. The tensional stresses present in the late Carboniferous and Early Permian gave rise to the development of North West-South East trending horsts and grabens. These structures were locally modified by minor wrench faults (Gast, 1988).

Continued subsidence and subsequent sediment loading (up to 1000 m) triggered halokinesis in the Zechstein during the Late Triassic. Diapir formation resulted in tectonic deformation of the overlying formations. Continued flow of the salt gave rise to the formation of discontinuous

anhydrite (Z3) blocks. These blocks are visible on seismic as 'rafts or floating blocks' within the salt. The upward movement of the salt triggered a series of tectonic re-adjustments in the Mesozoic succession resulting in collapse faulting of the overlying formations.

The effects of Alpine and Atlantic tectonism beginning in the Late Cretaceous gave rise to fault reactivation and basin inversion well into the Tertiary.

6.2.2.2 Stratigraphy

While the targets in this case study are restricted to the three main reservoir sands of the Rotliegend, it was necessary to include the overlying formations for seismic simulation purposes. Therefore, in the following section the general description of the regional stratigraphy covers not only the interval between Upper Carboniferous, through the Rotliegend, to the Zechstein, but also the Buntsandstein as well.

Late Carboniferous to Permian Rotliegend

Late Carboniferous to Early Permian red beds lie unconformably on rifted basement volcanics of the Variscan continent. There is no distinct unconformity at the top of the Carboniferous as there is with the Saalian unconformity (Ziegler, 1990) in the southern gas basin of the North Sea. The redbeds are dominated in the beginning by fan and dune deposits indicative of an arid aeolian environment which become more dune and shoreline dominated towards the top. These in turn are overlain by the shales and sandstones of the Heidberg-Bahnsen formation.

Of the reservoir formations, the lowermost is the Schneverdingen. This is followed by the Dethlingen This is in turn overlain by the Ebstorf formation. The uppermost reservoir formation of the Rotliegend in this region is the Wustrow formation.

Permian Zechstein

The base of the Zechstein is indicated by a copper shale, the Kupferschiefer. There follows a thin layer composed of interbedded anhydrite and carbonates of the Zechstein 1 and 2 cycles. This is overlain by the halite of the Zechstein 2 and 3 cycles. The thickness of this layer varies (due to halokinesis). The anhydrite of the Zechstein 3 series is present as discontinuous blocks or rafts in the Z2 and Z3 halite.

Triassic

The Triassic sediments overlie a Zechstein halite succession of variable thickness. The Lower Triassic (Bunter) is composed of terrestrial clastics (Buntsandstein) while the Upper Triassic comprises marine clastics carbonates, and evaporites.

6.2.2.3 Depositional Facies and Reservoir Geology

Deposition of the Lower Rotliegend was dominated by arid aeolian and alluvial fan processes in a horst and graben system. As deposition of the Lower Rotliegend progressed subsidence decreased and sabkha lakes to the north of the region began to transgress over the aeolian deposits as the grabens were filled in. By the end of deposition of the Wustrow the trough had essentially been filled in. Lake, shoreline and sabkha deposits dominated in the north while dunes and alluvial fans dominated the south. These deposits were then conformably overlain by the thick shale and sand deposits of the Upper Rotliegend, Heidberg-Bahnsen clastics. Sediment from the Upper Rotliegend was probably sourced by the Variscan mountains to the South (Kulke et.al., 1993).

The Rotliegend 'desert' was subsequently flooded by the shallow Zechstein Sea. This transgression is marked over N.W. Europe by a copper shale deposit (Kupferschiefer). Evaporation led to cyclical series of "evaporite" deposits being laid down conformably over the Upper Rotliegend clastics. The lower two evaporitic cycles, however, are dominated by the development of carbonate platforms with anhydrite sabkhas.

The lower clastic sequence of the Buntsandstein formation is a monotonous succession of silts, anhydritic shales and claystones deposited in fluvial, lacustrine and shallow marine environments (Ziegler, 1990).

The reservoir geology of the three main Rotliegend reservoir formations: the Wustrow, Dethlingen, and Schneverdingen Formations will be dealt with in more detail in the following three sections.

Schneverdingen Facies and Reservoir Geology

Deposited in arid conditions upon a rifted volcanic terrain the Schneverdingen comprises dune sandstone with locally thick fanglomeratic deposits. Coarse, proximal, conglomerates, breccias and gravels are to be found adjacent to, what were then active, faults. Fan material, however, becomes thinner and more mature towards the north of the grabens and distally, away from the edges of the graben. The large amount of volcanic material eroded off the horsts resulted in a high argillaceous (clay) content

within fan sediments. These clays were also deposited in the silty shales of the interdune areas.

Dunes were formed in the lows (ergs) away from the graben margins. The dunes are comprised, of "dry" dunes and "wet" dunes. This distinction has nothing to do with depositional environment but, instead, refers to the diagenetic history and subsequent reservoir quality of the dune sands. Dry dunes have hematite cements which formed above the water table during early diagenesis. Wet dunes underwent early diagenesis when saturated. as a result the pores are clogged with illite cement.

The Schneverdingen formation can be considered as a stack of fanglomerates, wet and dry dunes and silt/shale levels. There are occasional volcaniclastic or basaltic layers. The Schneverdingen may be completely absent on the horst blocks. The formation is capped by a sealing shale member separating it from the Dethlingen formation. While the fanglomerates and wet dunes may be gas charged, only the dry dunes have sufficient permeability and porosity to produce gas and are the target within this formation.

Dethlingen/Ebstorf Facies and Reservoir Geology

The lower members of the Dethlingen formation show a similar composition and distribution to the Schneverdingen formation. However, synsedimentary tectonism was reduced and the graben had begun filling up. Extensive fanglomerates were restricted to the south and graben margins with wet dunes predominating elsewhere.

The upper members of the Dethlingen formation show the onset of a marine transgression from the north. In this level fanglomerates are restricted to the faulted margins while dry dunes predominate in the south of the area. Moving northwards, the dry dunes pass into a belt of wet dunes then sandy sabkhas and finally shoreline sands. The shoreline sands have chlorite cement and are free from illite.

The overlying Ebstorf can be considered a result of the marine transgression that occurred prior to deposition of the Wustrow. The Ebstorf comprises a sandy member and a lower shale member. In places, the lower shale is missing and the sand member is considered to rest directly on the Dethlingen. The onset of this transgression explains the shoreline sands in the Dethlingen and the lack of shales in the presumed contact between the Ebstorf and the Dethlingen in places.

The porous and permeable shoreline sands are the main reservoir formation in the Dethlingen/Ebstorf interval. Both Dethlingen and Ebstorf sandstones are charged with gas. The sealing formation for this gas column is shale interval at the base of the Wustrow.

Wustrow Facies and Reservoir Geology

The Wustrow can be considered to be comprised of an upper and a lower member. The lower Wustrow comprises dune sandstones and fan deposits, and locally some volcaniclastics. Shoreline deposits occur only in the extreme northern part of the area.

The upper Wustrow unit comprises predominantly more shoreline and sabkha lake deposits and represents the onset of a major marine transgression prior to deposition of the Heidberg-Bahnsen shales. Wet dunes occur in the south of the depression, while fans are restricted to the southern extremities and, locally, along the margins. The north of the area comprises shoreline sands and sabkha deposits. The sabkhas are clay rich and reduce the reservoir quality of the sandstone when interbedded. Well studies indicate a pronounced asymmetry in the distribution of the shoreline sands towards the western edge of the depression. Shoreline deposits also thin out towards the south.

The shoreline deposits of the Wustrow are the uppermost reservoir formation of the Rotliegend in this area. The gas column is capped by a shale layer at the base of the Heidberg-Bahnsen.

6.2.3 Integration framework

The framework for the Rotliegend case study is shown Table 6.1. The framework entities correspond, in general, with sequence and lithological boundaries although some concessions were made to increase the flexibility of the well simulation algorithm. The following, is a description of the framework, describing the Rotliegend and overlying sediments in the study area:

 Nine main units and four seals were chosen. Each unit has one or several sub-unit (geological or seismic). The third column shows the lithologies comprising each sub-unit, while the fourth column shows the user-defined codes.

Unit	Sub-unit	Lithology	GeoProbe Code
Buntsandstein	Upper	Sandstone	bunt.up.snd
		Shale	bunt.up.shl
	Lower	Sandstone	bunt.low.snd
		Limestone	bunt.low.lim
		Shale	bunt.low.shl
Upper Zechstein	Z3 to Z7	Halite	uze.z37.hal
		Anhydrite (A3)	uze.z37.a3
		Shale	uze.z37.shl
Basal Zechstein	Z2 to Z1	Anhydrite (A2)	bze.z12.a2
		Carbonate	bze.z12.car
		Anhydrite	bze.z12.anh
		Copper Shale	bze.z12.cop
Heidberg-Bahnsen	Top Rotliegend	Sandstone	heid.topr.snd
		Shale	heid.topr.shl
Seal 1	Seal	Shale	seal1.seal.shl
Wustrow	Wustrow 1	Evaporite	wus.wul.eva
		Silt/Shale	wus.wu1.sil
	1	Shoreline Sandstone	wus.wul.sho
		Wet Dune Sandstone	wus.wul.wet
	į.	Dry Dune Sandstone	wus.wul.dry
		Fanglomerate	wus.wul.fan
		Volcanics	wus,wul.vol
	Wustrow 2	Wet Dune Sandstone	wus.wu2.wet
		Dry Dune Sandstone	wus.wu2.dry
	ł	Fanglomerate	wus.wu2.fan
		Silt/Shale	wus.wu2.sish
		Volcanies	wus.wu2.vol
Seal 2	Seal	Shale	seal2.seal.shl
Ebstorf	Shoreline	Shoreline Sandstone	ebs.shor.shor
		Silt/Shale	ebs.shor.sish
	Wet Dune	Wet Dune Sandstone	ebs.wet.wet
		Silt/Shale	ebs.wet.sish
Seal 3	Seal	Shale	seal3.seal.shl
Dethlingen	Dethlingen 1	Shoreline Sandstone	det.det1.sho
		Wet Dune Sandstone	det.det1.wet
		Fanglomerate	det.det1.fan
		Silt/Shale	det.det1.sish
		Anhydrite/Carbonate	det.det1.anc
	Dethlingen 2	Wet Dune Sandstone	det.det2.wet
		Dry Dune Sandstone	det.det2.dry
		Fanglomerate	det.det2.fan
		Silt/Shale	det.det2,sish
		Anhydrite/Carbonate	det.det2.anc
Seal 4	Seal	Shale	seal4.seal.shl
Base	Schneverdingen	Wet Dune Sandstone	base.schn.wet
		Dry Dune Sandstone	base.schn.dry
		Fanglomerate	base.schn.fan
		Silt/Shale	base.schn.sish
Lower Rotliegend	Volcanics	Volcanics	lowr.vol.vol
	Carboniferous	Sandstone	lowr.car.snd
	1	Shale	lowr.car.shl

 Table 6.1
 Rotliegend case study integration framework

- Within the Buntsandstein, the names of the lithologies may not represent the real lithology observed in the well. However, these names have been kept since they will not influence the final outcome.
- The Wustrow unit was divided into two sub-units: Wustrow 1 and Wustrow 2. The main difference is the presence of shoreline sands and evaporites in the Wustrow 1 sub-unit. The Dethlingen unit was similarly divided into two sub-units.
- Reservoir sands occur in the Wustrow, Ebstorf, Dethlingen and Schneverdingen units. Most important reservoir sands are the chlorite and hematite rich sands. Chlorite sands correspond to shoreline sands. Hematite rich sands correspond to the dry dunes lithology. Wet dune sands contain illite, which kills the porosity and permeability, so reducing the reservoir quality of these sands. For the purpose of this study they are regarded as waste rocks.
- Each sub-unit entity has several lithologies.
- Seals between different units have been placed in order to define the separate hydrocarbon columns. This is a requirement of the GeoProbe system. In order to identify hydrocarbons in the system, columns must be attached to a sealing layer. In factual wells the last shale layer above a reservoir was called the seal. No seal was entered in cases where no shale was present between subsequent reservoir units.
- Seal 3 (between Ebstorf and Dethlingen) may or may not be present in southern wells. The Ebstorf is always sandy; sometimes with shale at the base, although, this may be absent. When this occurs the Ebstorf appears "welded" to the top of the Dethlingen. (On logs it is impossible to differentiate the two when this occurs).
- Seal 4 has been arbitrarily introduced as a 1 m shale since there seems to be a new gas column starting at the top of the Schneverdingen. However, the lithology of what may constitute the seal, is not clear from the well data.

6.2.4 Well data preparation

The factual wells had to be entered into GeoProbe. First, the well stratigraphy was described in terms of framework entities. This description was based primarily on the elan-litho logs. Next, the sonic and density logs were entered into the system. These logs were parameterised (i.e. blocked)

at the lithology scale of the integration framework. The gas-content of reservoir layers was not entered, due to the absence of information.

Simulated well data was additionally required in order to supplement factual wells and include aspects of the geological reasoning. For this reason, factual well data were analysed in order to obtain information on the variations in thickness, sonic and density properties, per framework entity. These analyses yielded the stochastic input for the well simulation algorithm. Geological input to the simulation was based primarily on regional knowledge. The main geological rules are presented in Table 6.2. The complete simulation specifications are given in App. II.

Units	Rule	Sub-unit	Rule
Buntsandstein	Sum S.	Upper	Iterate S.
		Lower	Iterate S.
Upper Zechstein	Sum S.	Z3 to Z7	Iterate S.
Basal Zechstein	Sum S.	Z2 to Z1	Iterate S.
Heidberg- Bahnsen	Sum S.	Top Rotliegend	Sum S.
Seal1	Sum S.	Seal	Sum S.
Wustrow	XOR	Wustrow1	Iterate R.
		Wustrow2	Iterate R.
Seal2	Sum S.	Seal	Sum S.
Ebstorf	XOR	Shoreline	Iterate R.
		Wet dune/Fluv.	Iterate R.
Seal3	Sum S.	Seal	Sum S.
Dethlingen	XOR	Dethlingen1	Iterate R.
		Dethlingen2	Iterate R.
Seal4	Sum S.	Seal	Sum S.
Base	Sum R.	Schneverdingen	Iterate R.
Lower Rotliegend	Sum S.	Volcanics	Sum S.
		Carboniferous	Relative R.

Sum:

The thickness of the entity is constructed by taking the sum of the

thicknesses of the smaller scale entities.

Iterate:

The entity is filled with smaller scale entities

XOR:

Only one of the smaller scale entities is selected

S.

Sequential selection of minor scale entities

R.

Random selection of minor scale entities

 Table 6.2
 Geological rules for the simulation algorithm

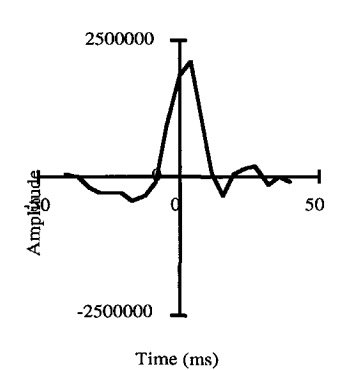


Fig. 6.2 Wavelet used to generate synthetic seismograms. The wavelet was derived at well location B.

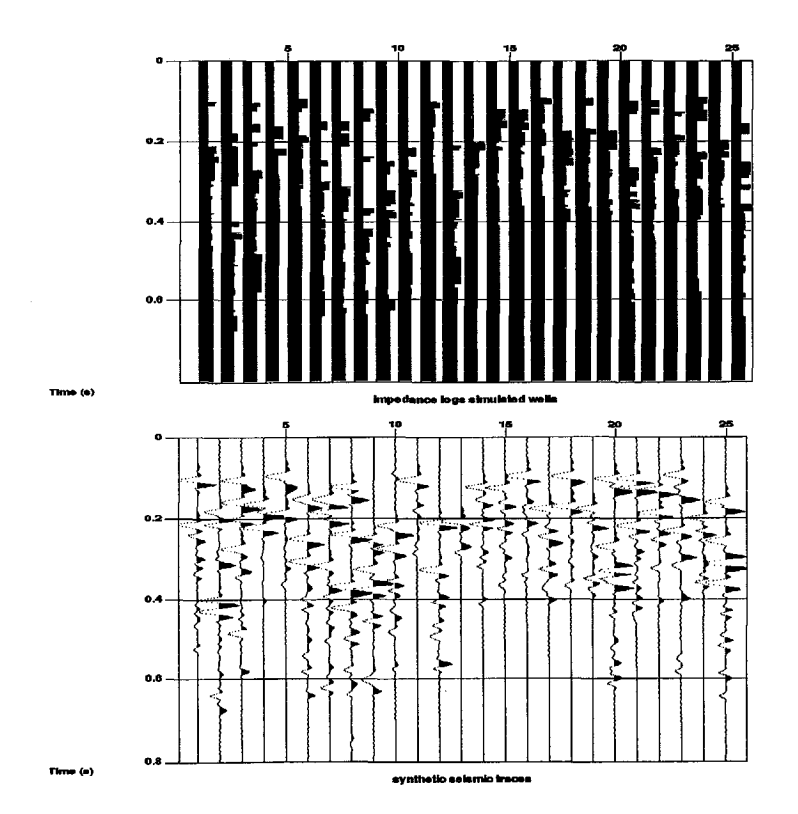


Fig. 6.3 Example of impedance logs and corresponding synthetic seismic traces of simulated wells.

In addition to the geological rules, simulation constraints were set. The most important constraints were generation rules applied to lithologies and subunit entities. These constraints act in combination with the defined geological rule. E.g. an iteration rule applied to a sand-shale sequence with 10% shale generation and 100% sand generation yields a sand-prone subunit. The Bundsandstein was excluded in the simulation; it was given a presence of 0%. A percentage was assigned also to entities with an XOR rule attachment. The simulation algorithm was further constrained by the correlation of sonic and density distributions with a correlation coefficient of -1. Effectively this implies that acoustic impedances were simulated rather than independent sonic and density variables.

The acoustic properties of the simulated wells were used to create reflectivity logs. These were then converted into synthetic seismograms by depth-time conversion, anti-alias filtering to 4 ms and convolution with a wavelet derived at well location B (Fig. 6.2). Some acoustic logs with corresponding synthetic seismograms are shown in Fig. 6.3.

6.2.5 Direct inversion

In this section the application of the direct inversion approach is described. A representative dataset for network training was created in total space. The training data set comprised 500 simulated wells with corresponding synthetics extended with 19 factual well, each with 25 factual traces. Two test dataset were used: one consisting of 500 simulated wells with corresponding synthetic seismic data and one consisting of the factual wells with one factual seismic trace. Note, that these seismic traces had been used in training the network and, therefore, cannot be considered an independent test case. A 200 ms RMS trace equalisation was applied to all seismic data. The target variable is the weighted average impedance of the Wustrow, calculated as:

$$Z = \frac{\sum_{i=1}^{n} Z_i \lambda_i}{\sum_{i=1}^{n} \lambda_i},$$
(6.1)

Direct inversion	
Training data	500 simulated wells +
	19 factual wells with 25 traces each
Test data	A) 500 simulated wells
	B) 19 factual wells with 1 factual
	trace
Network paradigm	Multi-Layer-Perceptron
No.of nodes: input-hidden-output	15-9-1
Input time gate	-10 to 50 ms, relative to Top
	Wustrow
Output	weighted average impedance
	Wustrow
Activation function input layer	none
Activation function hidden layer	prime tangent hyperbolic
Activation function output layer	linear
Training algorithm	backpropagation

Table. 6.3 Network specifications. All seismic data have been balanced using a 200 ms RMS scaling around the reference horizon.

Training variables	Normalised RMS	RMS	Mean Absolute	Max Absolute
Impedance	0.85	714460 kg/s*m ²	586098 kg/s*m ²	2075477 kg/s*m ²
Test variables A	Normalised RMS	RMS	Mean Absolute	Max Absolute
Impedance	0.72	671576 kg/s*m ²	546593 kg/s*m ²	2495753 kg/s*m ²
Test variables B	Normalised RMS	RMS	Mean Absolute	Max Absolute
Impedance	0.93	746647 kg/s*m ²	670127 kg/s*m ²	1237221 kg/s*m ²

Table. 6.4 Network performance statistics. A) 500 simulated wells B) factual wells with one factual seismic trace.

where:

Z is the impedance, λ the layer thickness, i the layer index and n the number of layers.

The network specifications are given in Table 6.3. The results are shown in Fig. 6.4 and Table 6.4. The prediction of the network on the factual wells is shown in Fig. 6.6.

It is concluded that the weighted average impedance of the Wustrow formation can be predicted from seismic data. The accuracy of the network

prediction has a RMS error of 671576 kg/s*m² on simulated data. This corresponds to less than 6%. The RMS error on the factual seismic traces at the factual well locations is 746647 kg/s*m², which corresponds to less than 7%. Note, however that these traces have been used in training the network and therefore, this RMS error cannot be used to quantify the prediction error. The trained network was subsequently applied to the seismic horizon slice yielding a lateral prediction grid for the weighted average impedance of the Wustrow formation (Fig. 6.7).

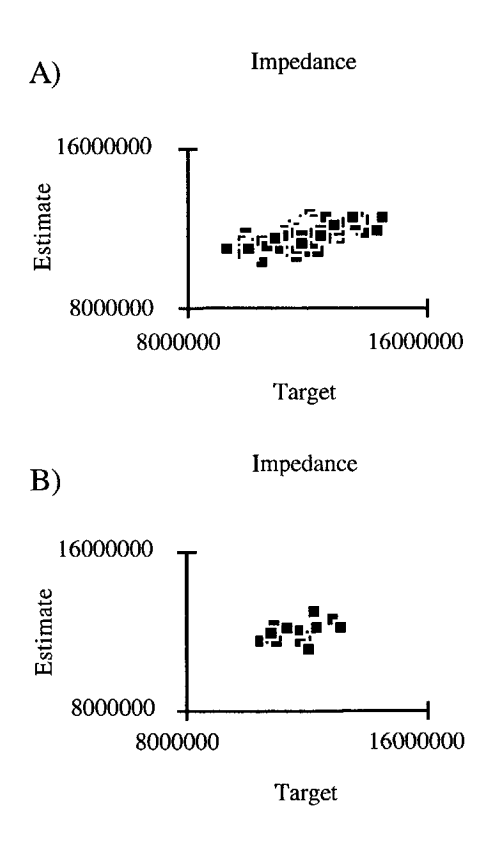


Fig. 6.4 Network performance on the test datasets A) 500 simulated wells B) factual wells with one factual seismic trace.

85

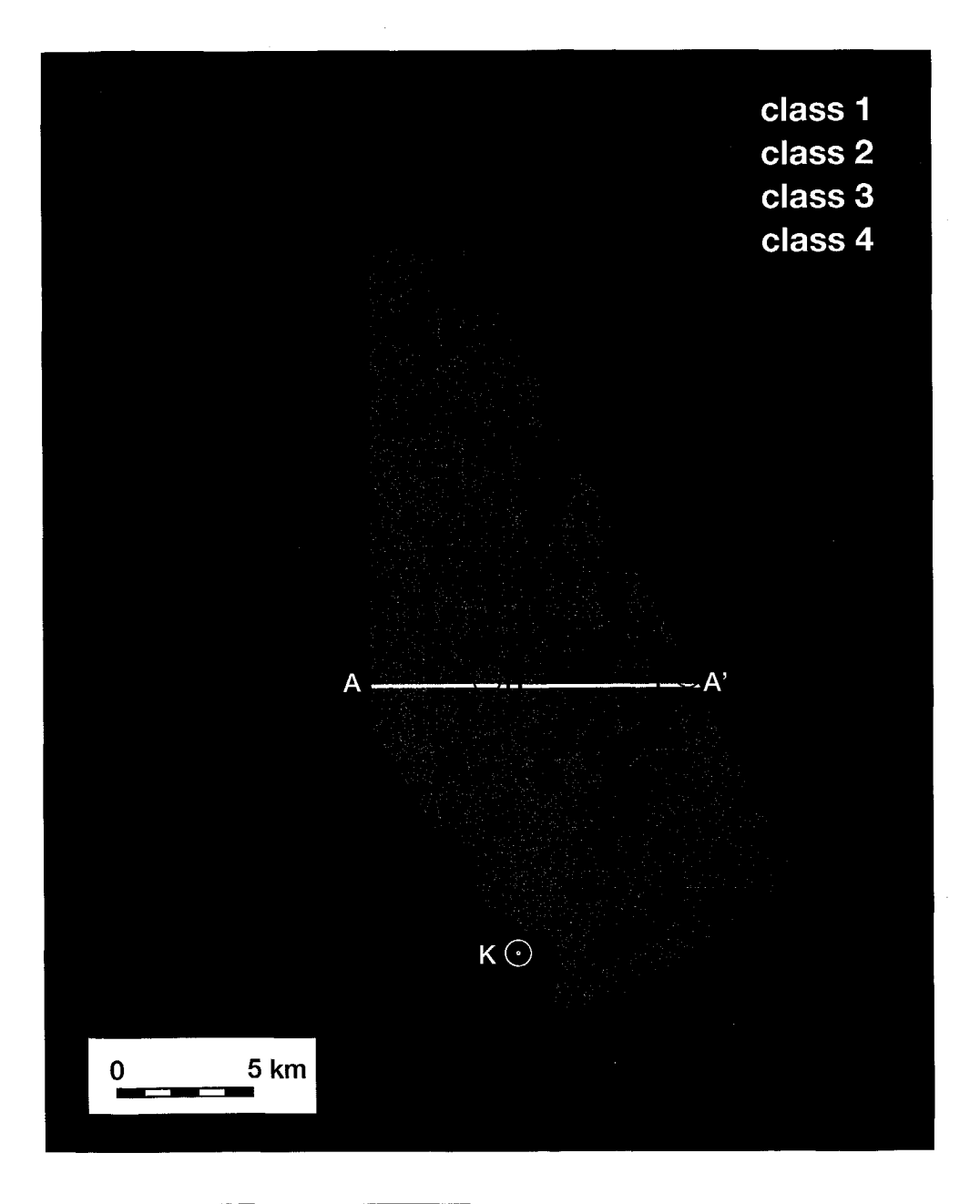


Fig. 6.5

UVQ segmentation of the Wustrow seismic response into 4 classes. The time-gate is -10 to 50 ms with respect to the Top Wustrow reference horizon

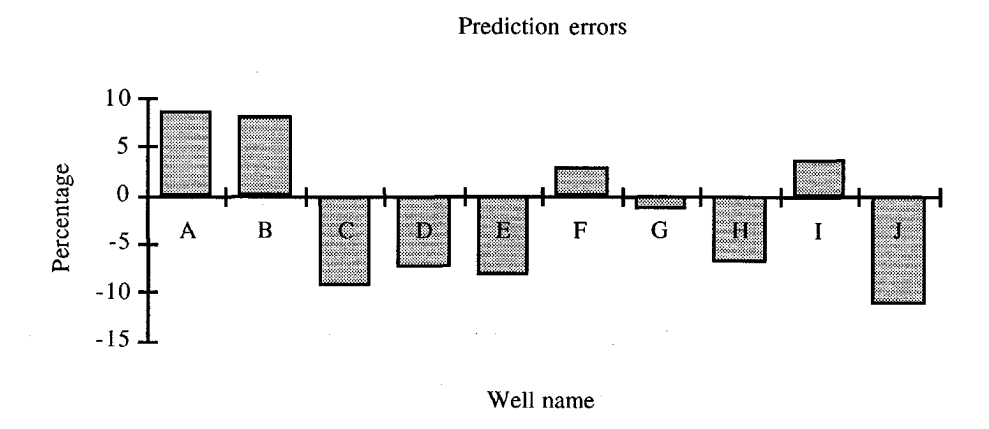


Fig. 6.6

Network errors when predicting the weighted average impedance of the Wustrow on factual wells using the factual seismic response at the well location. Note, that these seismic traces have also been used to train the network and, therefore, this is not an independent test of the network prediction performance.

6.2.6 Segmentation

In this section the segmentation approach is described. First a subset of the seismic horizon slice was created by selecting 25 (5x5) traces around the factual and dummy well locations (Fig. 6.1). Seismic data was selected in a gate of -100 to +100 ms around the reference horizon. The seismic traces were balanced using a 200 ms RMS equalisation. A gate of -10 to 50 ms around the reference horizon (15 samples) was used to train 5 separate UVO networks with 2, 3, 4, 5 and 6 classes, respectively. Output of the UVO's is the index of the winning network node (the class) plus a degree of match between input vector and centroid of the class (Equation 3.10). Trained networks were then applied to the seismic horizon slice yielding seismic class distribution maps and grids showing the degree of match. The seismic class distribution map of the UVQ network with four output classes is shown in Fig. 6.5 and the corresponding degree of match map in Fig. 6.10. Note, that, apparently, the area around wells C and D could not be clustered. Interpretation of the top Wustrow is difficult in this area because of halokinesis in the overburden. The top Wustrow amplitude map is shown in Fig. 6.12. A comparison with the segmentation map reveals that the classes are not merely a function of seismic amplitudes.

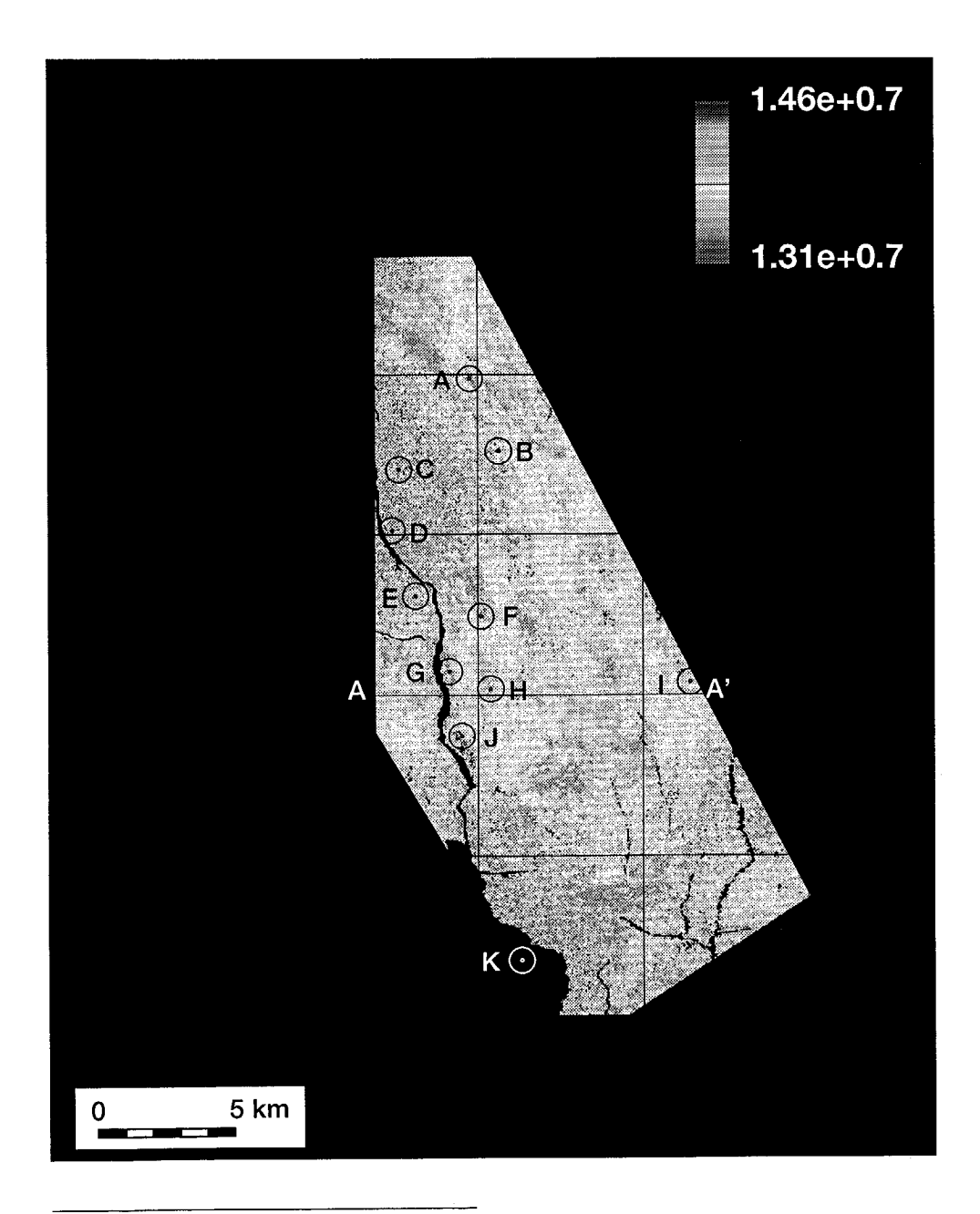


Fig. 6.7 Neural network lateral prediction grid for the weighted average impedance of the Wustrow formation.

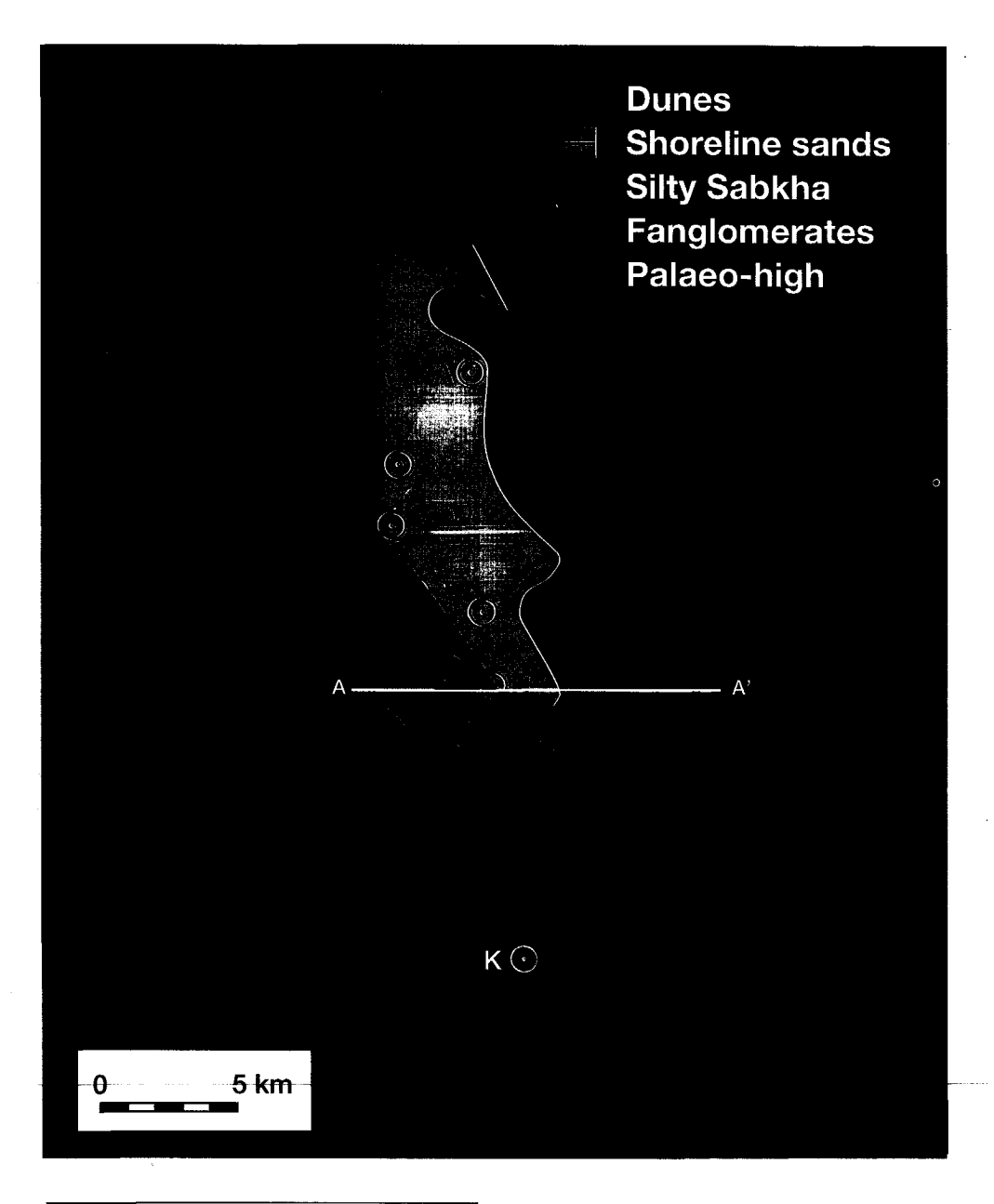
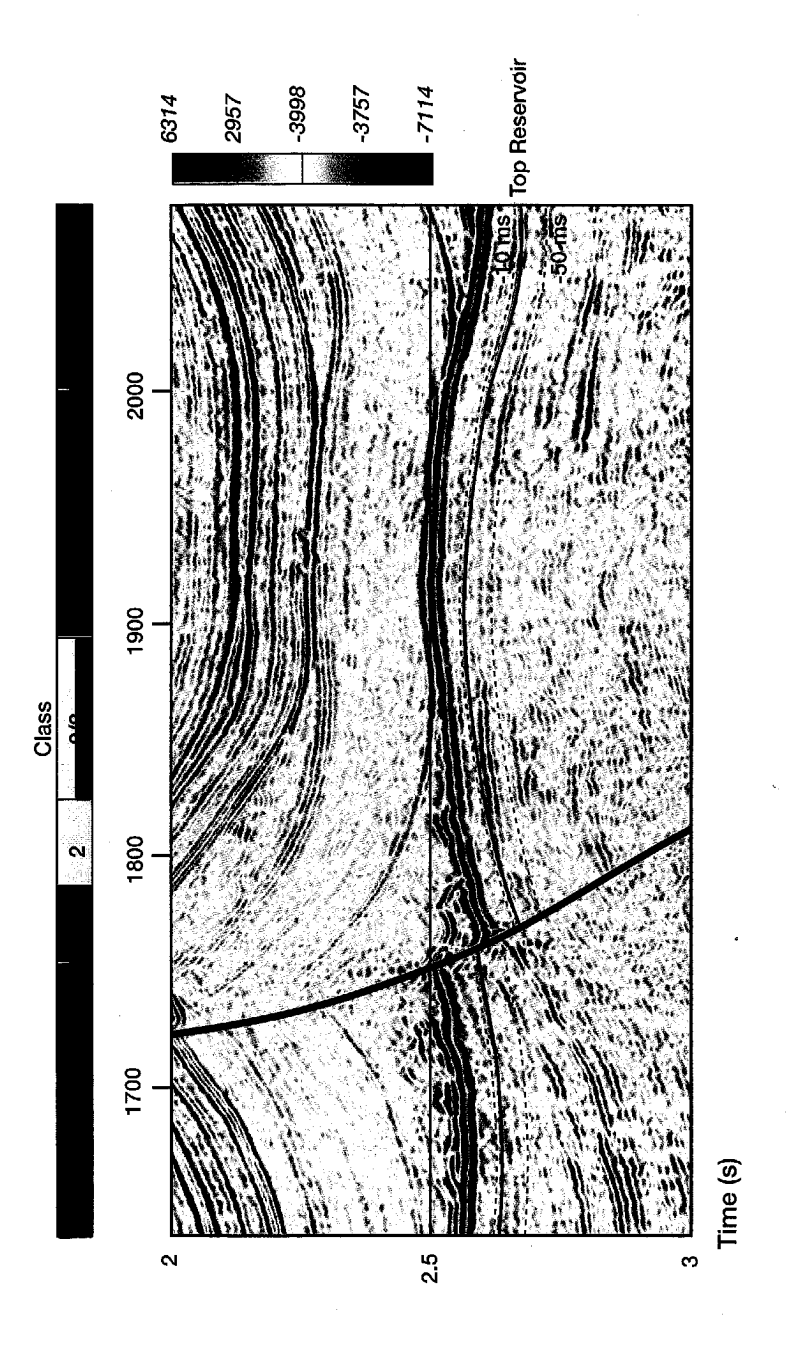


Fig. 6.8 Average distribution of sedimentary facies and palaeogeography over the Wustrow formation interval based on well data only.



Rotliegend study. Seismic line A-A' (see Fig. 6.5) showing different class responses.

6.9

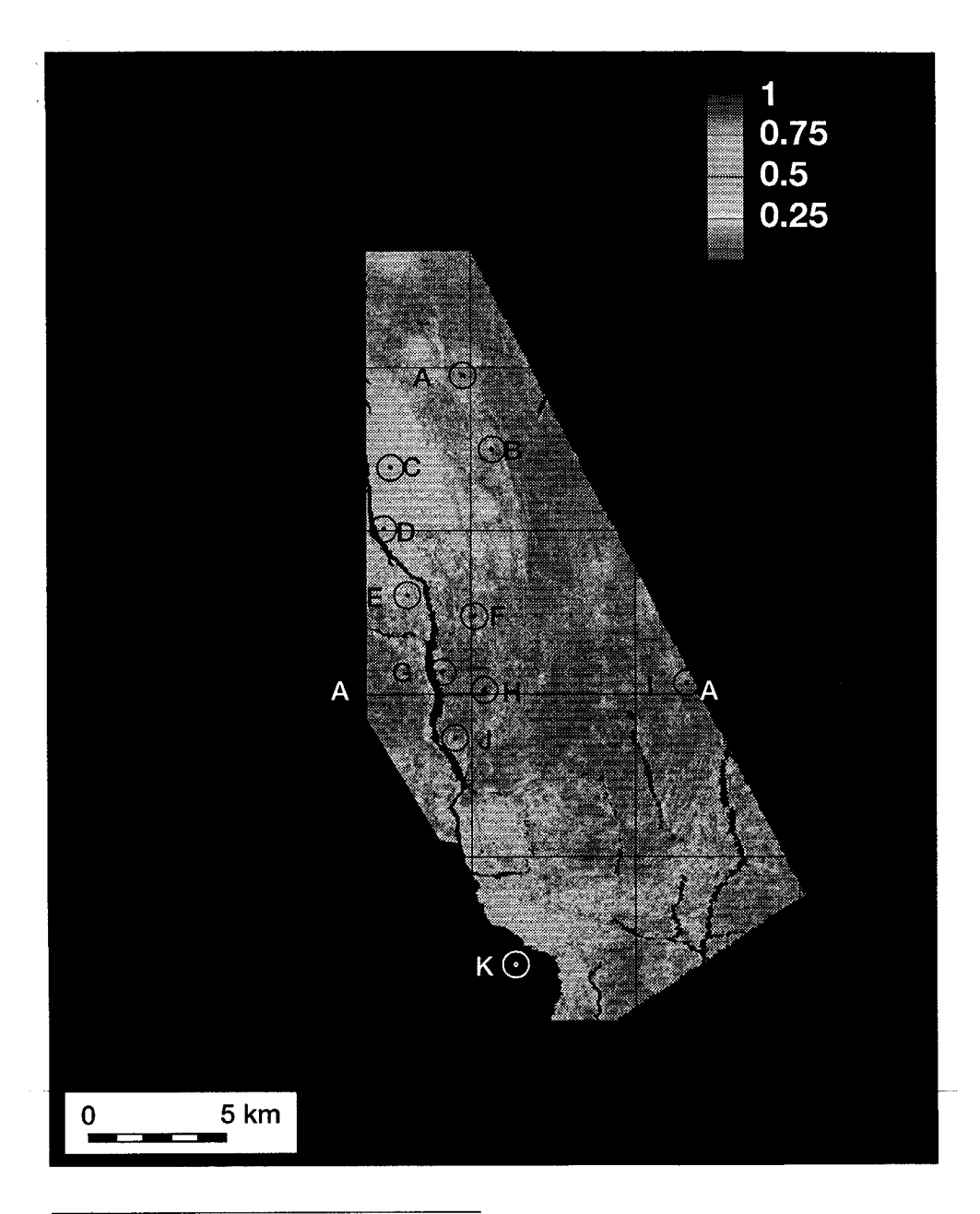


Fig. 6.10

UVQ degree of match corresponding to seismic response segmentation of the Wustrow into 4 classes. The degree of match indicates the Euclidean distance to the class centroid. It can vary from 0 (minimum match) to 1 (perfect match).

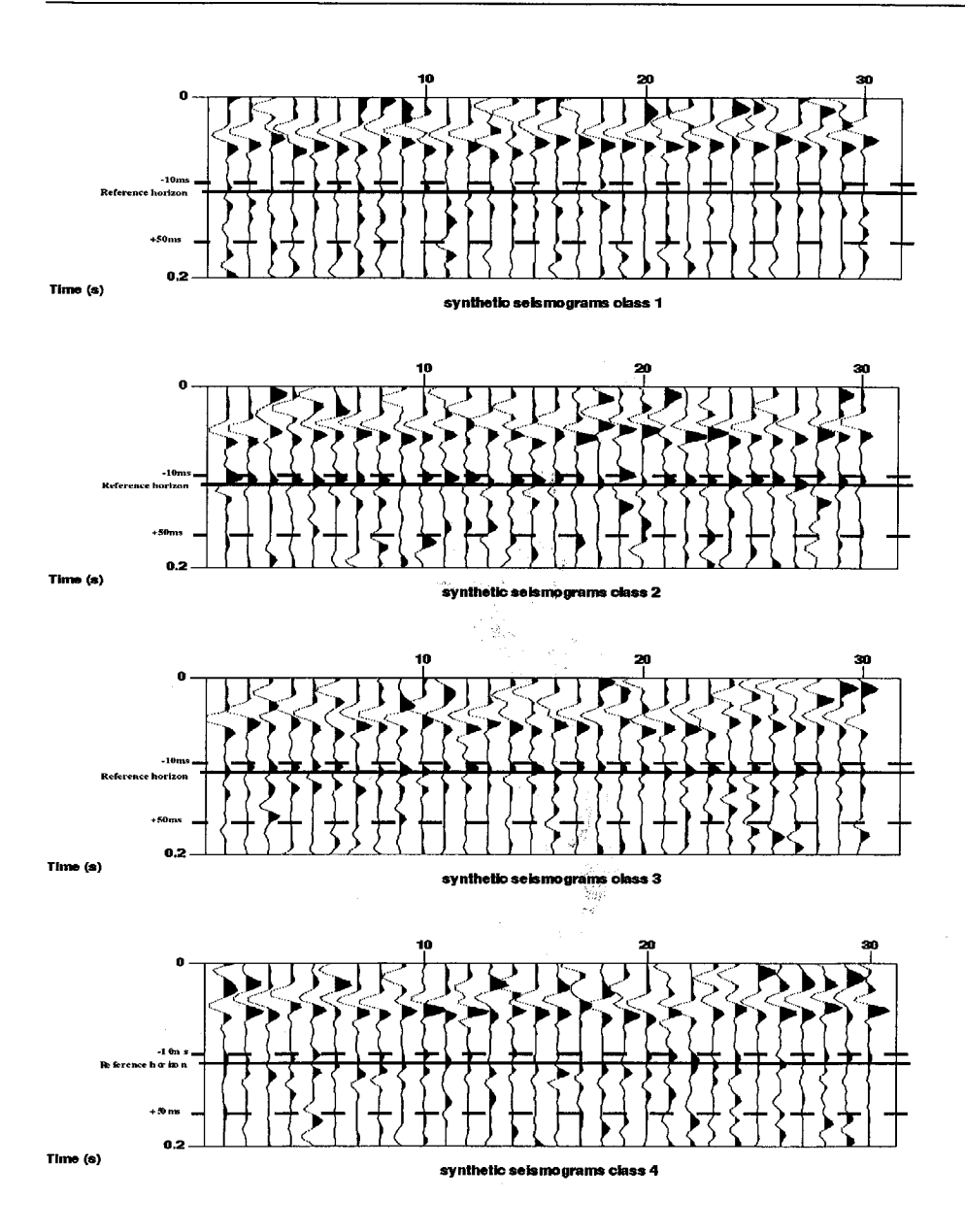


Fig. 6.11 Trained UVQ with 4 classes applied to synthetic seismograms. The top of the Wustrow is at 100 ms. The seismic gate used by UVQ to classify the response is -10 to 50 ms (15 samples) relative to Top Wustrow.

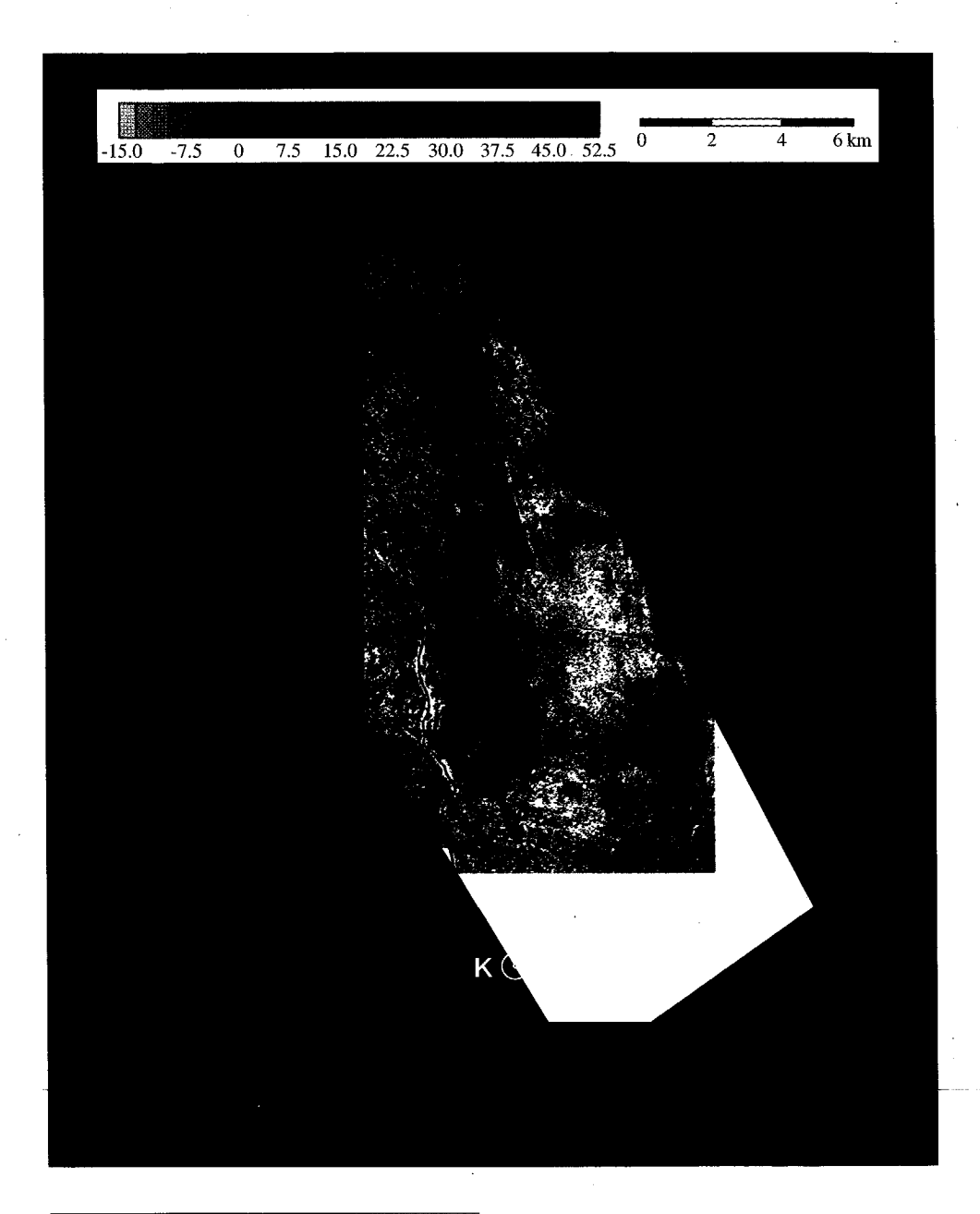


Fig. 6.12 Top Wustrow amplitude map (Courtesy Autonini, BEB Erdöl und Erdgas GMBH).

Comparison of the distribution map of seismic classes with the well-based sedimentary facies & palaeo-geography map of the Wustrow formation (Fig. 6.5 and 6.8, respectively), shows an excellent correlation. The classes appear to correspond to the sedimentary facies identified by the client. To verify this hypothesis the UVQ classifier was also applied to the seismic signals of a representative dataset.

First 500 wells were simulated. The synthetics from these well were balanced in the same way as the factual seismic traces with a 200 ms RMS scaling in a gate of 100 to 100 ms relative to the top Wustrow. Application of the trained UVQ to the selected time-gate of -10 to 50 ms yielded four classes that were analysed. The synthetic seismic responses of these classes are shown in Fig. 6.11. The seismic responses are clearly different. Class 1 is characterised by a low energy response, class 2 has a strong first loop, class 3 shows a double loop and class 4 has a hybrid response. The classes can be clearly identified on seismic inline A-A' (Fig. 6.9).

The simulated classified datasets were analysed in terms of relative abundance of framework entities (Fig. 6.13). These results, in combination with their shape and aerial distribution led to the following interpretation:

Class 1 (Red on Fig. 6.5) corresponds to the (poor reservoir) wet dune distribution of the sedimentary facies map of the Wustrow interval. The simulation specification indicated a thick Lower Wustrow with wet dunes predominating.

Class 2 (Yellow on Fig. 6.5) corresponds to the (good reservoir) shoreline sands of the sedimentary facies distributions. The simulation specifications emphasised a thicker Upper Wustrow with a predominantly shoreline composition. Class 2 occurs to the north of the area and adjacent to the western margin of the graben.

Class 3 (Green on Fig. 6.5) follows the trend of sabkha and southern fan deposits. The simulation specification detailed a thick Lower Wustrow with a large percentage of wet dunes with a relatively large silty/shale content. The UVQ class may be picking up the effect of interbedded shale in both the sabkha and distal alluvial fans. Alternations between class 2 and 3 may indicate belts of shoreline deposits separated by interdune sabkhas.

Class 4 (Cyan on Fig. 6.5) corresponds strongly to the position of marginal fanglomerates on the sedimentary facies map. While the simulation specification is similar to that of Class 1, the seismic signature is a hybrid of the Class 1 and 3. This could represent the interbedded and more random nature of acoustic impedance distributions within interfingering fan units.

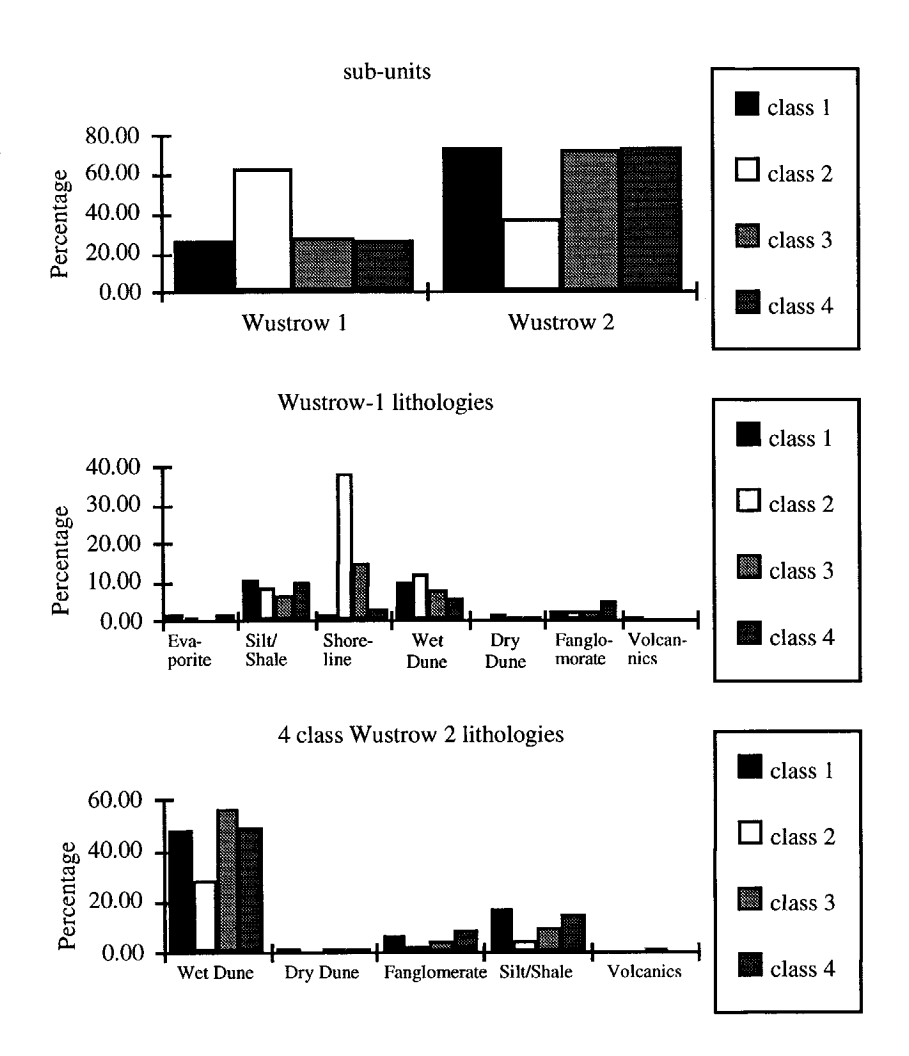


Fig. 6.13

Relative thickness of Wustrow framework entities per class. Classes were generated by applying the trained UVQ to a dataset comprising 500 simulated wells. The total Wustrow thickness per class sums to 100%.

This concludes the discussion on the Rotliegend example. In the following section the Middle Eastern case study will be described.

6.3 Middle Eastern case study

6.3.1 Available data

The Middle Eastern study area is covered by a 1992 vintage 3D-seismic dataset. The data have been acquired using vibroseis sources generating 10-80 Hz frequencies with a 10 s sweep length. The field layout consisted of 4 parallel receiver lines, each with 96 geophone groups. Source and receiver group intervals were 50 m, yielding a 25 by 25 bin size with a nominal fold of 24. Acquisition sampling rate of 2 ms was resampled to 4 ms in processing. A post-stack zero-phasing filter was applied at the end of the processing sequence which included linear noise removal using a Radon transform, 2 passes of residual statics and velocity analyses and post-stack D2D finite difference migration.

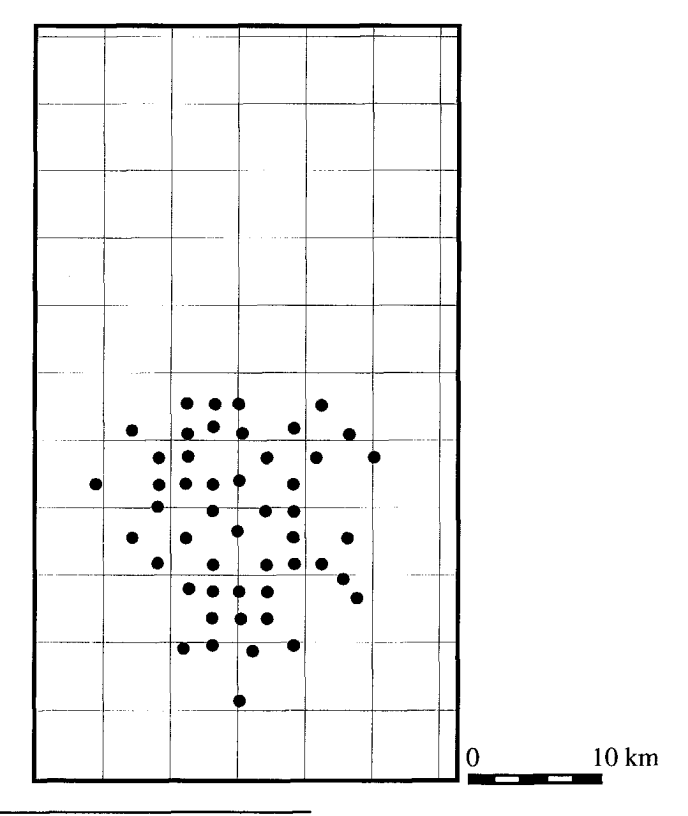


Fig. 6.14 Well locations

Several seismic horizons were mapped by the client. The top reservoir horizon has been used in this study as the reference horizon (Fig. 6.17).

Horizon maps in time and depth at top carbonate, top reservoir and top source unit were available on paper copies.

The well database consisted of 88 wells. Not all wells had a complete set of information, however. Eventually, 61 wells were loaded into GeoProbe, 49 of which fell inside the 3D-seismic data area (Fig. 6.14). For these wells, the following information was available on paper:

- Full suite of logs; most wells had FDC/CNL, BHC-Sonic, Gamma-ray, Resistivity and Calliper, some wells also had Dipmeter, Induction, Formation micro-scanner and ELAN-litho logs
- Correlation panels
- Core descriptions
- · Well log and sample description
- Well testing reports
- Cluster formation analyses reports
- Composite logs
- Formation tops; print out from the corporate database
- Sedimentology reports
- Various other reports on casing, perforations, formation analyses etc.

6.3.2 Geology

6.3.2.1 Tectonic Overview

The area is located onshore in the Middle East. Early Palaeozoic epicratonic sagging of the crust led to the deposition of marine sediments on a Precambrian basement complex (Beydoun, 1991). Deposition took place from the Early Cambrian till the Devonian. Orogenic rejuvenation towards the end of the Palaeozoic (al Laboun, 1986) led to uplift which resulted in a Late Devonian unconformity and erosion of the Early Palaeozoic sediments to the level of the Silurian shales. Late Carboniferous to Early-Middle Permian terrigineous clastics were then deposited. Continued margin subsidence resulted in a marine transgression and the development of

extensive carbonate shelves. Deformation took place during the Cretaceous which resulted in gentle folding and the development of the trap structures in the field. Additional deformation took place during the Early Tertiary as a result of the collision of the Arabian plate with Asia. The field architecture is a gentle structural dome with a parasitic fold on the limb of a regional monocline.

6.3.2.2 Stratigraphy

The zone of interest can be divided stratigraphically into three components. The lowermost formation is the 'source' unit comprising shales which are unconformably overlain by the 'reservoir' formation which in turn is conformably overlain by the 'carbonate' formation comprising carbonates and anhydrites.

Source Unit

Within the study area the source unit comprises marine shales with a moderately high clay content and correspondingly high gamma ray signature. The shales are massive in nature where encountered.

Reservoir Formation

The reservoir formation is of Late Carboniferous to Early Permian in age. Its base is an unconformity which in the study area is eroded into the top of the source unit shales (Fig. 6.15). The reservoir comprises terriginous clastic material in an alluvial plane setting. To the south of the study area the lowermost beds of the formation are comprised of massive silty-shales which appear to infill the erosion topography at the basal unconformity. In the east of the area there is a trough like structure which is infilled with massive sands. It is impossible to correlate major events from well to well over any great distance. No laterally extensive vertical layering in the reservoir unit is discernible. The final few beds in the reservoir unit comprise restricted marine sandstones with caliche and root horizons towards the top. There is occasionally evidence for a thin limestone horizon below the carbonate unit. The upper surface of the reservoir unit can be considered to be a peniplain. The upper beds mark the development of a marine transgression and development of a carbonate shelf.

Carbonate Formation

Conformably overlying the reservoir formation are the capping carbonates and anhydrites of the carbonate unit. This formation is of Middle Permian to Late Permian in age. The carbonate unit represents the formation of an extensive evoporitic carbonate platform shelf (Murris, 1980) and is divided into four members A, B, C and D. The lowermost carbonate is the D member which was included in our study. The member comprises well

bedded limestone-shale alternations at its base. These alternations become progressively more massive towards the top of the D unit where the limestones become more dolomitic. The succession contains more bedded anhydrite towards the upper D member which is capped by a massive anhydrite layer. All well logs were blocked to the top of the massive D unit anhydrite. The D unit is constant and unvarying throughout the study area and was in turn overlain by a thick succession of C member carbonates.

6.3.2.3 Depositional facies and reservoir geology

Oil is trapped in the sands and silts of the reservoir formation. The reservoir unit is capped by the D unit carbonate-shales in a gentle dome structure. The oil column is limited to the upper beds of the reservoir, which has a maximum thickness of app. 200 m in the study area. The source unit shales are considered regional source rocks by Beydoun (1991) and are possibly the source for the oil in the field.

Reservoir sedimentology

Both wireline logs and cores show discrete lithological divisions with very few fining or coarsening upward trends. The blocky nature of the beds and the lack of distinct fining upwards trends is indicative of bedload channels on a riverine or montaine alluvial plain (Galloway and Hobday, 1983). The terrestrial alluvial-plane deposits, typical of the reservoir unit, give way to marine dominated sandstones with rootlet beds and caliche horizons in the top few metres prior to the onset of evaporitic shelf conditions.

The silty sands are indicative of suspended load or lower energy deposits. On the flood plain, this may take the form of sheet-like crevasse splays. The flood plain sands are well bedded and interspersed with distributary channels and braided river deposits. There is little clay present throughout the reservoir unit. What little there is, appears to be confined to clay plugs of abandoned channels. The shales, silts and very fine grained non-porous sandstones were considered to be one lithotype for the purposes of this study, namely low-energy, suspended load units.

The channels and associated sands may be clustered into trends that were initially controlled by the erosional relief of the basal unconformity. The laterally non-correlatable lower reservoir unit has a tendency to be massive (either silty shale or sandstone) in the south of the study area and in the zone of the trough. These trends may have become less important as the palaeorelief was filled up and the peniplain developed.

Reservoir geology

The reservoir formation shows all the features of a classic labyrinth type reservoir (Weber & van Geuns, 1990). The reservoir formation deposits are predominantly alluvial plain deposits with reduced sand:shale ratios. From well-to-well, there are no laterally correlatable horizons within the reservoir formation, even though the top reservoir can be mapped on seismic data. Earlier interpretations by the client had divided the reservoir unit into an A and B member with a 'silt plug' in the middle of the A member. There seems to be no evidence for this division, however. Within the area of the field, there are no lacustrine or laterally extensive clay horizons throughout the formation that would act as field wide permeability barriers or seals.

High production rates occur in all sandstone types, including the thinner laminated sands. The production rate depends on the presence of sandbodies within the oil column and is seemingly independent of structural setting and stratigraphic position within the formation. Considerable volumes of oil can be produced from relatively thin (3-8 m) sandstone intervals.

Laminated sands of the alluvial plain, while thinner and less likely to interconnect, may be more laterally extensive. Channel sands, however, may be locally thicker and laterally less extensive but more likely to interconnect with other bodies at different levels. More massive flow units may trend parallel to larger channel cluster trends. It is impossible to predict distribution and connectivity of the various sand bodies from the well data. Understanding the distribution of these sandstone flowunits within the structural closure is crucial in understanding the reservoir response. The objective of the study was to extract geological information from the 3D-seismic data that would help in delineating and describing the complex reservoir architecture of this field.

6.3.3 Integration framework

The framework for the Middle Eastern case study is shown in Table 6.6. Special attention was given to the reservoir formation, as it was the target interval. Using a combination of the gamma-ray and formation analysis logs, four genetic sub-units were recognised within the reservoir unit. These units were averaged over 50 foot intervals and plotted on scaled depth sections at each well location. The genetic units served as an indicator for the average depositional energy (grainsize/porosity). Also plotted were production rates for each unit for each well. No spatial relationships or correlations were observed, underlining the high degree of stochastic behaviour in this labyrinth type reservoir.

The framework for this study is as follows:

- The framework consists of 4 main units. Each unit has one or several sub-units (geological or seismic). The third column shows the lithologies used, and the fourth column shows the GeoProbe codes given.
- The four main units occur sequentially as shown in the framework. Subunits within the carbonate units occur sequentially while sub-units within the reservoir can vary. The reservoir unit has been divided into four sub-units: Massive Type 3, Massive Type 2, Massive Silt-Shale, and Laminated. This subdivision is based on common grouping of certain lithologies observed in the Formation Analysis logs and corresponds to the genetic units of the formation. In individual wells, the sub-units order may vary. Sub-unit could be completely absent or present multiple times.

Unit	Sub-unit	Lithology	Code
Carbonate C	Carbonate	Carbonate	crbc.crb.crb
		Shale	crbc.crb.shl
Carbonate D	Massive	Anhydrite	crbd.msv.anh
		Carbonate	crbd.msv.crb
	Anhydrite	Anhydrite	crbd.anh.anh
		Carbonate	crbd.anh.crb
		Shale	crbd.anh.shl
	Alternating	Carbonate	crbd.alt.crb
		Shale	crbd.alt.shl
Seal	Seal	Seal	seal.seal
Reservoir	Massive Type 3	Type 3 Sand	res.mt3.t3s
		Silt/Shale	res.mt3.slt
	Massive Type 2	Type 2 Sand	res.mt2.t2s
		Silt/Shale	res.mt2.slt
	Massive SiltShale	Silt/Shale	res.msl.slt
		Type 2 or 3 Sand	res.msl.snd
	Laminated	Type 2 or 3 Sand	res.lam.snd
		Silt/Shale	res.lam.slt
Source	Marine	Shale	sou.mar.shl

 Table
 6.6
 Middle Eastern case study integration framework

- Each sub-unit is assigned several lithologies. The lithological composition of an interval determines a particular sub-unit type. Type 3 sandstones, for example, can only occur in Massive Type3 sub-unit or Laminated sub-unit while Type 2 sandstones will only be found in Laminated or massive Type 2. Lithologies could occur in any order, repeat themselves, or be completely absent.
- Oil-bearing sands occur only in the reservoir unit. Essentially, all sand lithologies, regardless of which sub-unit they belong to, are considered to be producing if they occur within the oil column. The fine grained non-producing sandstones, silts and shales were grouped into one lithotype (Silt/Shale) for the purposes of this study and are considered waste zones.
- There is only one hydrocarbon column, which is attached to the overlying seal at the base of the carbonate unit.

GeoProbe recognises hydrocarbon columns by the seal to which the column has been attached. If the lithology of the layer directly overlying the reservoir can vary, as in this case, GeoProbe has a problem. For this reason a virtual seal has been introduced immediately above the reservoir unit. In the factual wells and the simulations this seal is given a constant thickness of 0.1 foot.

6.3.4 Segmentation

In this case study it has been attempted, without success, to train Multi-Layer-Perceptrons to recognise the weighted average impedance and the overall thickness of the reservoir unit from its seismic response. In separate runs, training and test datasets were constructed from simulated data and from factual data respectively. It was concluded that direct inversion could not be used to quantify properties of the reservoir unit. It was decided to apply the segmentation approach in order to visualise and interpret the resulting seismic patterns. Segmentation requires the UVQ network to be trained on a representative seismic dataset. In the examples described in this thesis, the representative seismic dataset was created by selecting 25 (5x5) traces around the factual well locations (Fig. 6.14). Seismic data was selected in a gate of -50 to +50 ms around the top reservoir reference horizon. This seismic response was balanced using a 100 ms RMS

equalisation¹. A gate of -8 to 32 ms around the reference horizon (10 samples) was used to train the UVQ's. The seismic response of the reservoir unit has, in this way, been segmented into 2, 3 and 4 classes, (Fig. 6.21, 6.24 and 6.25, respectively). Given the remarkably constant acoustic impedance profile of the overlying carbonate unit and the unvarying nature of the source unit, any variation in the seismic must be due to lateral variations within the reservoir formation.

Comparison of the UVQ segmentation maps reveals general trends that are present on all maps. The dominant channel-like trends in the data are apparent, even on the 2 class segmentation map. Comparison with the basal unconformity depth map (Fig. 6.15) shows that the basic trends are related to the palaeo-topography.

Channel distribution may have become more random as the alluvial plain matured and relief diminished. The channel-like features are major sedimentary distribution trends. They consist of stacked deposits of massive sands and silts. The areas outside the channel-like trends have higher compositions of laminated, well-bedded, alluvial-plain sub-unit. The layered and more heterogeneous impedance distribution is reflected in the higher frequency content of the seismic response.

Comparison of the 2 and 3 class segmentation maps reveal that the channel-like features have been sub-divided into two classes. An interesting seismic pattern is mapped in the centre of the field (Fig. 6.24). The shape, location and aerial distribution indicated the tool was indeed picking up the depositional architecture. The three seismic classes were analysed using the factual well information in order to attach a geological significance to these patterns.

The 49 factual wells were combined with the factual seismic traces at the corresponding well locations in a -50 to 50 ms window either side of the reference horizon. These traces were offered to the UVQ classifier with 3 classes after trace balancing over the 100 ms window. The impedance logs and seismic responses of the resulting classes are shown in Fig. 6.16 and 6.17, respectively. The classification results are indicated on seismic inline A-A' (Fig. 6.26).

Trace balancing was applied because it was anticipated that simulated wells with corresponding synthetic seismic traces would be used in the analysis. It was later decided to analyse factual wells only, making the trace balancing step unnecessary.

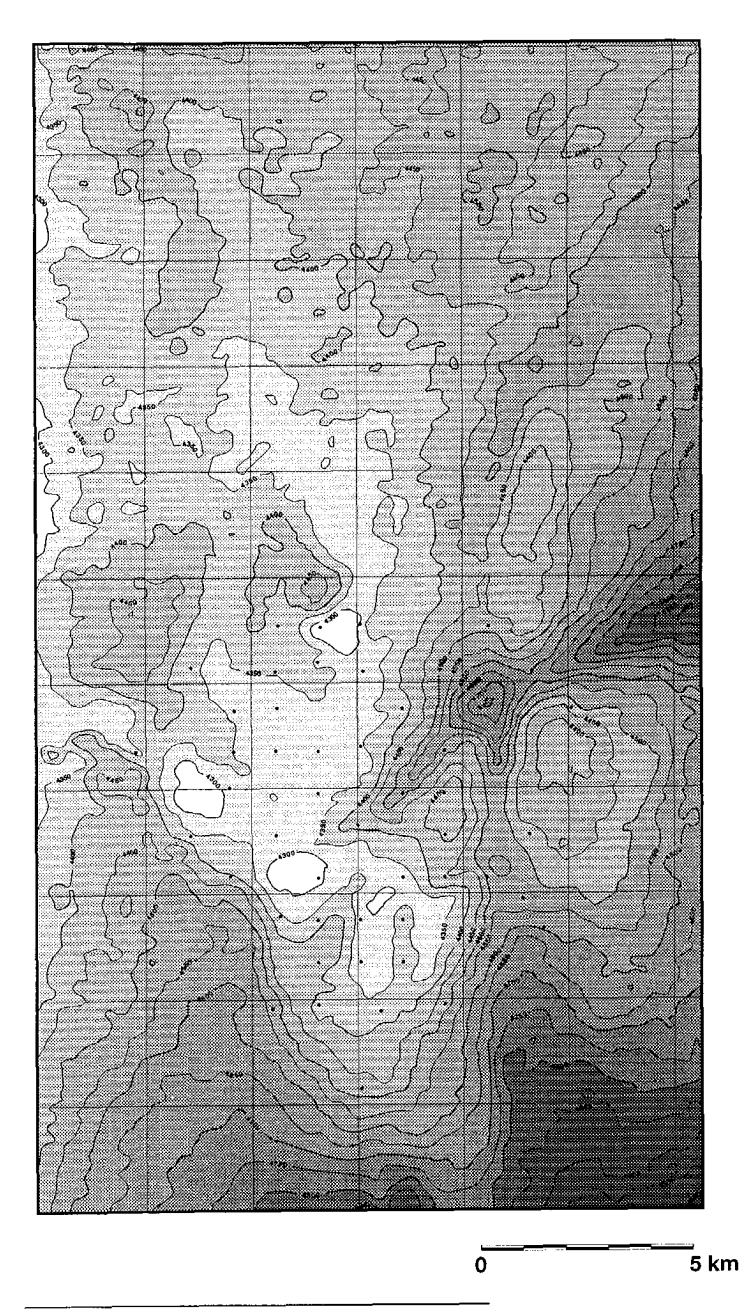


Fig. 6.15 Basal reservoir unconformity.

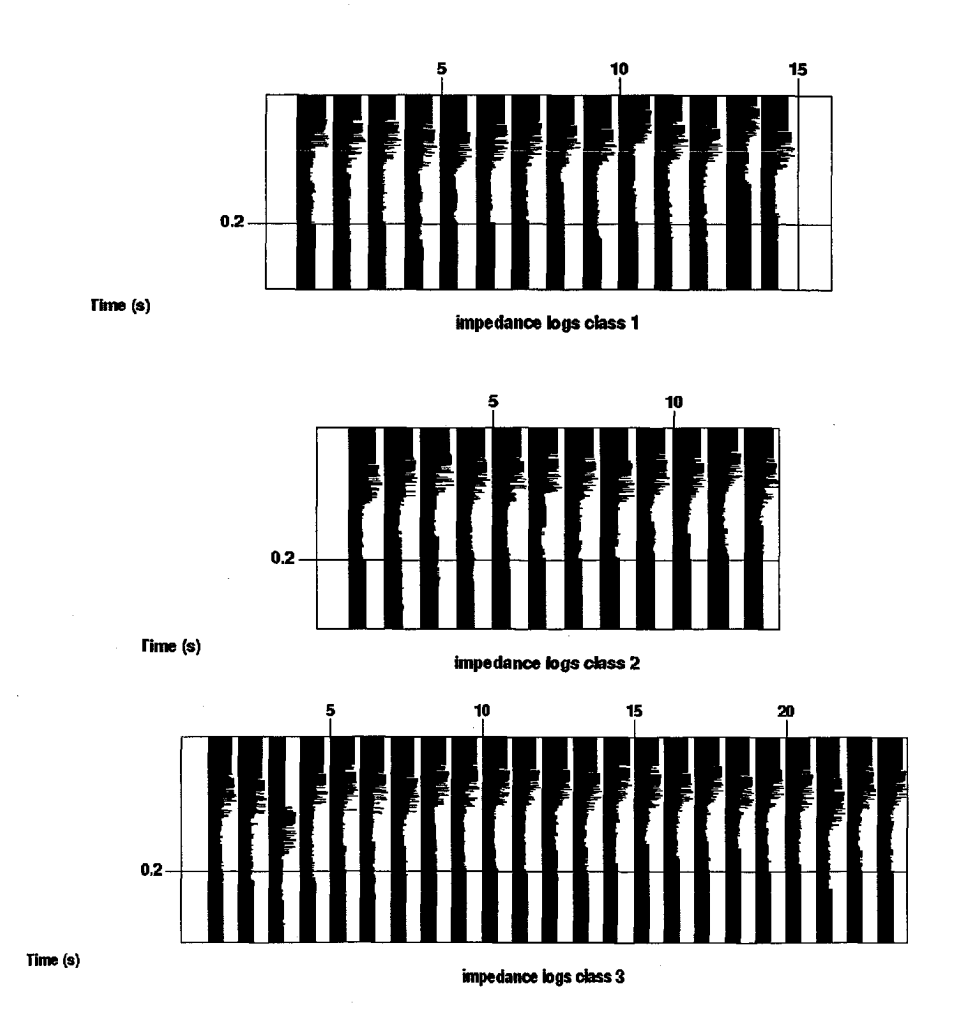
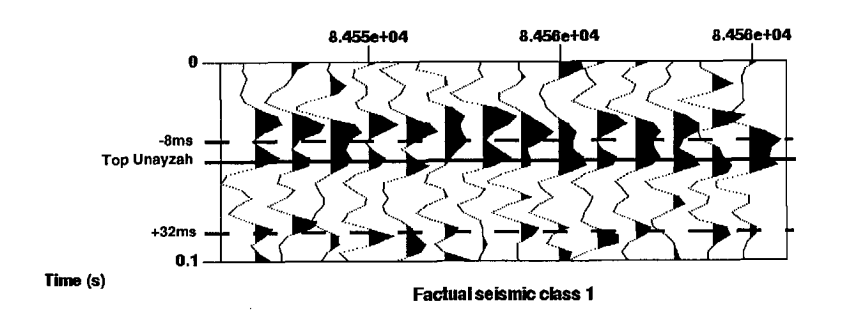
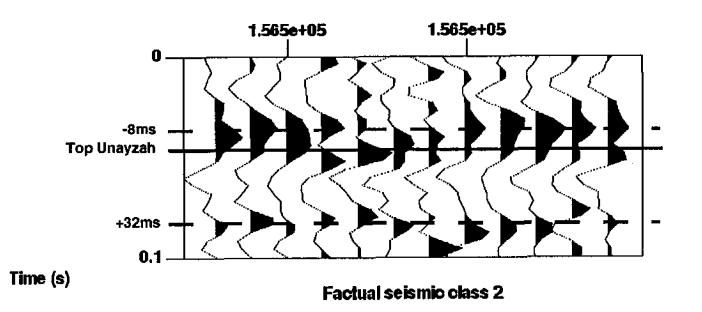


Fig. 6.16 Impedance logs of factual wells classified by the trained UVQ network into 3 classes. Classification is based on the seismic response within a time-gate of -8 to 32 ms relative to the top reservoir horizon. The top reservoir reference marker is floating at app. 150 ms at the base of the alternating high impedance layers.





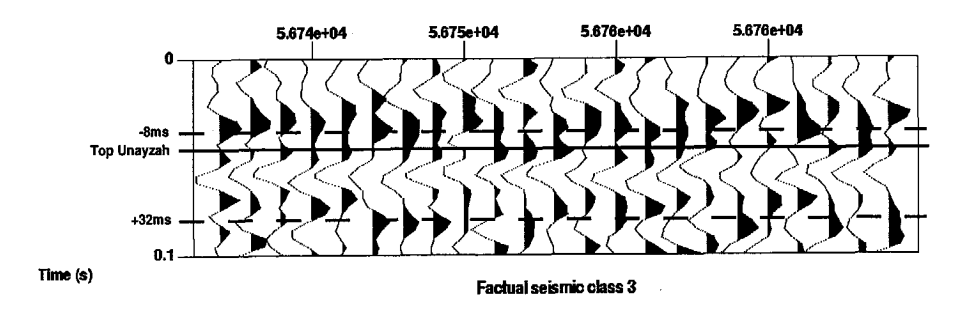


Fig. 6.17 Factual seismic traces at factual well locations, classified by the trained UVQ network into 3 classes. Classification is based on the seismic response in a gate of -8 to 32 ms relative to the top reservoir horizon.

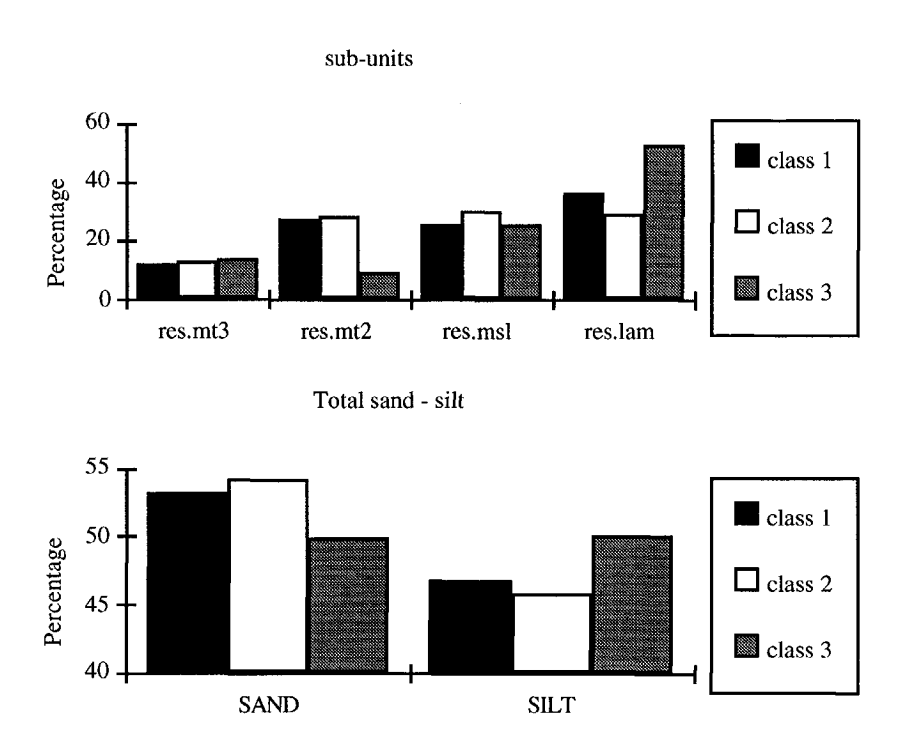


Fig. 6.18 Relative proportion of framework sub-units per class (top) and relative proportion sands and silts (bottom). Total thickness of the reservoir unit per class equals 100%.

The seismic classes are characterised by:

- a small positive kick in the middle of the broad white loop for class 1
- a slope in the lower part of the broad white loop for class 2
- a higher frequency content for class 3

The stratigraphic and lithologic differences have been analysed per class (Fig. 6.18 and 6.19). These analysis in combination with the shape and aerial distribution of the seismic patterns have led to the following geological interpretation:

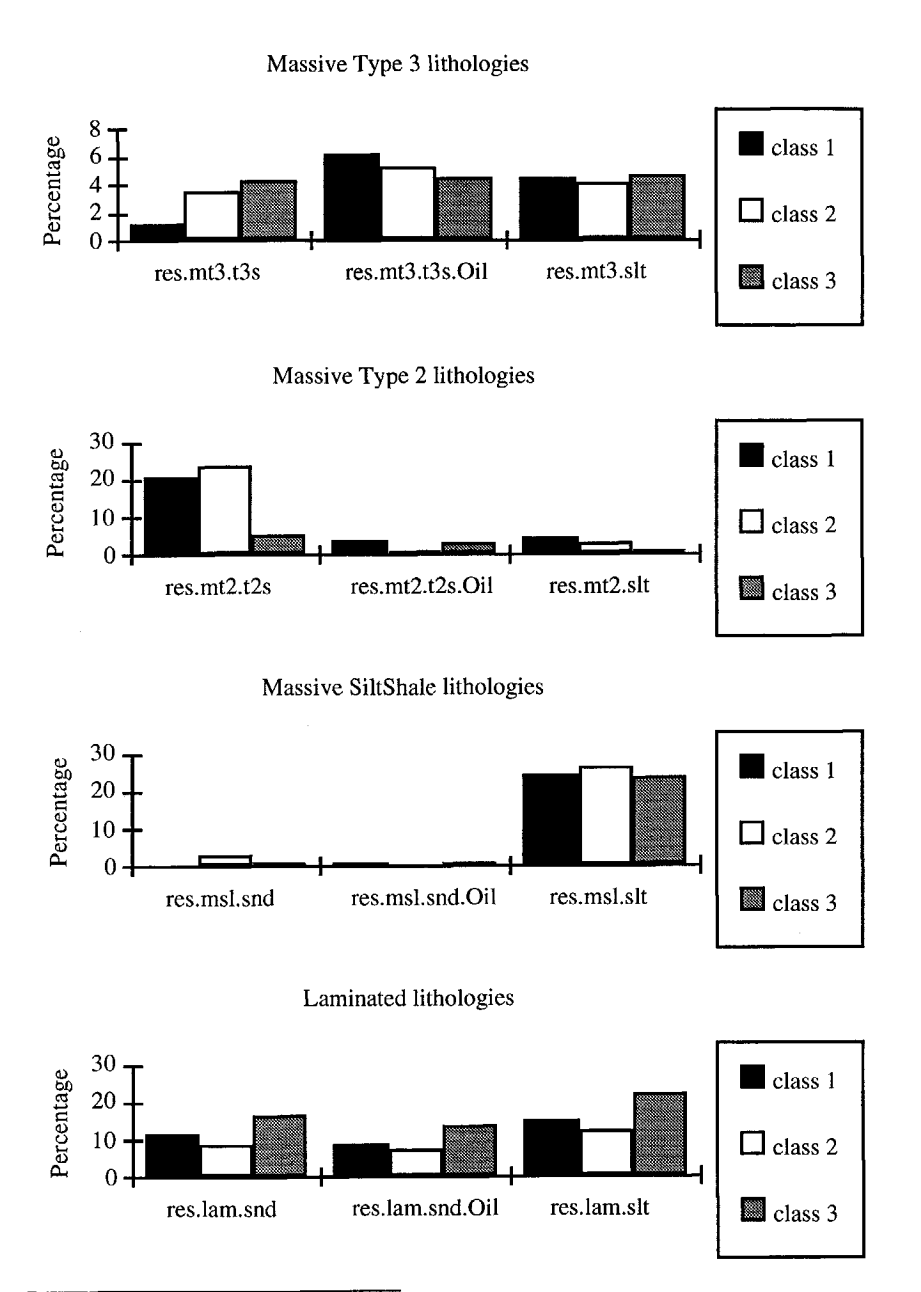


Fig. 6.19 Relative proportion of framework litologies per sub-unit and per class. Total thickness of the reservoir unit per class equals 100%.

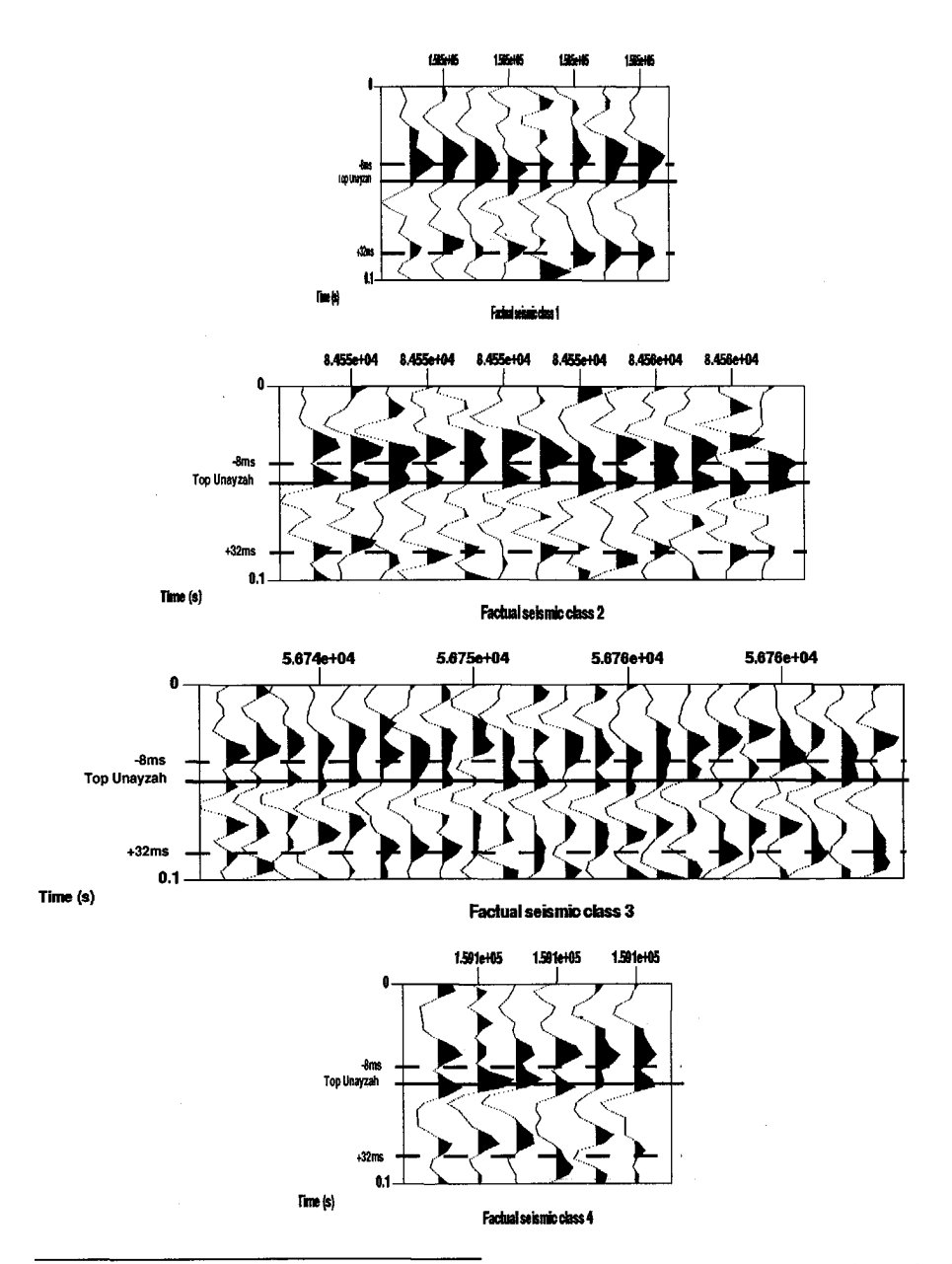


Fig. 6.20 Factual seismic traces at real well locations, classified by the trained UVQ network into 4 classes. Classification is based on the seismic response in a gate of -8 to 32 ms relative to the top reservoir horizon.

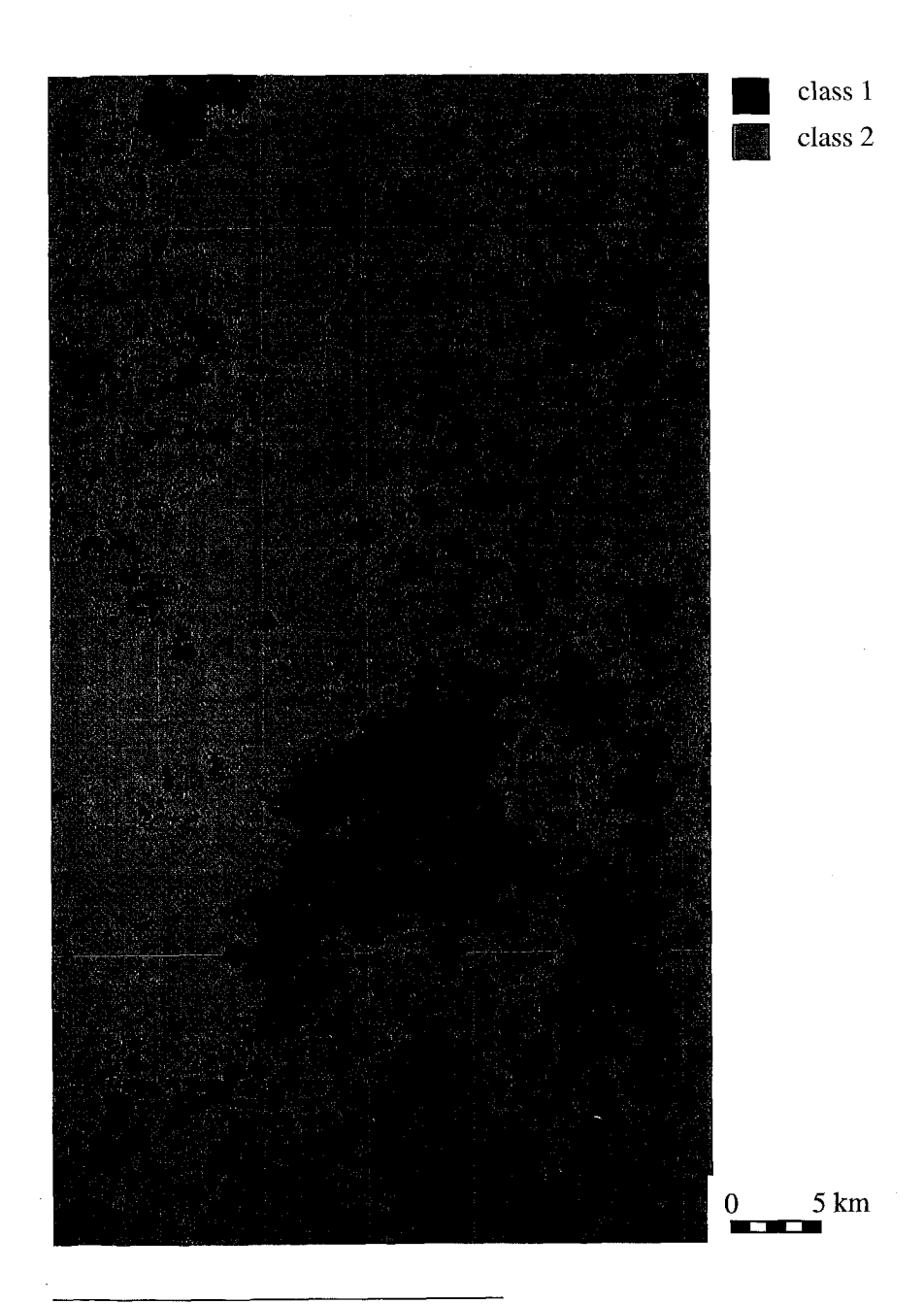


Fig. 6.21 Segmentation result for 2 classes.

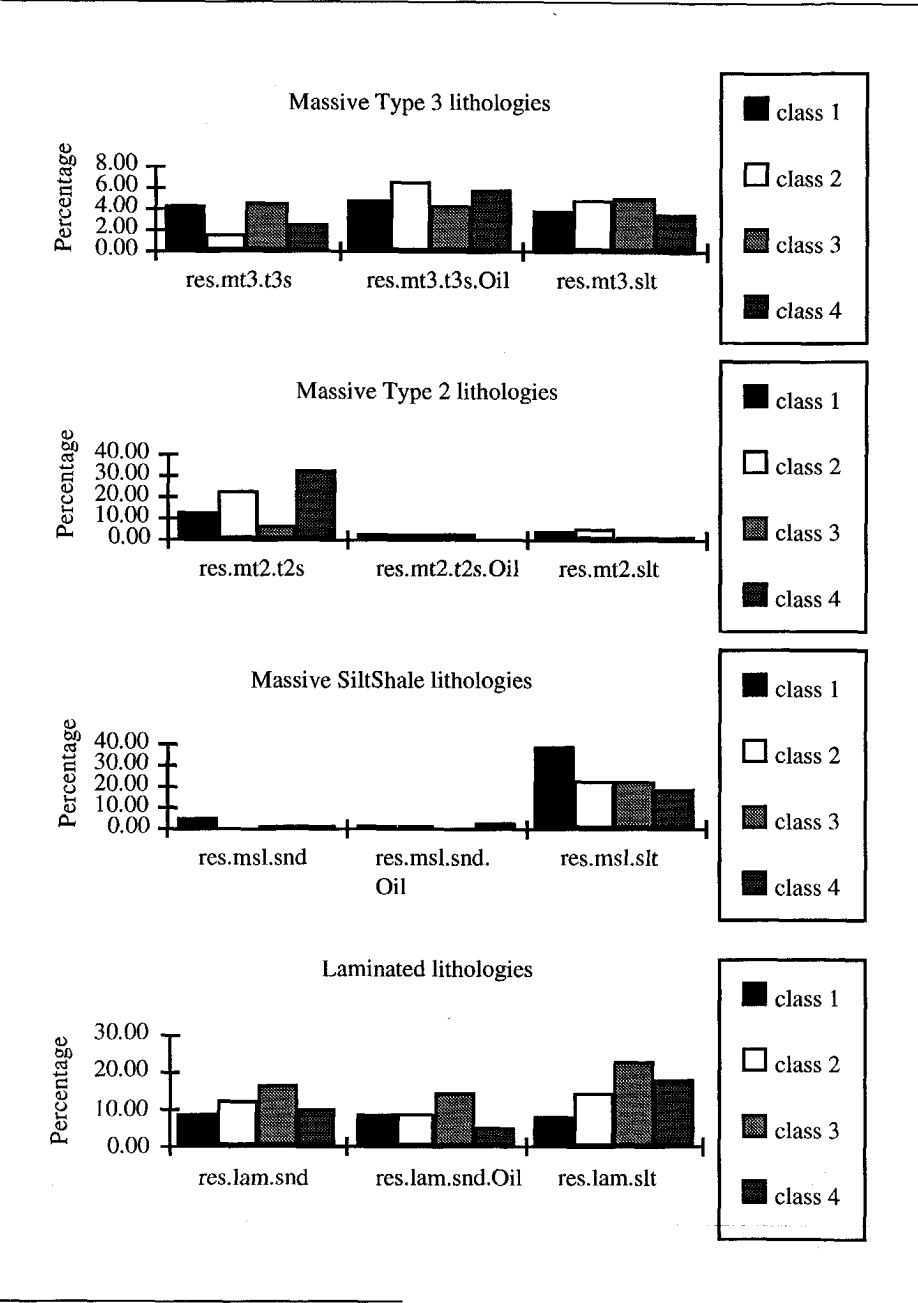


Fig. 6.22 Relative proportion of framework litologies per sub-unit and per class. Total thickness of the reservoir unit per class equals 100%.

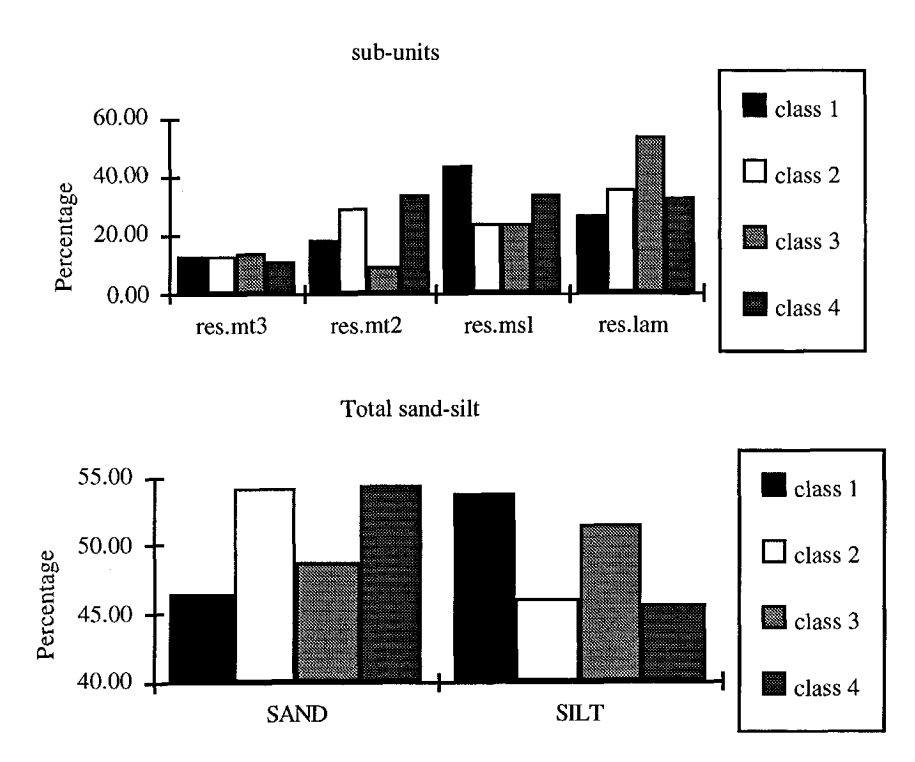


Fig. 6.23 Relative proportion of framework sub-units and relative proportion sand and silt per class. Total thickness of the reservoir unit per class equals 100%.

• Class 1 maps inside a channel-like trend. The sediment composition of the reservoir shows a relative abundance of the massive sub-unit types (either sand or silt). The overall sand percentage for this class is 53%. The massive sands and silts in this class are most likely to be distributary channel and braided river deposits while occasionaly point bars may be also present within the braided trend. Lateral continuity of individual sandbodies is limited, but sandbodies are likely to erosionally interconnect in such environments. Examination of the wells showed the positive peak between the double trough to be associated with a possible lacustrine level in the middle of the succession. This interval was characterised by thick clays or large washouts on the log data. The wells in this class do not support the theory that this pattern is associated with a "silt-plug" but there is a tendency towards non-bedload sedimentation over intervals in the log.

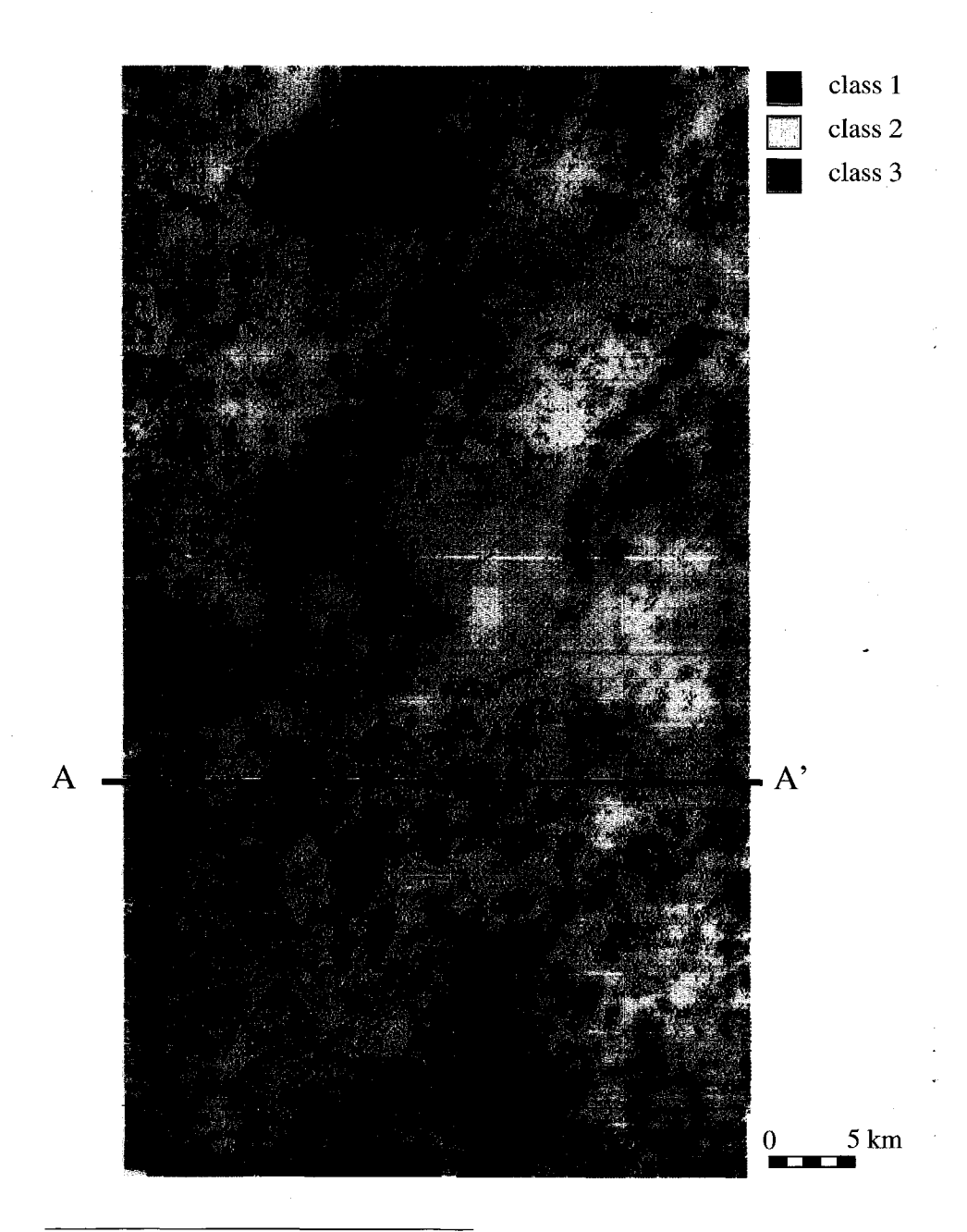


Fig. 6.24 Segmentation result for 3 classes.

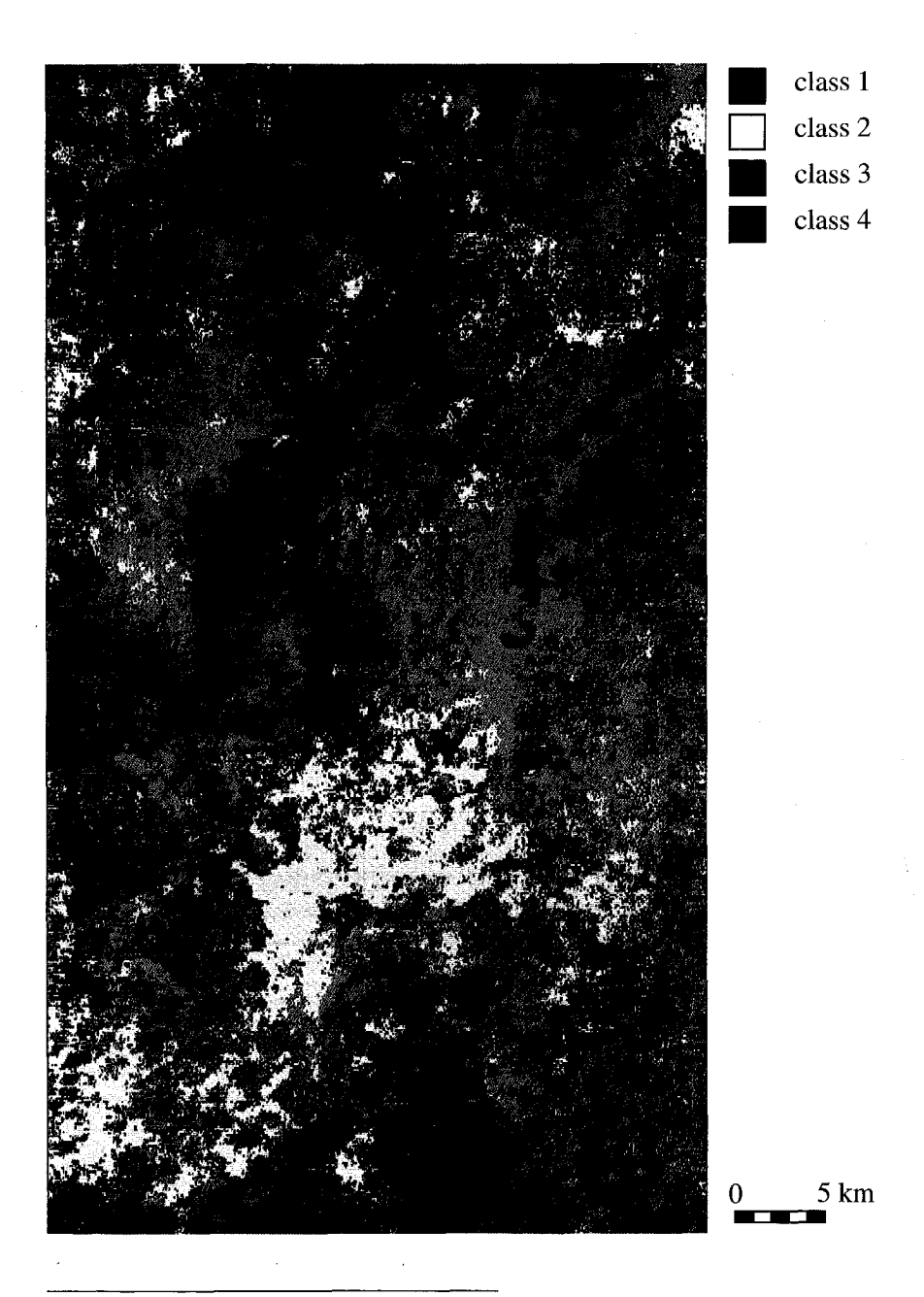


Fig. 6.25 Segmentation result for 4 classes.

• Class 2 also maps inside the channel-like trend. The sediment composition is very comparable with that of class 1, with a relative abundance of the more massive sub-unit types. Massive sands and silts are predominantly distributary channel and braided river deposits. Overall sand percentage is 54%. The positive peak between the double trough might be associated with a possible lacustrine level. However, in this class, the level is multiple and generally occurs higher-up in the succession. The main difference between class 1 and class 2, is a gentle stepwise trend for acoustic impedance towards the base of the succession in class 2. This trend might be geologically explained by differences in diagenesis and early compaction of the topographic fill.

• Class 3 maps outside the channel-like trend. The sediment composition shows a high abundance of the laminated, well-bedded sub-unit. The overall sand percentage is 50%. The laminated sands appear as sheet-like crevasse splays, interspersed with flood-plain silts. Lateral continuity of the sheet-like sands is probably greater than the continuity of the sands in classes 1 and 2.

It can be concluded that interpretation of general trends in the seismic patterns can be confidently made for the segmentation result with two seismic classes. Interpretation of the segmentation run with three classes, is more complicated. The difference between massive trends and floodplain are also clearly revealed on the three class segmentation result. However, the seismic classes 1 and 2 are too similar for the analysis to reveal any differences. Given the remarkably constant impedance of the overburden, there seems to be no doubt, however, that the seismic patterns are related to geological variations within the reservoir unit. The analysis results indicate that the geology within the seismic classes is overlapping. Consequently, it seems logical to also analyse the 4 class segmentation result.

Comparison of the segmentation maps with 3 and 4 classes (Fig. 6.24 and 6.25, respectively) reveals that the basic difference is a further sub-division of what has been mapped as class 2 in the 3 class segmentation run.

The 4 class UVQ classifier was applied to the 49 balanced factual seismic traces. The classified seismic responses are shown in Fig. 6.20. Comparison with Fig. 6.17 reveals that:

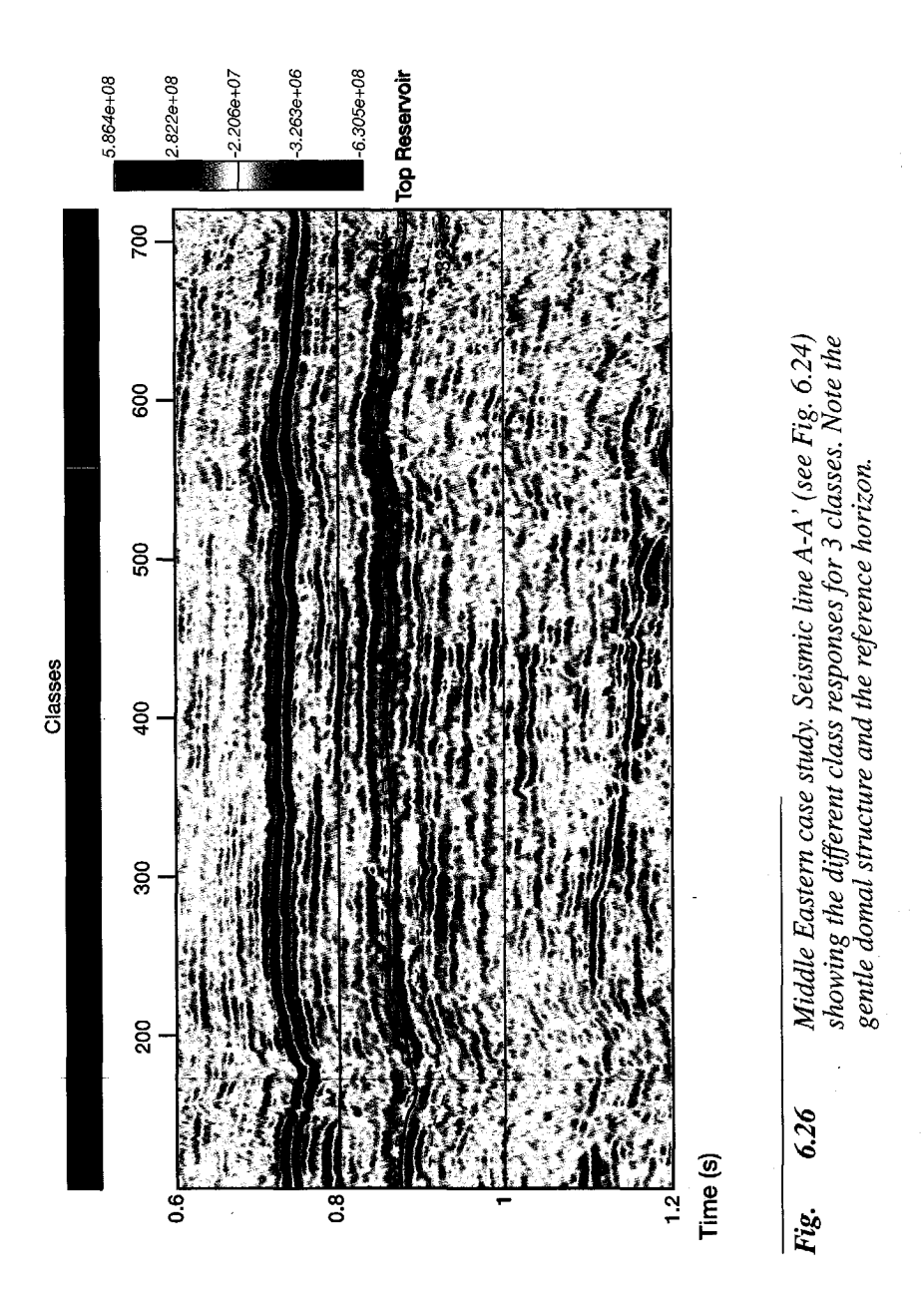
• Class 1 is characterised by the slope in the lower part of the broad white loop in combination with the small positive kick in the middle of the broad white loop.

• Class 2 is characterised by the small positive kick in the middle of the broad white loop (class 1 in the 3 class UVQ, only one well has not been classified in this class by the 4 class UVQ)

- Class 3 is characterised by the higher frequency content (also class 3 in the 3 class UVQ, only one well has not been classified in this class by the 4 class UVQ).
- Class 4 is characterised by the slope in the lower part of the broad white loop and the absence of the small positive kick in the middle of the broad white loop.

The analysis results are shown in Figs. 6.22 and 6.23. The separation of the classes in terms of the sedimentological composition has improved with respect to the 3 class result (Figs. 6.18 and 6.19). The interpretation for these 4 classes is as follows:

- Class 1 (red in Fig. 6.25) has the largest amount of the massive Silt/Shale sub-unit (43%) and the largest amount of the silt/shale lithology (38%). The overall sand content is 46% (Fig 6.23) which is the lowest for any class. The predominance of silty shale in the massive trend indicated by the analyses points to this class being the trend of abandoned channels that filled with ponded and suspended-load sediments. Porous, high producing, sands do occur but are less likely than in the other classes.
- Class 2 (yellow in Fig. 6.25) while containing relatively high percentages of Massive Type 2 and Laminated sub-units (29 and 36%, respectively, Fig. 6.23) also contains the highest percentage Type 3 sand lithology producing oil (Fig. 6.22). This lithology is the most productive of all the sand lithologies due to its coarseness and high porosity and permeability. Class 2 is the most silt/shale poor and represents a sand rich channel trend whose distribution (NE-SW, Fig. 6.25) may have been controlled by the palaeo-relief shown in Fig 6.15. This class statistically contains the most oil saturated Type 3 sands. These sands are the most productive if located within the oil column and, hence, class 2 should be considered a major target if located within the area of structural closure of the field.

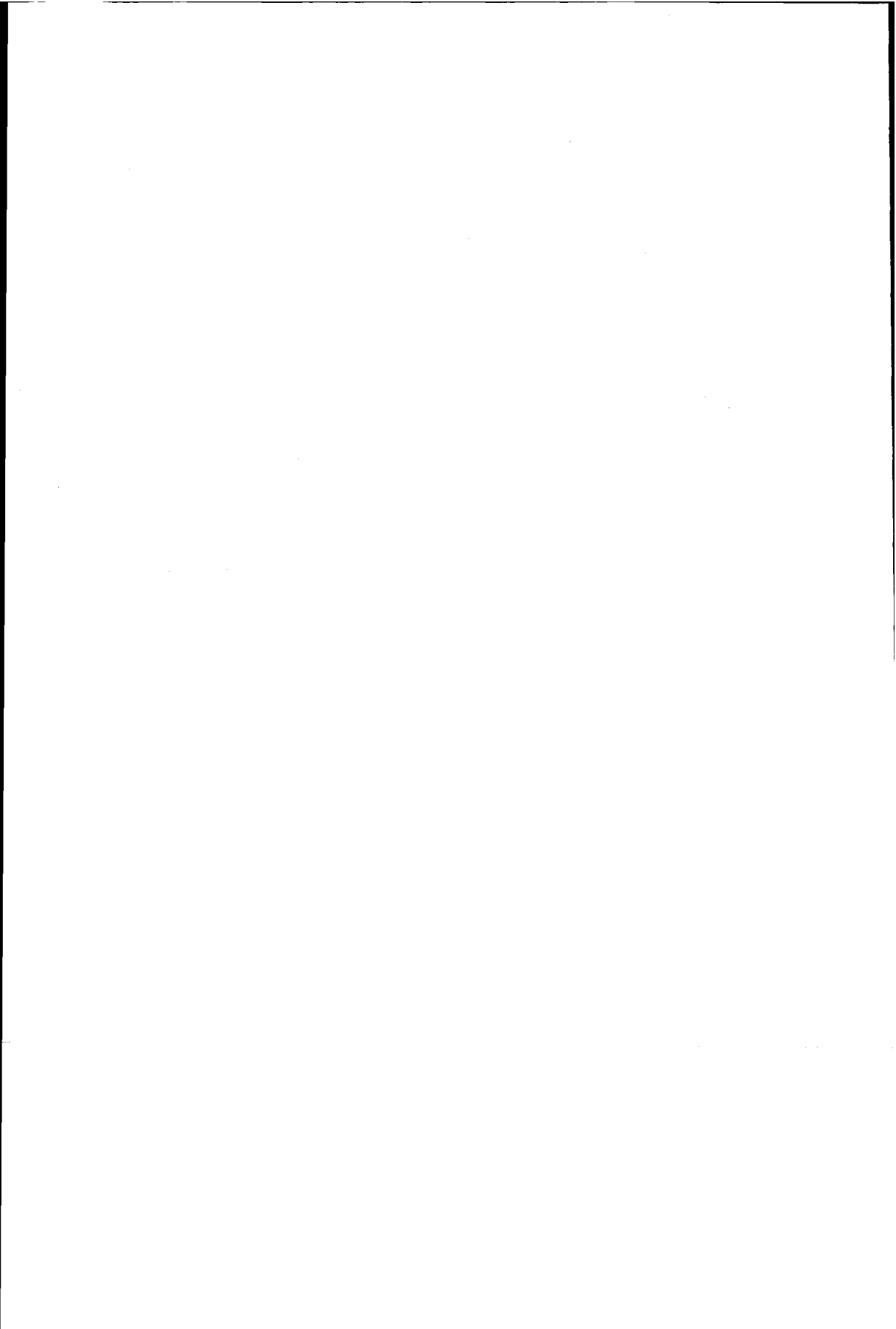


• Class 3 (green in Fig. 6.25) has the highest percentage of the Laminated sub-unit (53%). While the overall sand percentage is only 49% and the class is high in silt, high production rates can be achieved from the coarser, of what are thin and probably laterally more extensive, sheet sands. The Laminated sub-unit of Class 3 represents the well-bedded flood plain deposits where sheet sand and suspended load deposits alternated away from the massive channel trends. Class 3 corresponds to the locations of the highs in the palaeo-topography (Fig. 6.15).

• Class 4 (blue in Fig. 6.25) has the highest percentage of the Massive Type 2 sub-unit (33%) in addition to the laminated sub-unit (32%). The overall sand content is high (54%). Examinations of the wells associated with Class 4 show the Massive Type 2 sub-unit to be predominantly associated with very massive Type 2 sand beds that appear to fill in the palaeo-relief of the base reservoir unit. The aerial distribution of this class corresponds to this hypothesis while the relatively high percentage of Laminated sub-unit would indicate that the relief had been filled and a 'normal' alluvial distributory architecture had been established halfway during the deposition of the reservoir formation.

6.4 Conclusions

In this chapter the total space inversion method has been applied to two case studies. It has been shown that in both studies useful geological information could be extracted from the seismic signals. Especially the horizon slice segmentation approach yielded exciting results. In the Rotliegend study, it has been possible to map the extent of the good reservoir shoreline sands by segmentation. In the Middle Eastern study, the segmentation results revealed seismic patterns that could be related to sediment architecture and deposition of genetic units.



PRACTICAL ASPECTS

7.1 Introduction

In the previous chapter two case studies have been presented. It has been shown that, in both cases, interesting results were obtained with the total space inversion method. The segmentation approach, especially, yielded exciting results. As with other seismic reservoir characterisation techniques, total space inversion is not a trivial process. The reason being that data types and knowledge from different sources and disciplines need to be combined for an optimal result (Chapter 2).

In this chapter, practical aspects related to the total space inversion method will be discussed. First, seismic processing and the importance of preserving amplitudes in the seismic processing sequence is reviewed. This is followed by a discussion on trace balancing. This is a necessary, but unwanted, process in the inversion scheme. Trace balancing is required when simulated data and factual data are both taken into account. Then the importance of the reference horizon is highlighted. Finally the applicability of total space inversion and other post-stack seismic reservoir characterisation techniques are discussed.

7.2 True amplitude seismic processing

The aim of seismic inversion methods is to relate variations in seismic response to variations in geology, especially those associated with lithology, porosity and fluid content. It is, therefore, of great importance that no artificial variation is introduced during acquisition and processing of the

seismic data. This implies that the total seismic wavefield, both signal and noise events, must be sampled correctly during the acquisition phase. The noise can then be removed in the subsequent processing phase. The processing sequence should be aimed at preserving the amplitude information of the seismic refection events. This is called true amplitude processing.

In any processing sequence the recorded amplitudes must be corrected for attenuation, caused by spherical spreading, reflection and transmission losses and absorption. Spherical spreading refers to the decay in amplitude caused by the fact that the seismic energy is spread over an increasing area as the wavefront spreads out. Transmission and reflection losses occur at each interface and inhomogeneity in the earth. Amplitude attenuation has a frequency dependent and a frequency independent component. The frequency independent component is often compensated for with a deterministic scaling function. The frequency dependent component is often difficult to estimate. To some extent it can be compensated for by time dependent deconvolutions. Sometimes Automatic Gain Control (AGC), also called Automatic Volume Control (AVC) is applied to correct the effects of amplitude attenuation. With AGC, the energy within a sliding time window is equalised. If the window is larger than, say 1000 ms, the relative amplitude strengths are still maintained. With smaller time windows the relative amplitudes are distorted. The resulting seismic data should, hence, not be used in a seismic inversion exercise.

Another important step in the seismic processing sequence with respect to amplitude information is deconvolution. Many different types of deconvolution can be applied during a seismic processing sequence. If predictive deconvolution is applied to sharpen the wavelet, or, to remove multiples, the prediction gap needs to be chosen such that the seismic wavelet is not altered. In practice, this means that prediction gaps should not be smaller than the dominant wavelength of the seismic wavelet. When predictive deconvolution is applied, it must be realised that the seismic data is assumed to be minimum phase. If this assumption is not valid, the deconvolution process will affect the seismic wavelet and, hence, the amplitude/phase characteristics of the seismic data. Another type of deconvolution that is nowadays routinely applied, is wavelet deconvolution. This process removes the effect of the seismic wavelet on the seismic record yielding zero phase data. Wavelet deconvolution improves the vertical resolution and interpretability of the data. To apply wavelet deconvolution, the seismic wavelet needs to be estimated. The assumption made in most wavelet deconvolution processes, is that the wavelet is spatially invariant. If the seismic wavelet does change, the resulting seismic data set will have laterally varying amplitude/phase characteristics.

7.3 Seismic trace balancing

In this thesis two types of seismic wavelets have been used:

- Synthetic wavelets, such as the 30 Hz Ricker wavelet (Fig. 4.2), and
- Wavelets derived statistically (Fig. 6.2).

The latter type of wavelet has been calculated as the transfer filter between reflectivity well log and seismic trace. The seismic trace may have been averaged over a number of traces near the well location. Both types of wavelets have been used to generate synthetic seismograms for simulated wells. Generated synthetic seismograms are scaled to the level of the factual seismic traces around the well bore, in case the wavelet has been calculated as a transfer filter. If, on the other hand, a synthetic wavelet has been used in the seismic synthesis process, factual and synthetic seismic amplitudes are not comparable. In this case, a trace balancing step is required to equalise both datasets.

In practice it seems unavoidable to balance synthetic and factual seismic traces. Even in the case of transfer filters, trace balancing will be carried out to eliminate the effect of laterally varying wavelets. Trace balancing can be carried out in various ways. For example, if a large impedance break occurs within the simulated stratigraphic sequence, the corresponding seismic event can be used to equalise the factual and synthetic seismic traces. This approach assumes the acoustic impedance break to be constant within the survey area. Although this condition will never be met completely in many geological settings, it can be applied with success. For example, in the Rotliegend case study, the acoustic impedance break occurring at the top of the Z2 Anhydrite could have been used. In this thesis, however, a RMS equalisation has been used in both case studies. In the Middle Eastern case study trace balancing was not a pre-requisite, since only factual data was ultimately used. The trace balancing was included because, at the start of the Middle Eastern study, it was anticipated that synthetic seismic data would also be required. It is important to use a large equalisation gate, in case RMS trace equalisation is applied. This implies that the simulated stratigraphic interval must be as large as possible. In practice this means that part of the overburden and underlying sediments must be included in the simulation.

If seismic amplitudes change laterally, not because of geological variations, but due to processing artefacts or laterally changing wavelets, the lateral prediction results will deteriorate. For this reason, it is important to estimate wavelets at different spatial positions, e.g. using the statistical approach at the well locations. Well-to-seismic matches must also be investigated at all well locations (Fig. 2.1). If the match is poor, additional well log editing might be required. In practice, sonic logs often require squeezing, or stretching, to match the seismic response. In addition fluid-replacement editing must be considered to eliminate acoustic hydrocarbon effects. It is also possible that a poor match is caused by a disturbance of the seismic response, e.g. as a result of multiple interference, migration noise etc. Even the location of the seismic-to-well match must be examined carefully. When laterally varying overburden velocities exist, points in the sub-surface are migrated to the wrong spatial position, in the time-migration process. This phenomenon is known as the 'Hubral' effect. The proper location is found by shifting the synthetic seismogram to the seismic position where the best match is observed.

Different wavelets might well be used when synthesising seismic traces, if the wavelet changes laterally. Separate data sets could then be compiled for neural network training and testing. Trained networks are subsequently applied to separate parts of the factual seismic dataset. This approach might be considered for datasets comprising more than one vintage.

7.3 Reference horizon

The seismic time-gate to be analysed is selected relative to a reference horizon, during the inversion process. This means that the reference horizon determines which seismic samples are offered to a particular network node. The reference time, as interpreted on a 3D-seismic workstation, will generally not coincide with a seismic sample. Certainly not, when an autotracker has been used, or when the interpreted horizon has been 'snapped' to the nearest event. Therefore, a maximum error of one sample position can occur. This error is eliminated here by resampling the selected samples relative to the reference horizon.

The reference horizon should be as close as possible to the geological target. There are in principle two types of reference horizons (Fig. 7.1):

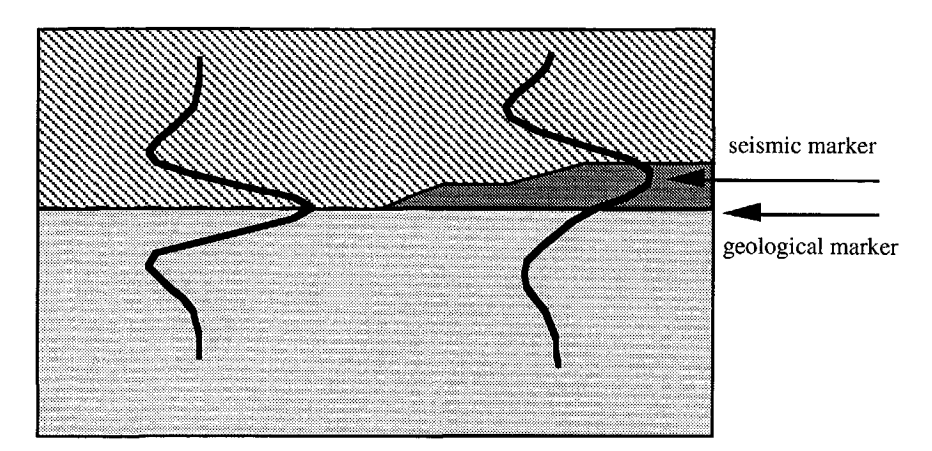


Fig. 7.1 Two types of reference horizons; geological markers and seismic markers. The position of the seismic marker can change laterally relative to the position of the geological marker.

- geological markers
- seismic markers

In general the seismic markers are mapped. In a seismic interpretation a good seismic reflector, closest to the target event is followed. Let us assume, the top of a reservoir has been mapped on seismic data. When the geology of the reservoir changes laterally, the seismic event will change as well, which is exactly what we need for the reservoir characterisation process. If, on the other hand, the overburden geology changes, the seismic event will change as well, irrespective of changes in the reservoir (see Experiment 6, Section 5.3.2). As a consequence, prediction performance of a reservoir property from the corresponding seismic response will deteriorate. Overburden effects may also cause the position of the seismic event to change relative to the top reservoir. The implication of this is that a different seismic response is selected for the inversion process, resulting also in a deterioration of the prediction performance.

It can, therefore, be argued, that the geological marker is the preferred reference horizon. Within the GeoProbe system, it is possible to investigate the difference in prediction performance between geological and seismic markers. As stated above, the majority of seismic interpretations seismic markers are mapped. Let us, therefore, assume that a seismic event, say a maximum amplitude, has been mapped close to the top of a reservoir. Wells can be simulated that describe the variations in the target zone using the

simulation algorithm in GeoProbe. When synthetic seismograms are generated for these wells, the reference time is also determined. Two sets of synthetic seismograms are generated in this way:

- one set with the reference time picked at the maximum amplitude near the top reservoir (seismic marker) and
- one set with the reference time picked exactly at the top reservoir (geological marker).

It can now be established for both datasets, whether, or not, well properties can be predicted from the synthetic seismic response. If good results are obtained for the seismic marker experiment for training and test datasets, the trained network can be applied to the entire 3D-seismic dataset. If, on the other hand, the seismic marker experiment does not give acceptable results, whilst the geological marker experiment does, the interpreted seismic horizon can be converted to a geological marker horizon.

The following procedure is proposed for converting seismic markers into geological markers:

- Generate synthetic seismograms for all wells in the survey.
- Measure the two-way time difference between the geological marker and the seismic marker.
- Map the time differences, e.g. using a Kriging algorithm.
- Add the time difference map to the seismic marker horizon map.

7.4 Applicability

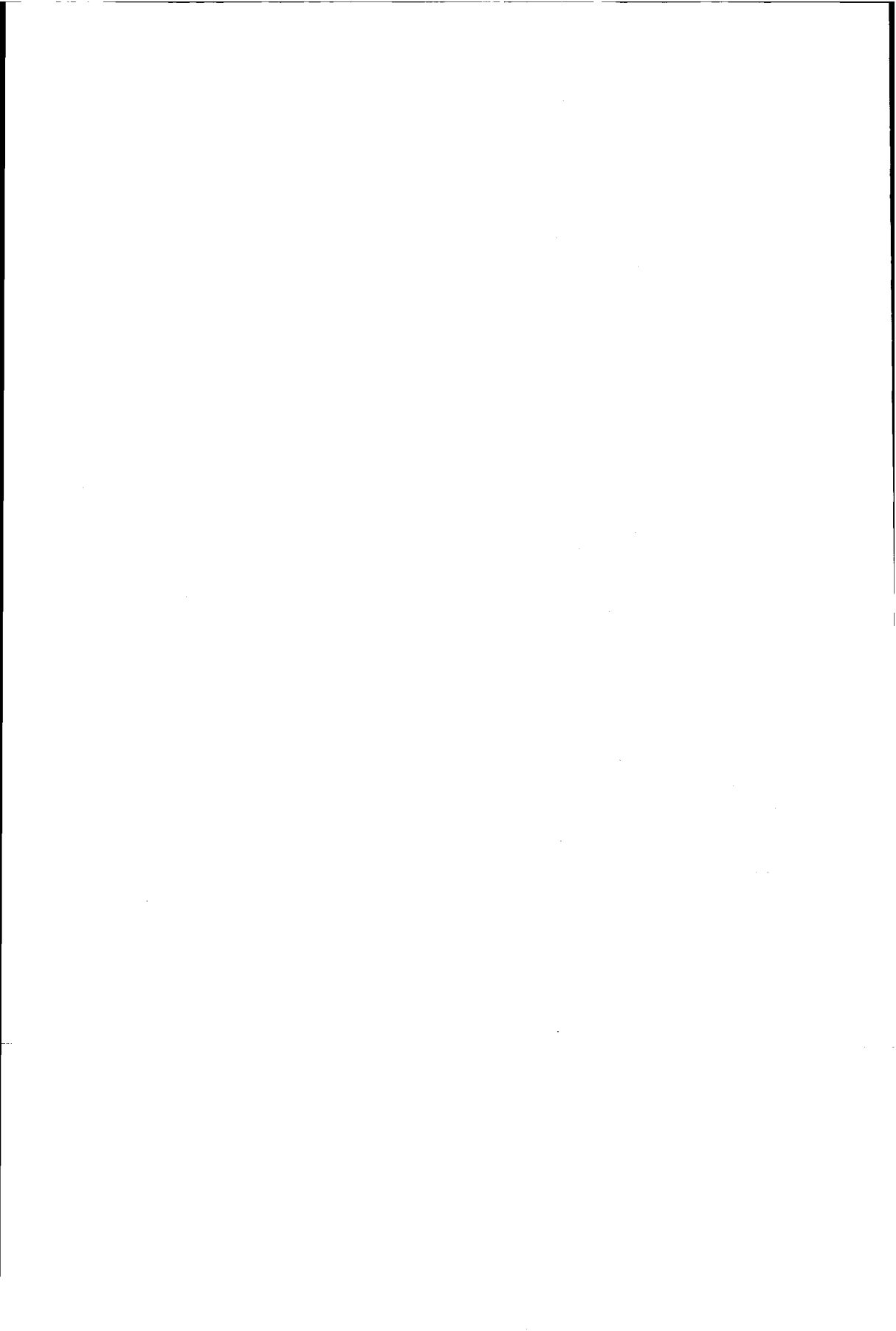
In this section the seismic reservoir characterisation techniques mentioned in Chapter 2 are compared with the total space inversion method. Total space inversion offers two options for seismic reservoir characterisation; direct inversion and segmentation. Direct inversion aims at establishing a relationship between seismic response and the relevant well property. The established relation is subsequently applied in a lateral prediction exercise (Fig. 2.5). Segmentation is applied in two steps (Fig. 2.6). In the first step the seismic response is clustered. This is followed by a step in which a representative dataset, comprising well data and corresponding seismic

traces, is compiled and classified by the same classifier. The resulting classes are then analysed to give a geological description of the clusters.

Most seismic reservoir techniques have been applied to a variety of different geological settings. For example, successful acoustic impedance inversions have been reported in fluvio-deltaic environments, carbonates, aeolian deposits and turbidites. The same is true for attribute analysis. In addition stochastic modelling successes have been reported for different settings. It is therefore, argued that the choice of technique is primarily determined by the objective of the study and the kind of data and knowledge available.

If limited well data is available, acoustic impedance inversion or segmentation can be applied. The advantage of segmentation is that it is completely data-driven, whereas most algorithms for acoustic impedance inversion require considerable user-interaction to obtain a useful result. Interpretation of the inverted impedances, or the segments, in terms of rock and fluid properties, however, is not trivial and requires further study and additional information.

If the area is well known, attribute analysis, the direct inversion approach of total space inversion and stochastic simulations can be applied. Attribute analysis and direct inversion have the same objectives, i.e. to relate the seismic response to salient well properties. The benefit of total space inversion is that factual wells can be combined with simulated wells to create a more representative dataset. Moreover, by using artificial neural networks for the inversion, it is possible to use the complete seismic response, rather than just a few attributes. The benefit of stochastic modelling is that it can incorporate the existence of spatial patterns in the variations of the rock patterns into the model. Spatial relations are ignored in the simulation algorithm used in this thesis (Chapter 4). The advantage of this particular simulation algorithm is that geological knowledge and stochastic input can be combined to yield realistic 1D-stratigraphic profiles with attached physical properties.



SUGGESTIONS FOR FUTURE WORK

8.1 Introduction

In this thesis a method for seismic reservoir characterisation has been described: the total space inversion method. In this method factual and simulated data are made commensurable by being described in terms of the same subsurface model: the integration framework. The application of the method has been limited to post-stack seismic data and wells (1D-stratigraphic profiles with attached physical properties) without spatial information. An algorithm has been used for the simulation of wells, in which geological knowledge and stochastic input can be combined to yield realistic wells. Seismic traces are synthesised for the simulated wells using the convolutional forward model. Artificial neural networks are then used to segment seismic responses and to establish relationships between seismic response and salient reservoir properties.

In this chapter suggestions are made about how the work presented in this thesis may be continued and improved. This work has been closely related to the Probe project in which the GeoProbe software was developed. Suggestions are made in this section about a number of ways in which GeoProbe may be improved. One suggestion is to extend the well simulation algorithm with a geostatistical option. in this way spatial information is taken into account by use of simulated wells. A suggestion is then made to implement a pre-stack option, in order to extract additional information from Amplitude Versus Offset data. Also improvements in the modelling of acoustic hydrocarbon effects can be made by using the Biot-Gassmann equation. It is further suggested to implement a pre-processor for well logs data. The preprocessor clusters well log responses in framework

entities and blocks sonic and density logs according to the required format. Improvements in the quantification of properties, may be possible by applying the total inversion in two steps; segmentation followed by direct inversion of the segments. Finally it is suggested that the integration framework concept is a powerful new technique with relevance for other geoscientific applications.

8.2 Geostatistical implementation

The simulation algorithm in this thesis simulates 1D-stratigraphic profiles with attached physical properties. No spatial locations are attached to the simulated wells. Therefore, an important information source is not utilised; the spatial relation to existing wells. It is possible to extend the algorithm to include this information. The extension involves attaching a variogram to each of the integration framework entities. The inversion scheme comprises the following steps:

- Selection by random draw of a location.
- Simulate a well conditionally to existing wells.
- Generate a synthetic seismogram for the simulated well.
- Correlate the synthetic trace with the factual seismic trace, if the correlation is not considered satisfactory, simulate another well (go back to step 2).
- A simulated well that is retained is merged with the data. It is now
 considered to be an existing well and will be used to condition other
 wells.
- Go back to step 1 until all locations have been processed following a random path.

The algorithm described above has been used by Haas and Dubrule (1994) to simulate acoustic impedance traces. The difference with the proposed scheme is that geological profiles with attached physical properties would be simulated rather than the physical properties alone. There are two advantages to this approach: first and foremost, the spatial relationships belong to geological entities and not to physical properties. In the scheme described by Haas and Dubrule, one variogram is used to describe the impedance variations in a heterogeneous shaly sandstone reservoir. In an

environment with sand-shale intercalations, it is expected however, that the shales are laterally more extensive than the sands. Different variogram could be attached to these entities in the proposed scheme. The second advantage is that the final objective of an inversion, i.e. the derivation of petrophysical variables (porosity, permeability etc.), or lithology, is considerably easier because it follows automatically from the simulations.

8.3 Pre-stack implementation

Amplitude Variation with Offset (AVO) analysis is a seismic reservoir characterisation technique in which amplitude variations as a function of offset are studied on pre-stack seismic data. AVO studies are of particular interest in the exploration for gas. Several successful AVO case studies. aimed at predicting gas-fill, have been reported in literature (e.g. Allen et. al., 1993). The theory behind AVO exploration for gas is based on the differences in the response of both compressional (P-waves) and shearwaves (S-waves) of a porous reservoir rock, depending on its gassaturations. Even a relatively low gas-saturation will substantially lower the P-wave velocities, whilst the S-wave velocities will be relatively unaffected. The ratio of P-wave velocity to S-wave velocity is an important factor in the partitioning of an incident P-wave when it strikes an interface. Thus, a change in amplitude can be expected along a reflector (i.e. as a function of offset) depending on the gas-fill. For some reservoirs the reflections associated with gas-bearing rock increase in amplitude with offset relative to other reflections. Such an increase with offset is anomalous; most reflections decrease in amplitude with offset. Most AVO studies try to detect such anomalies.

The concept of total space inversion can be applied equally well to pre-stack data. The additional AVO information can then be utilised to push the inversion results even further. A considerable effort is, required, however, for a pre-stack implementation. For the simulation, the module generating the synthetic seismograms should be modified. The simple convolutional model must be replaced with a wave-equation based algorithm which correctly models AVO effects. The input to the inversion software should also be modified to accept pre-stack data. Finally the pre-stack data must be made available for each study. This requires a change in conventional seismic processing practice. Input to the inversion algorithm should ideally be depth migrated pre-stack data. In this case, the reference horizon must be interpreted on the same depth migrated data. Both these conditions of depth migration and corresponding interpretation are, however, never met in practice. Alternatively, time migrated pre-stack data can also be used. As

with depth migration, it is not standard practice, however, to apply time migration pre-stack due to the computational effort required. Moreover, standard pre-stack migration algorithms will not save pre-stack results. This implies, that in most cases, a special pre-stack migration must be applied prior to a pre-stack lateral prediction exercise.

8.4 Fluid replacement simulations

In the current version of the well simulation algorithm, hydrocarbon effects are simulated by drawing acoustic reservoir properties from different distributions depending on the layer's fluid-fill. In general hydrocarbon-filled and brine-filled acoustic properties are correlated in the simulation's input specifications to reflect that rock matrix properties are independent of fluid-fill. This implies that acoustic hydrocarbon properties are assumed to be linearly related to brine-filled acoustic properties. This assumption is an oversimplification, as will be explained in the following section.

The velocity and density of a porous medium are influenced by the fluids that are present in the pore space. The bulk density ρ as a function of porosity ϕ is formulated in the following equation:

$$\rho = (1 - \phi)\rho_{\mathcal{S}} + \phi\rho_{f},\tag{8.1}$$

where:

 ho_s denotes the density of the solid fraction and ho_f the density of the pore fluid.

The relationship between velocity, porosity and fluid content is more complicated. Willie's time average equation, or (empirical) extensions to this formula have been used by many workers (e.g. de Haas, 1992). Willie's equation (Wyllie et.al., 1958) is formulated as:

$$t = (1 - \phi)t_S + \phi t_f , \qquad (8.2)$$

where t denotes sonic travel time of the rock, t_s the travel time in the solid matrix (i.e. empty porous rock), t_f travel time for the pore fluid and ϕ is the porosity.

This equation and the empirical extensions thereof, are not very reliable when used as fluid replacement algorithms, especially not for the gas-fill replacements.

The most widely used fluid-replacement algorithms, is the so-called Biot-Gassmann equation (see, e.g. Crans and Berkhout):

$$c_p = \sqrt{\frac{\kappa_s}{\rho} \left(3 \left(\frac{1 - \sigma_b}{1 + \sigma_b} \right) \beta + \frac{\left(1 - \beta \right)^2}{1 - \beta + \phi \left(\kappa_s / \kappa_f - 1 \right)} \right)}, \tag{8.3}$$

where:

 c_p denotes the seismic velocity for compressional waves. For an explanation of the other symbols see Table 8.1.

Parameter	Description	Unit
κ_s	compressibility modulus solid	N/m ²
κ_f	compressibility modulus fluid	N/m ²
σ_b	Poisson ratio	-
φ	Porosity	-
ρ_s	density solid	kg/m ³
ρ_f	density fluid	kg/m ³
ρ	density bulk	kg/m ³
c_p	P-wave velocity	m/s

 Table 8.1
 Rock and pore parameter definitions.

Direct application of this equation to calculate rock velocities is of limited use since the Poisson ratio σ_b and the compressibility moduli K_f , K_s are, in general unknown. However, if the velocity of a rock with a given saturation is known, then the Gassmann equation can be used to calculate

the velocity of the same rock with a different saturation. The proposed modification of the current simulation algorithm would be to specify acoustic reservoir probability density functions for brine-filled rocks only and calculate the hydrocarbon-filled properties when required. Simulating wells with hydrocarbon effects in the proposed scheme comprises the following steps:

- Generate a lithology (see chapter 6).
- Simulate the acoustic properties. For reservoir rocks, use the brine-filled acoustic probability density functions. Evaluate whether hydrocarbon effects are to be simulated. If so continue with the next step, else skip it.
- Comput the hydrocarbon-filled properties from the simulated brine-filled properties. It is assumed that K_w , K_{hc} , S_w , S_{hc} , σ_b , ρ_s , ρ_w and ρ_{hc} are input parameters specified by the user. For a description see Table 8.1; the index hc denotes hydrocarbons. First calculate the porosity ϕ using (8.1) for the brine-filled case. Then calculate ρ_f using s_w , s_{hc} , ρ_w and ρ_{hc} . Now calculate the density of the hydrocarbon-filled case using (8.1). Use Wood's law for the compressibility modulus of the fluid mixture K_f . Wood's law is formulated as:

$$1/\kappa_f = s_w/\kappa_w + s_{hc}/\kappa_{hc}. \tag{8.4}$$

Now the Gassmann equation (8.3) can be employed to calculate the velocity of the hydrocarbon-filled rock. The Gassmann equation, as a fluid replacement algorithm is applied in two steps. In the first step, the frame strength β defined as κ_m/κ_s where κ_m is the compressibility modulus of the matrix, is derived from the sound velocity of the brine-filled rock. Defining γ as:

$$\gamma = 3(1 - \sigma_b)/(1 + \sigma_b)$$
, (8.5)

and B as:

$$B = \phi(\kappa_s/\kappa_f - 1) , \qquad (8.6)$$

then β can be calculated as:

$$\beta = 1 - A \pm \sqrt{(A+B)^2 - (B^2/(1-\gamma))}, \tag{8.7}$$

with:

$$A = ((\rho c_p^2 / \kappa_s) + \gamma (B - 1)) / 2(1 - \gamma). \tag{8.8}$$

In the second step of the fluid replacement algorithm the assumption is made that ϕ , β and σ_b are independent from the fluid properties. Substitution of these variables together with the properties of the fluid mixture in (8.3), yields the velocity of the hydrocarbon filled rock. The sonic travel time follows as the reciprocal of this velocity.

It is noted, that the Gassmann equation assumes the velocity to be independent from frequency. Biot (1956b) has proved, however, that velocity does depend on frequency. At low (seismic) frequencies this effect can in general be ignored. Anderson (1984) proved that this effect can be significant in special cases, e.g. low permeability rocks with low saturation gas in the pores.

8.4 Well log preprocessor

In this thesis, well log data have been entered manually in a spreadsheet. Sonic and density logs have been parameterised at top and bottom of each layer. Subsequently, framework entities were attached to these layers. This is a time-consuming effort that can be automated in various ways.

One possibility is to use existing detailed stratigraphic interpretations to parameterise the data. These interpretations can, either, be downloaded from a corporate database, or, taken from ELAN-type logs.

Another possibility is to implement an option to make litho-stratigraphic interpretations based on available well logs. This requires an import facility for all relevant well logs, such as gamma-ray, SP, FDC/CNL, sonic, neutron, resistivity etc. In the proposed algorithm the UVQ network is employed to divide the well log responses into a number of segments. The

number of segments equals the number of framework lithlogies. The output of the UVQ is a segment number at each well log sample position. This, is, obviously, too detailed for well log parameterisation. Therefore, the segmentation must be followed by an upscaling process, e.g. with a moving average algorithm, in which the segments are grouped to the blocking scale. Sonic and density logs are then automatically parameterised at block boundaries. Next, the framework entities must be attached to the well-log blocks. As a first approximation the block segment numbers can be transformed into the framework lithologies. The user can attach the larger scale entities; units and sub-units to the parameterised logs in following interactive sessions.

8.5 Supervised segmentation

The segmentation described in this thesis is an unsupervised, or competitive learning approach. The seismic data itself determines how it can be classified. The UVO's input consists of seismic data vectors (time-samples) selected relative to a reference horizon, and the number of classes into which the data is to be segmented. No information is required about the classes themselves. However, if class information is available, it seems logical to utilise it. In other words, train a network on a representative dataset, to recognise classes from the corresponding seismic expressions. Application of the trained network to a 3D-seismic horizon slice then yields the spatial distribution of these classes. This approach is quite similar to the direct inversion approach, described in this thesis. With the direct inversion approach, MLP and RBF networks were trained to obtain a quantitative measure of a property of interest. With the supervised segmentation approach a different network is used to obtain a qualitative description of the data. The obvious network for supervised segmentation is the Learning Vector Quantiser (LVO, see Section 3.2.3).

Class information is, off course, available at well locations, but sometimes class information can also be inferred from spatial positions. For example, consider a gas discovery in a faulted structure. Based on the well information and the structural depth-map, the lateral extent of the gas can be derived within the drilled fault-block. Other undrilled fault-blocks might, or might not, contain gas. Either possibility might be supported by the seismic data if a supervised segmentation is carried out. The representative dataset for training the LVQ could be compiled as folllows:

- Seismic traces within the drilled fault block are selected to represent class 1; the gas-filled reservoir.
- Seismic traces off-structure are selected to represent class 2; the brinefilled reservoir.

If the LVQ can be trained, i.e. when the network converges, it can be applied to the entire 3D-horizon slice. In the ideal case, undrilled fault blocks will be classified, either, entirely as a 2, or, as a 1 above the GWC and as 2 below it.

8.6 Step-wise inversion

In chapter 5, it has been shown that the direct inversion approach breaks down as soon as many non-unique solutions exist in the representative data set. MLP and RBF networks do not converge in these cases, hence no meaningful lateral prediction results can be obtained. Convergence of networks can be achieved only, if additional geological constraints can reduce the solution space (Experiment 8, Section 5.3.4).

One obvious way to constrain the solution space is to divide the space into a number of segments. In other words, apply segmentation prior to direct inversion. If the segments are interpreted as representing different geological facies, then for each of the segments a different data set can be created in total space. Separate networks must now be trained for each dataset. Network predictions are valid only within each corresponding segment.

8.7 General use of the integration framework

In this thesis, a integration framework is used to describe simulated and factual wells. Data, described in terms of this integration framework are commensurable. As a consequence, it is feasible to combine factual and simulated data: the total space concept. The framework, as defined in this thesis, has proven to be a powerful way of describing geology in a generic way. The concept allows events, occurring multiple times, to be described in the framework, once only. For example, a succession of sands and shales need only be described in the framework by one sand and one shale lithology. The grouping of lithologies into sub-units and sub-units into units, ensures that data can be described at different scale levels. Because, there are no constraints to this grouping, it possible to describe the

subsurface as a combination of lithologies, stratigraphic sequences and genetic units, dictated only by the geological setting.

It is suggested here, that this concept of describing data in terms of the integration framework be used for other geoscientific applications. For example, in production history matching, the objective is to establish a subsurface model, that can be used to forecast and explain the production behaviour of a hydrocarbon reservoir. This is done in a reservoir simulator. The reservoir model is a description of the reservoir in terms of physical parameters, such as horizontal and vertical permeabilities. These parameters are updated, by the simulator, until a satisfactory match is obtained with the measured production data. It is possible, but unlikely, that the final subsurface model is consistent with a seismic reservoir characterisation result. As argued in this thesis, the only way to obtain consistent results is to describe all relevant data in terms of the same subsurface model. This model must be based on geological parameters (Section 2.4.1). In the case of reservoir simulations, it is suggested that the reservoir model be built with the aid of the integration framework. Relevant physical properties can then be attached to framework entities. In the matching process, the geological model with its attached physical properties is updated. Operating in this way, a final model is obtained that can be compared directly with results obtained from seismic reservoir characterisation studies. Moreover, it becomes feasible to combine the two inversion processes. For example, it is then possible to constrain the updating of the reservoir model, in the history matching process, with results obtained from seismic inversion studies.

CONCLUSIONS

9.1 General

In this thesis a technique for post-stack seismic reservoir characterisation has been described: the 'total space inversion method'. In this method seismic reservoir characterisation is approached from a geological perspective. It has been demonstrated that factual and simulated data are commensurable, when they have been described in terms of an acoustic-stratigraphic integration framework. The objective of total space inversion is to analyse a dataset comprising well information and corresponding seismic responses, that is representative of the zone of interest. Two approaches have been described:

- Direct inversion: in this approach the representative dataset is tested for relations between seismic response and salient reservoir properties. The established relations are subsequently applied to the factual seismic horizon slice.
- Segmentation: in this approach the factual seismic response is segmented into a number of classes. Subsequently, a representative dataset is classified and the well information is analysed to arrive at a geological description of the seismic classes.

In Chapter 5, various artificial neural network paradigms and architectures have been tested on different simulated datasets. In Chapter 6, the method has been applied, successfully, to two separate case studies: the Rotliegend case study and the Middle Eastern case study.

9.2 Conclusions

The conclusions related to the theoretical and practical aspects of the total space inversion method are as follows:

- Simulated data can be combined with factual data, if both datasets have been made commensurable. In this study, this was achieved by describing the datasets in terms of the integration framework.
- The integration framework defines the acoustic-stratigraphic entities, of a target zone in a study area, at three scale levels (Section 3.3). As a consequence, seismic reservoir characterisation results in total space inversion can be related to three scale levels.
- The integration framework allows the subsurface to be described as a combination of litho-stratigraphic-, sequence-stratigraphic- and genetic-units. The framework has the potential to be used for other geoscientific applications (Section 8.7).
- Simulating correlated stochastic multivariate variables one-by-one, makes it feasible to control the random draws by using geological reasoning and to evaluate the drawn value against hard constraints (Section 3.3). This is the basis for the simulation algorithm that has been used in this thesis to simulate 1D-stratigraphic profiles with attached physical properties.
- Horizon slice segmentation, as presented in this thesis, is a tool to visualise seismic patterns. The patterns can be interpreted, either directly, or, with the support of a classified representative dataset. Poor seismic data areas, or areas where the seismic horizon interpretation is poor, will show up in the segmented result as areas with random class distributions. Therefore, horizon slice segmentation is also a qualitycontrol tool.
- Direct inversion, as presented in this thesis, is feasible, only if the problem space is unique. If the problem space is non-unique, as in most factual cases, it must be constrained. Two possible approaches have been formulated to constrain the problem space:
 - 1. Feed additional (non-seismic) information to the inversion algorithm (Experiment 8, Section 5.3.4).
 - 2. Apply segmentation before direct inversion (Section 8.6).
- Performance of RBF networks is comparable to MLP networks (Chapter 5). RBF networks performed slightly better on the thickness inversion problem and slightly worse on the density inversion problem.

- Network performance can be controlled by the design, i.e. choice of paradigm, number of layers, number of nodes, activation functions etc.
- The total space inversion technique has been tested on post-stack seismic data and wells (1D-stratigraphic profiles with attached physical properties) without spatial information. The method can, in principle be extended to pre-stack data and wells with spatial information (Section 9.3 and 9.2, respectively).

In conclusion it may be stated that total space inversion, especially the segmentation approach, is a powerful new technique for inferring geological information from seismic signals.

	•			
			•	

REFERENCES

- al Laboun, A.A., 1986. Stratigraphy and Hydrocarbon Potential of the Paleozoic succession in Both Tabuk and Widyan Basins, Arabia, in Future Petroleum Provinces of the World. M.T. Halbouty (ed.), AAPG Memoir 40, pp. 373-397.
- Allen, J.L. & Peddy, C.P., 1993. Amplitude Variation with Offset: Gulf Coast Case Studies. Society of Exploration Geophysicists.
- Anderson, 1984. Fluid and Frequency effects on sonic velocities, SWPLA twenty fifth annual sonic logging symposium, June 10-13 1984.
- Archer, J.S. & Wall, P.G., 1986. Petroleum Engineering Principles and Practice. Graham and Trotman Ltd.
- Bashore W.M and Araktingi U.G., 1994. Examples of improved reservoir modeling through geostatistical data integration. SEG 64th annual meeting, L.A.
- Beydoun, Z.R., 1991. Arabian Plate Hydrocarbon Geology and Potential: A Plate Tectonic Approach. AAPG Studies in Geology 33, 77 p.
- Biot, M.A., 1956a. Theory of propagation of elastic waves in a fluid-saturated porous solid. I Low-frequency range. J. Acoust. Soc. Am., v. 28, p 168-178.
- Biot, M.A., 1956b. Theory of propagation of elastic waves in a fluid-saturated porous solid. II High-frequency range. J. Acoust. Soc. Am., v. 28, p 179-191.
- Broomhead, D.S., and Lowe, D., 1988. Multivariable functional interpolation and adaptive networks, Complex systems, 2:231-355, 1988.
- Brown, A.R., 1991. The Three-Dimensional Interpretation of Seismic Data (3rd Ed.). AAPG Memoir 42, 341 p.
- Bruin, C.G.M. de, 1992. Linear AVO Inversion by Prestack Depth Migration, PhD. Thesis, N.K.B. Offset B.V.

- Bunch, A.W.H. and Dromgoole, P.W., 1995. Lithology and fluid prediction from seismic and well data. Petroleum Geoscience, Vol 1, No. 1, Jan. 1995.
- Galloway, W.E. and Hobday, D.K., 1983. Terrigineous Clastic Depositional Systems Applications to Petroleum, Coal and Uranium Exploration. Springer-Verlag, New York, 416 p.
- Campbell C.V., 1967. Lamina and laminaset, bed and bedset. Sedimentology 8, 7-26.
- Campbell E.C., Scheffers B, de Groot P.F.M., 1994. Geophysics desperately seeking geology. poster presentation at the 56th EAEG conference, 6-10 June 1994, Vienna.
- Carlin, M., 1992. Radial Basis Function Networks and Nonlinear Data Modelling. Proceedings of Neuro-Nimes'92, Neural Networks and their Application, EC2, France, 1992, pp.623-633.
- Chessa, A.G.,1995. Conditional Simulation of Spatial Stochastic Models for Reservoir Heterogeneity. PhD. thesis, Delft University Press, Delft, The Netherlands.
- Chiburis, E. et.al., 1993. Hydrocarbon detection with AVO. Oilfield Review, January 1993, Elsevier Science Publishers, B.V.
- Crans, W., and Berkhout, A.J., 1980. Assessment of seismic amplitude anomalies. Oil and Gas Journal, no. 11, pp. 156-168.
- Dai, H., MacBeth, C., 1994. Split shear-wave analysis using an artificial neural network?. First Break Vol 12, December 1994.
- Dake, L.P., 1978. Fundamentals of reservoir engineering, Developments in Petroleum Science. Elsevier Science Publishers B.V.
- Danbom, S.H. & Domenico S.N., 1989. Shear-wave Exploration, Geophysical Developments No. 1. Society of Exploration Geophysicists.
- Dankbaar, J.W.M., 1989. Seismic Exploration with Shear Waves. PhD. Thesis.
- Davis, J.C., 1986. Statistics and Data Analysis in Geology. John Wiley & Sons.
- Degro, T., et.al., 1993. The Application of Amplitude Anomalies to Rotliegend Reservoir Delineation in Northern Germany. AAPG conference 19-10-1993, The Hague.
- Doveton, J.H., 1994. Geologic Log Analysis Using Computer Methods. AAPG Computer Applications in Geology, No. 2. Association of American Petroleum Geologists.
- Dubrule, O., 1989. A review of stochastic Models for Petroleum Industry. Geostatistics, M. Armstrong (ed.), 493-506, Kluwer, Dordrecht.
- de Groot, P.F.M. et.al., 1993. Seismic Reservoir characterisation using artificial neural networks and stochastic modelling techniques. presented at the 55th EAEG conference, June 1993, Stavanger.

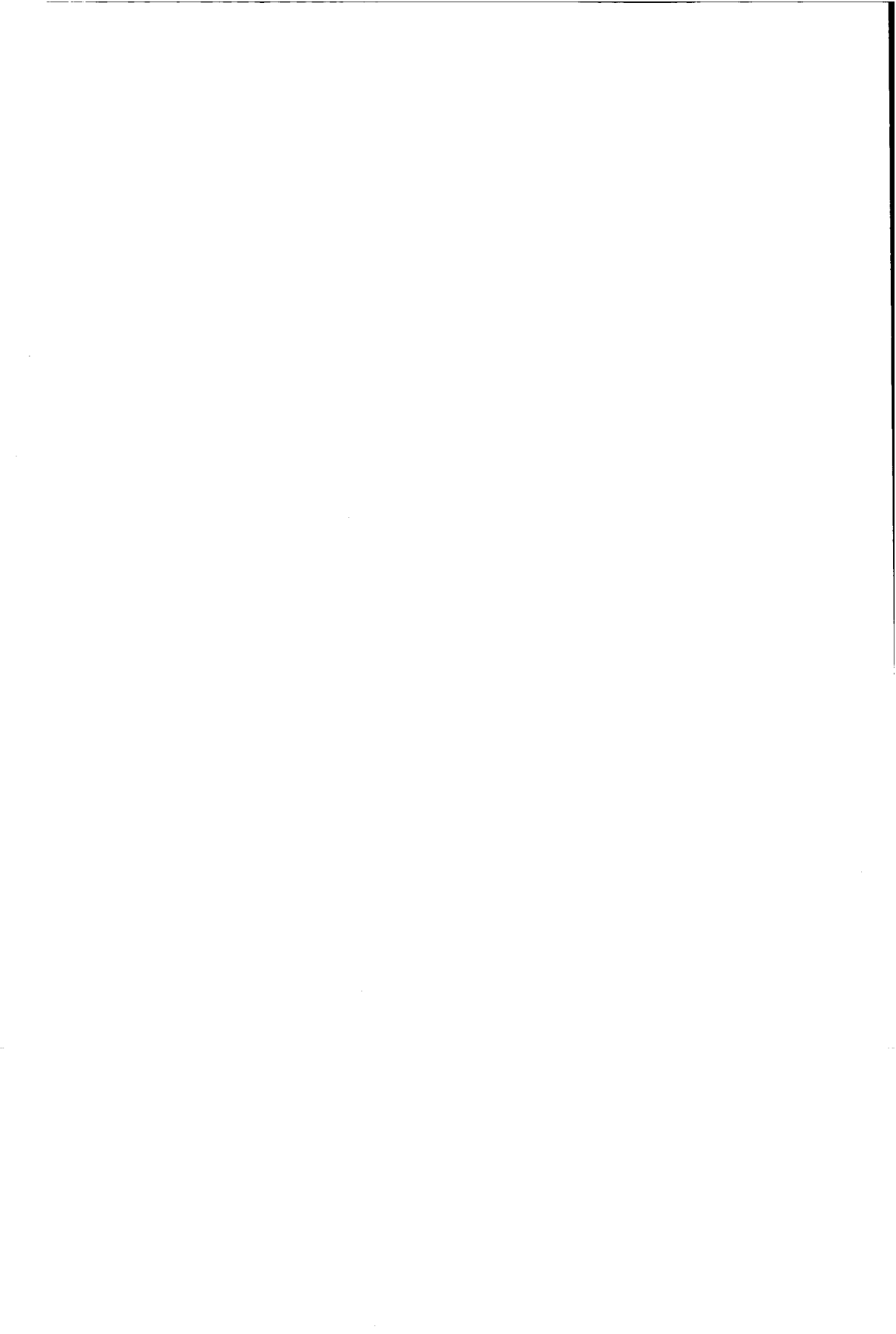
- de Groot, P.F.M., Bril, A.H., Floris F.J.T, Campbell, E.C., 1995. Monte Carlo simulation of wells, submitted to Geophysics.
- de Groot P.F.M., 1995. "Total Space Inversion"; Concept and Experiments in model space. accepted for oral presentation at 57th. EAEG conference, Glasgow.
- Dickey, P.A., 1986. Petroleum Development Geology. PennWell Books, PennWell Publishing Company.
- Duijndam, A.J.W. 1988. Bayesian Estimation in Seismic Inversion. Part I: Principles. Geophysical Prospecting 36, 899-918.
- Duijndam, A.J.W. 1988. Bayesian Estimation in Seismic Inversion. Part II: Uncertainty Analysis. Geophysical Prospecting 36, 878-898.
- Fahlman, 1988. An Empirical Study of Learning Speed in BackPropagation Networks. Technical Report CMU-CS-88-162, 1988.
- Fokkema, J.T. and Diephuis, G., 1994. Seismiek klankbeeld van de diepte. Natuur & Techniek '94, 62^e jaargang, no. 9.
- Gast, R.E., 1991. The Perennial Rotliegend Saline Lake in NW Germany. Geol. Jb. A 119, p 25-29.
- Gast, R.E., 1988. Rifting im Rotliegenden Niedersachsens. Die Geowissenschaften, 6. Jahrg. 1988/ Nr. 4.
- Goldberg, D.E., 1989. Genetic Algorithms in Search, Optimization, and Machine Learning. Addison-Wesley, Reading, M.A.
- Gevers, E.C.A. and Watson, S.W., 1978. Quantative Interpretation of Seismic data using Well logs. SPE, paper presented at the 53d. Annual Fall Technical Conference and Exhibition of the Society of Petroleum Engineers of AIME, Houston, Texas, Oct. 1978.
- Grieves, R.J., and Fulp, T.J., 1987. Three-dimensional seismic monitoring of an enhanced oil recovery process. Geophysics, 52, pp 1175-1187.
- Haas, A., and Dubrule, O., 1994. Geostatistical inversion a sequential method of stochastic reservoir modelling constrained by seismic data. First Break Vol 12, No 11, Nov. 1994.
- Haas, J.C. de, 1992. Elastic Stratigraphic Inversion, An Integrated Approach. PhD. Thesis, Gebotekst.
- Haatvedt, G. et.al., 1993. A comparative study of post-stack inversion techniques. EAEG 55th annual meeting, Stavanger
- Haykin, S., 1994. Neural Networks, A Comprehensive Foundation. Macmillan College Publishing Company, New York.
- Hecht-Nielsen, 1990. Neurocomputing. Addison-Wesley Publ..
- Hertz, J., Krogh, A. and Palmer, R.G., 1991. Introduction to the theory of neural computation, Lecture notes volume I. Santa Fe intsitute studies in the sciences of complexity, Addison-Wesley Publ. Comp.
- Holland, J.H., 1975. Adaptation in Natural and Artificial Systems. The University of Michigan Press, Ann Arbor.

- Hush and Horne, 1993. Progress in Supervised Neural Networks. What is new since Lippmann. IEEE Signal Processing Magazine, Jan. 1993.
- Haldorsen H.H., and Damsleth, E., 1990. Stochastic modeling. Joornal of Petroleum Scientists 42, pp. 404-412.
- Kavli, T.Ø., 1992. Learning Priciples in Dynamic Control. PhD.Thesis University of Oslo, ISBN no. 82-411-0394-8.
- Kulke, H. et.al., 1993. Harz Area, Germany: Typical Rotliegend and Zechstein Reservoirs in the Southern Permian Basin (Cental Europe). Excursion guide field trip No. 4, AAPG International Conference & Exhibition, The Hague, Oct. 1993. Association of American Petroleum Geologists.
- Lake, L.W., and Carrol, H.B. Jr., 1986. Reservoir characterization, Proceedings of the Reservoir Characterization Conference, held April 29-May 1, 1985, Dallas, Texas. Academic Press, Inc., ISBN 0-12-434065-2.
- LeCun, Y., 1985. Une procedure d'apprentissage pour réseau à seauil asymétrique (A learning procedure for asymmetric threshold networks). Proceedings of Cognitiva 85, 599-604, Paris.
- Lee, S. and Kil, R.M., 1988. Multilayer feedforward potential function network. IEEE International Conference on Neural Networks, I-161 I-171, San Diego, 1988.
- Lee, S. and Kil, R.M., 1989. Bidirectional Continuous Associator Based On Gaussian Potential Function Network. International Joint Conference on Neural Networks, vol.1, 1989, pp.45-53.
- Lippmann R.P., 1989. Pattern Classification Using Neural Networks. IEEE Communications Magazine, November 1989.
- Mardia, K.V., Kent, J.T. and Bibby, J.M., 1979. Multivariate Analysis, Academic Press London.
- Martinez, R.D. et.al., 1992. Complex reservoir characterization by multiparameter constrained inversion. Reservoir geophysics, Investigations in Geophysics No. 7. Society of Exploration Geophysicists. Editor: Sherrif, R.E.
- McCulloch, W.S. and Pitts, W., 1943, A logical calculus of idea's immanent in nervous activity. Bulletin of Mathematical Biophysics 5, page 115-133. Reprinted in Anderson, J.A. and Rosenfield, E., 1988. Neurocomputing: Foundations of Research, Cambridge MIT Press.
- Meeuwissen, A.M.H. and Cooke, R.H., 1994. Modelling joint probability distributions using graph and tree-dependence. submitted.
- Mijnssen, F.C.J., Tyler, N. and Weber, K.J., 1993. Knowledge base developments for the estimation of reservoir rock properties in the interwell area: examples from the Texas Gulf coast. Special Publication Number 15. International Association of Sedimentologists. Editors: Flint, S.S, and Bryant, I.D.

- Minsky, M. and Papert, S., 1969. Perceptrons: An Introduction to Computational Geometry. MIT Press, Cambridge, MA.
- Moody, J., and Darken, C.J., 1988. Learning with localized receptive fields, in Proceedings of the 1988 Connectionist Models Summer School. pp. 133-143, editors: Touretzky et.al., Morgan-Kaufman.
- Mosegaard K. and Vestergaard P.D., 1991. A simulated annealing approach to seismic model optimization with sparse prior information. Geophysical Prospecting 39, pp.599-611.
- Murris, R.J., 1980. Middle East: Stratigraphic Evolution and Oil Habitat. AAPG Bulletin, v. 64, pp.597-618.
- Neff, D.B., 1992, Estimated pay mapping using 3-D seismic data and incremental pay thickness modeling. Reservoir geophysics, Investigations in Geophysics No. 7. Society of Exploration Geophysicists. Editor: Sherrif, R.E.
- Neidell, N.S., Beard, J.H., Cook, E.E., 1986. Use of Seismic-Derived Velocities for Exploration on Land: Seismic Porosity and Direct Gas Detection. Seismic Stratigraphy II An Integrated Approach. AAPG Memoir 39. Editors: Berg, O.R. and Woolverton, D.G. Association of American Petroleum Geologists.
- Øhrn, 1993. Fast Learning Methods for Artificial Neural Networks. Master's thesis, Norwegian Institute of Technology (NTH) & SINTEF, December 1993.
- Parker, D.B., 1985. Learning-Logic, Tech.Rep.TR-47. MIT Center for Computational Research in Economic and Management Science, Cambridge, MA.
- Ping An, 1994. The effect of random noise in lateral reservoir characterization using feed-forward neural networks. SEG 64th annual meeting, L.A., October 1994.
- Platt, J., 1991. A resource-allocating network for function interpolation. Neural Computation, 3(2):213-225, 1991.
- Poggio, T. and Girosi, F., 1989. A theory of networks for approximation and learning. Technical report, Artificial Intelligence Laboratory, Massachusets Institute of Technology, Jul. 1989.
- Powel, M.J.D., 1987. Radial basis functions for multivariable interpolation: A review, in Algorithms for Approximation. editors: Mason, J.C., and Cox, M.G., Clarendon Press, London.
- Rich, E. and Knight, K., 1991. Artificial Intelligence second edition. McGraw-Hill, Inc.
- Reading, H.G., 1986. Sedimentary Environments and Facies. Blackwell Scietific Publications.
- Reineck, H.E. and Singh, I.B., 1980. Depositional Sedimentary Environments, Springer Verlag.

- Richardson, J.G., and Sneider, R.M., 1992. Synergism in Reservoir Management. Reservoir geophysics, Investigations in Geophysics No. 7. Society of Exploration Geophysicists. Editor: Sherrif, R.E.
- Robertson, J.D., 1989. Reservoir management using 3-D seismic data: Geophysics. The Leading Edge of Exploration, 8, No. 2, 25.
- Rosenblatt, F., 1962. Principles of Neurodynamics: Perceptrons and the Theory of Brain Mechanisms. Washington D.C., Spartan Books.
- Rumelhart, D.E., Hinton, G.E., and Williams, R.J., 1986. Learning internal representations by error propagation, Parallel Distributed Processing. Editors: Rumelhart, D.E., McClelland, J.L. and the PDP Research group, 318-362, Cambridge, MA, MIT Press.
- Sambrige, M. and Drijkoningen, G., 1992. Genetic Algorithms in seismic waveform inversion. Geophys. J. Int. 109, 323-342.
- Savit, C.H., and Changseng Wu, 1982. Geophysical Characterization of Lithology Application to Subtle Traps. The Deliberate Search of the Subtle Trap, AAPG Memoir 32. Editor: Halbouty, M.T., Association of American Petroleum Geologists.
- Schmidt, W.F., 1994, Neural Pattern Classifying Systems. PhD. thesis, TU Delft, CIP-DATA Koninklijke Bibliotheek, Den Haag, ISBN 90-9006716-7.
- Schultz et.al.,1994. Seismic-guided estimation of log properties, Part 1: A data-driven interpretation methodology. The Leading Edge, May 1994; Part 2: Using artificial neural networks for nonlinear attribute calibration. The Leading Edge, June 1994; Part 3: A controlled study. The Leading Edge, July 1994.
- Sherrif, R.E. et.al., 1992. Reservoir geophysics, Investigations in Geophysics No. 7. Society of Exploration Geophysicists.
- Siereveld, F.M., 1992. The Integration of Petrophysical, Geological, and Geophysical Information by "Constrained Stochastic Simulation". Msc. Thesis, Delft University of Technology, Faculty of Applied Physics.
- Sinvhal A. and Sinvhal H., 1992. Seismic Modelling and Pattern Recognition in Oil Exploration. Kluwer Academic Publishers.
- Skålnes, Å., Sandø, I.A., Brændsøi, H. and Mangerøy, G., 1993. A comparitive study of poststack inversions techniques. EAEG 55th Annual Meeting, Stavanger, June 7-11, 1993, Paper B001.
- Tarantola A., 1987. Inverse Problem Theory, Methods for Data Fitting and Model Parameter Estimation. Elsevier Science Publishing Company Inc.
- Turing A.M., 1937. On computable numbers, with an application to the Entscheidungsproblem. Proc. Lond. Math. Soc. (ser. 2), 42, 230-65; a correction 43, 544-6.
- Vail, P.R. et.al., 1977. Seismic Stratigraphy and Global Changes in Sea Level. AAPG Memoir 26, Seismic Stratigraphy - Applications to

- Hydrocarbon Exploration. Editor: Payton, C.E. American Association of Petroleum Geologists.
- Verschuur, D.J., 1991. Surface-related multiple elimination, an inversion approach. PhD. Thesis, University of Delft, ISBN 90-9004520-1.
- Vestergaard P.D. and Mosegaard K., 1991. Inversion of post-stack seismic data using simulated annealing. Geophysical Prospecting 39, pp. 613-624.
- Wagoner, Mitchum, Champion and Rahmanian, 1990. Siliciclastic Sequence Stratigraphy in Well Logs Cores and Outcrops. AAPG Methods in Exploration Series No. 7. Society of Sedimentary Geology Special Publication 42 (1988). Sea Level Changes - An Integrated Approach. American Association of Petroleum Geologists.
- Walden, A.T., 1994. Spatial Clustering: using Simple Summaries of Seismic Data to Find the Edge of an Oil-field. Applied Statistics 43, No. 2, pp. 385-398.
- Weber, K.J. and van Geuns, L.C., 1990. Framework for Constructing Clastic Reservoir Simulation Models. Jour. Petrol. Technology, 42, pp. 1248-1297.
- Werbos, P.J., 1974. Beyond Regression: New Tools for Prediction and Analysis in the Behavioral Sciences. PhD thesis, Harvard University, Cambridge, MA.
- Wilson, J.L., 1975. Carbonate Facies in Geologic History. Springer Verlag.
- Wyllie, M.R., Gregory, A.R., and Gardner, G.H.F., 1958. An Experimental Investigation of Factors Affecting Elastic Wave Velocities in Porous Media. Geophysics, v. 23., p459-493.
- Ziegler, P.A., 1990. Geological Atlas of Western and Central Europe. Geological Society Publishing House, London.



Appendix I

MONTE CARLO STATISTICS; SIMULATING CORRELATED MULTI-VARIATE STOCHASTIC VARIABLES

The following mathematical description is used in a simulation algorithm aimed at simulating wells, i.e. 1D-stratigraphic profiles with attached physical properties. In the algorithm, wells are constructed from so-called integration framework entities. These entities are grouped at three different scale levels. It is considered important that geological knowledge controls the selection of framework entities and that unrealistic realisations of variables can be redrawn. This implies that wells must be constructed one-by-one, entity-by-entity and variable-by-variable.

Variables in a computer are simulated using a (pseudo-) random number generator. When random variables are correlated, it is not simple, however, to simulate random draws using such a (pseudo-) random number generator. This is especially true when the variables must be drawn one-byone, as in our application. The realisations of already drawn variables will in that case influence the realisation of the variable to be drawn. For example, let us assume that a positive correlation exist between the thicknesses of two layers. When for the first layer a small thickness is drawn, then also for the second layer a small thickness must be drawn. In the case of normally distributed random variables, it is possible to draw the variables consecutively from the marginal distributions. Each time a variable is to be drawn, its marginal distribution must first be updated for the already drawn variables to which it is correlated.

In the following discussion \underline{X} is a stochastic vector. In our algorithm, \underline{X} comprises all stochastic variables required for the simulation. A component of \underline{X} is denoted by X_i . Examples of components are sonic, density, thickness and user-defined variables attached to framework entities. Each component X_i is assumed to be normally distributed with expectation μ_i and variance σ_i^2 , symbolically written as: $X_i \sim N(\mu_i, \sigma_i^2)$. The vector of expectation will be denoted $\underline{\mu}_i$. The components are assumed to be correlated. The covariance between components i and j is indicated by σ_{ij} . Note, that the covariance between component i and itself, σ_{ii} equals σ_i^2 . The matrix of covariances will be denoted as Σ . When the covariance σ_{ij} is normalised with the standard deviations σ_i and σ_j , we obtain the

correlation coefficient ρ_{ij} , symbolically written as: $\rho_{ij} = \sigma_{ij} / (\sigma_i * \sigma_j)$.

The matrix of correlation coefficients will be denoted by C. Sets of components can be grouped into subvectors of \underline{X} denoted by $\underline{X}^{(i)}$, An example of a subvector $\underline{X}^{(i)}$ is that part of stochastic vector \underline{X} comprising correlated thicknesses of a set of layers. The theorems given hereafter apply to the general case of drawing entire subvectors. However, for design reasons, the variables are, drawn one-by-one, in the final implementation of the algorithm. In other words the subvector $\underline{X}^{(i)}$ to be drawn has only one component. This is illustrated by the example at the end of this Appendix.

We require two theorems for our algorithm to work. Theorem 1.1 is used for updating the expectation and covariance matrix of a variable to be drawn, given some already drawn correlated variables (Mardia, 1979). This theorem requires the covariance matrix to be specified completely. In general, the user will not be in a position to specify all coefficients. Therefore, the unspecified correlation coefficients must be approximated first. This is accomplished with Theorem 1.2 (Meeuwissen et.al., 1994).

In the following discussion, first the two theorems are given, followed by an illustration of their use with an example.

Theorem 1.1

First we introduce some notation. Let \underline{X} be a n-dimensional stochastic vector which is partitioned as follows:

$$\underline{X} = \begin{pmatrix} \underline{X}^{(1)} \\ \underline{X}^{(2)} \end{pmatrix}, \tag{1.1}$$

with expectation E[X] equal to μ :

$$\underline{\mu} = \mathbf{E}[\underline{X}] = \left(\frac{\underline{\mu}^{(1)}}{\underline{\mu}^{(2)}}\right),\tag{1.2}$$

and a positive definite covariance matrix Cov(X) given by:

$$\Sigma = Cov(\underline{X}) = \begin{pmatrix} \Sigma_{11} & \Sigma_{12} \\ \Sigma_{21} & \Sigma_{22} \end{pmatrix}. \tag{1.3}$$

Suppose \underline{X} is multivariate normally distributed with expectation $\underline{\mu}$ and covariance matrix Σ , which can be symbolically written as:

$$\underline{X} \sim MVN(\mu, \Sigma).$$
 (1.4)

Here \sim denotes 'is distributed as' and MVN indicates multivariate normally distributed. Then the conditional distribution of $\underline{X}^{(1)}$ given a realisation $\underline{x}^{(2)}$ of $\underline{X}^{(2)}$ is multivariate normally distributed with expectation:

$$\underline{\hat{\mu}}^{(1)} = \underline{\mu}^{(1)} + \Sigma_{12} \Sigma_{22}^{-1} (\underline{x}^{(2)} - \underline{\mu}^{(2)}), \tag{1.5}$$

where $\underline{\hat{\mu}}^{(1)}$ is the updated expectation. The updated covariance matrix $\hat{\Sigma}_{11}$ is given by:

$$\hat{\Sigma}_{11} = \Sigma_{11} - \Sigma_{12} \Sigma_{22}^{-1} \Sigma_{21}. \tag{1.6}$$

Theorem 1.2

Suppose X_1 , X_2 and X_3 are correlated random variables which satisfy:

$$E[X_1|X_2 = x_2]$$
 is linear in x_2 , (1.7)

and

$$E[X_1|X_3 = x_3]$$
 is linear in x_3 . (1.8)

Then, given the correlation coefficients ρ_{12} between the pairs X_1 and X_2 and ρ_{13} between X_1 and X_3 , the correlation coefficient ρ_{23} is given by:

$$\rho_{23} = \rho_{12}\rho_{13}.\tag{1.9}$$

The conditions in the theorem imply, say for X_1 , X_2 , that given a realisation x_2 of variable X_2 , the expectation of X_1 shifts linearly towards x_2 . For normal distributions this is always satisfied, as can be seen from theorem 1.1, equation (1.5).

Although this theorem applies to three variables with one missing correlation coefficient only, we are going to use it also, without strict theoretical justification, for more than three variables where several correlation coefficients may be missing. We must note here, that, for more then three correlated variables, the positive definiteness of the covariance matrix may be violated by this procedure. In practice we have seen this happen only in some rare cases.

We will illustrate the use of these theorems with the following example. Suppose the correlation matrix has been specified for five variables as follows:

$$C = \begin{bmatrix} 1 & 0 & 0 & 0 & 0 \\ 0 & 1 & * & 0.8 & * \\ 0 & * & 1 & * & 0.6 \\ 0 & 0.8 & * & 1 & 0.4 \\ 0 & * & 0.6 & 0.4 & 1 \end{bmatrix}.$$
 (1.10)

In this particular example, ρ_{24} , ρ_{35} and ρ_{45} are known coefficients and ρ_{34} , ρ_{25} and ρ_{23} are unknown, which is indicated in the matrix by the * symbol. Using 1.9 we can determine two of the unspecified correlation coefficients.

$$\rho_{34} = \rho_{35}\rho_{54} = 0.24,\tag{1.11}$$

and

$$\rho_{25} = \rho_{24}\rho_{45} = 0.32. \tag{1.12}$$

However, ρ_{23} cannot be determined by combination of two of the given correlation coefficients. In a second step, we can approximate it using the previously determined correlation coefficients:

$$\rho_{23} = \rho_{24}\rho_{43},\tag{1.13}$$

which can be expanded using 1.11 to:

$$\rho_{23} = \rho_{24}\rho_{35}\rho_{54} = 0.192. \tag{1.14}$$

Note, that we could also have used:

$$\rho_{23} = \rho_{25}\rho_{53} = \rho_{24}\rho_{45}\rho_{53}. \tag{1.15}$$

In this particular case, the same value for ρ_{23} will be obtained for (1.14) and (1.15). In general, however the approximation is not unique. If several combinations are possible, in which the number of initially specified correlation coefficients differs, then a selection is made from the

combinations with the least number of initial coefficients. From these we, arbitrarily choose one of the possible combinations. Thus, if in a different example, ρ_{23} , ρ_{34} , ρ_{35} , ρ_{45} would have been specified, then we can obtain ρ_{25} , either from:

$$\rho_{25} = \rho_{23}\rho_{35},\tag{1.16}$$

or, from:

$$\rho_{25} = \rho_{23}\rho_{34}\rho_{45}.\tag{1.17}$$

The former expression is favoured because it contains less specified correlation coefficients.

With respect to the approximate nature of the procedure, we emphasise that after multiplying correlation coefficients, the resulting number comes closer and closer to zero. Therefore, the effect of the resulting approximation of the correlation coefficient decreases rapidly. Hence, we argue that making an error in the approximation has little effect when many terms are involved.

After application of the above procedure, the correlation matrix of (1.10) can be approximated by:

$$\tilde{C} = \begin{bmatrix} 1 & 0 & 0 & 0 & 0 \\ 0 & 1 & 0.192 & 0.8 & 0.32 \\ 0 & 0.192 & 1 & 0.24 & 0.6 \\ 0 & 0.8 & 0.24 & 1 & 0.4 \\ 0 & 0.32 & 0.6 & 0.4 & 1 \end{bmatrix}. \tag{1.18}$$

We can now draw samples for all variables. Suppose we would like to draw them in the order X_3 , X_5 , X_1 , X_2 , X_4 . When selecting X_3 , no other has been drawn, so we can just draw it from its marginal probability density function $X_3 \sim N(\mu_3, \sigma_3^2)$. Now X_5 must be drawn, conditioned on the x_3 value. Using theorem 1.1, we find:

$$\hat{\mu}_5 = \mu_5 + \sigma_{35}(\sigma_3^2)^{-1}(x_3 - \mu_3), \tag{1.19}$$

and

$$\hat{\sigma}_5^2 = \sigma_5^2 - \sigma_{35}(\sigma_3^2)^{-1}\sigma_{53},\tag{1.20}$$

where

$$\sigma_{35} = \rho_{35}\sigma_3\sigma_5,\tag{1.21}$$

is the covariance between X_3 and X_5 . Now X_5 can be drawn from $N(\hat{\mu}_5, \hat{\sigma}_5^2)$.

Now X_1 is to be drawn. Since it is independent of X_2 , X_3 , X_4 and X_5 it can be drawn from its marginal distribution $N(\mu_1, \sigma_1^2)$. Finally, for X_2 and X_4 we use:

$$\hat{\mu}_2 = \mu_2 + \left[\sigma_{23}\sigma_{25}\right] \begin{bmatrix} \sigma_3^2 & \sigma_{35} \\ \sigma_{35} & \sigma_5^2 \end{bmatrix}^{-1} \begin{bmatrix} x_3 - \mu_3 \\ x_5 - \mu_5 \end{bmatrix}, \quad (1.22)$$

$$\hat{\sigma}_{2}^{2} = \sigma_{2}^{2} - \left[\sigma_{23}\sigma_{25}\right] \begin{bmatrix} \sigma_{3}^{2} & \sigma_{35} \\ \sigma_{35} & \sigma_{5}^{2} \end{bmatrix}^{-1} \begin{bmatrix} \sigma_{23} \\ \sigma_{25} \end{bmatrix}, \quad (1.23)$$

and

$$\hat{\mu}_{4} = \mu_{4} + \begin{bmatrix} \sigma_{24}\sigma_{34}\sigma_{54} \end{bmatrix} \begin{bmatrix} \sigma_{2}^{2} & \sigma_{23} & \sigma_{25} \\ \sigma_{23} & \sigma_{3}^{2} & \sigma_{35} \\ \sigma_{25} & \sigma_{35} & \sigma_{5}^{2} \end{bmatrix}^{-1} \begin{bmatrix} x_{2} - \mu_{2} \\ x_{3} - \mu_{3} \\ x_{5} - \mu_{5} \end{bmatrix},$$
(1.24)

$$\hat{\sigma}_{4}^{2} = \sigma_{4}^{2} - \begin{bmatrix} \sigma_{24}\sigma_{34}\sigma_{54} \end{bmatrix} \begin{bmatrix} \sigma_{2}^{2} & \sigma_{23} & \sigma_{25} \\ \sigma_{23} & \sigma_{3}^{2} & \sigma_{35} \\ \sigma_{25} & \sigma_{35} & \sigma_{5}^{2} \end{bmatrix}^{-1} \begin{bmatrix} \sigma_{24} \\ \sigma_{34} \\ \sigma_{54} \end{bmatrix},$$
(1.25)

respectively.

This allows us to draw the variables one by one in any order. Also, we can redraw any one of the variables when needed, and condition on the latest drawn value for each of the correlated variables.

Appendix II

SIMULATION SPECIFICATIONS

In the GeoProbe software system simulation specifications are entered in three separate tables:

- A general table to specify geological rules and probability density functions (pdfs) for thicknesses of framework entities and for sonic and density variables at top and bottom of each lithology. Separate sonic and density pdfs can be specified for brine-filled and hydrocarbon-filled reservoir lithologies. Also pdfs for user-defined parameters can be specified in this table.
- A correlation table in which correlations between pairs of variables are specified.
- A special constraints table in which hydrocarbon columns, simulation constraints and hard constraints are specified.

In the general table the integration framework can be recognised in the columns 1, 4 and 7. Geological rules are specified in the columns 2 and 5. The rules are attached to the entity in the preceeding column. The S. and R. in the rule name refer to sequential and random selection, respectively. Two types of pdfs can be specified: normal distributions and constant distributions. Normal distributions are specified by the letter n followed by two values: the mean and standard deviation. Constant distributions are specified by the letter c followed by the value. SonicTop indicates the sonic variable at the top of a lithology. SonicTopOil indicates the oil-filled sonic variable at the top of a reservoir lithology.

In the following tables the simulation specifications, as used in this thesis, are presented. The first three tables correspond to the Middle Eastern case study simulation (Chapter 4). The next three tables correspond to the Rotliegend case study (Chapter 6).

Park	٩	Thickness nof	Facies	Rule	Thickness odf	Lithology	Thickness pdf	Type	SonicTop pdf	SonicTopOil pdf	Density Top pdf	Density TopOil pdf
S Cum C	2	0.09	Carbonate	Herate S.	0.600	Carbonate	n 50 35	Waste	n 53 3		n 2.8 0.04	
Ognate Con	5	200				Shale	n 10 8	Waste	n 602		n 2.65 0.04	
Nonate D Sum	S.	n 230 15	Massive	Sum S.	n 75 5	Anhydrite	n 30 7	Waste	n 512		n 2.96 0.01	
						Carbonate	n 40 10	Waste	n 49 2		n 2.82 0.03	
-			Anhydrite	Iterate R.	n 70 15	Anhydrite	n83	Waste	n 503		n 2.93 0.04	
						Carbonate	n73	Waste	n 55 4		n 2.83 0.06	
						Shale	n63	Waste	629 u		n 2.65 0.13	
-		-	Alternating	Iterate R.	n 95 20	Carbonate	n 8 5	Waste	n 55 8		n 2.8 0.06	
						Shale	n84	Waste	п 73 10		n 2.6 0.09	
						Anhydrite	n63	Waste	n 483		n 2.9 0.03	
Sm	Sum	_	Seal	Sum S.		seal	c.1	Seal	c73		c 2.6	
pronir Tree	Irerate R	0.310.100	Massive Tyne 3	Iterate R.	09 06 0	Type 3 Sand	n 128	Reservoir	n 865	n 85.56	n 2.32 0.05	п 2.33 0.07
1						Silt/Shale	n 8 5	Waste	908 u		n 2.46 0.09	
			Massive Type 2	Iterate R.	n 140 100	Type 2 Sand	n 25 20	Reservoir	n 764	n 796	n 2.34 0.05	n 2.32 0.07
1						Silt/Shale	n84	Waste	n 75.5 S		n 2,41 0.09	
+			Massive Silt/Shale Herate R.	Herate R.	n 110 60	Type 2 or 3 Sand	n75	Reservoir	n 78 7	n 817	n 2.4 0.07	n 2.38 0.08
+						Silt/Shale	n 25 20	Waste	n 79 5		n 2.49 0.09	
			Laminated	Herate R.	n 145 70	Type 2 or 3 Sand	n 8.7	Reservoir	n 74 10	n 76 10	n 2.35 0.07	2.32 0.05
-						Silt/Shale	n86	Waste	n 784		n 2.45 0.05	
S. Car	Sum	the same of the same	Marine	Sim		Shale	c 550	Waste	n 78 5		n 2.6 0.07	

Middle Eastem case study Framework, see Table 4.1 Units: thickness in ft, sonic in µs/ft, density in g/cc.

Correlation table

Code	Parameter	Code	Parameter	Coefficient
crbc.crb.crb	SonicTop	crbc.crb.crb	DensityTop	-1
crbc.crb.shl	SonicTop	crbc.crb.shl	DensityTop	-1
crbd.msv.anh	SonicTop	crbd.msv.anh	DensityTop	-1
crbd.msv.crb	SonicTop	crbd.msv.crb	DensityTop	-1
crbd.anh.anh	SonicTop	crbd.anh.anh	DensityTop	-1
crbd.anh.crb	SonicTop	crbd.anh.crb	DensityTop	-1
crbd.anh.shl	SonicTop	crbd.anh.shl	DensityTop	-1
crbd.alt.crb	SonicTop	crbd.alt.crb	DensityTop	-1
crbd.alt.shl	SonicTop	crbd.alt.shl	DensityTop	-1
crbd.alt.Anh	SonicTop	crbd.alt.Anh	DensityTop	-1
seal.seal	SonicTop	seal.seal.seal	DensityTop	-1
res.mt3.t3s	SonicTop	res.mt3.t3s	DensityTop	-1
res.mt3.slt	SonicTop	res.mt3.slt	DensityTop	-1
res.mt2.t2s	SonicTop	res.mt2.t2s	DensityTop	-1
res.mt2.slt	SonicTop	res.mt2.slt	DensityTop	-1
res.msl.snd	SonicTop	res.msl.snd	DensityTop	-1
res.msl.slt	SonicTop	res.msl.slt	DensityTop	-1
res.lam.snd	SonicTop	res.lam.snd	DensityTop	-1
res.lam.slt	SonicTop	res.lam.slt	DensityTop	-1
sou.mar.shl	SonicTop	sou.mar.shl	DensityTop	-1
res.mt3.t3s	SonicTopOil	res.mt3.t3s	SonicTop	1
res.mt3.t3s	SonicTopOil	res.mt3.t3s	DensityTopOil	-1
res.mt2.t2s	SonicTopOil	res.mt2.t2s	SonicTop	1
res.mt2.t2s	SonicTopOil	res.mt2.t2s	DensityTopOil	-1
res.msl.snd	SonicTopOil	res.msl.snd	SonicTop	1
res.msl.snd	SonicTopOil	res.msl.snd	DensityTopOil	-1
res.lam.snd	SonicTopOil	res.lam.snd	SonicTop	1
res.lam.snd	SonicTopOil	res.lam.snd	DensityTopOil	-1

Middle Eastern case study Framework, see Table 4.1

Constraints table

Code	Parameter	Constraint	Value
seal.seal	OilColumn	Distribution	n 50 50
seal.seal.seal	OilColumn	MaximumRedraw	150
seal.seal.seal	OilColumn	MinimumRedraw	0
crbc.crb.crb	Carbonate	Generation	100
crbc.crb.shl	Shale	Generation	100
crbd.msv.anh	Anhydrite	Generation	100
crbd.msv.crb	Carbonate	Generation	100
crbd.anh.anh	Anhydrite	Generation	45
crbd.anh.crb	Carbonate	Generation	20
crbd.anh.shl	Shale	Generation	35
crbd.alt.crb	Carbonate	Generation	55
crbd.alt.shl	Shale	Generation	40
crbd.alt.Anh	Anhydrite	Generation	5
res.mt3		Generation	20
res.mt3.t3s	Type 3 Sand	Generation	35
res.mt3.slt	Silt/Shale	Generation	65
res.mt2		Generation	20
res.mt2.t2s	Type 2 Sand	Generation	55
res.mt2.slt	Silt/Shale	Generation	45
res.msl		Generation	30
res.msl.snd	Type 2 or 3 Sand	Generation	20
res.msl.slt	Silt/Shale	Generation	80
res.lam		Generation	35
res.lam.snd	Type 2 or 3 Sand	Generation	40
res.lam.slt	Silt/Shale	Generation	60

Middle Eastern case study Framework, see Table 4.1

General table		;					Interesting and the	Time	Contoffen	DencityTon
Unit	- 1	Thickness pdf	Facies		Thickness par	Littology	n 72 S.d	Waste	200000	n 2 14 0 08
Buntsandstein	Sum S.		Opper	Iterate 5.	n 120 IS	Sandstone	1,00,00	W ASIC	200	7 5 08
				Î	3,7,5=7	Shale	1100.20	TT/SOLO	2000	200 14 0 08
			Lower	Iterate S.	n 475 140	Sandstone	n 200 200	wasie	0 00 11	0.14 0.00
						Limestone	n 200 200	Waste	n5/5	0.77.00
						Shale	n 330 222	Waste	n 65 6	n 2.63 .07
Upper Zechstein	Sum S.		Z2 to Z7	Iterate S.	n 361 238	Halite	n 90 131	Waste	n 68 5	n 2.08 .05
	1					Anhydrite (A3)	n 49 52	Waste	n 523	n 2.97 .03
						Shale	n 20 20	Waste	n 50 5	n 2.5 0.08
Basal Zechshtein	Sum		Z1 to Z2	Sum S.	n 594	Anhydrite (A2)	п31	Waste	n 52 2	n 2.97 .01
				1		Carbonate	n 63	Waste	n 57 2	n 2.71 .01
						Anhydrite	n 49.4	Waste	n 48 2	n 2.97.02
						Conner Shale	1 2	Waste	n642	n 2.68 0.5
Hoidberg-Rahnean	Sum C		Ton Dodingand	Sum	100 ×	Sandstone	n.5.5	Waste	n 68 5	n 2.65 0.05
ricing-parimen	Comme of		top tomogram	1	200	Chale	n 109 8	Waste	n 58 4	n 2.7 0.05
Casil	-		Cani	Sum S		Shale	- 0	Seal	593	c 2.75
Whetrow	S down	40.50	Whetron, 1	Ι,	243	Fvanorite	n 2 2	Waste	n 55 2	n 2.80 0.1
u Chon u		OC* CO	- HOROLL		2.5	Sitt/Shale	n93	Waste	n 64 4	n 2.67.05
						Shoreline sandstone	n 14 10	Reservoir	n 74 3	n 2.46 .05
						Wet dune / Fluvial sandstone	n 7.5	Reservoir	n 68 4	n 2.54 .03
						Dry dune sandstone	n 5 2	Reservoir	n 75 2	n 2,42 0.05
				-		Fanolomerate	n 10 8	Waste	n 63 1	n 2.69 0.03
						Volcanics	n 54	Waste	n 52 3	n 2.8 0.02
			Wistrow 2	Iterate R.	n 34 3	Wet dune / Fluvial sandstone	n 178	Reservoir	п 663	n 2.57 0.03
						Dry dune sandstone	n S 2	Reservoir	n 75 2	n 2.42 0.05
						Fanelomerate	n 126	Waste	n 63 J	n 2.69 0.03
						Silt/Shale	n 8.5	Waste	n 63 3	n 2.67 0.05
						Volcanics	n 53	Waste	n 523	п 2.8 0.02
Sea!?	Sums		Seal	SumS		Shale	n73	Seal	282	c 2.77
Ebstorf	XOK	30.70	Shoreline	1.	n43	Shoreline sandstone	n43	Reservoir	n 61 15	n 2.44 .04
						Sitt/Shale	n54	Waste	n 633	n 2.67 0.05
			Wet dune / Fluvial	Iterate R.	n 12 3	Wet dune / Fluvial sandstone	n 84	Reservoir	n 64 4	n 2.62 0.09
						Sitt/Shale	n53	Waste	n 64 2	n 2.68 0.03
Seal3	Sum S.		Seal	Sum S.		Shale	c.1	Seal	293	c 2.68
Dethlingen	XOX	10.90	Dethlingen 1	L	n 173 36	Shoreline sandstone	n 50 45	Reservoir	n 72 3	n 2.49 0.02
-		2.5				Wet dune / Fluvial sandstone	ก 50 50	Reservoir	n 61 4	n 2.6 0.06
						Fanglomerate	n 36 27	Waste	n 58 5	п 2.59 0.08
						Silvshale	n 5 2	Waste	n 572	n 2.68 0.02
						Anhydrite / Carbonate	n 2 2	Waste	n 55 2	n 2.76.0.5
			Dethlingen 2	Iterate R.	n 135 36	Wet dune / Fluvial sandstone	п 29 29	Reservoir	n 66 4	n 2.54 .07
						Dry dune sandstone	n43	Reservoir	n 71 3	n 2.47 .02
						Fanglomerate	n 13 13	Waste	n 623	n 2.66 0.04
						Silt/Shale	29 u	Waste	n 62 2	n 2.69 0.02
						Anhydrite / Carbonate	0.1	Waste	n 55 3	n 2.8 0.1
Sea14	Sum S.		Seal	Sum S.		Shale	c.1	Seal	c 62	c 2.69
Base	Sum R.		Schneverdingen	Iterate R.	n 140 136	Wet dune / Fluvial sandstone	n 1721	Reservoir	n 663	n 2.53 .04
	1					Dry dune sandstone	n 25 22	Reservoir	n 72 3	п 2.45 0.03
						Fanglomerate	n 27 40	Waste	n 63 3	n 2.66 0.03
						Silt/Shale	n 2 2	Waste	n 66 1	In 2.62 .01
Lower Rotliegend	Sum S.		Volcanics	Sum S.		Volcanics	n 82 111	Waste	n 63 7	n 2.64 0.12
			Carboniferous	Relative R.	n 50 20	Sandstone	n63	Waste	n 663	п 2.53 .04
						Shale	n63	Waste	n 62 3	п 2.62 .01

Rottiegend case study Framework, see Table 6.1 Units: thickness in m, sonic in µs/ft, density in g/cc.

Corre	lation	tabl	e

wus.wul.eva SonicTop wus.wul.sil DensityTop	Code	Parameter	Code	Parameter	Coefficient
wus.wu1.sil SonicTop wus.wu1.sil DensityTop -1 wus.wu1.wet SonicTop wus.wu1.sho DensityTop -1 wus.wu1.wet SonicTop wus.wu1.wet DensityTop -1 wus.wu1.dry SonicTop wus.wu1.dry DensityTop -1 wus.wu1.fan SonicTop wus.wu1.fan DensityTop -1 wus.wu1.vol SonicTop wus.wu1.fan DensityTop -1 wus.wu1.vol SonicTop wus.wu1.fan DensityTop -1 wus.wu2.wet SonicTop wus.wu2.wet DensityTop -1 wus.wu2.fan SonicTop wus.wu2.dry DensityTop -1 wus.wu2.fan SonicTop wus.wu2.fan DensityTop -1 wus.wu2.sish SonicTop wus.wu2.fan DensityTop -1 wus.wu2.sish SonicTop wus.wu2.fan DensityTop -1 wus.wu2.sish SonicTop wus.wu2.vol DensityTop -1 wus.wu2.sish SonicTop wus.wu2.vol DensityTop -1 wus.wu2.vol SonicTop wus.wu2.vol DensityTop -1 bunt.up.snd SonicTop bunt.up.snd DensityTop -1 bunt.up.snd SonicTop bunt.up.shl DensityTop -1 bunt.low.snd SonicTop bunt.low.snd DensityTop -1 bunt.low.snd SonicTop bunt.low.snd DensityTop -1 bunt.low.snd SonicTop bunt.low.snd DensityTop -1 bunt.low.shl SonicTop bunt.low.snl DensityTop -1 bunt.low.snl SonicTop bunt.low.snl DensityTop -1 bunt.low.snl SonicTop bunt.low.snl DensityTop -1 bunt.low.snl SonicTop bunt.low.snl DensityTop -1 buze.z37.hal DensityTop -1 buze.z37.hal DensityTop -1 bze.z12.ac SonicTop bez.z12.ac DensityTop -1 bze.z12.ac SonicTop bez.z12.ac DensityTop -1 bze.z12.car SonicTop bez.z12.car DensityTop -1 bze.z12.car SonicTop bez.z12.car DensityTop -1 bze.z12.can SonicTop bez.z12.can DensityTop -1 bze.shor.shor SonicTop bes.shor.shor DensityTop -1 bed.dopr.snl SonicTop bes.shor.shor DensityTop -1 bes.shor.sish SonicTop bes.shor.shor DensityTop -1 bes.shor.sish SonicTop det.del.wet DensityTop -1 cbs.shor.sish SonicTop det.del.wet DensityTop -1 det.del.wet SonicTop det.del.an DensityTop -1 det.del.anc SonicTop det.del.anc DensityTop -1 det.del.anc SonicTop det.del.anc DensityTop -1 det.del.anc SonicTop det.del.anc DensityTop -1 det.del.anc SonicTop det.del.an	seal1.seal.shl	SonicTop	seal1.seal.shl	DensityTop	-1
wus.wu1.sil SonicTop wus.wu1.sil DensityTop -1 wus.wu1.wet SonicTop wus.wu1.sho DensityTop -1 wus.wu1.wet SonicTop wus.wu1.wet DensityTop -1 wus.wu1.dry SonicTop wus.wu1.dry DensityTop -1 wus.wu1.fan SonicTop wus.wu1.fan DensityTop -1 wus.wu1.vol SonicTop wus.wu1.fan DensityTop -1 wus.wu1.vol SonicTop wus.wu1.fan DensityTop -1 wus.wu2.wet SonicTop wus.wu2.wet DensityTop -1 wus.wu2.fan SonicTop wus.wu2.dry DensityTop -1 wus.wu2.fan SonicTop wus.wu2.fan DensityTop -1 wus.wu2.sish SonicTop wus.wu2.fan DensityTop -1 wus.wu2.sish SonicTop wus.wu2.fan DensityTop -1 wus.wu2.sish SonicTop wus.wu2.vol DensityTop -1 wus.wu2.sish SonicTop wus.wu2.vol DensityTop -1 wus.wu2.vol SonicTop wus.wu2.vol DensityTop -1 bunt.up.snd SonicTop bunt.up.snd DensityTop -1 bunt.up.snd SonicTop bunt.up.shl DensityTop -1 bunt.low.snd SonicTop bunt.low.snd DensityTop -1 bunt.low.snd SonicTop bunt.low.snd DensityTop -1 bunt.low.snd SonicTop bunt.low.snd DensityTop -1 bunt.low.shl SonicTop bunt.low.snl DensityTop -1 bunt.low.snl SonicTop bunt.low.snl DensityTop -1 bunt.low.snl SonicTop bunt.low.snl DensityTop -1 bunt.low.snl SonicTop bunt.low.snl DensityTop -1 buze.z37.hal DensityTop -1 buze.z37.hal DensityTop -1 bze.z12.ac SonicTop bez.z12.ac DensityTop -1 bze.z12.ac SonicTop bez.z12.ac DensityTop -1 bze.z12.car SonicTop bez.z12.car DensityTop -1 bze.z12.car SonicTop bez.z12.car DensityTop -1 bze.z12.can SonicTop bez.z12.can DensityTop -1 bze.shor.shor SonicTop bes.shor.shor DensityTop -1 bed.dopr.snl SonicTop bes.shor.shor DensityTop -1 bes.shor.sish SonicTop bes.shor.shor DensityTop -1 bes.shor.sish SonicTop det.del.wet DensityTop -1 cbs.shor.sish SonicTop det.del.wet DensityTop -1 det.del.wet SonicTop det.del.an DensityTop -1 det.del.anc SonicTop det.del.anc DensityTop -1 det.del.anc SonicTop det.del.anc DensityTop -1 det.del.anc SonicTop det.del.anc DensityTop -1 det.del.anc SonicTop det.del.an	wus.wu1.eva	SonicTop	wus.wu1.eva	DensityTop	-1
wus.wu1.wef SonicTop wus.wu1.wet DensityTop -1 wus.wu1.fn SonicTop wus.wu1.dry DensityTop -1 wus.wu1.fn SonicTop wus.wu1.fn DensityTop -1 wus.wu1.vol SonicTop wus.wu1.fn DensityTop -1 wus.wu2.wet SonicTop wus.wu2.wet DensityTop -1 wus.wu2.dry SonicTop wus.wu2.dry DensityTop -1 wus.wu2.fan SonicTop wus.wu2.dry DensityTop -1 wus.wu2.fan SonicTop wus.wu2.dry DensityTop -1 wus.wu2.fan SonicTop wus.wu2.sish DensityTop -1 wus.wu2.sish SonicTop wus.wu2.vol DensityTop -1 wus.wu2.vol SonicTop wus.wu2.vol DensityTop -1 seal2.seal.shl SonicTop bunt.up.snd DensityTop -1 bunt.up.snd SonicTop bunt.up.shl DensityTop -1 bunt.low.snd SonicTop bunt.low.snd DensityTop -1 bunt.low.snd SonicTop bunt.low.snd DensityTop -1 bunt.low.shl SonicTop bunt.low.snd DensityTop -1 bunt.low.shl SonicTop bunt.low.shl DensityTop -1 bunt.ze.z37.hal SonicTop uze.z37.hal DensityTop -1 buze.z37.shl SonicTop uze.z37.shl DensityTop -1 bze.z12.a2 SonicTop bze.z12.a2 DensityTop -1 bze.z12.a2 SonicTop bze.z12.a2 DensityTop -1 bze.z12.car SonicTop bze.z12.anh DensityTop -1 bze.z12.cop SonicTop bze.z12.anh DensityTop -1 bze.z12.cop SonicTop bez.z12.cop DensityTop -1 bze.z12.cop SonicTop bez.z12.cop DensityTop -1 bze.shor.sho SonicTop bez.z12.cop DensityTop -1 bes.shor.shor SonicTop bes.shor.shor DensityTop -1 cbs.shor.shor SonicTop bes.shor.shor DensityTop -1 cbs.shor.shor SonicTop det.del.sho DensityTop -1 cbs.wet.wet SonicTop det.del.sho DensityTop -1 cbs.wet.wet SonicTop det.del.sho DensityTop -1 cbs.wet.sish SonicTop det.del.sho DensityTop -1 cbs.wet.sish SonicTop det.del.sho DensityTop -1 cbs.wet.wet SonicTop det.del.sho DensityTop -1 cbs.wet.sish SonicTop det.del.sho DensityTop -1 cbs.shor.shor SonicTop det.del.sho DensityTop -1 cbs.sec.shn.sish DensityTop -1 cbs.se	wus.wu1.sil	SonicTop	wus.wu1.sil		-1
wus.wul.wet SonicTop wus.wul.wet DensityTop -1 wus.wul.fan SonicTop wus.wul.dry DensityTop -1 wus.wul.fan SonicTop wus.wul.dry DensityTop -1 wus.wul.vol SonicTop wus.wul.vol DensityTop -1 wus.wul.vol SonicTop wus.wul.vol DensityTop -1 wus.wul.wet SonicTop wus.wul.wet DensityTop -1 wus.wul.ard SonicTop wus.wul.wet DensityTop -1 wus.wul.fan SonicTop wus.wul.wet DensityTop -1 wus.wul.fan SonicTop wus.wul.ard DensityTop -1 wus.wul.fan SonicTop wus.wul.sish DensityTop -1 wus.wul.sish SonicTop wus.wul.vol DensityTop -1 wus.wul.vol SonicTop wus.wul.vol DensityTop -1 wus.wul.vol SonicTop bunt.up.sh DensityTop -1 bunt.up.sh SonicTop bunt.up.sh DensityTop -1 bunt.low.sh SonicTop bunt.low.sh DensityTop -1 buze.z37.ha DensityTop -1 bze.z12.a2 SonicTop bze.z12.a2 DensityTop -1 bze.z12.a2 SonicTop bze.z12.a2 DensityTop -1 bze.z12.cop SonicTop bze.z12.car DensityTop -1 bze.z12.cop SonicTop bze.z12.car DensityTop -1 bze.z12.cop SonicTop bez.z12.cop DensityTop -1 bed.dopr.sh SonicTop bes.shor.sho DensityTop -1 bebs.shor.sish SonicTop bes.shor.sho DensityTop -1 bebs.shor.sish SonicTop bes.shor.sho DensityTop -1 cbs.shor.sish SonicTop bes.shor.sho DensityTop -1 cbs.shor.sish SonicTop bes.shor.sish DensityTop -1 cbs.wet.wet SonicTop det.del.sho DensityTop -1 cbs.wet.wet SonicTop det.del.sho DensityTop -1 det.del.sho SonicTop det.del.sho DensityTop -1 det.del.sho SonicTop det.del.sho DensityTop -1 det.del.sho SonicTop det.del.sho DensityTop -1 det.del.san SonicTop det.del.sho DensityTop -1 det.del.san SonicTop det.del.sho De	wus.wu1.sho	SonicTop	wus.wu1.sho	DensityTop	-1
wus.wu1.dry SonicTop wus.wu1.dry DensityTop -1- wus.wu1.fan SonicTop wus.wu1.fan DensityTop -1- wus.wu1.vol SonicTop wus.wu1.fan DensityTop -1- wus.wu2.wet SonicTop wus.wu2.wet DensityTop -1- wus.wu2.dry SonicTop wus.wu2.dry DensityTop -1- wus.wu2.fan SonicTop wus.wu2.fan DensityTop -1- wus.wu2.sish SonicTop wus.wu2.fan DensityTop -1- wus.wu2.sish SonicTop wus.wu2.sish DensityTop -1- wus.wu2.sish SonicTop wus.wu2.sish DensityTop -1- wus.wu2.vol SonicTop wus.wu2.vol DensityTop -1- bunt.up.snd SonicTop bunt.up.snd DensityTop -1- bunt.up.snd SonicTop bunt.up.snd DensityTop -1- bunt.up.snd SonicTop bunt.up.snd DensityTop -1- bunt.low.snd SonicTop bunt.low.snd DensityTop -1- bunt.low.snl SonicTop bunt.low.snd DensityTop -1- buze.z37.hal SonicTop uze.z37.hal DensityTop -1- buze.z37.snl SonicTop uze.z37.a3 DensityTop -1- bze.z12.a2 SonicTop bze.z12.a2 DensityTop -1- bze.z12.a2 SonicTop bze.z12.a2 DensityTop -1- bze.z12.anh SonicTop bze.z12.an DensityTop -1- bze.z12.anh SonicTop bze.z12.car DensityTop -1- bze.z12.cop SonicTop bze.z12.car DensityTop -1- bze.z12.cop SonicTop bze.z12.can DensityTop -1- bze.shor.shor SonicTop heid.topr.snl DensityTop -1- bze.shor.shor SonicTop bes.shor.shor DensityTop -1- bzb.swet.sish SonicTop ebs.wet.sish DensityTop -1- cbs.wet.sish SonicTop det.del.ne DensityTop -1- cbs.wet.sish SonicTop det.del.ne DensityTop -1- cdt.del.ne SonicTop det.del.ne DensityTop -1- cdt.del.sho SonicTop det.del.ne DensityTop -1- cdt.del.anc SonicTop det.del.ne DensityTop -1- cdt.del.anc SonicTop det.del.anc DensityTop -1- cdt.del.anc SonicTop Dess.schn.sish DensityTop -1- cdt.d	wus.wu1.wet	SonicTop	wus.wu1.wet	DensityTop	-1
wus.wu1.fan SonicTop wus.wu1.fan DensityTop -1 wus.wu2.wet SonicTop wus.wu2.wet DensityTop -1 wus.wu2.wet SonicTop wus.wu2.wet DensityTop -1 wus.wu2.dry SonicTop wus.wu2.dry DensityTop -1 wus.wu2.fan SonicTop wus.wu2.fan DensityTop -1 wus.wu2.sih SonicTop wus.wu2.fan DensityTop -1 wus.wu2.vol SonicTop wus.wu2.sih DensityTop -1 wus.wu2.vol SonicTop wus.wu2.vol DensityTop -1 seal2.seal.shl SonicTop bunt.up.snd DensityTop -1 bunt.up.snd SonicTop bunt.up.snd DensityTop -1 bunt.up.snd SonicTop bunt.up.snd DensityTop -1 bunt.low.snd SonicTop bunt.low.snd DensityTop -1 bunt.low.snd SonicTop bez.212.a2 DensityTop -1 bunt.low.snd SonicTop bze.212.a2 DensityTop -1 bunt.low.snd SonicTop bze.212.a2 DensityTop -1 bunt.low.snd SonicTop bze.212.and DensityTop -1 bunt.low.snd SonicTop heid.topr.snd DensityTop -1 bunt.low.snd SonicTop heid.topr.snd DensityTop -1 bunt.low.snd SonicTop bze.212.and DensityTop -1 bunt.low.snd SonicTop ebs.shor.ssho DensityTop -1 ebs.shor.ssho SonicTop det.del.snd DensityTop -1 ebs.wet.sish SonicTop det.del.snd DensityTop -1 det.del.snd SonicTop det.del.snd DensityTop -1 det.del.snd SonicTop det.del.snd DensityTop -1 det.del.anc SonicTop det.del.snd DensityTop -1 det.del.anc SonicTop det.del.snd DensityTop -1 det.del.snd SonicTop det.del.snd DensityTop -1 det.del.anc SonicTop de	wus.wu1.dry	SonicTop	wus.wu1.dry	DensityTop	-1
wus.wu1.vol SonicTop wus.wu1.vol DensityTop ————————————————————————————————————	wus.wul.fan	SonicTop	wus.wu1.fan		-1
wus.wu2.wet SonicTop wus.wu2.wet DensityTop ————————————————————————————————————			wus.wu1.vol		-1
wus.wu2.dry SonicTop wus.wu2.dry DensityTop ————————————————————————————————————	wus.wu2.wet	SonicTop		DensityTop	-1
wus.wu2.sish SonicTop wus.wu2.sish DensityTop -1 wus.wu2.vol SonicTop wus.wu2.vol DensityTop -1 seal2.seal.shl SonicTop seal2.seal.shl DensityTop -1 bunt.up.snd SonicTop bunt.up.snd DensityTop -1 bunt.up.shl SonicTop bunt.up.shl DensityTop -1 bunt.low.snd SonicTop bunt.low.snd DensityTop -1 bunt.low.snd SonicTop bunt.low.snd DensityTop -1 bunt.low.snd SonicTop bunt.low.snd DensityTop -1 bunt.low.shl SonicTop bunt.low.shl DensityTop -1 bunt.low.shl SonicTop bunt.low.shl DensityTop -1 uze.z37.hal SonicTop uze.z37.hal DensityTop -1 uze.z37.sal SonicTop uze.z37.shl DensityTop -1 uze.z37.shl SonicTop uze.z37.shl DensityTop -1 uze.z37.shl SonicTop bze.z12.a2 DensityTop -1 bze.z12.a2 SonicTop bze.z12.a2 DensityTop -1 bze.z12.car SonicTop bze.z12.car DensityTop -1 bze.z12.car SonicTop bze.z12.car DensityTop -1 bze.z12.car SonicTop bze.z12.car DensityTop -1 bze.z12.cop SonicTop bze.z12.cop DensityTop -1 bze.z12.cop SonicTop bze.z12.cop DensityTop -1 beid.topr.shl SonicTop heid.topr.shl DensityTop -1 beid.topr.shl SonicTop heid.topr.shl DensityTop -1 cbs.shor.sish SonicTop ebs.shor.sish DensityTop -1 cbs.shor.sish SonicTop ebs.shor.sish DensityTop -1 cbs.wet.sish SonicTop bze.x12.cop DensityTop -1 cbs.wet.sish SonicTop det.del.sho DensityTop -1 cdt.del.sho SonicTop det.del.sho DensityTop -1 cdt.del.sish SonicTop det.del.sho DensityTop -1 cdt.del.sish SonicTop det.del.sho DensityTop -1 det.del.sish SonicTop det.del.sho DensityTop -1 det.del.anc SonicTop base.schn.sho D	wus.wu2.dry		wus.wu2.dry		-1
wus.wu2.vol SonicTop wus.wu2.vol DensityTop -1 seal2.seal.shl SonicTop seal2.seal.shl DensityTop -1 bunt.up.snd SonicTop bunt.up.snd DensityTop -1 bunt.up.shl SonicTop bunt.up.shl DensityTop -1 bunt.low.snd SonicTop bunt.low.snd DensityTop -1 bunt.low.snd SonicTop bunt.low.snd DensityTop -1 bunt.low.snd SonicTop bunt.low.snd DensityTop -1 bunt.low.shl SonicTop bunt.low.shl DensityTop -1 bunt.low.shl SonicTop bunt.low.shl DensityTop -1 uze.z37.hal SonicTop uze.z37.hal DensityTop -1 uze.z37.a3 SonicTop uze.z37.shl DensityTop -1 uze.z37.shl SonicTop uze.z37.shl DensityTop -1 bze.z12.a2 SonicTop bze.z12.a2 DensityTop -1 bze.z12.car SonicTop bze.z12.a2 DensityTop -1 bze.z12.car SonicTop bze.z12.car DensityTop -1 bze.z12.cop SonicTop bze.z12.cop DensityTop -1 bze.z12.cop SonicTop bze.z12.cop DensityTop -1 bze.shor.shd SonicTop heid.topr.snd DensityTop -1 heid.topr.snd SonicTop heid.topr.snd DensityTop -1 bes.shor.sish SonicTop ebs.shor.sish DensityTop -1 cbs.shor.sish SonicTop ebs.shor.sish DensityTop -1 cbs.wet.wet SonicTop ebs.shor.sish DensityTop -1 cbs.wet.wet SonicTop ebs.wet.wet DensityTop -1 cbs.wet.sish SonicTop det.del.sho DensityTop -1 det.del.sho SonicTop det.del.sho DensityTop -1 det.del.anc SonicTop det.del.anc DensityTop -1 det.del.anc SonicTop det.del.anc DensityTop -1 det.del.anc SonicTop base.schn.sho DensityTop -1 det.del.anc SonicTop base.schn.sho DensityTop -1 det.del.anc SonicTop base.schn.sho DensityTop -1 det.del.anc SonicTop det.del.anc DensityTop -1 det.del.anc SonicTop det.del.anc DensityTop -1 det.del.anc SonicTop Desc.schn.sho DensityTop -1 det.del.anc SonicTop Desc.sc	wus.wu2.fan	SonicTop	wus.wu2.fan	DensityTop	-1
wus.wu2.vol SonicTop wus.wu2.vol DensityTop -1 seal2.seal.shl SonicTop seal2.seal.shl DensityTop -1 bunt.up.snd SonicTop bunt.up.snd DensityTop -1 bunt.up.shl SonicTop bunt.up.shl DensityTop -1 bunt.low.snd SonicTop bunt.low.snd DensityTop -1 bunt.low.snd SonicTop bunt.low.snd DensityTop -1 bunt.low.snd SonicTop bunt.low.snd DensityTop -1 bunt.low.shl SonicTop bunt.low.shl DensityTop -1 bunt.low.shl SonicTop bunt.low.shl DensityTop -1 uze.z37.hal SonicTop uze.z37.hal DensityTop -1 uze.z37.a3 SonicTop uze.z37.shl DensityTop -1 uze.z37.shl SonicTop uze.z37.shl DensityTop -1 bze.z12.a2 SonicTop bze.z12.a2 DensityTop -1 bze.z12.car SonicTop bze.z12.a2 DensityTop -1 bze.z12.car SonicTop bze.z12.car DensityTop -1 bze.z12.cop SonicTop bze.z12.cop DensityTop -1 bze.z12.cop SonicTop bze.z12.cop DensityTop -1 bze.shor.shd SonicTop heid.topr.snd DensityTop -1 heid.topr.snd SonicTop heid.topr.snd DensityTop -1 bes.shor.sish SonicTop ebs.shor.sish DensityTop -1 cbs.shor.sish SonicTop ebs.shor.sish DensityTop -1 cbs.wet.wet SonicTop ebs.shor.sish DensityTop -1 cbs.wet.wet SonicTop ebs.wet.wet DensityTop -1 cbs.wet.sish SonicTop det.del.sho DensityTop -1 det.del.sho SonicTop det.del.sho DensityTop -1 det.del.anc SonicTop det.del.anc DensityTop -1 det.del.anc SonicTop det.del.anc DensityTop -1 det.del.anc SonicTop base.schn.sho DensityTop -1 det.del.anc SonicTop base.schn.sho DensityTop -1 det.del.anc SonicTop base.schn.sho DensityTop -1 det.del.anc SonicTop det.del.anc DensityTop -1 det.del.anc SonicTop det.del.anc DensityTop -1 det.del.anc SonicTop Desc.schn.sho DensityTop -1 det.del.anc SonicTop Desc.sc	wus.wu2.sish	SonicTop	wus.wu2.sish	DensityTop	-1
seal2.seal.shl SonicTop seal2.seal.shl DensityTop 1 bunt.up.snd SonicTop bunt.up.snd DensityTop -1 bunt.low.snd SonicTop bunt.low.snd DensityTop -1 bunt.low.snd SonicTop bunt.low.snd DensityTop -1 bunt.low.shl SonicTop bunt.low.shl DensityTop -1 uze.z37.hal SonicTop uze.z37.hal DensityTop -1 uze.z37.shl SonicTop uze.z37.shl DensityTop -1 uze.z37.shl SonicTop uze.z37.shl DensityTop -1 bze.z12.a2 SonicTop bze.z12.a2 DensityTop -1 bze.z12.a2 SonicTop bze.z12.ca DensityTop -1 bze.z12.cop SonicTop bze.z12.cop DensityTop -1 heid.topr.shl SonicTop bez.shc.sib.r.shor.shor DensityTop -1 ebs.shor.sish SonicTop ebs.shor.sish DensityTop -1 ebs.wet.wet SonicT	wus.wu2.vol		wus.wu2.vol		-1
bunt.up.sndSonicTopbunt.up.sndDensityTop-1bunt.low.sndSonicTopbunt.low.sndDensityTop-1bunt.low.sndSonicTopbunt.low.sndDensityTop-1bunt.low.shlSonicTopbunt.low.shlDensityTop-1bunt.low.shlSonicTopbunt.low.shlDensityTop-1uze.z37.halSonicTopuze.z37.halDensityTop-1uze.z37.a3SonicTopuze.z37.shlDensityTop-1uze.z37.shlSonicTopbze.z12.a2DensityTop-1bze.z12.a2SonicTopbze.z12.a2DensityTop-1bze.z12.a1SonicTopbze.z12.anDensityTop-1bze.z12.anhSonicTopbze.z12.anhDensityTop-1bze.z12.copSonicTopbze.z12.copDensityTop-1heid.topr.sndSonicTopbeid.topr.sndDensityTop-1heid.topr.sndSonicTopebs.shor.shorDensityTop-1ebs.shor.shorSonicTopebs.shor.shorDensityTop-1ebs.wet.wetSonicTopebs.wet.wetDensityTop-1ebs.wet.sishSonicTopebs.wet.sishDensityTop-1ebs.wet.sishSonicTopebs.wet.sishDensityTop-1det.de1.shoSonicTopdet.de1.shoDensityTop-1det.de1.shoSonicTopdet.de1.shoDensityTop-1det.de2.wetSonicTopdet.de2.shoDensityTop-1			seal2.seal.shl		-1
bunt.low.shl SonicTop bunt.low.shl DensityTop -1 bunt.low.snd SonicTop bunt.low.snd DensityTop -1 bunt.low.lim SonicTop bunt.low.shl DensityTop -1 bunt.low.shl SonicTop bunt.low.shl DensityTop -1 uze.z37.hal SonicTop uze.z37.hal DensityTop -1 uze.z37.shl SonicTop uze.z37.shl DensityTop -1 bze.z12.a2 SonicTop bze.z12.a2 DensityTop -1 bze.z12.a1 SonicTop bze.z12.car DensityTop -1 bze.z12.anh SonicTop bze.z12.cop DensityTop -1 bze.z12.cop SonicTop bze.z12.cop DensityTop -1 heid.topr.snd SonicTop bez.t12.cop DensityTop -1 heid.topr.snd SonicTop bes.shor.shor DensityTop -1 ebs.shor.sish SonicTop ebs.shor.shor DensityTop -1 ebs.shor.sish SonicTop	bunt.up.snd		bunt.up.snd		-1
bunt.low.snd SonicTop bunt.low.snd DensityTop -1 bunt.low.lim SonicTop bunt.low.lim DensityTop -1 bunt.low.shl SonicTop bunt.low.shl DensityTop -1 uze.z37.hal SonicTop uze.z37.hal DensityTop -1 uze.z37.hal SonicTop uze.z37.a3 DensityTop -1 uze.z37.shl SonicTop uze.z37.a3 DensityTop -1 uze.z37.shl SonicTop uze.z37.shl DensityTop -1 uze.z37.shl SonicTop uze.z37.shl DensityTop -1 bze.z12.a2 SonicTop bze.z12.a2 DensityTop -1 bze.z12.car SonicTop bze.z12.car DensityTop -1 bze.z12.can SonicTop bze.z12.can DensityTop -1 bze.z12.cop SonicTop bze.z12.cop DensityTop -1 bez.z12.cop SonicTop bze.z12.cop DensityTop -1 beid.topr.snd SonicTop heid.topr.snd DensityTop -1 beid.topr.snl SonicTop heid.topr.snl DensityTop -1 cbs.shor.sish SonicTop ebs.shor.sish DensityTop -1 ebs.wet.wet SonicTop ebs.wet.wet DensityTop -1 ebs.wet.sish SonicTop ebs.wet.sish DensityTop -1 ebs.wet.sish SonicTop det.del.sho DensityTop -1 det.del.sho SonicTop det.del.sho DensityTop -1 det.del.sho SonicTop det.del.sho DensityTop -1 det.del.sish SonicTop det.del.sish DensityTop -1 det.del.sish SonicTop det.del.anc DensityTop -1 det.del.anc SonicTop det.del.anc DensityTop -1 det.del.anc SonicTop det.del.anc DensityTop -1 det.del.anc SonicTop det.del.anc DensityTop -1 det.del.sish SonicTop det.del.anc DensityTop -1 det.del.anc SonicTop base.schn.sib DensityTop -1 lowr.vol.vol SonicTop base.schn.sib DensityTop -1 lowr.vol.vol DensityTop -1 lowr.vol.vol DensityTop -1 lowr.vol.vol DensityTop -1					-1
bunt.low.limSonicTopbunt.low.limDensityTop-1bunt.low.shlSonicTopbunt.low.shlDensityTop-1uze.z37.halSonicTopuze.z37.halDensityTop-1uze.z37.a3SonicTopuze.z37.a3DensityTop-1uze.z37.shlSonicTopuze.z37.shlDensityTop-1bze.z12.a2SonicTopbze.z12.a2DensityTop-1bze.z12.a1SonicTopbze.z12.a2DensityTop-1bze.z12.anhSonicTopbze.z12.copDensityTop-1bze.z12.copSonicTopbze.z12.copDensityTop-1heid.topr.sndSonicTopheid.topr.sndDensityTop-1heid.topr.shlSonicTopheid.topr.shlDensityTop-1ebs.shor.sishSonicTopebs.shor.shorDensityTop-1ebs.wet.wetSonicTopebs.shor.sishDensityTop-1ebs.wet.sishSonicTopebs.wet.wetDensityTop-1ebs.wet.sishSonicTopdet.del.shoDensityTop-1det.del.shoSonicTopdet.del.shoDensityTop-1det.del.shoSonicTopdet.del.lanDensityTop-1det.del.fanSonicTopdet.del.lanDensityTop-1det.del.ancSonicTopdet.del.ancDensityTop-1det.del.ancSonicTopdet.del.ancDensityTop-1det.del.ganSonicTopdet.del.ganDensityTop-1					-1
bunt.low.shl SonicTop bunt.low.shl DensityTop -1 uze.z37.hal SonicTop uze.z37.hal DensityTop -1 uze.z37.a3 SonicTop uze.z37.hal DensityTop -1 uze.z37.shl SonicTop uze.z37.shl DensityTop -1 uze.z37.shl SonicTop uze.z37.shl DensityTop -1 bze.z12.a2 SonicTop bze.z12.a2 DensityTop -1 bze.z12.car SonicTop bze.z12.car DensityTop -1 bze.z12.canh SonicTop bze.z12.car DensityTop -1 bze.z12.cop SonicTop bze.z12.cop DensityTop -1 bze.z12.cop SonicTop bze.z12.cop DensityTop -1 heid.topr.snd SonicTop heid.topr.snd DensityTop -1 heid.topr.shl SonicTop heid.topr.shl DensityTop -1 bes.shor.sish SonicTop ebs.shor.shor DensityTop -1 ebs.shor.sish SonicTop ebs.shor.sish DensityTop -1 ebs.wet.wet SonicTop ebs.wet.wet DensityTop -1 ebs.wet.sish SonicTop ebs.wet.sish DensityTop -1 ebs.wet.sish SonicTop det.del.sho DensityTop -1 det.del.sho SonicTop det.del.sho DensityTop -1 det.del.sho SonicTop det.del.sho DensityTop -1 det.del.wet SonicTop det.del.wet DensityTop -1 det.del.sish SonicTop det.del.anc DensityTop -1 det.del.anc SonicTop det.del.sho DensityTop -1 det.del.anc SonicTop det.del.sho DensityTop -1 det.del.sho SonicTop det.del.sho DensityTop -1 det.del.anc SonicTop det.del.sho DensityTop -1 det.del.sho SonicTop det.del.sho DensityTop -1 det.del.sea.sho SonicTop base.schn.sho DensityTop -1 det.del.sea.sho SonicTop base.schn.sho DensityTop -1 det.del.sea.sho.sonicTop base.schn.fan DensityTop -1 base.schn.fan SonicTop base.schn.fan DensityTop -1 lowr.vol.vol DensityTop -1 lowr.car.snd SonicTop lowr.car.snd DensityTop -1	bunt.low.lim		bunt.low.lim		-1
uze.z37.halSonicTopuze.z37.halDensityTop-1uze.z37.a3SonicTopuze.z37.shlDensityTop-1bze.z12.a2SonicTopbze.z12.a2DensityTop-1bze.z12.carSonicTopbze.z12.carDensityTop-1bze.z12.carSonicTopbze.z12.carDensityTop-1bze.z12.canhSonicTopbze.z12.canhDensityTop-1bze.z12.copSonicTopbze.z12.copDensityTop-1heid.topr.sndSonicTopheid.topr.sndDensityTop-1heid.topr.shlSonicTopheid.topr.shlDensityTop-1cbs.shor.shorSonicTopebs.shor.shorDensityTop-1cbs.shor.sishSonicTopebs.shor.sishDensityTop-1cbs.wet.wetSonicTopebs.wet.wetDensityTop-1cbs.wet.sishSonicTopebs.wet.sishDensityTop-1seal3.seal.shlSonicTopdet.del.shoDensityTop-1det.del.shoSonicTopdet.del.shoDensityTop-1det.del.ancSonicTopdet.del.sishDensityTop-1det.del.fanSonicTopdet.del.sishDensityTop-1det.de2.wetSonicTopdet.de2.sishDensityTop-1det.de2.drySonicTopdet.de2.fanDensityTop-1det.de2.fanSonicTopdet.de2.fanDensityTop-1det.de2.fanSonicTopdet.de2.sishDensityTop-1 <td></td> <td></td> <td></td> <td></td> <td>-1</td>					-1
uze.z37.a3SonicTopuze.z37.a3DensityTop-1uze.z37.shlSonicTopuze.z37.shlDensityTop-1bze.z12.a2SonicTopbze.z12.a2DensityTop-1bze.z12.carSonicTopbze.z12.carDensityTop-1bze.z12.anhSonicTopbze.z12.canDensityTop-1bze.z12.copSonicTopbze.z12.copDensityTop-1bze.z12.copSonicTopbeid.topr.sndDensityTop-1heid.topr.shlSonicTopheid.topr.shlDensityTop-1ebs.shor.shorSonicTopebs.shor.shorDensityTop-1ebs.shor.sishSonicTopebs.shor.sishDensityTop-1ebs.wet.wetSonicTopebs.wet.wetDensityTop-1ebs.wet.sishSonicTopebs.wet.sishDensityTop-1ebs.wet.sishSonicTopdet.del.shoDensityTop-1det.del.shoSonicTopdet.del.wetDensityTop-1det.del.wetSonicTopdet.del.wetDensityTop-1det.del.sishSonicTopdet.del.sishDensityTop-1det.del.ancSonicTopdet.del.sishDensityTop-1det.de2.wetSonicTopdet.del.ancDensityTop-1det.de2.fanSonicTopdet.de2.fanDensityTop-1det.de2.fanSonicTopdet.de2.sishDensityTop-1det.de2.ancSonicTopbase.schn.wetDensityTop-1 <tr< td=""><td></td><td></td><td></td><td></td><td>-1</td></tr<>					-1
uze.z37.shlSonicTopuze.z37.shlDensityTop-1bze.z12.a2SonicTopbze.z12.a2DensityTop-1bze.z12.carSonicTopbze.z12.carDensityTop-1bze.z12.anhSonicTopbze.z12.copDensityTop-1bze.z12.copSonicTopbze.z12.copDensityTop-1heid.topr.sndSonicTopheid.topr.sndDensityTop-1heid.topr.shlSonicTopheid.topr.shlDensityTop-1heid.spr.shor.shorSonicTopebs.shor.shorDensityTop-1ebs.shor.sishSonicTopebs.shor.sishDensityTop-1ebs.wet.wetSonicTopebs.wet.wetDensityTop-1ebs.wet.sishSonicTopebs.wet.sishDensityTop-1ebs.wet.sishSonicTopdet.del.shoDensityTop-1det.del.shoSonicTopdet.del.shoDensityTop-1det.del.shoSonicTopdet.del.wetDensityTop-1det.del.shoSonicTopdet.del.shoDensityTop-1det.del.sishSonicTopdet.del.sishDensityTop-1det.del.ancSonicTopdet.del.ancDensityTop-1det.de2.wetSonicTopdet.de2.wetDensityTop-1det.de2.fanSonicTopdet.de2.fanDensityTop-1det.de2.fanSonicTopdet.de2.sishDensityTop-1det.de2.ancSonicTopbase.schn.wetDensityTop-1				DensityTop	-1
bze.z12.a2 SonicTop bze.z12.a2 DensityTop -1 bze.z12.car SonicTop bze.z12.car DensityTop -1 bze.z12.anh SonicTop bze.z12.car DensityTop -1 bze.z12.cop SonicTop bze.z12.cop DensityTop -1 bze.z12.cop SonicTop bze.z12.cop DensityTop -1 heid.topr.snd SonicTop heid.topr.snd DensityTop -1 heid.topr.shl SonicTop heid.topr.shl DensityTop -1 cbs.shor.shor SonicTop ebs.shor.shor DensityTop -1 cbs.shor.sish SonicTop ebs.shor.shor DensityTop -1 cbs.wet.wet SonicTop ebs.wet.wet DensityTop -1 cbs.wet.sish SonicTop ebs.wet.sish DensityTop -1 cesal3.seal.shl SonicTop ebs.wet.sish DensityTop -1 det.de1.sho SonicTop det.de1.sho DensityTop -1 det.de1.sho SonicTop det.de1.sho DensityTop -1 det.de1.sish SonicTop det.de1.sish DensityTop -1 det.de2.wet SonicTop det.de1.sish DensityTop -1 det.de2.wet SonicTop det.de2.wet DensityTop -1 det.de2.wet SonicTop det.de2.wet DensityTop -1 det.de2.sish SonicTop det.de2.sish DensityTop -1 det.de2.sish SonicTop det.de2.anc DensityTop -1 det.de2.sish SonicTop det.de2.anc DensityTop -1 det.de2.anc SonicTop base.schn.dry DensityTop -1 base.schn.dry SonicTop base.schn.dry DensityTop -1 base.schn.sish SonicTop base.schn.sish DensityTop -1 base.schn.sish SonicTop base.schn.sish DensityTop -1 lowr.vol.vol SonicTop lowr.vol.vol DensityTop -1 lowr.car.snd SonicTop lowr.car.snd DensityTop -1					-1
bze.z12.carSonicTopbze.z12.carDensityTop-1bze.z12.anhSonicTopbze.z12.anhDensityTop-1bze.z12.copSonicTopbze.z12.copDensityTop-1heid.topr.sndSonicTopheid.topr.sndDensityTop-1heid.topr.shlSonicTopheid.topr.shlDensityTop-1cbs.shor.shorSonicTopebs.shor.shorDensityTop-1cbs.shor.sishSonicTopebs.shor.shorDensityTop-1cbs.wet.wetSonicTopebs.wet.wetDensityTop-1cbs.wet.sishSonicTopebs.wet.sishDensityTop-1seal3.seal.shlSonicTopseal3.seal.shlDensityTop-1det.de1.shoSonicTopdet.de1.shoDensityTop-1det.de1.shoSonicTopdet.de1.wetDensityTop-1det.de1.shoSonicTopdet.de1.sishDensityTop-1det.de1.sishSonicTopdet.de1.sishDensityTop-1det.de2.sishSonicTopdet.de2.wetDensityTop-1det.de2.wetSonicTopdet.de2.wetDensityTop-1det.de2.fanSonicTopdet.de2.fanDensityTop-1det.de2.sishSonicTopdet.de2.ancDensityTop-1det.de2.ancSonicTopbase.schn.wetDensityTop-1base.schn.drySonicTopbase.schn.fanDensityTop-1base.schn.fanSonicTopbase.schn.fanDensityTop <td></td> <td></td> <td></td> <td></td> <td>-1</td>					-1
bze.z12.anh SonicTop bze.z12.anh DensityTop -1 bze.z12.cop SonicTop bze.z12.cop DensityTop -1 heid.topr.snd SonicTop heid.topr.snd DensityTop -1 heid.topr.shl SonicTop heid.topr.shl DensityTop -1 ebs.shor.shor SonicTop ebs.shor.shor DensityTop -1 ebs.shor.sish SonicTop ebs.shor.sish DensityTop -1 ebs.wet.wet SonicTop ebs.wet.wet DensityTop -1 ebs.wet.sish SonicTop ebs.wet.sish DensityTop -1 ebs.wet.sish SonicTop det.de1.sho DensityTop -1 det.de1.sho SonicTop det.de1.sho DensityTop -1 det.de1.sho SonicTop det.de1.sho DensityTop -1 det.de1.sish SonicTop det.de1.sish DensityTop -1 det.de2.wet SonicTop det.de1.anc DensityTop -1 det.de2.wet SonicTop det.de2.wet DensityTop -1 det.de2.sish SonicTop det.de2.wet DensityTop -1 det.de2.fan SonicTop det.de2.fan DensityTop -1 det.de2.sish SonicTop det.de2.sish DensityTop -1 det.de2.anc SonicTop det.de2.sish DensityTop -1 det.de2.anc SonicTop det.de2.anc DensityTop -1 base.schn.wet SonicTop base.schn.dry DensityTop -1 base.schn.fan SonicTop base.schn.fan DensityTop -1 base.schn.fan SonicTop base.schn.fan DensityTop -1 base.schn.fan SonicTop base.schn.sish DensityTop -1 lowr.vol.vol SonicTop lowr.vol.vol DensityTop -1					-1
bze.z12.cop SonicTop bze.z12.cop DensityTop -1 heid.topr.snd SonicTop heid.topr.snd DensityTop -1 heid.topr.shl SonicTop heid.topr.shl DensityTop -1 ebs.shor.shor SonicTop ebs.shor.shor DensityTop -1 ebs.shor.sish SonicTop ebs.shor.sish DensityTop -1 ebs.wet.wet SonicTop ebs.wet.wet DensityTop -1 ebs.wet.sish SonicTop ebs.wet.sish DensityTop -1 edet.de1.sho SonicTop det.de1.sho DensityTop -1 det.de1.sho SonicTop det.de1.sho DensityTop -1 det.de1.wet SonicTop det.de1.sho DensityTop -1 det.de1.fan SonicTop det.de1.sish DensityTop -1 det.de2.wet SonicTop det.de1.anc DensityTop -1 det.de2.wet SonicTop det.de2.wet DensityTop -1 det.de2.dry SonicTop det.de2.wet DensityTop -1 det.de2.fan SonicTop det.de2.fan DensityTop -1 det.de2.fan SonicTop det.de2.sish DensityTop -1 det.de2.anc SonicTop det.de2.sish DensityTop -1 det.de2.anc SonicTop det.de2.anc DensityTop -1 base.schn.wet SonicTop base.schn.dry DensityTop -1 base.schn.fan SonicTop base.schn.dry DensityTop -1 base.schn.fan SonicTop base.schn.fan DensityTop -1 base.schn.fan SonicTop base.schn.sish DensityTop -1 lowr.vol.vol SonicTop lowr.vol.vol DensityTop -1 lowr.car.snd SonicTop lowr.car.snd DensityTop -1					-1
heid.topr.snd SonicTop heid.topr.snd DensityTop -1 heid.topr.shl SonicTop heid.topr.shl DensityTop -1 ebs.shor.shor SonicTop ebs.shor.shor DensityTop -1 ebs.shor.sish SonicTop ebs.shor.sish DensityTop -1 ebs.wet.wet SonicTop ebs.wet.wet DensityTop -1 ebs.wet.sish SonicTop ebs.wet.sish DensityTop -1 ebs.wet.sish SonicTop ebs.wet.sish DensityTop -1 seal3.seal.shl SonicTop seal3.seal.shl DensityTop -1 det.de1.sho SonicTop det.de1.sho DensityTop -1 det.de1.wet SonicTop det.de1.sho DensityTop -1 det.de1.fan SonicTop det.de1.sish DensityTop -1 det.de2.fan SonicTop det.de1.anc DensityTop -1 det.de2.wet SonicTop det.de2.wet DensityTop -1 det.de2.dry SonicTop det.de2.wet DensityTop -1 det.de2.fan SonicTop det.de2.fan DensityTop -1 det.de2.fan SonicTop det.de2.fan DensityTop -1 det.de2.fan SonicTop det.de2.sish DensityTop -1 det.de2.nc SonicTop det.de2.sish DensityTop -1 det.de2.anc SonicTop det.de2.anc DensityTop -1 base.schn.wet SonicTop base.schn.dry DensityTop -1 base.schn.fan SonicTop base.schn.fan DensityTop -1 base.schn.fan SonicTop base.schn.fan DensityTop -1 base.schn.sish SonicTop base.schn.sish DensityTop -1 lowr.vol.vol SonicTop lowr.vol.vol DensityTop -1 lowr.car.snd SonicTop lowr.car.snd DensityTop -1					-1
heid.topr.shl SonicTop heid.topr.shl DensityTop -1 ebs.shor.shor SonicTop ebs.shor.shor DensityTop -1 ebs.shor.sish SonicTop ebs.shor.sish DensityTop -1 ebs.wet.wet SonicTop ebs.wet.wet DensityTop -1 ebs.wet.sish SonicTop ebs.wet.sish DensityTop -1 ebs.wet.sish SonicTop ebs.wet.sish DensityTop -1 seal3.seal.shl SonicTop seal3.seal.shl DensityTop -1 det.de1.sho SonicTop det.de1.sho DensityTop -1 det.de1.wet SonicTop det.de1.sho DensityTop -1 det.de1.sish SonicTop det.de1.sish DensityTop -1 det.de1.fan SonicTop det.de1.sish DensityTop -1 det.de2.sish SonicTop det.de2.wet DensityTop -1 det.de2.wet SonicTop det.de2.wet DensityTop -1 det.de2.han SonicTop det.de2.wet DensityTop -1 det.de2.fan SonicTop det.de2.fan DensityTop -1 det.de2.fan SonicTop det.de2.fan DensityTop -1 det.de2.sish SonicTop det.de2.sish DensityTop -1 det.de2.anc SonicTop det.de2.sish DensityTop -1 det.de2.anc SonicTop det.de2.sish DensityTop -1 base.schn.wet SonicTop base.schn.wet DensityTop -1 base.schn.fan SonicTop base.schn.dry DensityTop -1 base.schn.fan SonicTop base.schn.fan DensityTop -1 base.schn.sish SonicTop base.schn.sish DensityTop -1 lowr.vol.vol SonicTop lowr.vol.vol DensityTop -1 lowr.car.snd SonicTop lowr.car.snd DensityTop -1					-1
ebs.shor.shor SonicTop ebs.shor.shor DensityTop -1 ebs.shor.sish SonicTop ebs.shor.sish DensityTop -1 ebs.wet.wet SonicTop ebs.wet.wet DensityTop -1 ebs.wet.sish SonicTop ebs.wet.sish DensityTop -1 ebs.wet.sish SonicTop det.del.sho DensityTop -1 det.del.sho SonicTop det.del.sho DensityTop -1 det.del.wet SonicTop det.del.wet DensityTop -1 det.del.fan SonicTop det.del.sish DensityTop -1 det.del.sish SonicTop det.del.sish DensityTop -1 det.del.anc SonicTop det.del.anc DensityTop -1 det.de2.wet SonicTop det.de2.wet DensityTop -1 det.de2.fan SonicTop det.de2.fan DensityTop -1 det.de2.fan SonicTop det.de2.fan DensityTop -1 det.de2.sish SonicTop det.de2.sish DensityTop -1 det.de2.anc SonicTop det.de2.anc DensityTop -1 base.schn.wet SonicTop base.schn.wet DensityTop -1 base.schn.dry SonicTop base.schn.dry DensityTop -1 base.schn.fan SonicTop base.schn.fan DensityTop -1 base.schn.sish SonicTop base.schn.sish DensityTop -1 lowr.vol.vol SonicTop lowr.vol.vol DensityTop -1 lowr.car.snd SonicTop lowr.car.snd DensityTop -1					-1
ebs.shor.sish SonicTop ebs.shor.sish DensityTop -1 ebs.wet.wet SonicTop ebs.wet.wet DensityTop -1 ebs.wet.sish SonicTop ebs.wet.sish DensityTop -1 seal3.seal.shl SonicTop seal3.seal.shl DensityTop -1 det.de1.sho SonicTop det.de1.sho DensityTop -1 det.de1.wet SonicTop det.de1.wet DensityTop -1 det.de1.fan SonicTop det.de1.sish DensityTop -1 det.de1.fan SonicTop det.de1.sish DensityTop -1 det.de1.sish SonicTop det.de1.sish DensityTop -1 det.de2.sish SonicTop det.de2.wet DensityTop -1 det.de2.wet SonicTop det.de2.wet DensityTop -1 det.de2.dry SonicTop det.de2.dry DensityTop -1 det.de2.fan SonicTop det.de2.fan DensityTop -1 det.de2.sish SonicTop det.de2.sish DensityTop -1 det.de2.sish SonicTop det.de2.sish DensityTop -1 det.de2.sish SonicTop det.de2.nc DensityTop -1 det.de2.anc SonicTop det.de2.anc DensityTop -1 base.schn.wet SonicTop base.schn.wet DensityTop -1 base.schn.dry SonicTop base.schn.dry DensityTop -1 base.schn.fan SonicTop base.schn.fan DensityTop -1 base.schn.sish SonicTop base.schn.fan DensityTop -1 lowr.vol.vol SonicTop lowr.vol.vol DensityTop -1 lowr.car.snd SonicTop lowr.car.snd DensityTop -1					-1
ebs.wet.wet SonicTop ebs.wet.wet DensityTop -1 ebs.wet.sish SonicTop ebs.wet.sish DensityTop -1 seal3.seal.shl SonicTop seal3.seal.shl DensityTop -1 det.de1.sho SonicTop det.de1.sho DensityTop -1 det.de1.wet SonicTop det.de1.wet DensityTop -1 det.de1.fan SonicTop det.de1.sish DensityTop -1 det.de1.sish SonicTop det.de1.fan DensityTop -1 det.de1.sish SonicTop det.de1.fan DensityTop -1 det.de2.wet SonicTop det.de2.wet DensityTop -1 det.de2.wet SonicTop det.de2.wet DensityTop -1 det.de2.fan SonicTop det.de2.fan DensityTop -1 det.de2.fan SonicTop det.de2.fan DensityTop -1 det.de2.sish SonicTop det.de2.sish DensityTop -1 det.de2.sish SonicTop det.de2.sish DensityTop -1 det.de2.sish SonicTop det.de2.sish DensityTop -1 det.de2.anc SonicTop det.de2.anc DensityTop -1 base.schn.wet SonicTop base.schn.wet DensityTop -1 base.schn.dry SonicTop base.schn.dry DensityTop -1 base.schn.fan SonicTop base.schn.fan DensityTop -1 base.schn.sish SonicTop base.schn.fan DensityTop -1 lowr.vol.vol SonicTop lowr.vol.vol DensityTop -1 lowr.car.snd SonicTop lowr.car.snd DensityTop -1					-1
ebs.wet.sish SonicTop ebs.wet.sish DensityTop -1 seal3.seal.shl SonicTop seal3.seal.shl DensityTop -1 det.de1.sho SonicTop det.de1.sho DensityTop -1 det.de1.wet SonicTop det.de1.wet DensityTop -1 det.de1.fan SonicTop det.de1.fan DensityTop -1 det.de1.sish SonicTop det.de1.sish DensityTop -1 det.de1.anc SonicTop det.de1.anc DensityTop -1 det.de2.wet SonicTop det.de2.wet DensityTop -1 det.de2.dry SonicTop det.de2.dry DensityTop -1 det.de2.fan SonicTop det.de2.fan DensityTop -1 det.de2.sish SonicTop det.de2.sish DensityTop -1 det.de2.sish SonicTop det.de2.sish DensityTop -1 det.de2.anc SonicTop det.de2.sish DensityTop -1 seal4.seal.shl SonicTop base.schn.wet DensityTop -1 base.schn.dry SonicTop base.schn.dry DensityTop -1 base.schn.fan SonicTop base.schn.fan DensityTop -1 base.schn.sish SonicTop base.schn.sish DensityTop -1 lowr.vol.vol SonicTop lowr.vol.vol DensityTop -1 lowr.car.snd SonicTop lowr.car.snd DensityTop -1					-1
seal3.seal.shlSonicTopseal3.seal.shlDensityTop-1det.de1.shoSonicTopdet.de1.shoDensityTop-1det.de1.wetSonicTopdet.de1.wetDensityTop-1det.de1.fanSonicTopdet.de1.fanDensityTop-1det.de1.sishSonicTopdet.de1.sishDensityTop-1det.de1.ancSonicTopdet.de2.wetDensityTop-1det.de2.wetSonicTopdet.de2.wetDensityTop-1det.de2.drySonicTopdet.de2.dryDensityTop-1det.de2.fanSonicTopdet.de2.fanDensityTop-1det.de2.sishSonicTopdet.de2.sishDensityTop-1det.de2.ancSonicTopdet.de2.ancDensityTop-1base.schn.wetSonicTopbase.schn.wetDensityTop-1base.schn.drySonicTopbase.schn.dryDensityTop-1base.schn.fanSonicTopbase.schn.fanDensityTop-1base.schn.sishSonicTopbase.schn.sishDensityTop-1lowr.vol.volSonicToplowr.vol.volDensityTop-1lowr.car.sndSonicToplowr.car.sndDensityTop-1					-1
det.de1.sho SonicTop det.de1.sho DensityTop -1 det.de1.wet SonicTop det.de1.wet DensityTop -1 det.de1.fan SonicTop det.de1.fan DensityTop -1 det.de1.sish SonicTop det.de1.sish DensityTop -1 det.de2.met SonicTop det.de2.wet DensityTop -1 det.de2.dry SonicTop det.de2.dry DensityTop -1 det.de2.fan SonicTop det.de2.fan DensityTop -1 det.de2.sish SonicTop det.de2.sish DensityTop -1 det.de2.anc SonicTop det.de2.anc DensityTop -1 base.sl.shl SonicTop base.schn.wet DensityTop -1 base.schn.dry SonicTop base.schn.dry DensityTop -1 base.schn.fan SonicTop base.schn.fan DensityTop -1 base.schn.sish SonicTop base.schn.sish DensityTop -1 lowr.vol.vol SonicTop </td <td></td> <td></td> <td>seal3.seal.shl</td> <td></td> <td>-1</td>			seal3.seal.shl		-1
det.de1.wet SonicTop det.de1.wet DensityTop -1 det.de1.fan SonicTop det.de1.fan DensityTop -1 det.de1.sish SonicTop det.de1.sish DensityTop -1 det.de2.met SonicTop det.de2.wet DensityTop -1 det.de2.wet SonicTop det.de2.wet DensityTop -1 det.de2.fan SonicTop det.de2.fan DensityTop -1 det.de2.sish SonicTop det.de2.sish DensityTop -1 det.de2.anc SonicTop det.de2.anc DensityTop -1 seal4.seal.shl SonicTop base.schn.wet DensityTop -1 base.schn.wet SonicTop base.schn.dry DensityTop -1 base.schn.fan SonicTop base.schn.fan DensityTop -1 base.schn.sish SonicTop base.schn.sish DensityTop -1 lowr.vol.vol SonicTop lowr.vol.vol DensityTop -1				<u>*</u>	-1
det.de1.fan SonicTop det.de1.fan DensityTop -1 det.de1.sish SonicTop det.de1.sish DensityTop -1 det.de1.anc SonicTop det.de1.anc DensityTop -1 det.de2.wet SonicTop det.de2.wet DensityTop -1 det.de2.dry SonicTop det.de2.fan DensityTop -1 det.de2.fan SonicTop det.de2.sish DensityTop -1 det.de2.sish SonicTop det.de2.anc DensityTop -1 seal4.seal.shl SonicTop seal4.seal.shl DensityTop -1 base.schn.wet SonicTop base.schn.wet DensityTop -1 base.schn.fan SonicTop base.schn.fan DensityTop -1 base.schn.sish SonicTop base.schn.sish DensityTop -1 lowr.vol.vol SonicTop lowr.vol.vol DensityTop -1 lowr.car.snd SonicTop lowr.car.snd DensityTop -1			det.de1.wet		
det.de1.sish SonicTop det.de1.sish DensityTop -1 det.de1.anc SonicTop det.de1.anc DensityTop -1 det.de2.wet SonicTop det.de2.wet DensityTop -1 det.de2.dry SonicTop det.de2.fan DensityTop -1 det.de2.sish SonicTop det.de2.sish DensityTop -1 det.de2.sish SonicTop det.de2.anc DensityTop -1 seal4.seal.shl SonicTop seal4.seal.shl DensityTop -1 base.schn.wet SonicTop base.schn.wet DensityTop -1 base.schn.dry SonicTop base.schn.fan DensityTop -1 base.schn.fan SonicTop base.schn.fan DensityTop -1 lowr.vol.vol SonicTop lowr.vol.vol DensityTop -1 lowr.car.snd SonicTop lowr.car.snd DensityTop -1			det.de1.fan		-1
det.de1.anc SonicTop det.de1.anc DensityTop -1 det.de2.wet SonicTop det.de2.wet DensityTop -1 det.de2.dry SonicTop det.de2.dry DensityTop -1 det.de2.fan SonicTop det.de2.fan DensityTop -1 det.de2.sish SonicTop det.de2.sish DensityTop -1 det.de2.anc SonicTop det.de2.anc DensityTop -1 seal4.seal.shl SonicTop seal4.seal.shl DensityTop -1 base.schn.wet SonicTop base.schn.wet DensityTop -1 base.schn.dry SonicTop base.schn.fan DensityTop -1 base.schn.sish SonicTop base.schn.sish DensityTop -1 lowr.vol.vol SonicTop lowr.vol.vol DensityTop -1 lowr.car.snd SonicTop lowr.car.snd DensityTop -1					-1
det.de2.wet SonicTop det.de2.wet DensityTop -1 det.de2.dry SonicTop det.de2.dry DensityTop -1 det.de2.fan SonicTop det.de2.fan DensityTop -1 det.de2.sish SonicTop det.de2.sish DensityTop -1 det.de2.anc SonicTop det.de2.anc DensityTop -1 seal4.seal.shl SonicTop seal4.seal.shl DensityTop -1 base.schn.wet SonicTop base.schn.wet DensityTop -1 base.schn.dry SonicTop base.schn.fan DensityTop -1 base.schn.sish SonicTop base.schn.sish DensityTop -1 lowr.vol.vol SonicTop lowr.vol.vol DensityTop -1 lowr.car.snd SonicTop lowr.car.snd DensityTop -1					-1
det.de2.dry SonicTop det.de2.dry DensityTop -1 det.de2.fan SonicTop det.de2.fan DensityTop -1 det.de2.sish SonicTop det.de2.sish DensityTop -1 det.de2.anc SonicTop det.de2.anc DensityTop -1 seal4.seal.shl SonicTop seal4.seal.shl DensityTop -1 base.schn.wet SonicTop base.schn.wet DensityTop -1 base.schn.dry SonicTop base.schn.fan DensityTop -1 base.schn.sish SonicTop base.schn.sish DensityTop -1 lowr.vol.vol SonicTop lowr.vol.vol DensityTop -1 lowr.car.snd SonicTop lowr.car.snd DensityTop -1					-1
det.de2.fan SonicTop det.de2.fan DensityTop -1 det.de2.sish SonicTop det.de2.sish DensityTop -1 det.de2.anc SonicTop det.de2.anc DensityTop -1 seal4.seal.shl SonicTop seal4.seal.shl DensityTop -1 base.schn.wet SonicTop base.schn.wet DensityTop -1 base.schn.fan SonicTop base.schn.fan DensityTop -1 base.schn.sish SonicTop base.schn.sish DensityTop -1 lowr.vol.vol SonicTop lowr.vol.vol DensityTop -1 lowr.car.snd SonicTop lowr.car.snd DensityTop -1		SonicTop			
det.de2.sish SonicTop det.de2.sish DensityTop -1 det.de2.anc SonicTop det.de2.anc DensityTop -1 seal4.seal.shl SonicTop seal4.seal.shl DensityTop -1 base.schn.wet SonicTop base.schn.wet DensityTop -1 base.schn.dry SonicTop base.schn.dry DensityTop -1 base.schn.sish SonicTop base.schn.sish DensityTop -1 lowr.vol.vol SonicTop lowr.vol.vol DensityTop -1 lowr.car.snd SonicTop lowr.car.snd DensityTop -1				Density Top	-1
det.de2.anc SonicTop det.de2.anc DensityTop -1 seal4.seal.shl SonicTop seal4.seal.shl DensityTop -1 base.schn.wet SonicTop base.schn.wet DensityTop -1 base.schn.dry SonicTop base.schn.dry DensityTop -1 base.schn.fan SonicTop base.schn.fan DensityTop -1 base.schn.sish SonicTop base.schn.sish DensityTop -1 lowr.vol.vol SonicTop lowr.vol.vol DensityTop -1 lowr.car.snd SonicTop lowr.car.snd DensityTop -1					
seal4.seal.shl SonicTop seal4.seal.shl DensityTop -1 base.schn.wet SonicTop base.schn.wet DensityTop -1 base.schn.dry SonicTop base.schn.dry DensityTop -1 base.schn.fan SonicTop base.schn.fan DensityTop -1 base.schn.sish SonicTop base.schn.sish DensityTop -1 lowr.vol.vol SonicTop lowr.vol.vol DensityTop -1 lowr.car.snd SonicTop lowr.car.snd DensityTop -1					-1
base.schn.wet SonicTop base.schn.wet DensityTop -1 base.schn.dry SonicTop base.schn.dry DensityTop -1 base.schn.fan SonicTop base.schn.fan DensityTop -1 base.schn.sish SonicTop base.schn.sish DensityTop -1 lowr.vol.vol SonicTop lowr.vol.vol DensityTop -1 lowr.car.snd SonicTop lowr.car.snd DensityTop -1		SonicTop			-1
base.schn.dry SonicTop base.schn.dry DensityTop -1 base.schn.fan SonicTop base.schn.fan DensityTop -1 base.schn.sish SonicTop base.schn.sish DensityTop -1 lowr.vol.vol SonicTop lowr.vol.vol DensityTop -1 lowr.car.snd SonicTop lowr.car.snd DensityTop -1					
base.schn.fan SonicTop base.schn.fan DensityTop -1 base.schn.sish SonicTop base.schn.sish DensityTop -1 lowr.vol.vol SonicTop lowr.vol.vol DensityTop -1 lowr.car.snd SonicTop lowr.car.snd DensityTop -1					-1
base.schn.sish SonicTop base.schn.sish DensityTop -1 lowr.vol.vol SonicTop lowr.vol.vol DensityTop -1 lowr.car.snd SonicTop lowr.car.snd DensityTop -1					-1
lowr.vol.vol SonicTop lowr.vol.vol DensityTop -1 lowr.car.snd SonicTop lowr.car.snd DensityTop -1					-1
lowr.car.snd SonicTop lowr.car.snd DensityTop -1					-1
				DensityTop	-1
	lowr.car.shl	SonicTop	lowr.car.shl	DensityTop	-1

Rotliegend case study Framework, see Table 6.1

Constraints table

Code	Parameter	Constraint	Value
wus.wu1.eva	Thickness	Generation	5
wus.wu1.sho	Thickness	Generation	45
wus.wu1.sil	Thickness	Generation	25
wus.wu1.wet	Thickness	Generation	35
wus.wu1.dry	Thickness	Generation	5
wus.wu1.fan	Thickness	Generation	5
wus.wu1.vol	Thickness	Generation	2
wus.wu2.wet	Thickness	Generation	50
wus.wu2.dry	Thickness	Generation	5
wus.wu2.fan	Thickness	Generation	10
wus.wu2.sish	Thickness	Generation	30
wus.wu2.vol	Thickness	Generation	5
bunt	Thickness	Presence	0
ebs.shor.shor	Thickness	Generation	100
ebs.shor.sish	Thickness	Generation	5
ebs.wet.wet	Thickness	Generation	80
ebs.wet.sish	Thickness	Generation	20
det.de1.sho	Thickness	Generation	10
det.de1.wet	Thickness	Generation	35
det.de1.fan	Thickness	Generation	25
det.de1.sish	Thickness	Generation	10
det.de1.anc	Thickness	Generation	20
det.de2.wet	Thickness	Generation	60
det.de2.dry	Thickness	Generation	5
det.de2.fan	Thickness	Generation	30
det.de2.sish	Thickness	Generation	5
det.de2.anc	Thickness	Generation	2
base.schn.wet	Thickness	Generation	30
base.schn.dry	Thickness	Generation	40
base.schn.fan	Thickness	Generation	30
base.schn.sish	Thickness	Generation	5

Rotliegend case study Framework, see Table 6.1

Appendix III

PERFORMANCE STATISTICS SIMULATED DATA EXPERIMENTS

The results of the experiments on simulated data, discussed in chapter 5, are presented in this appendix. The performance statistics on training and test datasets are presented in one table per experiment. The performance on the test dataset, is presented in three figures, for each experiment. The left-hand figure shows the normalised RMS error as a function of training patterns. The solid line indicates the training performance of the average density variable, the dashed line indicates the net gas-column thickness. The middle-and right-hand figure show the network estimated values versus the target values of the test variables (average density and net-gas column thickness, respectively). In the experiments 1 until 5, these values have been scaled to a range between -1 and +1. In experiment 8 unscaled values are shown.

1A Training variables	Normalised RMS	RMS	Mean Absolute	Max Absolute
Density	0.28_	13.47 kg/m ³	9.63 kg/m ³	51.48 kg/m^3
Gas column	0.33	3. <u>6</u> 7 m	2.26 m	16.56 m
1A Test variables	Normalised RMS	RMS	Mean Absolute	Max Absolute
Density	0.28	14.29 kg/m ³	11.20 kg/m ³	38.65 kg/m ³
Gas column	0.33	3.16 m	2.17 m	13.40 m

1B Training variables	Normalised RMS	RMS	Mean Absolute	Max Absolute
Density	0.29	14.33 kg/m ³	10.53 kg/m ³	57.95 kg/m ³
Gas column	0.46	5.16 m	3.12 m	22.48 m
1B Test variables	Normalised RMS	RMS	Mean Absolute	Max Absolute
Density	0.29	14.53 kg/m ³	10.92 kg/m ³	42.16 kg/m ³
Gas column	0.44	4.22 m	2.66 m	18.54 m

1C Training variables	Normalised RMS	RMS	Mean Absolute	Max Absolute
Density	0.32	14.53 kg/m ³	14.53 kg/m ³	14.53 kg/m ³
Gas column	0.56	6.23 m	4.17 m	24.84 m
1C Test variables	Normalised RMS	RMS	Mean Absolute	Max Absolute
Density	0.32	16.32 kg/m ³	12.10 kg/m ³	48.73 kg/m ³
Gas column	0.54	5.19 m	3.60 m	21.09 m

ID Training variables	Normalised RMS	RMS	Mean Absolute	Max Absolute
Density	0.54	26.15 kg/m ³	20.04 kg/m ³	104.10 kg/m ³
Gas column	0.98	10.95 m	9.03 m	28.47 m
1D Test variables	Normalised RMS	RMS	Mean Absolute	Max Absolute
Density	0.51	25.69 kg/m ³	20.49 kg/m ³	75,35 kg/m ³
Gas column	0.97	9 36 m	8.08 m	20.31 m

2A Training variables	Normalised RMS	RMS	Mean Absolute	Max Absolute
Density	0.22	10.91 kg/m ³	7.95 kg/m ³	42.51 kg/m ³
Gas column	0.31	3.43 m	2.09 m	15.79 m
2A Test variables	Normalised RMS	RMS	Mean Absolute	Max Absolute
Density	0.24	12.10 kg/m ³	9.10 kg/m ³	33.50 kg/m ³
Gas column	0.32	3.06 m	1.92 m	12.62 m

2B Training variables	Normalised RMS	RMS	Mean Absolute	Max Absolute
Density	0.92	44.85 kg/m ³	35.35 kg/m ³	114.50 kg/m ³
Gas column	0.44	4.92 m	3.56 m	19.08 m
2B Test variables	Normalised RMS	RMS	Mean Absolute	Max Absolute
Density	0.93	46.94 kg/m ³	38.34 kg/m ³	119.23 kg/m ³
Gas column	0.48	4.60 m	3.51 m	16.49 m

2C Training variables	Normalised RMS	RMS	Mean Absolute	Max Absolute
Density	0.30	14.71 kg/m ³	10.65 kg/m ³	53.70 kg/m ³
Gas column	0.41	4.59 m	2.84 m	18.86 m
2C Test variables	Normalised RMS	RMS	Mean Absolute	Max Absolute
Density	0.31	15.65 kg/m ³	12.45 kg/m ³	41.98 kg/m ³
Gas column	0,39	3.81 m	2.51 m	16.08 m

3A Training variables	Normalised RMS	RMS	Mean Absolute	Max Absolute
Density	0.46	22.51 kg/m ³	16.24 kg/m ³	70.51 kg/m ³
Gas column	0.45	4.97 m	3.05 m	21.44 m
3A Test variables	Normalised RMS	RMS	Mean Absolute	Max Absolute
Density	0.46	23.28 kg/m ³	17.59 kg/m ³	85.49 kg/m ³
Gas column	0.37	3.62 m	2.36 m	15.30m

3B Training variables	Normalised RMS	RMS	Mean Absolute	Max Absolute
Density	0.32	15.48 kg/m ³	11.22 kg/m ³	66.20 kg/m ³
Gas column	0.32	3.58 m	2.39 m	21.52 m
3B Test variables	Normalised RMS	RMS	Mean Absolute	Max Absolute
Density	0.33	16.49 kg/m ³	11.55 kg/m ³	78.70 kg/m ³
Gas column	0.30	2.86 m	1.88 m	15.58 m

3C Training variables	Normalised RMS	RMS	Mean Absolute	Max Absolute
Density	0.47	22.75 kg/m ³	17.22 kg/m ³	84.07 kg/m ³
Gas column	0.35	3.92 m	2.56 m	20.88 m
3C Test variables	Normalised RMS	RMS	Mean Absolute	Max Absolute
Density	0.45	22.67 kg/m ³	17.75 kg/m ³	64.95 kg/m ³
Gas column	0.31	3.04 m	2.30 m	12.37 m

3D Training variables	Normalised RMS	RMS	Mean Absolute	Max Absolute
Density	0.29	14.05 kg/m ³	10.48 kg/m ³	43.84 kg/m ³
Gas column	0.23	2.54 m	1.44 m	19.50 m
3D Test variables	Normalised RMS	RMS	Mean Absolute	Max Absolute
Density	0.29	14.48 kg/m ³	11.15 kg/m ³	40.34 kg/m ³
Gas column	0.19	1.81 m	1.33 m	7.86 m

4A Training variables	Normalised RMS	RMS	Mean Absolute	Max Absolute
Density	0.17	8.14 kg/m ³	6.29 kg/m ³	29.49 kg/m ³
Gas column	0.21	2.33 m	1.53 m	10,28 m
4A Test variables	Normalised RMS	RMS	Mean Absolute	Max Absolute
Density	0.18	9.02_ kg/m ³	7.08 kg/m ³	21.72 kg/m ³
Gas column	0.25	2.45 m	1.55 m	14.09 m

4B Training variables	Normalised RMS	RMS	Mean Absolute	Max Absolute
Density	0.18	8.55 kg/m ³	6.72 kg/m ³	25.97 kg/m ³
Gas column	0.24	2.72 m	1.92 m	9.15 m
4B Test variables	Normalised RMS	RMS	Mean Absolute	Max Absolute
Density	0.18	9.01 kg/m ³	7.04 kg/m ³	25.95 kg/m ³
Gas column	0.27	2.63 m	1.74 m	16.71 m

4C Training variables	Normalised RMS	RMS	Mean Absolute	Max Absolute
Density	0.21	10.13 kg/m ³	7.57 kg/m ³	40.13 kg/m ³
Gas column	0.35	3.93 m	2.46 m	14.96 m
4C Test variables	Normalised RMS	RMS	Mean Absolute	Max Absolute
Density	0.22	10.97 kg/m ³	8.20 kg/m ³	28.49 kg/m ³
Gas column	0.36	3.49 m	2.18 m	15.23 m

4D Training variables	Normalised RMS	RMS	Mean Absolute	Max Absolute
Density	0.13	6.32 kg/m ³	4.96 kg/m ³	17.33 kg/m ³
Gas column	0.39	4.30 m	3.12 m	15.91 m
4D Test variables	Normalised RMS	RMS	Mean Absolute	Max Absolute
Density	0.13	6.34 kg/m ³	5.01 kg/m ³	16.59 kg/m ³
Gas column	0.44	4.24 m	2.87 m	26.92 m

4E Training variables	Normalised RMS	RMS	Mean Absolute	Max Absolute
Density	0.12	5.85 kg/m ³	4.73 kg/m ³	13.91 kg/m ³
Gas column	0.40	4.42 m	3.05 m	17.76 m
4E Test variables	Normalised RMS	RMS	Mean Absolute	Max Absolute
Density	0.13	6.51 kg/m ³	5.17 kg/m ³	18.18 kg/m ³
Gas column	0.43	4.14 m	2.71 m	27.58 m

5 Training variables	Normalised RMS	RMS	Mean Absolute	Max Absolute
Density	0.22	11.69 kg/m ³	8.70 kg/m ³	41.43 kg/m ³
Gas column	0.50	5.17 m	3.93 m_	14.40 m
5 Test variables	Normalised RMS	RMS	Mean Absolute	Max Absolute
Density	0.29	14.47 kg/m ³	11.41 kg/m ³	41.64 kg/m ³
Gas column	0.58	5.73 m	4.20 m	20.08 m

6 Training variables	Normalised RMS	RMS	Mean Absolute	Max Absolute
Density	0.82	37.95_kg/m ³	29.19 kg/m ³	122.35 kg/m ³
Gas column	0.53	5.76 m	4.54 m	14.85 m
6 Test variables	Normalised RMS	RMS	Mean Absolute	Max Absolute
Density	0.83	41.73 kg/m ³	33.36 kg/m ³	112.32 kg/m ³
Gas column	0.60	6.52 m	4.75 m	23.54 m

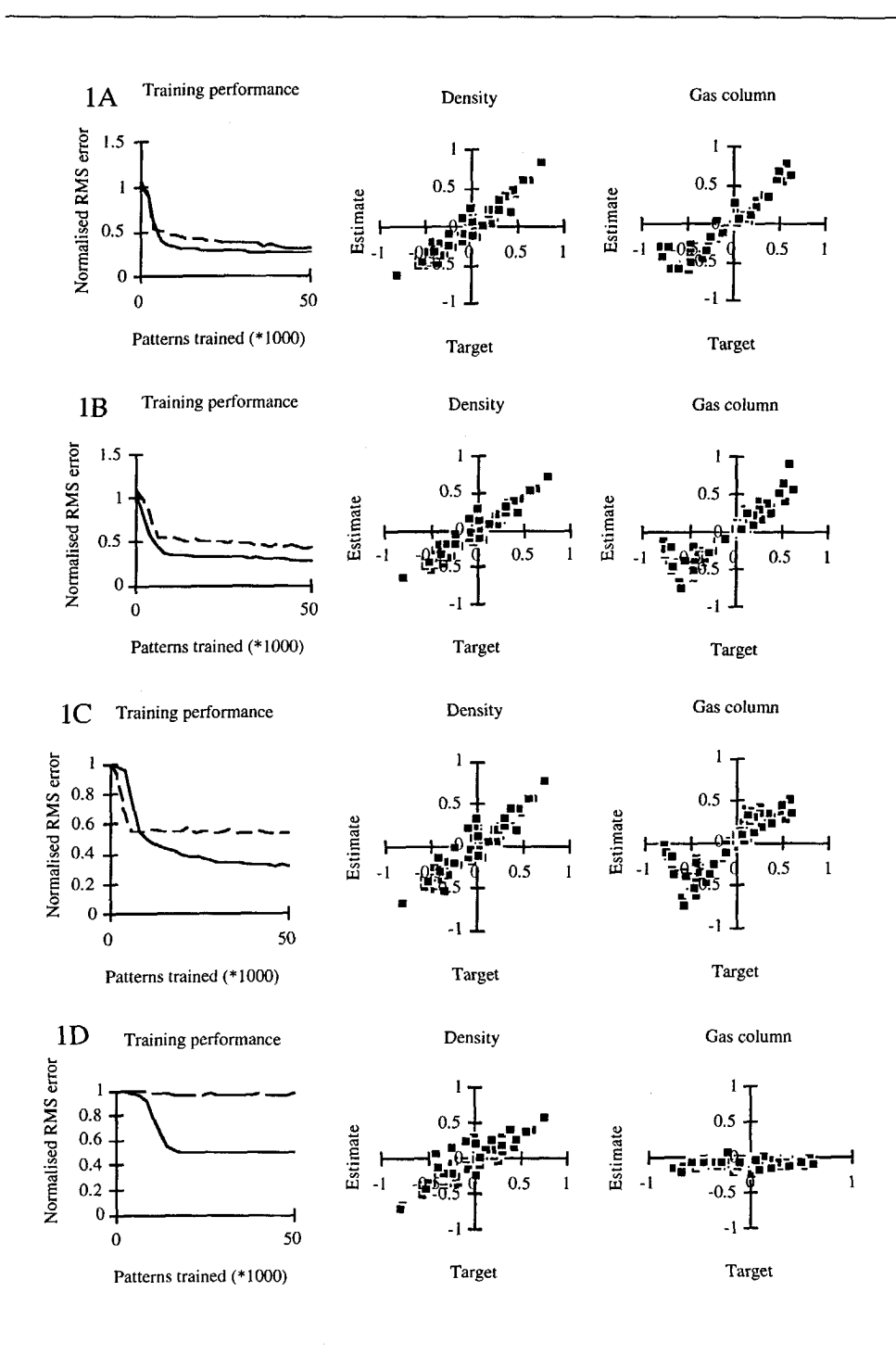
7A Training variables	Normalised RMS	RMS	Mean Absolute	Max Absolute
Density	0.80	37.11 kg/m ³	29.27 kg/m ³	118.03 kg/m ³
Gas column	0.54	5.83 m	4.53 m	14.21 m
7A Test variables	Normalised RMS	RMS	Mean Absolute	Max Absolute
Density	0.87	43.63 kg/m ³	34.53 kg/m ³	128.14 kg/m ³
Gas column	0.61	6.66 m	4.84 m	26.51 m

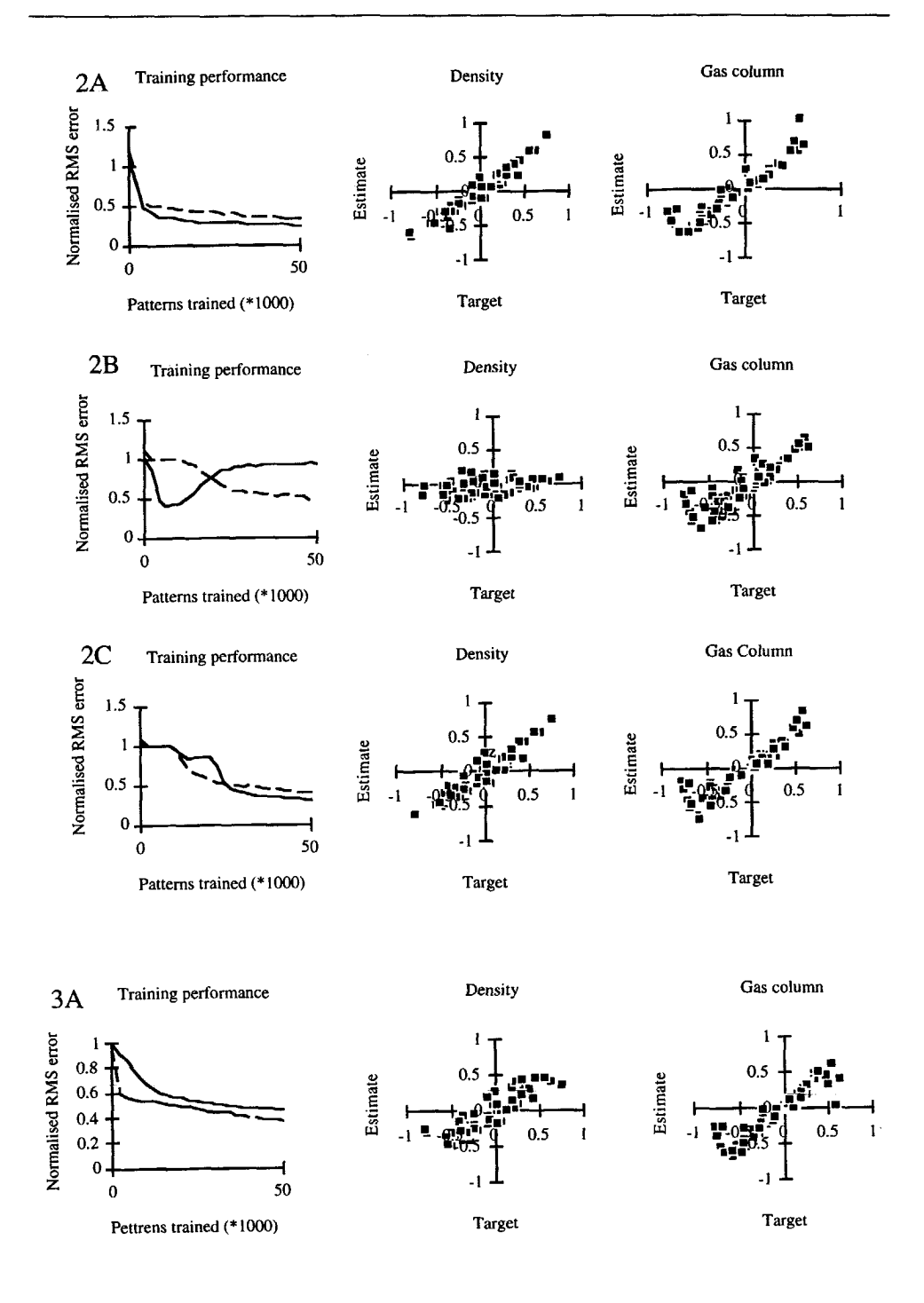
7B Training variables	Normalised RMS	RMS	Mean Absolute	Max Absolute
Density	0.82	37.95 kg/m ³	29.19 kg/m ³	122.35 kg/m ³
Gas column	0.53	5.76 m	4.54 m	14.85 m
7B Test variables	Normalised RMS	RMS	Mean Absolute	Max Absolute
Density	0.83	41.73 kg/m ³	33.36 kg/m ³	112.32kg/m ³
Gas column	0.60	6.52 m	4.75 m	23.54 m

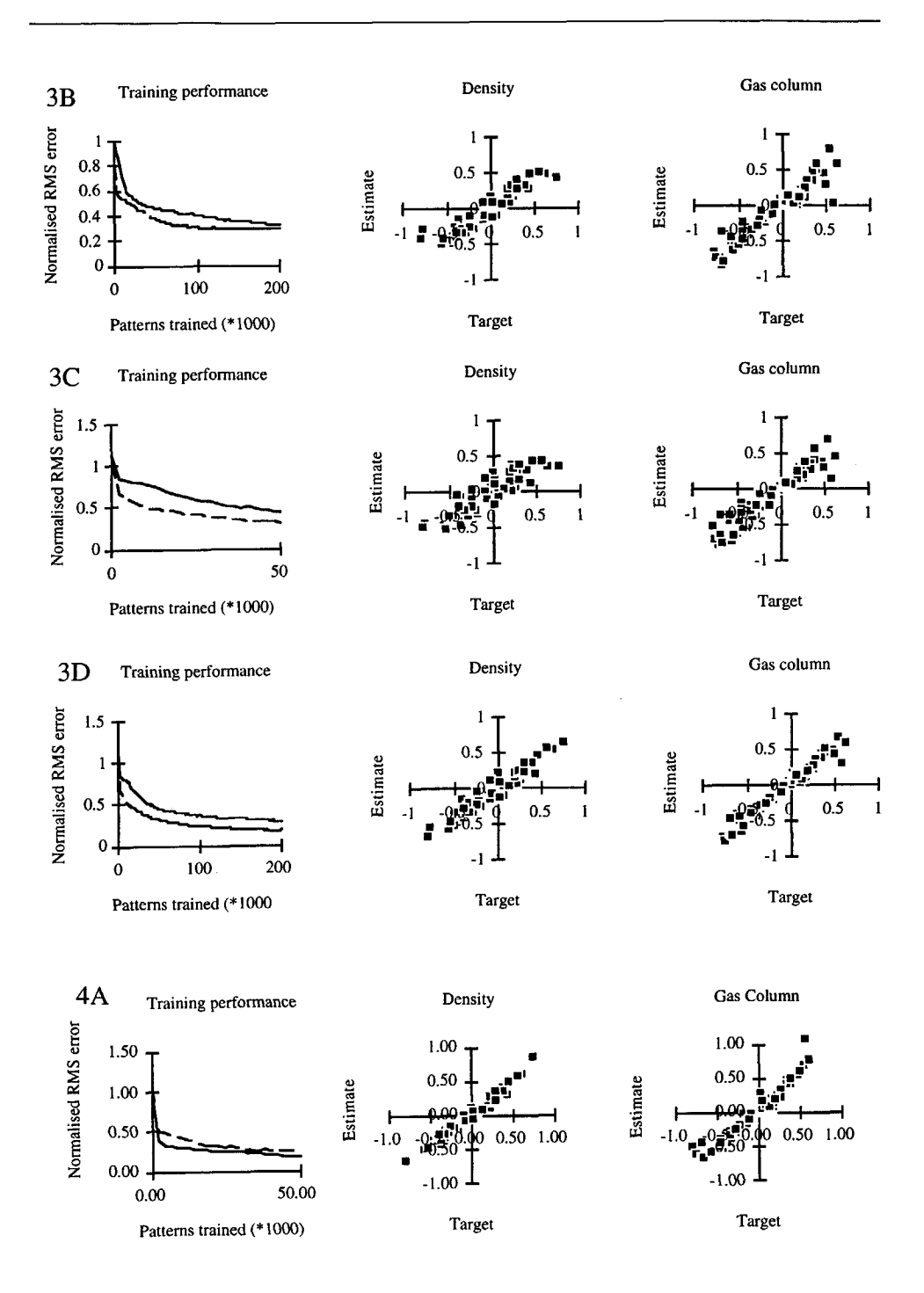
7C Training variables	Normalised RMS	RMS	Mean Absolute	Max Absolute
Density	0.82	37.93 kg/m ³	29.88 kg/m ³	114.71 kg/m ³
Gas column	0.59	6.37 m	4.93 m	14.89 m
7C Test variables	Normalised RMS	RMS	Mean Absolute	Max Absolute
Density	0.85	42.72 kg/m ³	34.26 kg/m ³	125.99 kg/m ³
Gas column	0.66	7.23 m	5.38 m	22.21 m

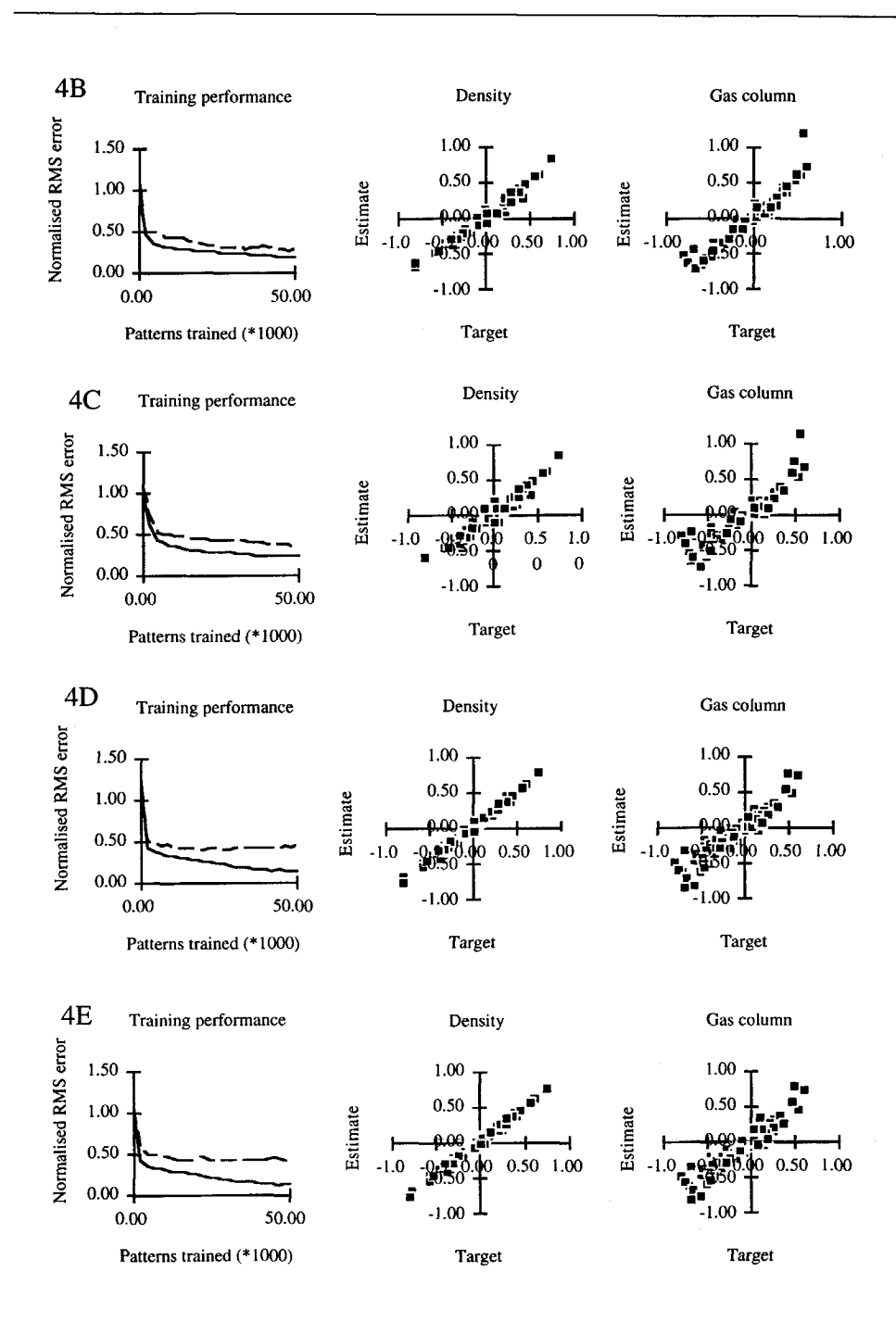
7D Training variables	Normalised RMS	RMS	Mean Absolute	Max Absolute
Density	0.82	37.95 kg/m ³	29.19 kg/m ³	122.35 kg/m ³
Gas column	0.53	5.76 m	4.54 m	14.85 m
7D Test variables	Normalised RMS	RMS	Mean Absolute	Max Absolute
Density	0.83	41.73 kg/m ³	33.36 kg/m ³	112.32 kg/m ³
Gas column	0.60	6.52 m	4.75 m	23.54 m

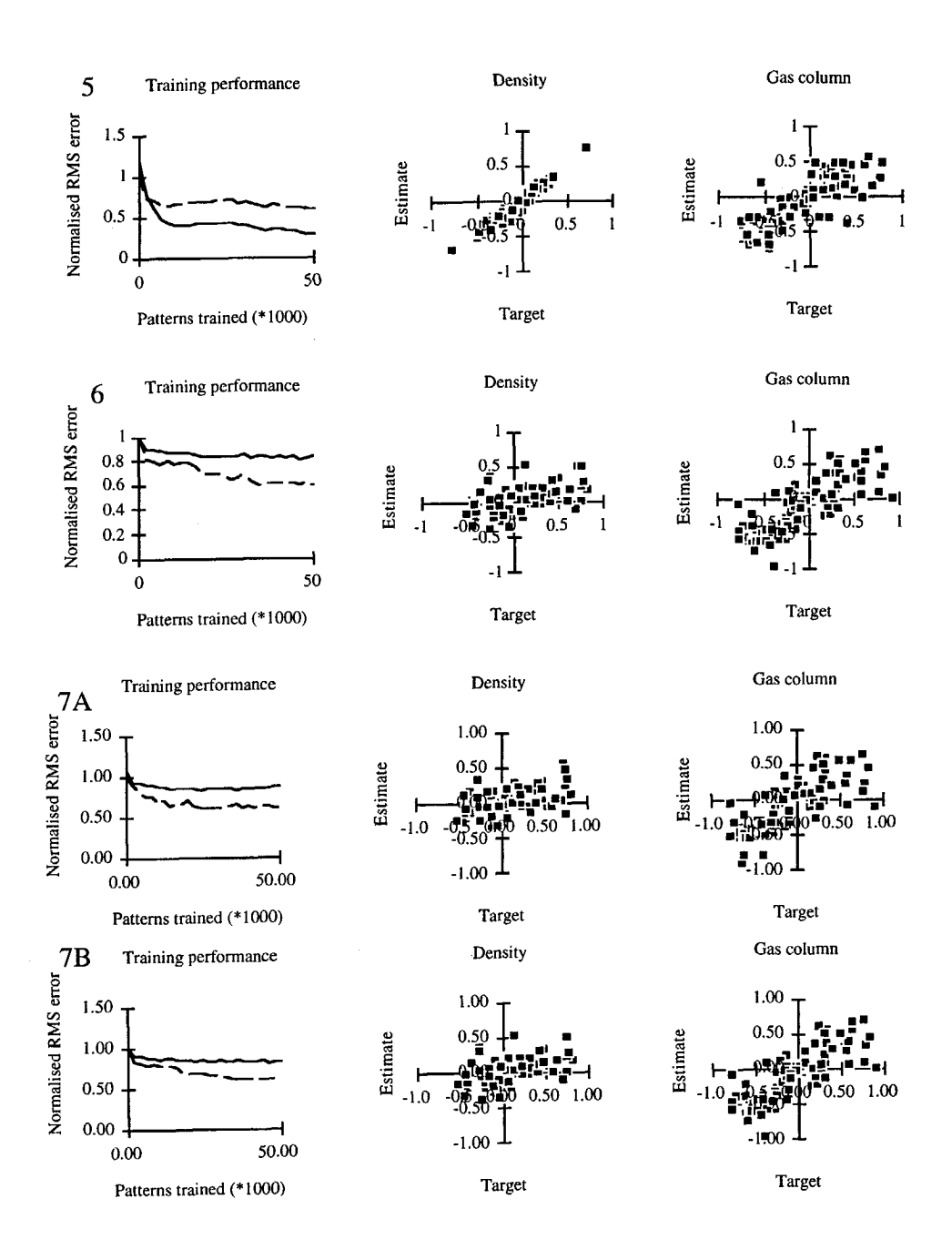
8 Training variables	Normalised RMS	RMS	Mean Absolute	Max Absolute
Density	0.25	13.62 kg/m ³	10.37 kg/m ³	35.86 kg/m ³
Gas column	0.13	1.34 m	0.91 m	5.69 m
8 Test variables	Normalised RMS	RMS	Mean Absolute	Max Absolute
Density	0.28	14.26 kg/m ³	11.20 kg/m ³	40.19 kg/m ³
	I	2.07 m	1.52 m	6.84 m

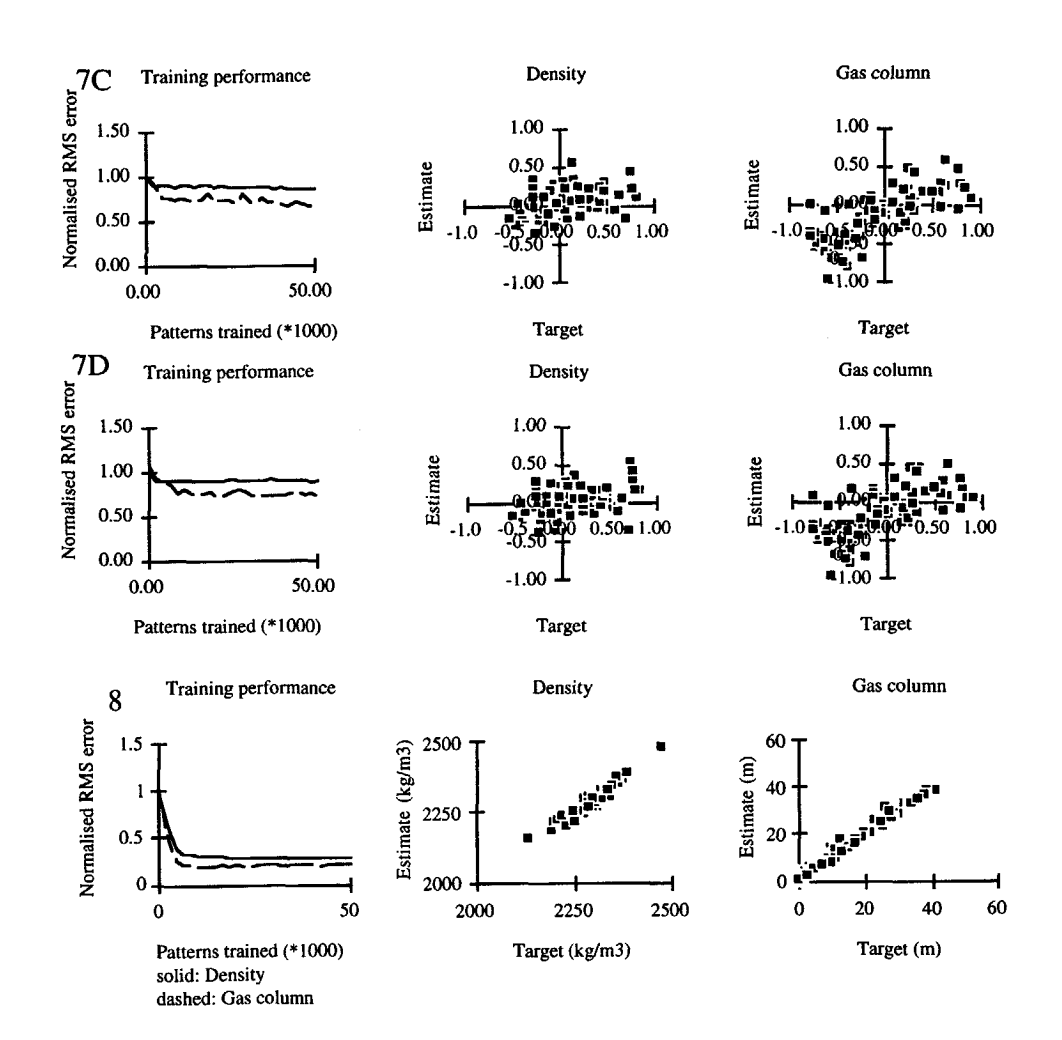












SUMMARY

In this thesis a new method for post-stack seismic reservoir characterisation is described. In this method the seismic reservoir characterisation process is approached from a geological perspective. Factual and simulated wells, i.e. one-dimensional stratigraphic profiles with attached physical properties are described in terms of a common subsurface model: the integration framework. The integration framework defines the acoustic-stratigraphic entities, at three scale levels within the target zone for a particular survey area. Factual and simulated wells described in this way, are commensurable. The factual wells are combined with the surface seismic traces at the well locations. Simulated acoustic properties of the simulated wells are used to generate synthetic seismic traces. Operating in this way, datasets consisting of well information and corresponding seismic responses are combined in what is defined as: *model space* (simulated data only), real space (factual data only), or total space (combined factual and simulated data). The objective is to arrive at a dataset that is representative of the geological and physical variations in the target zone. These data are used in the seismic characterisation process; the so-called total space inversion method.

In this study two approaches within the total space inversion concept are described:

 Direct inversion: in this approach the representative dataset is tested for relations between seismic response and salient reservoir properties. The established relations are subsequently applied to a factual seismic horizon slice, yielding lateral prediction results. • Segmentation: in this approach the factual seismic response is segmented into a number of classes. A representative dataset is subsequently segmented by the same classifier and the well information is analysed to arrive at a geological description of the seismic classes.

In this thesis, artificial neural networks are employed in the inversion phase. Unsupervised Vector Quantisers (UVQs) are used in the segmentation approach and Multi-Layer-Perceptrons (MLP) and Radial Basis Functions (RBF) networks are used in the direct inversion.

An algorithm is used for the simulation of wells, which combines geological reasoning with stochastic input. The algorithm makes use of an innovative Monte Carlo statistics procedure in which correlated multi-variate stochastic variables are drawn one-by-one.

A number of experiments on simulated data, describing different geological settings, are presented. Different network paradigms (MLP, RBF) and designs (number of layers, number of nodes, activation functions) are tested in these experiments.

The total space inversion method has been applied to two case studies. The first study deals with a Rotliegend unit comprising gas-filled aeolian sandstones. The second study involves an oil-filled fluviatile reservoir. It is shown that in both studies exciting results were obtained by visualising, analysing and interpreting seismic patterns. In the Rotliegend study, it was possible to map the extent of the good reservoir 'shoreline' sand-deposits. In the second study major sedimentary distribution trends and patterns in a labyrinth-type reservoir were revealed. Utilising the integration framework, the classes could be analysed for geological content. This revealed a number of distributary trends comprising channelised sandbodies, silts and clays within an ancient avulsing floodplain environment.

The information extracted from the seismic signals using total space inversion is useful to production geologists and reservoir engineers, as it helps explain reservoir body distribution, connectivity, drainage and injection models in addition to giving an indication of net oil in place.

In conclusion it may be stated that total space inversion, especially the segmentation approach, is a powerful new technique for inferring geological information from seismic signals.

SAMEN VATTING

Seismische reservoir karakterisatie met behulp van reëele en gesimuleerde putten

In dit proefschrift wordt een nieuwe methode beschreven voor post-stack seismische reservoir karakterisatie. In deze methode wordt het seismische reservoir karakterisatie process benaderd vanuit een geologisch perspectief. Reëele en gesimuleerde putten, d.w.z. één-dimensionale stratigrafische profielen met bijbehorende fysische eigenschappen, worden beschreven in termen van één en hetzelfde model van de ondergrond: het integratie kader. Het integratie kader definieert de akoestisch-stratigrafische entiteiten van het beoogde interval, in een bepaald studie gebied, op drie schaal nivo's. Putten die op deze wijze worden beschreven zijn vergelijkbaar. Reëele putten worden gecombineerd met de seismische sporen op de put lokaties. De gesimuleerde akoestische eigenschappen van gesimuleerde putten worden gebruikt om seismische sporen te synthetiseren. Door deze manier van werken worden gegevens, bestaande uit put informatie en seismische signalen gecombineerd, in, wat is gedefinieerd als: model ruimte (enkel gesimuleerde gegevens), reëele ruimte (enkel reëele gegevens), of totale ruimte (zowel reëele, alsook gesimuleerde gegevens). Het streven is, een databank te creëeren, die representatief geacht wordt voor de variaties in geologische- en fysische-eigenshappen van het beoogde interval. De gegevens worden gebruikt in het seismische reservoir karakterisatie process; de zogenaamde totale ruimte inversie methodiek.

In dit proefschrift worden twee methodieken binnen het totale ruimte inversie concept beschreven:

- Direkte inversie. In deze methodiek wordt de representatieve databank onderzocht naar relaties tussen seismische signalen en onderliggende, belangwekkende reservoir eigenschappen. Vastgestelde relaties worden vervolgens toegepast op de reëele seismische horizon-snede. Dit levert een ruimtelijke voorspelling van de eigenschap op.
- Segmentatie. In deze methodiek wordt de reëele seismische horizonsnede gesegmenteerd in een aantal klasses. Vervolgens wordt een representatieve databank geclassificeerd met behulp van dezelfde classificator. De putgegevens in de resulterende klasses worden dan geanalyseerd om tot een geologische beschrijving te komen van de seismische klasses.

In dit proefschrift worden kunstmatige neurale netwerken toegepast tijdens de inversie fase. Niet-begeleide vector kwantificeerders (UVQs) worden gebruikt voor de segmentatie methodiek en meer-laagse perceptrons (MLPs) en radiale basis functies (RBF) netwerken worden gebruikt voor de direkte methodiek.

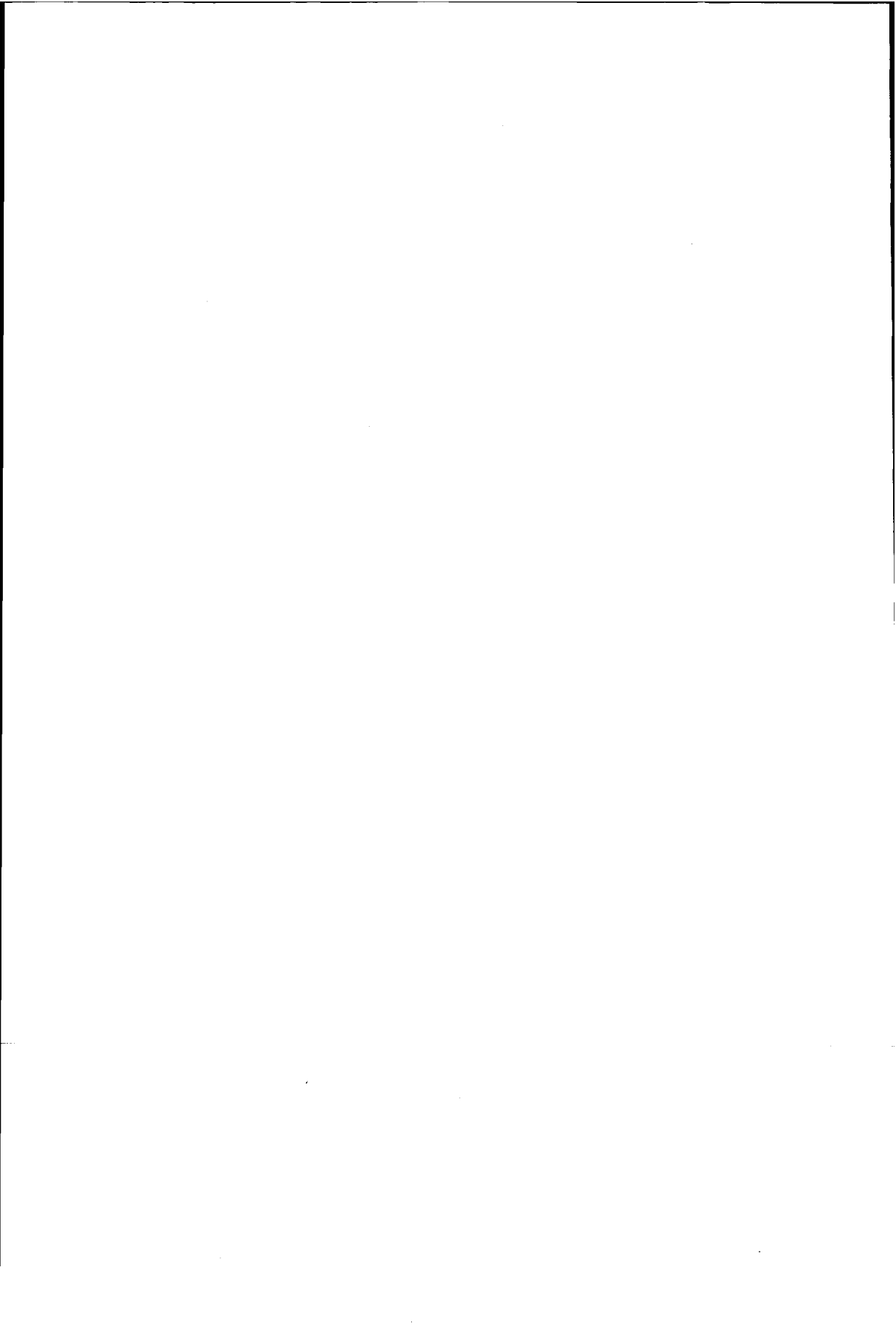
Voor het simuleren van putten is een algoritme gebruikt waarin geologische redenaties gecombineerd worden met stochastische invoer. Het algoritme maakt gebruik van een innovatieve procedure om gecorreleerde multivariaat verdeelde stochastische variabelen één-voor-één te trekken.

Een aantal experimenten met gesimuleerde data worden gepresenteerd. De simulaties beschrijven meerdere geologische modellen. Verschillende netwerk paradigma's (MLP, RBF) en ontwerpen (aantal lagen, aantal knopen, activatie functies) zijn getest in deze experimenten.

De totale ruimte inversie methodiek is toegepast in twee studies. De eerste studie betreft een Rotliegend eenheid bestaande uit gas-gevulde aeolische zanden. De tweede studie heeft betrekking op een fluviatiel olie reservoir. Beide studies laten zien dat bruikbare geologische informatie aan de seismische signalen kon worden onttrokken. Vooral de horizon-snede segmentatie methodiek leverde opwindende informatie op. In de Rotliegend study bleek het mogelijk door middel van segmentatie de, vanuit een reservoir perspectief gezien, goede 'kustzand' afzettingen, te karteren. In de tweede studie werden sediment distributie trends en patronen zichtbaar in een 'labyrint-type' reservoir. Door middel van het integratie kader konden de seismische klassen gerelateerd worden aan de geologische inhoud. Dit leidde tot de interpretatie van een aantal sediment distributie trends bestaande uit gekanaliseerde zandlichamen, silt- en klei-afzettingen in een avulsief overstromingsgebied.

De informatie die met behulp van de totale inversie methodiek aan de seismische signalen kon worden onttrokken, is van belang voor produktie geologen en reservoir ingenieurs. Het geeft inzicht in zandlichaam distributie, connectiviteit, drainage en injectie modellen en helpt bij de bepaling van de netto koolwaterstof reserves.

Concluderend kan worden gesteld dat, met name de segmentatie methodiek, in het totale ruimte inversie concept, een krachtige techniek is om geologische informatie te onttrekken aan seismische signalen.



CURRICULUM VITAE

Paul Franciscus Maria de Groot born on April 10th. 1956

Education:

1962-1968: Primary school in Enschede, The Netherlands.

1968-1974: Secondary school (Athenaeum-B) in Enschede.

1974-1975: Studied at the faculty of dental surgery of the

University of Nijmegen.

1975-1981: Studied at the faculty of Mining Engineering of the

University of Delft. Graduated in February 1981, with a thesis entitled: 'Real time quality control of seismic data in the acquisition phase' on an assignment for the Nederlandse Aardolie

Maatschappij.

Professional Career:

1981-1982: Joined 'Shell Internationale Petroleum Maatschappij'

in March 1981. Started at the 'Koninklijke Shell Exploratie en Produktie Laboratorium' with the acquisition research group, working on a project involving the interaction between two vibrators. Attended the basic training courses for Shell exploration staff and was subsequently trained as a seismic processor between August 1981 and

February 1982.

1982-1986: Transferred to 'Petroleum Development Oman'.

Worked as a seismic processor, from 1982 until

1984. Joined the interpretation studies group of P.D.O., dealing with lateral prediction studies, ray-tracing exercises, VSP's and seismic interpretation.

1986-1991:

Transferred to 'Shell Petroleum Development Company' of Nigeria. Worked from 1986 until 1988 as a seismic interpreter involved in acreage evaluation and prospect generation, based in Port Harcourt. In 1988 took over the position of Head Geological Databases, based in Warri, responsible for exploration data management and exploration computing.

March-July 1991:

Transferred to 'Shell Internationale Petroleum Maatschappij' in The Hague, to work in a section responsible for supporting seismic interpretation workstations and evaluating geophysical software. Resigned from S.I.P.M. in July 1991 to found 'Ouest Geophysical Services B.V.'.

July 1991-

June 1992:

Director Quest Geophysical Services B.V. Performed geophysical consultancy services and initiated the 'PROBE' consortium aimed at developing a seismic reservoir charcaterisation method based on artificial neural networks and stochastic modelling techniques.

1992-

present:

Joined TNO Institute of Applied Geoscience as senior geophysicist. Projectleader of the "DELSI" and the "PROBE" software development projects. In addition carried out extensive seismic acquisition, processing

and interpretation services, incl. reporting.

Publications:

Internal SHELL reports (all confidential) TNO reports (all confidential)

Campbell, A.E., Scheffers B., de Groot P.F.M., 1994. Geophysics desperately seeking geology. poster presentation at the 56th EAEG conference, 6-10 June 1994, Vienna.

de Groot, P.F.M. et.al., 1993. Seismic Reservoir characterisation using artificial neural networks and stochastic modelling techniques. presented at the 55th EAEG conference, June 1993, Stavanger.

de Groot, P.F.M., Bril, A.H., Floris F.J.T, Campbell, E.C., 1995. Monte Carlo simulation of wells. submitted to Geophysics.

Curriculum vitae

- de Groot P.F.M., 1995. "Total Space Inversion"; Concept and Experiments in model space. Presentated at the 57th. EAEG conference, Glasgow.
- de Groot, P.F.M., Campbell, A.E. and Cisneros, R., 1995. Seismic reservoir characterisation using 'total space inversion'. In preparation.
- Jugla, F., Julien, P., de Groot, P., Verschuur, E., 1994. A real case comparison between surface-related multiple elimination and other wave equation-based techniques, presented at the 64th SEG conference, October 1994. Los Angeles.
- Meekes, J.A.C., Scheffers, B., Cox, H.L.H. and de Groot, P.F.M., 1995. A Large 2D High Resolution Seismic Survey Optimum Data Quality as Related to Source Parameters. Presentated at the 57th. EAEG conference, Glasgow.

